



AUBURN UNIVERSITY

Samuel Ginn College of Engineering

Research Report for ALDOT Project 931-046

**USE OF TITANIUM ALLOY REINFORCEMENT TO
STRENGTHENED BRIDGES IN ALABAMA: LABORATORY
TESTING AND ANALYTICAL INVESTIGATIONS**

Submitted to

The Alabama Department of Transportation

Prepared by

Md Aminul Islam

Jack C. Flowers

Victor Aguilar

Kadir C. Sener

Anton K. Schindler

SEPTEMBER 2024

Highway Research Center

Harbert Engineering Center
Auburn, Alabama 36849

1. Report No. 931-046	2. Government Accession No.		3. Recipient Catalog No.	
4. Title and Subtitle Use of Titanium Alloy Reinforcement to Strengthened Bridges in Alabama: Laboratory Testing and Analytical Investigations			5. Report Date September 2024	
			6. Performing Organization Code	
7. Author(s) M. A. Islam, J.C. Flowers, V. Aguilar, K. C. Sener, and A. K. Schindler			8. Performing Organization Report No. 931-046	
9. Performing Organization Name and Address Highway Research Center Department of Civil Engineering 238 Harbert Engineering Center Auburn, AL 36849			10. Work Unit No. (TRAIS)	
			11. Contract or Grant No.	
12. Sponsoring Agency Name and Address Alabama Department of Transportation 1409 Coliseum Boulevard Montgomery, Alabama 36130-3050			13. Type of Report and Period Covered Technical Report	
			14. Sponsoring Agency Code	
15. Supplementary Notes Project performed in cooperation with the Alabama Department of Transportation.				
16. Abstract <p>This report presents findings from a comprehensive study evaluating the feasibility of using Near-Surface-Mounted (NSM) Titanium Alloy Bars (TiAB) to strengthen structurally deficient reinforced concrete (RC) bridges in Alabama. The research aimed to provide a cost-effective, efficient solution to extend the service life of aging and strength deficient highway infrastructure, focusing on a flexurally deficient bridge in Cullman. Three TiAB NSM anchorage methods were investigated: i) hooked-bonded, ii) straight-bonded, and iii) hooked-unbonded.</p> <p>The study was conducted in two phases. Phase 1 involved laboratory testing of 15 small-scale specimens to evaluate TiAB anchorage behavior and bond strength, essential for calculating the development length. The results confirmed the AASHTO NSM Guide bond strength recommendations for hooked-bonded anchorage, provided bond strength guidelines for straight-bonded anchorage, and evaluated the feasibility of hooked-unbonded anchorage.</p> <p>Phase 2 included full-scale testing of 16 girders representative of the Cullman bridge, assessing both positive- and negative-moment strengthening using the three anchorage methods. The results indicated the need for additional requirements for the hooked-bonded method for adequate strengthening, leading to proposed updates for the AASHTO TiAB NSM Guide. Design guidelines were also developed for the effective use of straight-bonded anchorage. Full-scale tests of the hooked-unbonded method indicated that this method might be suitable for temporary use but inadequate for permanent strengthening.</p> <p>The study developed detailed construction and field implementation guidelines for strengthening the Cullman bridge. While fatigue evaluations are necessary for final recommendations, these findings offer critical insights for ALDOT in implementing NSM TiAB as a reliable method to strengthen RC bridges.</p>				
17. Key Words Bond strength, bridge flexural strengthening, titanium-alloy bars, near-surface mounting, epoxy, groove cutting			18. Distribution Statement No restrictions.	
19. Security Classification (of this report) Unclassified	20. Security Classification (of this page) Unclassified	21. No. of Pages 196	22. Price None.	

Research Report

USE OF TITANIUM ALLOY REINFORCEMENT TO STRENGTHENED BRIDGES IN ALABAMA: LABORATORY TESTING AND ANALYTICAL INVESTIGATIONS

Submitted to

The Alabama Department of Transportation

Prepared by

Md Aminul Islam

Jack C. Flowers

Victor Aguilar

Kadir C. Sener

Anton K. Schindler

SEPTEMBER 2024

DISCLAIMERS

The contents of this report reflect the views of the authors who are responsible for the facts and accuracy of the data presented herein. The contents do not necessarily reflect the official views or policies of Alabama DOT, Auburn University, or the Highway Research Center. This report does not constitute a standard, specification, or regulation. Comments contained in this report related to specific testing equipment and materials should not be considered an endorsement of any commercial product or service; no such endorsement is intended or implied.

NOT INTENDED FOR CONSTRUCTION, BIDDING, OR PERMIT PURPOSES

Kadir C. Sener, Ph.D., P.E.

Anton K. Schindler, Ph.D., P.E.

Research Supervisors

ACKNOWLEDGEMENTS

Material contained herein was obtained in connection with a research project ALDOT 931-046, conducted by the Highway Research Center, Auburn University. Funding for the project was provided by the Federal Highway Administration (FHWA) and the Alabama Department of Transportation (ALDOT). The funding, cooperation, and assistance of many individuals from each of these organizations are gratefully acknowledged. The authors would like to acknowledge the various contributions of the following individuals:

Eric Christie	ALDOT, State Maintenance Engineer
Daniel Jones	ALDOT, Deputy State Maintenance Engineer
Stacey Glass	ALDOT, State Construction Engineer
Brad Williams	ALDOT, Deputy State Construction Engineer
Kidada Dixon	ALDOT, Research and Development Engineer
Kristy Harris	FHWA Alabama
Jill Adkins	Perryman Company

ABSTRACT

This report presents findings from a comprehensive study evaluating the feasibility of using Near-Surface-Mounted (NSM) Titanium Alloy Bars (TiAB) to strengthen structurally deficient reinforced concrete (RC) bridges in Alabama. The research aimed to provide a cost-effective, efficient solution to extend the service life of aging and strength deficient highway infrastructure, focusing on a flexurally deficient bridge in Cullman. Three TiAB NSM anchorage methods were investigated: i) hooked-bonded, ii) straight-bonded, and iii) hooked-unbonded.

The study was conducted in two phases. Phase 1 involved laboratory testing of 15 small-scale specimens to evaluate TiAB anchorage behavior and bond strength, essential for calculating the development length. The results confirmed the AASHTO NSM Guide bond strength recommendations for hooked-bonded anchorage, provided bond strength guidelines for straight-bonded anchorage, and evaluated the feasibility of hooked-unbonded anchorage.

Phase 2 included full-scale testing of 16 girders representative of the Cullman bridge, assessing both positive- and negative-moment strengthening using the three anchorage methods. The results indicated the need for additional requirements for the hooked-bonded method for adequate strengthening, leading to proposed updates for the AASHTO TiAB NSM Guide. Design guidelines were also developed for the effective use of straight-bonded anchorage. Full-scale tests of the hooked-unbonded method indicated that this method might be suitable for temporary use but inadequate for permanent strengthening.

The study developed detailed construction and field implementation guidelines for strengthening the Cullman bridge. While fatigue evaluations are necessary for final recommendations, these findings offer critical insights for ALDOT in implementing NSM TiAB as a reliable method to strengthen RC bridges.

Table of Contents

LIST OF TABLES.....	xi
LIST OF FIGURES.....	xiii
CHAPTER 1 INTRODUCTION	1
1.1 Background	1
1.2 Research objectives and tasks	3
1.3 Organization of the report	4
CHAPTER 2 LITERATURE REVIEW	6
2.1 Background	6
2.2 Near Surface Mounted (NSM) FRP	6
2.3 Limitation of FRP.....	7
2.4 Titanium Alloy Bars (TiABs)	8
2.4.1 Durability of TiAB to Extreme Environmental Conditions.....	10
2.4.2 NSM TiAB Bond Strength	11
2.4.3 NSM TiAB for Flexural Strengthening	15
2.4.4 NSM TiAB Fatigue Testing.....	20
2.5 Existing Design Standards Related to Flexural Strengthening	22
2.5.1 ASTM B1009 (2020).....	22
2.5.2 ACI 440.2 (2023)	24
2.5.3 AASHTO NSM TiAB Guide	24
2.5.4 ACI 318-19: Effect of stress discontinuity for internal bar cutoff	27

2.6 Summary of Literature Review and Knowledge Gaps	28
CHAPTER 3 MATERIAL PROPERTIES	30
3.1 Background	30
3.2 Concrete.....	30
3.3 Reinforcing Steel.....	32
3.4 Titanium	35
3.5 Epoxy	36
CHAPTER 4 SPECIMEN AND TEST SETUP DETAILS FOR PHASE 1	37
4.1 Introduction	37
4.2 Test Matrix and Specimen Design	37
4.2.1 Hooked-bonded Specimens.....	39
4.2.2 Straight-bonded Specimens.....	40
4.2.3 Hooked-unbonded Specimens.....	41
4.3 Specimen Construction.....	41
4.4 Instrumentation	44
4.5 NSM Strengthening.....	46
4.5.1 Pre-cracking	46
4.5.2 Preparing the TiAB for Installation	48
4.5.3 Preparing the Specimens for NSM Strengthening	50
4.5.4 Strengthening the Specimens.....	53

4.6 Test Setup and Load Protocol	53
CHAPTER 5 TEST RESULTS, ANALYSIS, AND DISCUSSION FOR PHASE 1	55
5.1 Introduction	55
5.2 Experimental Behavior and Response.....	55
5.2.1 Experimental Results of Hooked-bonded Specimens.....	55
5.2.2 Experimental Results of Straight-bonded Specimens.....	69
5.2.3 Experimental Results of Hooked-unbonded Specimens.....	80
5.3 Summary of Tested Specimens	89
5.4 Results and Discussion of Hooked-bonded Specimens	93
5.5 Results and Discussion of Straight-bonded Specimens	95
5.6 Results and Discussion of Hooked-Unbonded Specimens	97
5.7 Summary and Conclusions of Phase 1 Testing	98
5.7.1 Hooked-bonded specimens	98
5.7.2 Straight-bonded specimens	99
5.7.3 Hooked-unbonded specimens	99
CHAPTER 6 SPECIMEN AND TEST SETUP DETAILS FOR PHASE 2	101
6.1 Introduction	101
6.2 Test Matrix	101
6.3 Design of Specimens	102
6.3.1 Positive-Moment Test.....	102
6.3.2 Negative-Moment Test.....	103

6.4 Construction of Specimens	104
6.5 Instrumentation	106
6.6 TiAB NSM Strengthening	108
6.6.1 Pre-cracking	108
6.6.2 Preparing the TiAB for Installation	111
6.6.3 Preparing the specimens for NSM strengthening	112
6.6.4 Strengthening the Specimens	115
6.7 Test Setup and Load Protocol	120
CHAPTER 7 TEST RESULTS, ANALYSIS, AND DISCUSSION FOR PHASE 2	123
7.1 Introduction	123
7.2 Hooked-bonded Specimens	123
7.2.1 Strengthening of Specimens	124
7.2.2 Test Results	124
7.2.3 Discussion of test results	126
7.3 Straight-bonded Specimens	132
7.3.1 Strengthening Specimens	133
7.3.2 Test Results	134
7.3.3 Discussion of test results	136
7.4 Hooked-Unbonded Specimens	141
7.4.1 Strengthening of Specimens	142
7.4.2 Test Results	142
7.4.3 Discussion of test results	143
7.5 Fatigue load test	145
7.5.1 Strengthening of Specimens	146
7.5.2 Discussion of Test Results	146

7.6 Summary and Conclusions of Phase 2 Testing	153
7.6.1 Hooked-bonded specimens	153
7.6.2 Straight -bonded specimens	156
7.6.3 Hooked-unbonded specimens	158
7.6.4 Fatigue Test Specimens	159
CHAPTER 8 PROPOSED STRENGTHENIG METHOD FOR THE CULLMAN BRIDGE	160
8.1 Introduction	160
8.2 Overall Bridge Design	160
8.3 Bridge Deficiencies	161
8.3.1 Preliminary Analytical Work	162
8.3.2 Detailed Structural Analysis and Proposed Strengthening Method	164
CHAPTER 9 SUMMARY, CONCLUSION, AND RECOMMENDATIONS	170
9.1 Phase 1 Work.....	170
9.1.1 Conclusion of Phase 1 Work.....	170
9.2 Phase 2 Work.....	171
9.2.1 Conclusion of Phase 2 Work.....	171
9.3 Recommendations	172
REFERENCES	173
APPENDIX	176

LIST OF TABLES

Table 2-1 Tensile test results of titanium with surface roughness (Barker, 2014)	10
Table 2-2 Results and Comparison of Fatigue and Freeze/Thaw Test (Vavra, 2016)	21
Table 2-3 Ti-6Al-4V Chemical Composition (Adapted from ASTM B1009, 2020)	23
Table 2-4 Pin Diameters and Overall Tail Lengths (AASHTO, 2020)	27
Table 2-5 Groove Dimension and Spacing Requirements (AASHTO, 2020)	27
Table 3-1 Concrete Mixture Proportions	30
Table 3-2 Reinforcing rebar tension test results of #4 bar	33
Table 3-3 Fully cured epoxy properties (HILTI, 2021)	36
Table 4-1 Hooked-Bonded Test Matrix with TiAB embedment length	39
Table 4-2 Straight-Bonded Test Matrix with TiAB embedment length	40
Table 4-3 Straight-Bonded Effective Bond Stresses using Nominal and Measured f_{yTi}	41
Table 4-4 Hooked-Unbonded Test Matrix with TiAB length	41
Table 4-5 Concrete Properties	43
Table 5-1 Calculated strength for all Specimens based on different models and assumptions. ...	56
Table 5-2 Summary of experimental results (Hooked-bonded)	57
Table 5-3 Bond stress at failure and observed behavior	65
Table 5-4 Summary of the experimental results (straight-bonded TiAB)	70
Table 5-5 Bond stress at failure and observed behavior	77
Table 5-6 Summary of the experimental results (hooked-unbonded TiAB)	81
Table 5-7 Summary of test results	89
Table 5-8 Crack width comparison	89
Table 5-9 Strength Comparison to Control	92
Table 5-10 Hooked-Bonded Load and Displacements	94
Table 5-11 Summary of Hooked-Bonded TiAB Results	95
Table 5-12 Straight-Bonded Loads and Displacements	96
Table 5-13 Straight-Bonded Yield Results	97

Table 5-14 Hooked-Unbonded Loads and Displacements	97
Table 6-1 Test Matrix for Member Level Test	102
Table 6-2 TiAB length for hooked-unbonded specimen.	119
Table 7-1 Test Matrix and Specimen Designation for Hooked-bonded Specimens.....	123
Table 7-2 Test Matrix and Specimen Designation for Straight-bonded Specimens.....	133
Table 7-3 Test Matrix and Specimen Designation for Hooked-unbonded Specimens.....	142
Table 7-4 Test Matrix and Specimen Designation for Fatigue Load Test	146
Table 7-5 Summary Results of Hooked-bonded Tested Specimens.....	154
Table 7-6 Service-Level Crack Width Comparisons (hooked-bonded specimens)	155
Table 7-7 Summary Results of Straight-bonded Tested Specimens.....	156
Table 7-8 Service-Level Crack Width Comparisons (straight-bonded specimens)	157
Table 7-9 Summary Results of Hooked-unbonded Tested Specimens.....	158
Table 8-1 Locations with Flexural Strength Deficiencies Based on EV3 Load Case (Positive Mom. in Yellow, Negative Mom. in Orange, Most Critical Locations Circled)	162

LIST OF FIGURES

Figure 1-1 Picture of the Cullman Bridge and the Posted Weight Limit Sign	2
Figure 1-2 NSM strengthening Method.....	3
Figure 2-1 Minimum groove dimension and spacing for NSM FRP applications (ACI 440.2, 2023)	7
Figure 2-2 Stress-strain curves of CFRP, BFRP, and hybrid composites with different numbers of basalt fiber layers (Subagia and Kim, 2014).....	8
Figure 2-3 Stress-strain curves of Stainless Steel and TiAB (#5) (Amneus, 2014).....	9
Figure 2-4 Stress-strain curves of TiAB (#5) with different surface treatments (Barker, 2014).....	10
Figure 2-5 Pull-out test setup for TiAB (Barker 2014).....	12
Figure 2-6 Modified ASTM A944-10 for Bond Length Test (Amneus 2014).....	13
Figure 2-7 Inverted Half Beam Bond Test Setup (Vavra, 2016).....	14
Figure 2-8 ASTM A615 #5 bar (left) and titanium bar (right, with red arrow) (Platt and Harries, 2018a).....	14
Figure 2-9 Schematic fixture for beam end test (Platt and Harries, 2018a)	15
Figure 2-10 Specimen with preformed diagonal crack and strengthened with TiAB (Amneus, 2014)	16
Figure 2-11 Mosier Bridge with Critical Section circled (Higgins, Amneus, Barker, 2015).....	16
Figure 2-12 Mosier Girder and Cross Section with NSM TiAB (Higgins, Amneus, & Barker, 2015)	17
Figure 2-13 Straight Bar (Top) and Hooked Bar (Bottom) NSM Retrofit (Unit - mm) (Platt, Harries, and McCabe, 2020)	18
Figure 2-14 Specimen with preformed diagonal crack and strengthened with TiAB (Barker, 2014)	19
Figure 2-15 Epoxy Anchors (left) and Prestressing Chuck Anchors (right) (Vavra, 2016)	20
Figure 2-16 S-N curve of fatigue test (Platt, 2018)	22
Figure 2-17 Free-Body Diagram for Section to Assess Flexural Tension Demand in Reinforcing (AASHTO, 2020).....	25
Figure 3-1 Compressive strength gain of concrete over time	31

Figure 3-2 Tensile test of #4 reinforcing steel	33
Figure 3-3 Stress-strain response of steel reinforcement tension test used in Phase 1 (#4 bar) ..	34
Figure 3-4 Stress-strain response of steel reinforcement tension test Phase 2 (#8 and #9 bar) ..	34
Figure 3-5 The two TiAB types evaluated in this project	35
Figure 3-6 Comparison of stress-strain plot for both TiABs (Type 1 and Type 2 - #4 TiAB)	36
Figure 4-1 Beam sections and detailing of reinforcement	38
Figure 4-2 Specimen naming configuration	39
Figure 4-3 Hooked-bonded Specimen R.HB.40	40
Figure 4-4 Rebar Cage (Left) and Lifting Hardware (Right).....	42
Figure 4-5 Concrete forms and sliding funnel	42
Figure 4-6 Concrete casting, vibrating and finishing.....	43
Figure 4-7 Cylinder preparation for strength evaluation	44
Figure 4-8 Beam after placement (Left) and moist curing (Right)	44
Figure 4-9 Instrumentation layout (Elevation View)	45
Figure 4-10 Instrumentation layout: strain gauges in TiAB (Top) and LPTs (Bottom)	46
Figure 4-11 Example Load vs Displacement (Top) and Load vs Displacement (Bottom)	47
Figure 4-12 Crack initiation during pre-cracking (Top) and typical crack pattern at end of pre-cracking (Bottom)	48
Figure 4-13 TiAB heating (heating) and bending (right)	49
Figure 4-14 TiAB with wedge and strain gauges	50
Figure 4-15 Custom 0.75 in. wide blade and groove in the beam	51
Figure 4-16 Track saw mounted on beam	51
Figure 4-17 Hammer drill used for hole (left), beveling (middle), and chiseling to refine bevel.....	52
Figure 4-18 Low-pressure water blasting with abrasives.....	52
Figure 4-19 First lift of epoxy application (left and middle), and Installed TiAB after final epoxy lift (right).....	53
Figure 4-20 Test setup for NSM TiAB bond test (material-level test)	54
Figure 5-1 Condition of Specimens at yielding of the tension steel reinforcement.	58

Figure 5-2 Condition of Specimens during detection of concrete crushing.	59
Figure 5-3 Condition of Specimens after peak load.....	60
Figure 5-4 Load-displacement response for specimens and AASHTO NSM Guide strength prediction	61
Figure 5-5 Moment-curvature response for strengthened specimens and section fiber analysis prediction	64
Figure 5-6 Strain profiles along the TiAB for HB60 at different force levels	65
Figure 5-7 Post-test specimen pictures of anchorage failure (HB 15 and HB20) or concrete-epoxy interface failure (HB30 and HB40).....	66
Figure 5-8 Displacement capacity ratio for each specimen: (a) measured from the yielding of the steel; (b) measured from the yielding of the TiAB	68
Figure 5-9 Measured load at concrete crushing and peak load for NSM TiAB strengthened specimens.....	69
Figure 5-10 Cracking condition of specimens at yielding of the tension reinforcement steel.....	71
Figure 5-11 Cracking condition of specimens at 0.005 steel strain	72
Figure 5-12 Cracking condition of specimens after peak load.....	73
Figure 5-13 Load-displacement response for specimens and AASHTO NSM TiAB Guide strength prediction	74
Figure 5-14 a) Inclined crack formation and b) concrete-epoxy interface delamination of SB40 ..	75
Figure 5-15 a) Epoxy rupture in SB60 and b) debonding and TiAB rupture in SB80	76
Figure 5-16 Horizontal crack formation in the shear span of SB96	76
Figure 5-17 Displacement capacity ratio for each specimen: (a) measured from the yielding of the steel; (b) measured from the yielding of the TiAB	78
Figure 5-18 Measured load at peak load for NSM TiAB strengthened specimens	80
Figure 5-19 Cracking condition of specimens at yielding of the tension reinforcement steel.....	82
Figure 5-20 Cracking condition of specimens at 0.005 steel strain	82
Figure 5-21 Cracking condition of specimens after peak load.....	83
Figure 5-22 Load-displacement response for specimens and AASHTO NSM TiAB Guide strength prediction	84

Figure 5-23 Inclined cracks formation near hook ends of HU10	85
Figure 5-24 Inclined cracks formation near hook ends of HU30	86
Figure 5-25 a) Widened and inclined cracks in the central region and b) widened cracks near hook ends of HU40	87
Figure 5-26 Cracking in the beam HU60 (a) at peak load (23.36 kips) (b) after failure	87
Figure 5-27 Displacement capacity ratio for each specimen: (a) measured from the yielding of the steel; (b) measured from the yielding of the TiAB	88
Figure 5-28 All Specimens Load versus Displacement Response	90
Figure 5-29 Peak Load versus TiAB Length for all Anchorage Methods	91
Figure 5-30 Deflections at Failure for Specimens that reached TiAB Yielding	91
Figure 5-31 Hooked-Bonded TiAB Load versus Displacement	94
Figure 5-32 Straight-Bonded Load versus Displacement	96
Figure 5-33 Hooked-Unbonded Load versus Displacement	98
Figure 6-1 Specimen dimensions and reinforcement details for the positive-moment test configuration	103
Figure 6-2 Specimen dimensions and reinforcement details for the negative-moment test configuration	104
Figure 6-3 Rebar cage formation (Left) and formwork ready for casting with lifting device (Right)	105
Figure 6-4 (a) Consolidation using vibrator, (b) air content test, and (c) slump test	105
Figure 6-5 Specimen after casting (Left) and Lifting of the specimen (Right)	106
Figure 6-6 Instrumentation layout	107
Figure 6-7 Strain gauge layout for fatigue test	107
Figure 6-8 Load versus reinforcing rebar tensile strain in mid-span (Top), and load versus mid-span displacement (Bottom)	109
Figure 6-9 Cracks in the specimen (Positive-moment test)	110
Figure 6-10 Cracks in the specimen (Negative-moment test)	111
Figure 6-11 TiAB hook and section through hook end epoxied to concrete	112

Figure 6-12 Cutting groove for positive bending test (Top) and for negative bending test (Bottom)	114
Figure 6-13 Low-pressure water blasting to clean the groove (Left) and Cleaned groove (Right)	115
Figure 6-14 Moment diagram for hooked-bonded and un-bonded strengthened specimens (positive-moment test)	116
Figure 6-15 Moment diagram for hooked-bonded (negative-moment test)	117
Figure 6-16 Moment diagram for straight-bonded strengthened specimens (positive- moment bending test)	118
Figure 6-17 Moment diagram for straight-bonded strengthened specimens (negative moment bending test)	119
Figure 6-18 Fatigue test load protocol	121
Figure 6-19 Load steps and cycles for a cyclic load test (Casadei et al., 2005)	122
Figure 7-1 Load-deflection behavior of the positive-moment specimens (hooked-bonded specimens)	125
Figure 7-2 Load-deflection behavior of the negative-moment specimens (hooked-bonded specimens)	126
Figure 7-3 Inclined shear cracks near hook ends and interface failure for Specimen TB.G.H.P.01	128
Figure 7-4 Concrete-epoxy interface failure for Specimen TB.G.H.P.02	129
Figure 7-5 Concrete-epoxy interface failure for Specimen TB.G.H.P.03	130
Figure 7-6 Crack formation at the hook and delamination for Specimen TB.G.H.N.01	131
Figure 7-7 Cracking in Specimen TB.G.H.N.02 at 86 kips	132
Figure 7-8 Load-deflection behavior of the positive-moment specimens (straight-bonded specimens)	135
Figure 7-9 Load-deflection behavior of the negative-moment specimens (straight-bonded specimens)	136
Figure 7-10 Concrete-epoxy interface failure for Specimen TB.G.S.P.01 at 100 kips	137
Figure 7-11 Concrete-epoxy interface failure for Specimen TB.G.S.P.02 at 108 kips load	138
Figure 7-12 Concrete-epoxy interface failure for Specimen TB.G.S.P.03 at 112 kips load	139

Figure 7-13 Wide crack formation at the end of TiAB and concrete-epoxy interface delamination for Specimen TB.G.S.N.01	140
Figure 7-14 Concrete cracking pattern for Specimen TB.G.S.N.02 at 4.44 inches of mid-span displacement.....	141
Figure 7-15 Load-deflection behavior of the positive-moment specimens (hooked-unbonded specimens).....	144
Figure 7-16 Anchorage failure of Specimen TB.U.H.P.01	144
Figure 7-17 Anchorage failure of Specimen TB.U.H.P.02	145
Figure 7-18 Strain variation in tensile steel under fatigue load cycles.....	148
Figure 7-19 Variation of mid-span displacement under fatigue load	148
Figure 7-20 Loading protocol for fatigue test	149
Figure 7-21 Mid-span displacement versus applied force response during step loads.....	150
Figure 7-22 Applied load versus mid-span displacement response of control specimen post-fatigue testing	151
Figure 7-23 Applied load versus mid-span displacement during step loads for the strengthened specimen.....	151
Figure 7-24 Tension test results of steel and TiAB (with and without fatigue load cycles).....	153
Figure 8-1 Plan View Showing Half of the Cullman Bridge (courtesy of ALDOT)	160
Figure 8-2 Cross Section at Mid of the Span (Section A-A in Figure 8.1) of the Cullman Bridge (figure not to scale)	161
Figure 8-3 Sectional view of the bridge girder with reinforcement detailing	162
Figure 8-4 Illustration of Portions with Insufficient Flexural Strength of the Cullman Bridge (Delineated with blue lines).....	163
Figure 8-5 Moment-curvature Comparison Plots using Titanium-Allow Reinforcement to Strengthen the Cullman Bridge	164
Figure 8-6 Positive- and Negative-moment Deficiencies for Span 1 (green circle)	165
Figure 8-7 Positive-moment deficiencies for Span 2 (green circle)	166
Figure 8-8 Strengthened and moment-deficient lengths in the Cullman Bridge	167
Figure 8-9 Groove size and location for #5 and #3 TiAB.....	167

Figure 8-10 Positive-moment strengthened capacity for span 1	168
Figure 8-11 Negative-moment strengthened capacity for span 1	168
Figure 8-12 Positive-moment strengthened capacity for span 2	169

Chapter 1

INTRODUCTION

1.1 BACKGROUND

According to a report by the American Road and Transportation Builders Association (ARTBA, 2023), approximately 16,102 bridges in Alabama need repair. Of these, 3.5 percent (about 559 bridges) are classified as structurally deficient, meaning that at least one key element is in poor or worse condition. The report also states that the most heavily traveled structurally deficient bridges in Alabama were built before 1981. Therefore, it is necessary to develop a cost-effective method to extend their service life which is also critically important for the state's economy. Enhancements to load-carrying capacity or fatigue performance may be necessary for older reinforced concrete bridges to extend their service life further or adapt to new load conditions. Common reasons for bridge strengthening include: (i) outdated design or detailing practices, (ii) repurposing of the bridge, (iii) increases in traffic volume, (iv) increases in the weight of vehicles crossing the bridge, and (v) repairs due to damage (e.g., fire or vehicle collision).

In recent years, the use of near-surface mounted (NSM) titanium alloys has emerged as a feasible option in the right applications, offering a simple and economical alternative to conventional flexural-strength methods (Higgins et al., 2017). Currently, carbon-fiber reinforced polymer (CFRP) is used in some instances for strengthening RC members; however, CFRP may not always provide satisfactory results due to material deficiencies and limitations in their implementation. These materials often suffer from a brittle stress-strain response. Additionally, research has demonstrated issues related to the premature failure of CFRP retrofits due to debonding and environmental exposure issue (Smith and Teng 2002).

On the other hand, titanium-alloy reinforcement offers several desirable properties as a strengthening material, including: (i) high yield strength in the 130-140 ksi range (Amneus, 2014), (ii) a steel-like stress-strain response with a well-defined yield point and significant ductility (Adkins & George, 2017), (iii) robust corrosion resistance and high durability under environmental exposure (Higgins et al. 2017), (iv) high deformability allowing for bar bending (Adkins & George, 2017), and (v) cost-effectiveness compared to other alternatives (e.g., CFRP) by reducing strengthening costs and enabling an expedited field repair schedule (Higgins et al. 2017).

Although the NSM TiAB method is an attractive alternative with promising research results, no studies have been conducted on its application to bridges in Alabama. There is a need to evaluate the implementation of this method in practical field applications, particularly for scenarios beyond the common hooked-bonded cases, such as unbonded-hooked or bonded-unhooked anchorage

methods. In this project, additional research was performed to assess whether the desired structural performance can be achieved, especially in situations where accessibility for field operations is limited, as is the case with some Alabama bridges. If successfully implemented, this research could introduce a new structural strengthening method for strength-deficient reinforced concrete bridges, which constitute the majority of ALDOT's bridge inventory (out of a total of 3,324 bridges, 2,726 are reinforced concrete and were built prior to 1980).

ALDOT Maintenance Bureau engineers have identified several flexural-deficient bridges with similar structural attributes, specifically three-span continuous reinforced concrete bridges built in the early 1960s. One of these bridges, located in Cullman (NBI ID: 7755), has been identified as a potential candidate for implementing this novel strengthening technique. The bridge is on US Route 278 (State Route 74), which is part of the main street (3rd St.) of downtown Cullman. As shown in Figure 1-1, this bridge is an overpass over the S&N Alabama subdivision railroad line of CSX Transportation. The bridge has been weight-restricted due to both positive and negative flexural strength deficiencies for several different truck types, as indicated by the posted weight limit sign in Figure 1-1.



Figure 1-1 Picture of the Cullman Bridge and the Posted Weight Limit Sign

Limited research studies have investigated the use of titanium alloy bars for strengthening RC bridge members. Dr. Chris Higgins' research group at Oregon State University has conducted most of these studies, reporting about 30% cost savings when titanium-alloy bars were used to strengthen RC bridges (Higgins et al., 2017). These studies have led to the development of an AASHTO design and construction guideline (AASHTO, 2020) and an ASTM standard for titanium alloy reinforcing for use in civil infrastructure applications (ASTM B1009-20, 2020). These

documents were developed based on a limited number of experiments and are focused primarily on using TiAB that is bonded to the concrete with epoxy in a groove with hooks at the ends as the flexural-strengthening method (Figure 1-2, more details in Appendix C, Figure 1). Other researchers have also investigated potential corrosion issues associated with the use of titanium bars in reinforced concrete members and have concluded that the response is favorable (Platt and Harries, 2018). The details of these documents and additional research studies are presented in the literature review chapter.

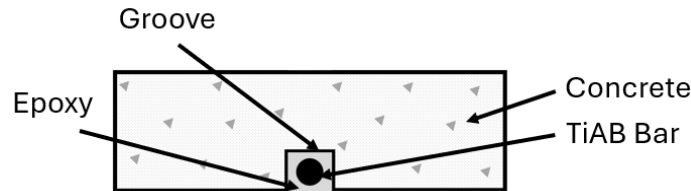


Figure 1-2 NSM strengthening Method

1.2 RESEARCH OBJECTIVES AND TASKS

The primary objectives of the research covered in this report are to determine the feasibility of using NSM TiAB for strengthening structurally deficient ALDOT reinforced concrete bridges, with a particular focus on a bridge in Cullman that exhibits both positive and negative flexural strength deficiencies,. These objectives were achieved through two research testing phases. Phase 1 testing involved laboratory experimental investigations to assess the bond strength of TiAB, while Phase 2 testing focused on laboratory experimental investigations of full-scale bridge girder specimens, representative of the Cullman bridge, addressing both positive and negative flexural strength deficiencies.

The research objectives were pursued by addressing several critical design and detailing parameters when strengthening with titanium-alloy reinforcement that have not been previously explored, such as:

- (i) Implementation of additional strengthening methodologies, including straight bars (without hooked ends) for bonded applications and hooked reinforcement bars for unbonded applications.
- (ii) Conducting full-scale testing for positive- and negative-flexural strengthening schemes while considering practical field implementation.
- (iii) Investigating the applicability of strength design requirements in existing AASHTO design guidelines.
- (iv) Developing analytical models to accurately predict measured behavior.

(v) Developing detailed construction and implementation guidelines specific to strengthening the Cullman Bridge.

This research also aims to address any limitations or deficiencies of the recently developed AASHTO (2020) and provide ALDOT with the necessary information to implement titanium-alloy reinforcement as a strengthening method for reinforced concrete bridges with similar flexural strength deficiencies as those observed in the Cullman Bridge.

The main objectives of Phase 1 testing are listed below:

- Experimentally evaluate the effective bond strength required to achieve yielding (development length) of NSM TiABs with hooked bonded anchorage, and compare it to the assumed 1.0 ksi average bond strength provided in the current AASHTO design guidelines.
- Experimentally evaluate the development length of NSM TiABs with straight bonded (unhooked) anchorage, and develop effective bond strength recommendations for design.
- Investigate the experimental behavior of hooked-unbonded NSM TiABs and evaluate their feasibility for member strengthening.

The main objectives of Phase 2 testing are listed below:

- Experimentally evaluate the flexural behavior of reinforced concrete bridge girders strengthened with hooked-bonded TiABs with optimal bonded TiAB lengths.
- Experimentally evaluate the flexural behavior of reinforced concrete bridge girders strengthened with straight-bonded (unhooked) TiABs with optimal bonded TiAB lengths.
- Experimentally evaluate the flexural behavior of reinforced concrete bridge girders strengthened with hooked-unbonded TiABs, and provide design recommendations for effective implementation.
- Experimentally evaluate the fatigue performance of reinforced concrete bridge girders strengthened using the most effective NSM TiAB method.

1.3 ORGANIZATION OF THE REPORT

- Chapter 2: Presents a literature review of the NSM TiAB strengthening method and a detailed overview of existing standards or guidelines.
- Chapter 3: Discusses the mechanical properties of the materials used in both research phases.
- Chapters 4 and 5: Document the specimen design and construction, as well as the test results, analysis, and discussion for Phase 1.
- Chapters 6 and 7: Document the specimen design and construction, as well as the test results, analysis, and discussion for Phase 2.

- Chapter 8: Discusses the existing conditions and deficiencies of the Cullman Bridge and proposes strengthening options.
- Chapter 9: Provides a summary and conclusion of the findings of this project.

Chapter 2

LITERATURE REVIEW

2.1 BACKGROUND

This chapter provides an overview of research conducted on near-surface mounted (NSM) strengthening techniques with an emphasis on past TiAB research. The NSM method encompasses various applications, including: (i) strengthening for flexural deficiencies, (ii) strengthening for shear deficiencies, (iii) strengthening for fatigue, and (iv) bond strength testing. These strengthening techniques involve the use of NSM fiber-reinforced polymer (NSM-FRP) and NSM titanium alloy bars (NSM-TiABs). The following sections will discuss the details of bond strength tests, specific strengthening methods, and relevant design methods and standards for these strengthening approaches.

2.2 NEAR SURFACE MOUNTED (NSM) FRP

Several strengthening techniques have become popular for enhancing the service life of reinforced concrete (RC) structures. Klaiber, et al. (1987) identified some of the most popular strengthening techniques for existing highway bridges. These techniques include: (a) the addition of steel cover plates, (b) the addition of external shear reinforcement, (c) jacketing, (d) post-tensioning, (e) adding or replacing members, and (f) developing additional bridge continuity. They also highlighted the use of composite fiber materials, such as fiberglass, Kevlar, carbon or graphite, as the most widely adopted materials in the construction industry.

Chajes et al. (2019) provided a comprehensive overview of the advantages and disadvantages of various bridge-strengthening methods, emphasizing externally bonded FRP (fiber-reinforced polymer) as the most prevalent composite material applications for bridge strengthening and rehabilitation. Externally bonded FRP systems were developed as an alternative to traditional external strengthening techniques, such as steel plate bonding and steel or concrete column jacketing (ACI 440, 2023). However, a significant drawback of externally bonded FRP is its susceptibility to peeling or delamination from the structure due to high shear stresses at the end locations (Chajes et al., 2019). This issue can be mitigated by using mechanical anchorage at the ends of the externally bonded FRP (Chajes, et al., 2019).

An alternative method to reduce the risk of debonding is the near-surface mounting (NSM) technique (Lorenzis and Nanni, 2001; Hassan and Rizkalla, 2003; Daly, Shave, & Denton, 2006; Yost, et al. 2007; Razaqpur, Shedid, and Petrina, 2011). This method involves cutting grooves on the surface of the concrete, applying epoxy, placing the FRP material, and filling the remaining

groove spaces with epoxy. ACI 440.2 (2023) prescribes the size of the grooves and spacing, as illustrated in Figure 2-1. With fiber-reinforced polymers, the NSM method can be implemented with strips, plates, and circular or rectangular rods, ensuring that three sides of the FRP are bonded to the concrete member, which minimizes the chance of debonding and enhances force transfer (Chajes et al., 2019). Additionally, this method provides greater protection to the retrofit from environmental impacts. Near-surface mounting offers a substantial increase in moment capacity with relatively little repair material required (Chajes et al., 2019).

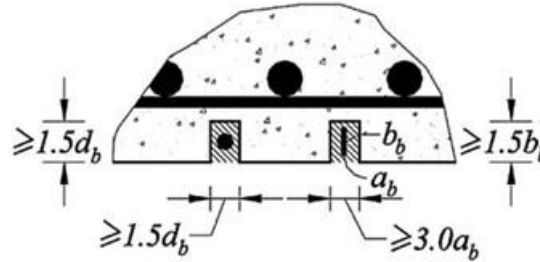


Figure 2-1 Minimum groove dimension and spacing for NSM FRP applications (ACI 440.2, 2023)

2.3 LIMITATION OF FRP

Despite the advantages of having a high modulus, high strength, good creep and corrosion resistance, and low unit weight, CFRP sheets or plates have some notable limitations: (i) they exhibit brittle behavior and thus lack a yield plateau (Subagia and Kim, 2014; Higgins et al., 2017), and (ii) they cannot be bent to form hooks for improved anchorage performance (Subagia and Kim, 2014; Higgins et al., 2017). Subagia and Kim (2014) conducted tensile strength tests on CFRP, basalt fiber-reinforced polymer (BFRP), and hybrid composites—where basalt fabric layers were placed between carbon fabric layers (designated as B1–B5)—using a universal testing machine following ASTM D 638 standards (D20 Committee, 2022). The results, shown in Figure 2-2, indicated that the tensile strength and tensile strain of CFRP were 687 MPa (99.6 ksi) and 1.062%, respectively. The tensile strain increased with the number of basalt fabric layers (B1–B5, where the number beside B indicates the number of basalt layers). This means that the composite with the highest number of basalt layers, B5, exhibited the highest tensile strain. On the other hand, BFRP displayed lower tensile strength (402 MPa or 58 ksi) but greater tensile strain (2.2%). In all cases, it is evident that FRP composites demonstrate brittle behavior.

Another type of FRP is Glass-FRP (GFRP), which is commonly chosen due to its lower cost compared to Carbon-FRP (CFRP) (Barris et al., 2020). GFRP is a composite material with a generally lower modulus of elasticity than steel, which means that GFRP-RC elements typically experience more deflection and larger crack widths (Barris et al., 2013). Additionally, the linear

stress-strain relationship of GFRP materials can lead to brittle and sudden failure of the member (Nanni, 2003; Vavra, 2016). Some studies suggest that NSM FRP flexural-strengthened RC beams are still prone to failure due to FRP end debonding, despite the relatively strong bond between NSM FRP and concrete (Teng et al., 2006; Sharaky, Torres, and Sallam, 2015; Zhang et al., 2022).

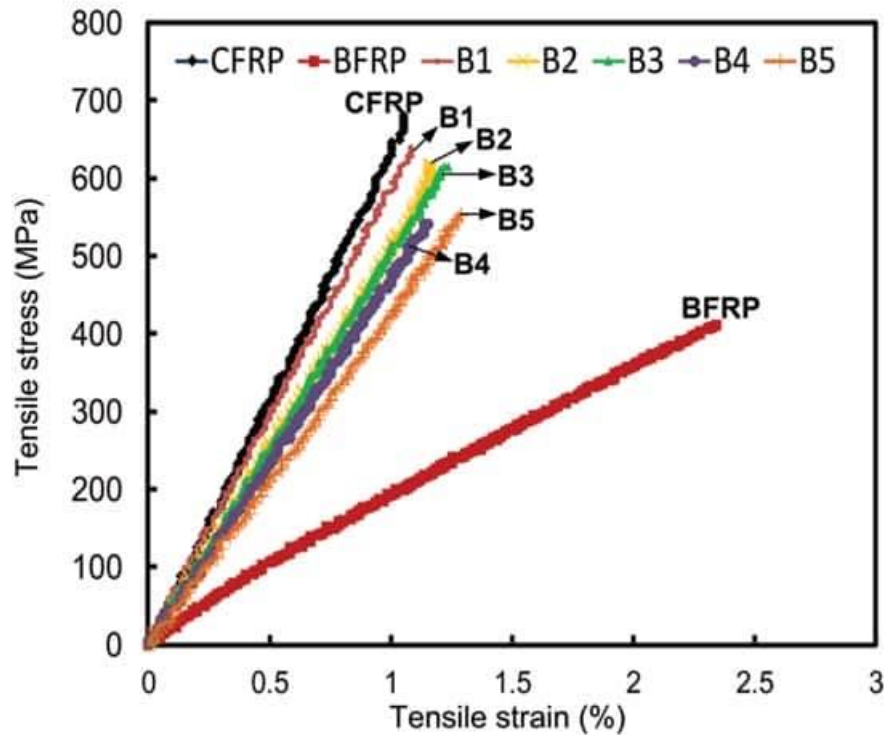


Figure 2-2 Stress-strain curves of CFRP, BFRP, and hybrid composites with different numbers of basalt fiber layers (Subagia and Kim, 2014)

2.4 TITANIUM ALLOY BARS (TiABs)

Strengthening using NSM titanium-alloy bars (TiABs) has emerged as a feasible option, offering a simple and economical solution compared to conventional alternatives (Higgins et al., 2017). The use of TiABs for bridge strengthening applications using the NSM method has several favorable characteristics, including: (a) high yield strength (Adkins and George, 2017; Bomberger, Cambourelis, and Hutchinson, 1954; Platt and Harries, 2019), (b) a well-defined yield point (Adkins and George, 2017; AASHTO, 2020; Amneus, 2014), (c) sufficient ductility (Adkins and George, 2017), (d) good environmental durability (Higgins et al., 2017; Adkins and George, 2017; Vavra, 2016), (e) lower overall cost compared to other alternatives (Higgins et al., 2017; Adkins and George, 2017), (f) high shear strength and resistance to mechanical damage (Adkins and George, 2017), (g) high maximum service temperature and thermal expansion compatibility with concrete (Adkins and George, 2017), and (h) the ability to form mechanical anchorage (Adkins and George,

2017; Vavra, 2016; Amneus, 2014; Higgins, Amneus, and Barker, 2015). The titanium alloy most commonly used for strengthening purposes is Ti-6Al-4V, which consists of 5.5–6.75% aluminum and 3.5–4.5% vanadium (ASTM B1009-20, 2020).

Amneus (2014) conducted a study comparing NSM strengthening using TiABs and stainless steel. The stress-strain responses of both stainless steel and TiABs, tested according to ASTM E8 (2011), are shown in Figure 2-3. The results indicate that TiABs exhibit higher strength than stainless steel and similar ductility while also displaying a well-defined yield plateau.

Tensile tests were performed on TiABs with five different surface treatments to assess the impact of surface treatment on material properties (Barker, 2014). The measured stress-strain responses are shown in Figure 2-4. The titanium alloy bars generally exhibited a well-defined yield plateau, though a 0.2% offset was used to determine yield values. The measured yield stress and ultimate stress values for each titanium surface treatment are summarized in Table 2-1. The results show that material properties were similar across all five surface treatments, leading to the conclusion that surface treatments do not have a significant impact on the material properties of TiABs.

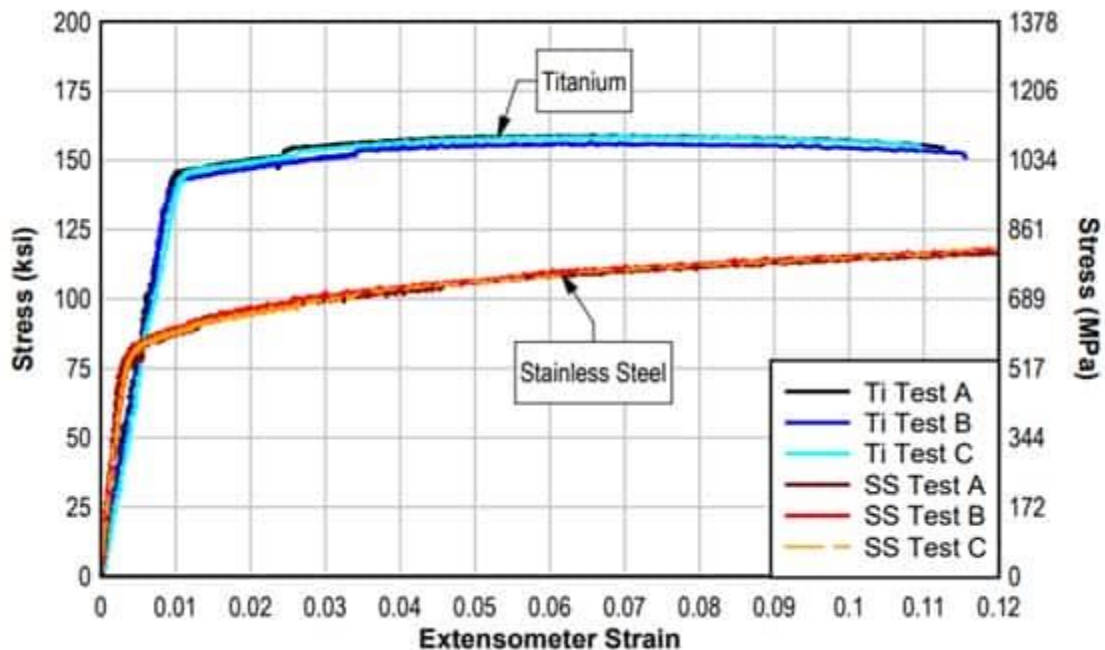


Figure 2-3 Stress-strain curves of Stainless Steel and TiAB (#5) (Amneus, 2014)

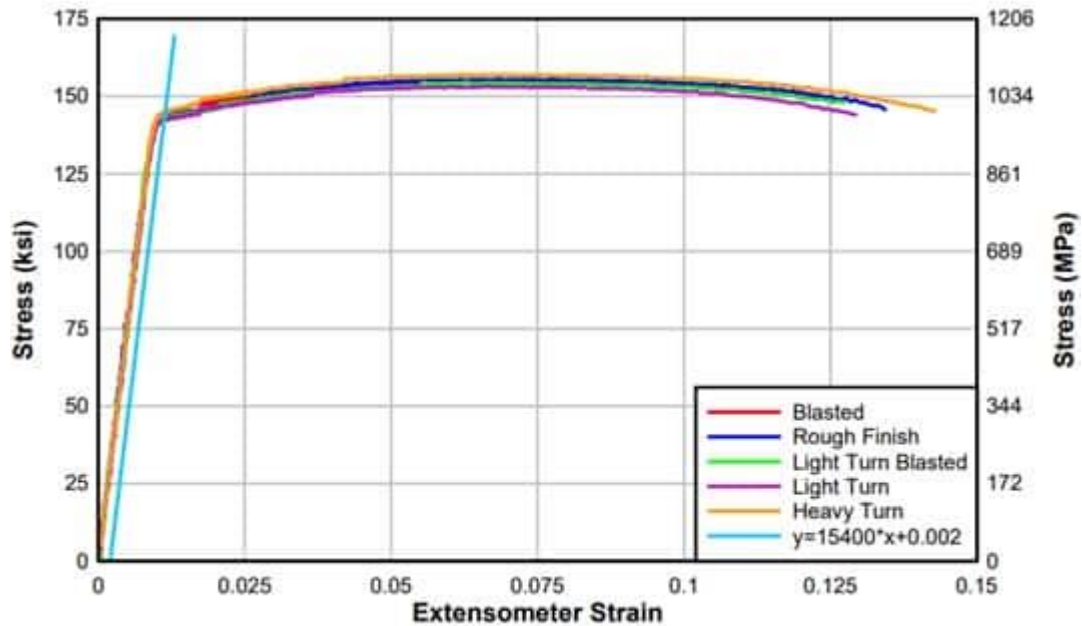


Figure 2-4 Stress-strain curves of TiAB (#5) with different surface treatments (Barker, 2014)

Table 2-1 Tensile test results of titanium with surface roughness (Barker, 2014)

Surface Treatment	0.2% offset yield stress, ksi	Ultimate stress, ksi
Blasted	144.5	155.5
Rough Finish	143.8	155.6
Blasted Light Turn	143.2	154.7
Light Turn	142.4	153.4
Heavy Turn	144.6	157.2

2.4.1 DURABILITY OF TiAB TO EXTREME ENVIRONMENTAL CONDITIONS

Titanium has proven to be highly resistant to marine environments and galvanic corrosion (Bomberger, Cambourelis, and Hutchinson, 1954), making it an excellent material for NSM applications, particularly because NSM placements are close to the surface of the concrete where reinforcement is more vulnerable to environmental conditions. The NSM method also positions titanium near existing reinforcing steel. If galvanic corrosion were to occur, the condition of the

existing reinforcing steel could be compromised, potentially reducing the overall strength of the RC structure compared to its state before the introduction of titanium.

Bomberger, Cambourelis, and Hutchinson (1954) conducted a study on the corrosion properties of titanium in marine environments. They tested commercially pure cold-rolled titanium strips, measuring 6 inches by 1.5 inches by 1/32 to 1/16 inch thick, to evaluate titanium's corrosion properties. The titanium was exposed to three different conditions: (i) sea air at distances of 80 and 800 feet from the ocean for five years, (ii) the industrial atmosphere of Bridgeport, Connecticut for four years and eleven months, and (iii) seawater flowing at 3 feet per second for up to 4.5 years. The study concluded that the titanium remained completely unaffected by these harsh marine conditions.

Platt and Harries (2018) focused on the galvanic corrosion potential of NSM titanium reinforcing bars in their study. They investigated the effects of coupling Ti-6Al-4V titanium with ASTM A615 black steel in NSM applications. The study involved testing 62 concrete prisms, each measuring 152 x 152 x 152 mm (6 x 6 x 6 in.) and containing a single embedded No.4 ASTM A615 (grade 60) black steel bar. A 0.5-inch diameter titanium bar, CFRP, or 2205 stainless steel NSM bar was embedded along one side of each prism into NSM slots. The specimens were conditioned in a cyclic temperature and humidity environment for two years, during which half-cell potential and macro-couple current were continuously monitored. The study concluded that the presence of Ti-6Al-4V titanium reinforcing bars in proximity to or in electrical contact with A615 steel reinforcing bars did not result in any change in the rate or nature of corrosion.

2.4.2 NSM TiAB BOND STRENGTH

Some researchers have conducted bond strength tests to evaluate the NSM TiAB method. However, the lack of understanding regarding the development length of NSM TiAB necessitated the Phase 1 research performed in this project. This section reviews bond characterization studies of NSM TiAB, primarily performed at Oregon State University (OSU).

Barker (2014) conducted pull-out tests to evaluate the bond strength of several titanium-epoxy interfaces. Five TiABs with different surface deformations/treatments—surface blasted, rough finish, light turn, light turn blasted, and heavy turn—were tested. The pull-out test involved drilling a 0.75-inch diameter hole 5 inches deep into concrete blocks, filling the hole halfway with epoxy, and setting the bar perpendicular to the concrete, allowing it to cure for seven days. A picture of the pull-out test setup is shown in Figure 2-5. The results indicated that the light and heavy turn deformations performed best in the pull-out test. Bars with blasted and rough surface deformations failed at bond stresses between 1.0 and 1.5 ksi, while the light-turned, heavy-turned, and light-

turned blasted bars failed at bond stresses above 4.5 ksi, based on the average bond stress calculations using Equation 2.1.

$$\mu_{avg} = \frac{\Delta f_s d_b}{4\Delta l} \quad 2.1$$

Where, μ_{avg} = average bond stress, Δf_s = change in stress, d_b = diameter of the bar, Δl = change in length over which the stress was measured. Average bond stresses were also calculated around the locations of the NSM material hooks in the full-scale beams. The average and peak bond stresses at failure ranged from 0.236-0.399 ksi and 0.566-0.861 ksi, respectively. Based on the pull-out and tensile tests, Barker (2014) used the heavy-turn surface deformation on TiABs for NSM retrofitting purposes.



Figure 2-5 Pull-out test setup for TiAB (Barker 2014)

Amneus (2014) also conducted a bond length study of NSM TiAB, using an adapted version of ASTM A944-10. Six 9x12x24-inch blocks were constructed with a 15/16" square groove cut into the top. Three of the specimens had 4-inch No. 5 TiABs, and three had 12-inch No. 5 TiABs, which were epoxied into the groove and pulled using a 110-kip actuator. The test configuration is depicted in Figure 2-6. The 4-inch embedment length specimens failed along the concrete-epoxy interface, with an average bond stress calculated as 2.091 ksi using Equation 2.1. The maximum stress achieved in the NSM titanium bar was around 60 ksi, less than half the yield stress of the TiAB. The bars with a 12-inch embedment length failed at similar loads as the 4-inch tests, and the TiABs did not achieve yield. The average bond stress achieved before failure in the 12-inch bars was 0.802 ksi. The NSM titanium alloy bars in the full-scale T-specimens had a bond stress of 0.296 ksi over the bonded length until the cutoff bar termination. The specimen design was the limiting factor in the test, preventing definitive conclusions regarding bond performance. However, the tests revealed that the development length for a No. 5 TiAB was greater than 4 inches.

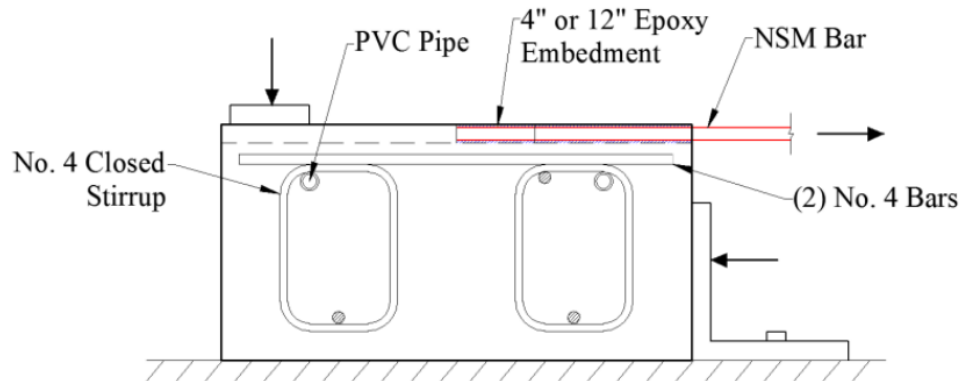


Figure 2-6 Modified ASTM A944-10 for Bond Length Test (Amneus 2014)

Vavra (2016) conducted bond stress tests for NSM TiAB using an inverted half-beam test, as depicted in Figure 2-7. This test was designed to exhibit slender flexural response under four-point loading with a 12-inch long constant moment region. The inverted half beams were 56 inches long, 14 inches tall, and 6 inches wide. A total of 12 straight-bonded bars were tested with three tests for 4, 6, 8, and 12-inch embedment lengths using 5/8" diameter (#5) spiral surface TiABs. Three hooked-bonded bars were also tested with embedment lengths of 4, 6, and 8 inches and 90° hooks. The straight-bonded bars experienced an average bond stress before failure of 0.5 to 0.6 ksi, calculated using Equation 2.1. The failure mechanism for the straight-bonded bars in this study was a wedge-shaped concrete failure plane extending from the embedded end of the bar to the free face of the beam. The hooked bars exhibited similar results, failing in bar pull-out and crushing of the concrete at the hook-bearing area. The TiABs achieved an average bar stress of 80 ksi (all three performed similarly), corresponding to about 62% of the nominal yield strength (130 ksi). The bond stress was not measured in the hooked specimens. Vavra (2016) concluded that "given the lower confinement for the pullout specimens in comparison to hooks in the girder specimen T.45.Ld3(10).Ti.FT/FTG, crushing of the concrete in the hook bend exhibited by the three pullout specimens might not represent the failure mode of the NSM TiABs with the given hook detail." The study also examined the possible effect of epoxy type on the resulting active bond length by comparing the results of two specimens strengthened with different epoxies (E1 and E2). Each epoxy type exhibited a different failure mechanism: E1 specimens developed a failure wedge in the concrete, whereas E2 specimens slipped and failed at the bar-epoxy interface. The study concluded that the chosen epoxy type significantly impacted the bond strength.

Platt and Harries (2018a) conducted tests to investigate the bond characteristics of titanium reinforcing bars using ASTM D7913 pull-out tests, ASTM A944 beam-end tests, and concrete prism tension tests. The TiAB used in this study (red arrow in Figure 2-8) had surface deformations similar to A615 steel, as shown in Figure 2-8. Five specimens of TiABs with three different heat treatments

and a control series of ASTM A615 bars were tested with three concrete batches. The specimens were cast into 203 mm concrete cubes for the pull-out test. All bars had a bonded region of 5 bar diameters (5db), equal to 80 mm (3.15 in.) long. The average calculated bond stress at slip initiation ranged from 0.19 to 0.42 ksi. The beam-end test specimens, shown in Figure 2-9, had #5 reinforcing bars of titanium, A615 steel, and GFRP cast into 216 x 603 x 622 mm concrete forms. Bars had bonded regions of 0.5 l_d , 1.0 l_d , or 1.5 l_d . The calculated average bond stress at 0.004 mm slip (initial slip) ranged from 0.33 to 0.75 ksi. The bond performance of the titanium bars was influenced by the rib ratio, which was similar to that of A615 bars.

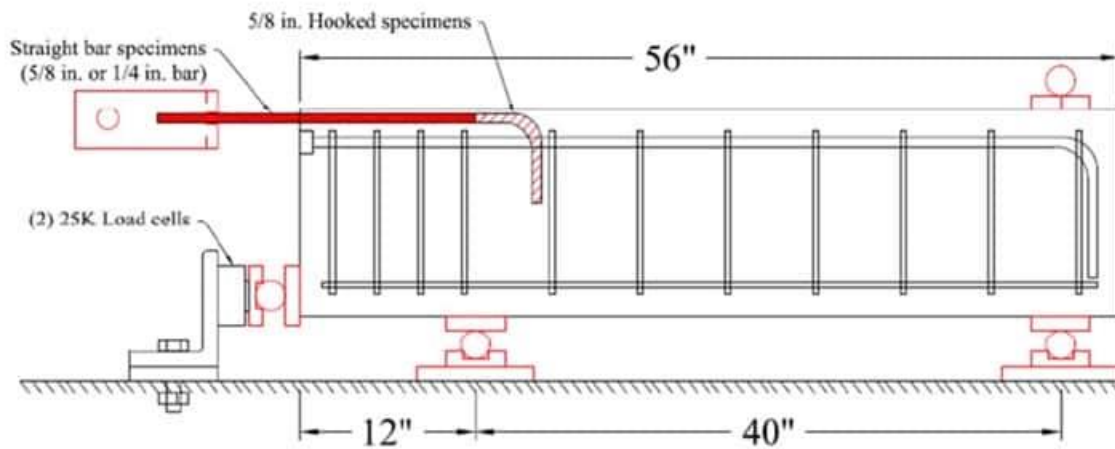


Figure 2-7 Inverted Half Beam Bond Test Setup (Vavra, 2016)



a) deep deformations on Ti bar from Heat 1



b) shallow deformations on Ti bar (rotated 120° from Figure a)

Figure 2-8 ASTM A615 #5 bar (left) and titanium bar (right, with red arrow) (Platt and Harries, 2018a)

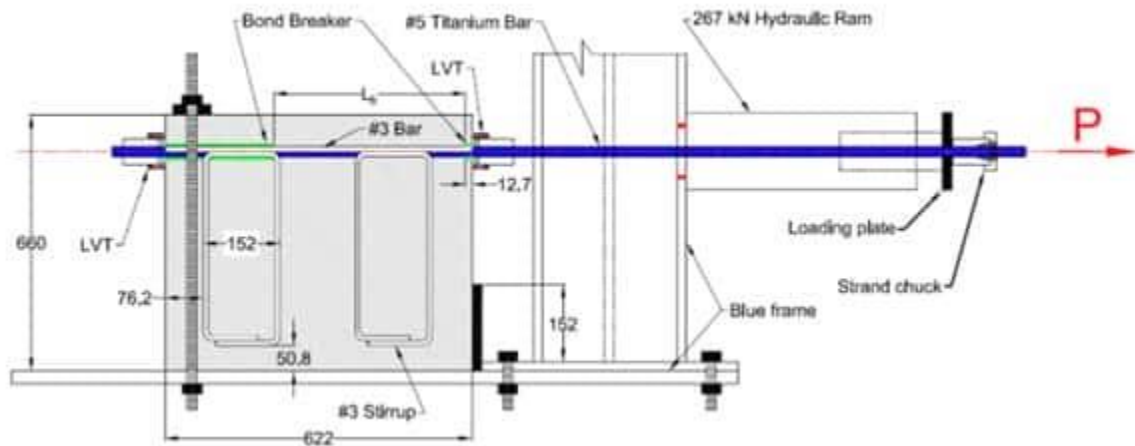


Figure 2-9 Schematic fixture for beam end test (Platt and Harries, 2018a)

2.4.3 NSM TiAB FOR FLEXURAL STRENGTHENING

This section of the literature review focuses on large-scale tests that have utilized NSM TiAB as a method for bridge strengthening.

2.4.3.1 Positive-Moment Flexural Strengthening Tests (Bonded TiAB)

Amneus (2014) reported on three specimens that were strengthened to increase the positive moment capacity of beams with flexural deficiencies. Two of the specimens were reinforced with hooked TiAB, while the third was reinforced with hooked stainless steel. Inverted versions of these beams were also tested to study negative-moment flexural strengthening, as discussed in the next section (Barker, 2014). Figure 2-10 shows one of the beams retrofitted for positive-moment strengthening. The test results demonstrated that NSM metallurgic bar reinforcement led to an increase in load capacity of at least 31% and a midspan displacement increase of at least 85% compared to the baseline unstrengthened specimen. The failures shifted from non-ductile diagonal-tension failures to ductile flexural failures. The use of TiAB bars required approximately half the amount of material compared to stainless steel to achieve the same capacity and ductility, making titanium-alloy bars a more suitable option for NSM strengthening.

A case study conducted by OSU researchers successfully repaired a bridge in Mosier, Oregon, using NSM TiAB (Higgins, Amneus, & Barker, 2015). The 4-span bridge (shown in Figure 2-11), built in the 1950s and crossing I-84 in Mosier, Oregon, was identified during a biennial bridge inspection in 2013 to have wide cracks (0.03 inches). The Oregon Department of Transportation conducted tests using sweeping trucks over the span with the prescribed rating. It was determined that the demand at the critical section was 219 k-ft, which was 46 k-ft above the AASHTO-designed moment capacity. To experimentally test the repair application before implementing it on the Mosier

[illegible]

A photograph of a multi-span concrete highway bridge. The bridge has a series of metal guardrails along its length. On the right side, a red circle is drawn around a section of the guardrail, indicating a specific area of interest. The bridge spans a road that leads into a valley with hills in the background.

In a study conducted at the University of Pittsburgh (UP) by Platt, Harries, and McCabe (2020), the flexural capacity of four intentionally damaged slabs was tested using NSM TiAB strengthening. The objective was to evaluate whether the reduced flexural capacity (reduced by about 40%) could be restored using NSM TiAB. The four specimens were tested and compared to an undamaged control slab. Two slabs were reinforced with 72-inch straight TiABs—one with a single No. 5 TiAB and the other with four No. 5 TiABs. The other two slabs were reinforced with

16-inch hooked TiABs, with one slab using a single No. 5 TiAB and the other using four No. 5 TiABs. Figure 2-13 shows the elevation view of the retrofits and the cuts made to the longitudinal rebar to damage the slab. The slabs were then tested under three-point loading until failure and compared to the original slab. The researchers concluded that NSM TiAB could restore the slab's load capacity. The reinforced slabs exceeded the capacity of the original slab, with the exception of the singular hooked TiAB slab. However, all tested specimens exhibited premature failure with reduced ductility. The hooked (stapled) specimens were deemed to have a bond length shorter than necessary and exhibited premature failure at the hooks. The specimens with straight TiABs exhibited ductility similar to the undamaged control Slab A but showed significant slip at ultimate capacity.

Lastly, Vavra (2016) conducted a flexural test on a reinforced concrete beam subjected to combined fatigue and freeze-thaw cycles. After completing the fatigue and freeze-thaw cycles, the beams were moved to the strong floor, where they were tested to failure in four-point bending. The results of the test are detailed in Section 2.4.4.

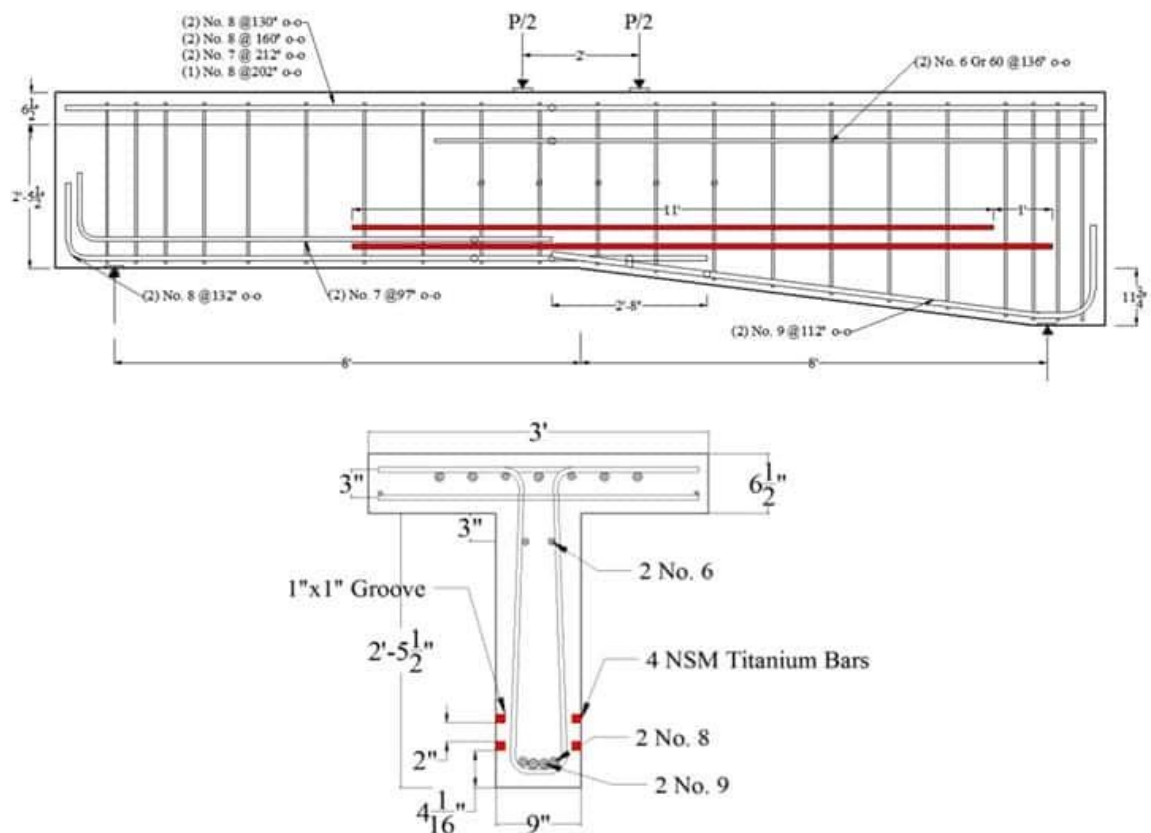


Figure 2-12 Mosier Girder and Cross Section with NSM TiAB (Higgins, Amneus, & Barker, 2015)

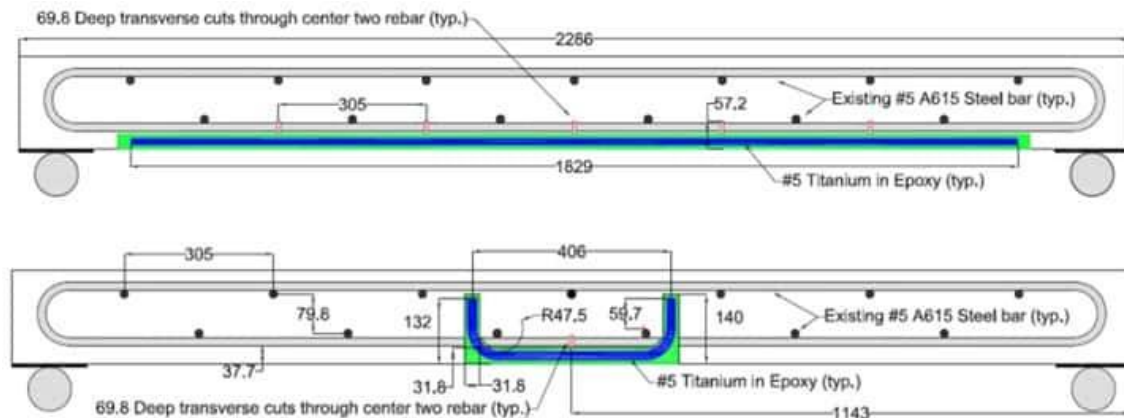


Figure 2-13 Straight Bar (Top) and Hooked Bar (Bottom) NSM Retrofit (Unit - mm) (Platt, Harries, and McCabe, 2020)

2.4.3.2 Negative-Moment Flexural Strengthening Tests (Bonded TiAB)

Barker (2014) conducted inverted beam tests to demonstrate the effectiveness of the NSM TiAB method for negative-moment flexural strengthening. Four large-scale girders were designed with deficient anchorages and tested to investigate near-surface mounted retrofitting techniques. Three of the specimens were constructed with a 45° preformed diagonal crack (Figure 2-14), which precluded aggregate interlock, and cutoff flexural reinforcing steel bars that terminated one-third of the minimum development length (as per ACI 318) past the crack. The fourth specimen did not have a preformed crack and had the main flexural steel terminated at midspan.

The specimens strengthened with NSM TiABs achieved 17% to 39% greater capacities compared to the control specimens (Barker, 2014). They also demonstrated higher overall deformation capacity and more distributed cracking before failure than the control specimen. While the stainless-steel specimen achieved similar capacity increases as the titanium alloy, it required twice the reinforcing area. The fourth specimen, designed to evaluate the performance of NSM titanium alloy bars in pure flexure, showed that the titanium alloy bars contributed significantly to the flexural strength of the specimen. Additionally, the use of titanium alloy bars enabled high ductility at failure, with distributed cracking along the retrofitted length.

Analytical methods were also employed to verify the performance of the strengthened specimens. For the three inverted beams tested with preformed cracks, the initial diagonal crack crossing the developing section of the longitudinal cutoff bars did not control the failure location of the specimen. Instead, the reinforcement detailing and load patterns determined the final failure crack.

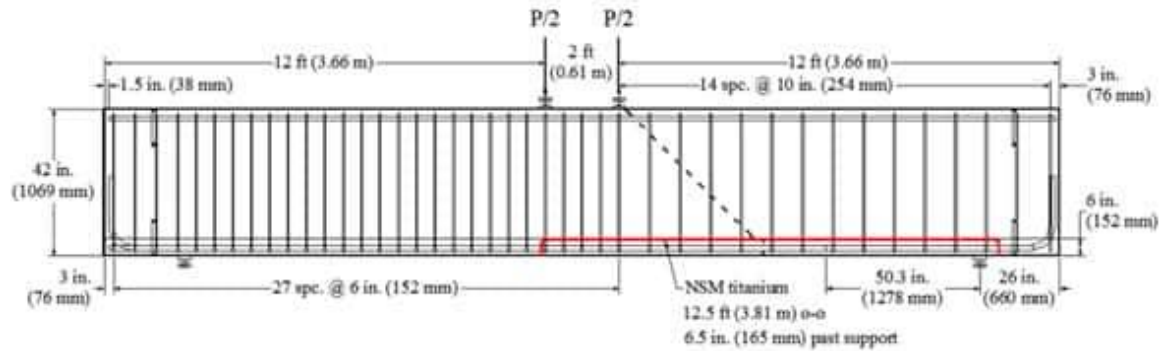


Figure 2-14 Specimen with preformed diagonal crack and strengthened with TiAB (Barker, 2014)

2.4.3.3 Positive-Moment Flexural Strengthening Tests with Unbonded TiAB

Vavra (2016) conducted tests on NSM TiAB using a hooked-unbonded mounting method, also referred to as the stapling method. This method was tested using two identical beams, each containing three #11 longitudinal bars as positive-moment reinforcement in the stem of the beam. Two of the three #11 bars were cut in the middle of the beam to create a weak region. The study examined two different methods of hooked-unbonded bars: epoxy anchors and anchors using prestressing chucks. Both methods involved prestressing the bars using deflectors, as shown in Figure 2-15. The prestressing force in each bar ranged from 1.6 kips to 5.9 kips.

Response2000 (R2K) was used to determine the theoretical final load and displacement of an unstrengthened beam (control beam). Both specimens failed due to concrete crushing in the compression zone and exhibited ductile responses. The R2K specimen theoretically failed at 106.1 kips with 5.12 inches of displacement, the epoxy-anchored specimen failed at 171.3 kips with 4.76 inches of displacement, and the prestressing chuck-anchored specimen failed at 216.3 kips with 5.06 inches of displacement. The specimen strengthened with epoxied anchors exhibited slipping, which resulted in softening and an overall lower capacity compared to the beam with prestressing chuck anchorage. In contrast, the prestressing chucks prevented the pull-out of the hooks, allowing the specimen to reach a higher applied load. Local concrete crushing at the hook bend was observed in both specimens.

The results demonstrated that flexural capacity can be increased using unbonded TiAB. However, the researchers recommended that this method be considered a short-term fix rather than a long-term solution due to the system's low stiffness.



Figure 2-15 Epoxy Anchors (left) and Prestressing Chuck Anchors (right) (Vavra, 2016)

2.4.4 NSM TiAB FATIGUE TESTING

Vavra (2016) also studied the performance of NSM TiAB during simultaneous freeze-thaw and fatigue cycles. The specimens tested for fatigue and freeze-thaw were the T.45.Ld3(10) beams previously tested by Amneus (2014) at OSU, shown in Figure 2-10 (referred to as T.45.Ld3(10) NSM.FTG/FT in this study). This beam was subjected to 1,600,000 cycles to simulate a 50-year service life using Miner's rule, assuming concrete cracking caused by an 80,000 lb semi-truck. The cycles were performed at a rate of 1.2 Hz, designed to bring the stress in the internal reinforcement to 20 ksi, which is considered the upper limit for maintaining long life in internal steel reinforcement according to ACI Committee 215 (1992). The mean load for these cycles was 80 kips in a 3-point loading test setup. Three pseudo-static cycles were run from 3 kips to 210 kips at the beginning of the test and every 250,000 cycles. These tests were conducted in an environmental chamber that simultaneously underwent freeze-thaw cycles. The temperature range was from 45°F to 21°F, with a 30-minute ramp time between the two extremes and a 60-minute hold time at those temperatures. This was equivalent to 8 cycles per day, totaling 200 cycles over 25 days. During the thaw portion of the cycle, the beam was wetted daily to ensure sufficient moisture penetration into the cracks before freezing. After the fatigue and freeze-thaw cycles were completed, the beam was moved to the strong floor, where it was failed monotonically in four-point bending. The fatigue test results are summarized in Table 2-2, showing that the fatigue and freeze-thaw cycles had negligible impacts on the beam's performance with the NSM TiAB. The applied load was 1% greater, and the final displacement was 1% less than an identical beam that did not undergo fatigue and freeze-thaw cycles. Compared to the beam without NSM TiAB, the capacity was increased by 32%, and the midspan displacement increased by 83%. Vavra's study demonstrated that NSM TiAB is negligibly affected by fatigue and freeze-thaw cycles.

A material-level axial-loaded bar fatigue study on 18 TiAB deformed reinforcing bars was conducted using ASTM E466-15 at the University of Pittsburgh (Platt, 2018). As-received deformed bars were inserted into hydraulic wedge grips and clamped with a gauge length of 51 mm ($3.2d_b =$

2 in.). Specimens were loaded to the midpoint of their fatigue range, which is the average of maximum and minimum loads, and cycling began at a rate of 20 Hz. Testing continued until failure or until reaching 2 million cycles, which is typically used in experimental work for structural engineering. All stresses were reported based on the nominal cross-sectional area of a #5 TiAB (0.31 in²). Two target stress ranges were used: 24 ksi and 48 ksi (165 MPa and 331 MPa, respectively). In all cases except one, the minimum stress was approximately 69 MPa (10 ksi). Six specimens of #5 ASTM A615 steel were tested as control specimens, following standard practice for reinforcing bar fatigue testing. For deformed steel reinforcing bars tested in air, the following general equation is most often used to describe fatigue behavior (Helgason and Hanson, 1974): $\log N = 6.969 - 0.0055S$ (where S is expressed in MPa units; $\log N = 6.969 - 0.0383S$ in ksi units). The results for the ASTM A615 specimens tested by Platt (2018) correlated well with this relationship, thereby validating the test setup and procedure. The fatigue test results of the TiAB are also shown in Figure 2-16, where despite their higher yield strength, the titanium bars exhibited poorer fatigue performance than expected and poorer than that observed for steel bars.

Table 2-2 Results and Comparison of Fatigue and Freeze/Thaw Test (Vavra, 2016)

Specimen	Applied Load, kip	V_{APP}, ksi	V_{DL}, ksi	V_{EXP}, ksi	Midspan Disp., in.	Failure Crack Angle (deg)
T.45.Ld3(10)	299.5	149.8	3.1	152.9	1.14	33
T.45.Ld3(10).Ti	392.9	196.5	3.5	200.0	2.11	33
T.45.Ld3(10).Ti.FT/FTG	395.5	197.8	3.6	201.4	2.09	33

Knudtsen (2016) conducted experimental research to evaluate the effectiveness of the NSM TiAB strengthening method. Seven full-scale T-shaped reinforced concrete girders were built and strengthened with NSM titanium alloy bars to enhance shear strength. Two of these girders, strengthened with two different types of epoxy, were subjected to simultaneously applied high-cycle fatigue and freeze-thaw cycles before being tested to failure. The specimens were subjected to 2.4 million cycles at a frequency of 2 Hz, with a stress range of 13.8 ksi in the internal stirrups. The test was conducted under a three-point loading configuration, with an applied load range of 13.2–24.3% for one specimen and 16.1–29.6% for the other.

Higgins et al. (2007) performed high-cycle fatigue tests to assess potential deterioration in shear capacity. They designed and constructed nine full-size specimens (T-shaped and inverted T-shaped) reflecting the details and materials of 1950s vintage conventionally reinforced concrete bridge girders. Previously conducted field test data related to diagonal cracks and stirrup stress range were used for the laboratory specimens. Pre-cracking was done to produce the desired

diagonal crack widths in the specimens. The specimens were then moved to a separate test frame to apply high-cycle fatigue loading. The test rate was 2.4 Hz with a stress range of 13.8 ksi. The specimens were subjected to 2 million cycles under a point loading configuration with a force control loading protocol.

Chou et al. (2023) tested eleven reinforced concrete beams strengthened with prestressed NSM CFRP under fatigue loading to determine the influence of bond length, fatigue load amplitude, CFRP prestressing force, and end-plate anchorage. The specimens were tested using a four-point bending flexural test. The fatigue test was conducted at a rate of 2 Hz, with a stress range of 13.6 and 15.7 ksi for two different groups of specimens.

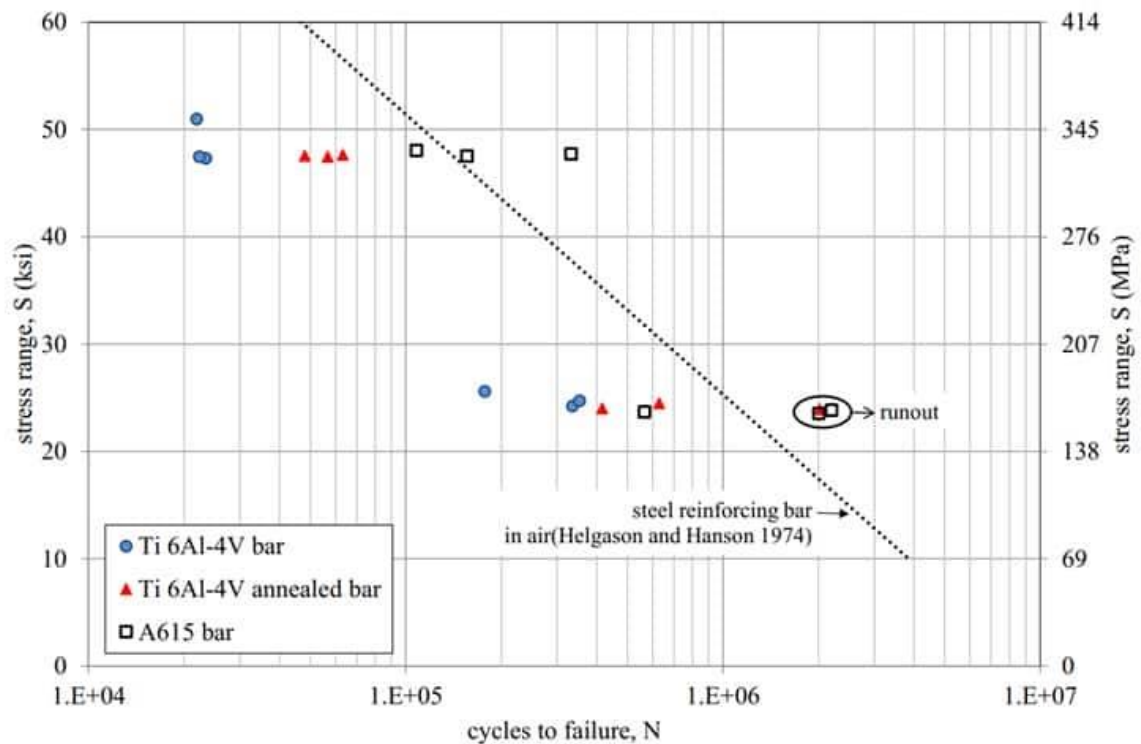


Figure 2-16 S-N curve of fatigue test (Platt, 2018)

2.5 EXISTING DESIGN STANDARDS RELATED TO FLEXURAL STRENGTHENING

This section reviews the AASHTO and ACI guidelines regarding bond strength and development length used for NSM FRP and TiAB, as well as design guidelines for strengthening purposes.

2.5.1 ASTM B1009 (2020)

This ASTM standard covers TiAB with surface deformations and 90-degree anchorage hooks for use in NSM applications for flexural and shear strengthening of concrete beams. The titanium alloy

bars specified for these applications are Grade 5 (Ti-6Al-4V). This alloy is primarily composed of titanium, with small amounts of other elements such as aluminum and vanadium, as shown in the chemical composition provided in Table 2.3.

Two material grades are recognized for the titanium alloy bars in (ASTM B1009-20, 2020): Class 120 and Class 130. The minimum yield stress corresponds to 120 ksi and 130 ksi for each class, respectively. The specification requires that: (i) all bars should achieve a minimum elongation of 10% at failure; (ii) the surface deformations must be sufficient to prevent failure along the TiAB-bonding material interface; and (iii) the deformations must be capable of producing an average bond stress of 1.0 ksi (6.9 MPa) over the bar surface area based on nominal circumference along the straight length of the titanium alloy bar in a direct pullout configuration, enabling the development of the nominal yield stress. Dimensions, weight, permissible variations, bending requirements (e.g., without cracking on the outside radius of the bend portion with the note that bars may be heated up to 1200°F prior to bending), bonding material (e.g., epoxy, polyester, vinyl ester resins, and cementitious grouts), and other restrictions are also included and listed in ASTM B1009 (2020).

Table 2-3 Ti-6Al-4V Chemical Composition (Adapted from ASTM B1009, 2020)

Composition By Weight Percentage	
Grade	5
Carbon Max	0.08
Oxygen Max	0.2
Nitrogen Max	0.05
Hydrogen Max	0.015
Iron Max	0.4
Aluminum	5.500-6.750
Vanadium	3.500-4.500
Other Elements Max Each	0.1
Other Elements Max Total	0.4
Titanium	Balance

2.5.2 ACI 440.2 (2023)

ACI 440.2 (2023) is a guide for the design and construction of FRP systems to strengthen concrete structures, covering two systems: (i) FRP laminate sheets and (ii) FRP rods and strips for NSM applications. FRP laminates consist of dry unidirectional or multidirectional fiber sheets, partially cured unidirectional or multidirectional fiber sheets, and various composite shapes manufactured off-site. Surface-embedded NSM FRP systems consist of circular or rectangular bars or plates. For NSM FRP applications, ACI 440.2 (2023) provides information on required groove spacing, depth, effective strain, and required development length. The details of the groove dimensions are shown in Figure 2-1.

For single-layer straight FRP laminates, it is necessary to terminate the FRP at a distance equal to or greater than the development length (l_{df}) beyond the point where the resisted moments become lower than the cracking moment (M_{cr}). In the case of multiple-ply straight laminates, the outermost ply should be terminated no less than the development length (l_{df}) past the point where the resisted moments fall below the cracking moment (M_{cr}). Each successive ply should be terminated no less than an additional 6 inches beyond the previous ply. However, there are no specific guidelines for the termination of the hooked-bonded NSM FRP rod. The formula provided to calculate the development length (l_{db}) for straight bonded NSM FRP circular rod is (ACI 440.2, 2023):

$$l_{db} = \frac{d_b}{4 \tau_b} f_{fd} \quad 2.2$$

where, τ_b is the average bond strength, recommended as 1 ksi; f_{fd} is the debonding stress of FRP based on the debonding strain of the section.

For rectangular bars, the development length is (ACI 440.2, 2023):

$$l_{db} = \frac{a_b b_b}{2 (a_b + b_b) \tau_b} f_{fd} \quad 2.3$$

where, a_b is the smallest bar dimension and b_b is the largest bar dimension.

2.5.3 AASHTO NSM TiAB GUIDE

The American Association of State Highway and Transportation Officials (AASHTO) published a design and construction guide for strengthening existing reinforced concrete structures for flexure and shear with titanium alloy bars (TiABs) using the near-surface mounted (NSM) construction method, referred to as the “AASHTO NSM TiAB Guide.” The recommended approach for flexural

strengthening involves incorporating a standard 90-degree hook at both ends of the TiAB to ensure secure anchorage. Additionally, a minimum compressive strength of 3000 psi for the concrete is required. Conformity to the ASTM B1009 specification (Section 2.5.1) is required for the titanium alloy bars used in the strengthening process. The average bond stress of the TiABs along the bond length is 1 ksi, consistent with that used for NSM-FRP in ACI 440.2 (2023). The flexural tension reinforcement, comprising both steel and TiABs, must be capable of resisting the flexural tension requirements in the presence of shear cracks. Therefore, in calculating the embedment length of TiAB, the development length is added to $d_v \cot \theta$, as conceptually described in Figure 2-17.

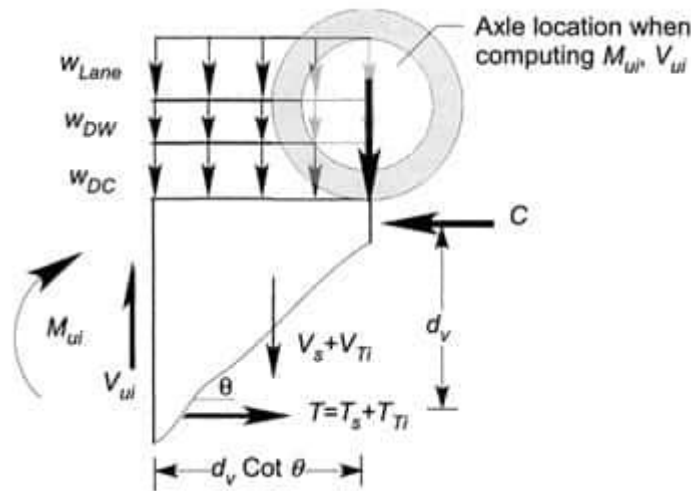


Figure 2-17 Free-Body Diagram for Section to Assess Flexural Tension Demand in Reinforcing (AASHTO, 2020)

The nominal moment capacity of the strengthened section is determined from the equilibrium conditions of the cross-section, idealizing the concrete stress as an equivalent rectangular stress block (Whitney stress block). For the case in which the steel and the TiABs are yielding, the nominal moment capacity can be computed with the equation provided in the AASHTO NSM TiAB Guide (Equation 2.4). The equation is based on the following assumptions: negligible tensile strength of concrete; neglecting the compression reinforcement steel; plane sections remain plane; strain compatibility between concrete, steel, and TiABs; idealized elastic-plastic behavior of steel and TiABs; and no relative slip between concrete steel or TiABs. Furthermore, the strain in the concrete at the ultimate stage is considered to be 0.003.

$$M_n = A_s f_y \left(d_s - \frac{\beta_1 c}{2} \right) + A_{Ti} \alpha_E f_{yTi}^* \left(d_{Ti} - \frac{\beta_1 c}{2} \right) \quad 2.4$$

Where, A_s and A_{Ti} represent the area of flexural tension steel and TiABs respectively, the minimum specified yield stress of steel and TiABs is denoted by f_y and f_{yTi} respectively, d_s and d_{Ti}

refer to the distance from the extreme compression fiber to the centroid of the flexural steel and TiABs respectively, $\beta_1 c$ is the height of the equivalent rectangular stress block, α_E refers to the environmental sensitivity factor for the bonding material with a value of 0.85 for routine exposure environments and 1.0 for insensitive exposure environments.

In accordance with the equation mentioned in the AASHTO NSM guide, the development length of TiABs with hooks can be computed as,

$$l_{dTi} = \frac{D_{Ti}}{4} \frac{\alpha_E f_{yTi}^*}{\bar{\mu}_u} \quad 2.5$$

In this equation, D_{Ti} is the diameter of TiAB and $\bar{\mu}_u$ represents the average bond strength of TiAB, which is assumed to be 1 ksi. When used in the calculations, the environmental sensitivity factor, α_E , is considered to be 1.0 in this research due to the controlled laboratory conditions. The AASHTO NSM TiAB Guide requires that any bonding material used in conjunction with TiAB to achieve an average bond stress of 1.0 ksi along the bond length in a pullout test configuration to achieve the nominal yield stress of the TiAB.

The bond strength ($\bar{\mu}_u$) provided in this guideline is for the hooked-bonded TiABs. The expected average bond strength of 1.0 ksi is referenced from ACI 440.2 (2023) which is based on the bond test of straight-bonded CFRP strips ACI 440.2 (2023). The straight-bonded bars without hooked ends are not considered in the AASHTO NSM TiAB Guide and therefore do not have a recommended average bond strength for design.

For the design of NSM TiAB, the AASHTO NSM TiAB Guide provides a flexural resistance factor (ϕ_b). This resistance factor depends on the strain distribution in the section when the extreme concrete compression fiber reaches the assumed crushing strain of 0.003. When the strain in the extreme layer of tension steel is 0.005, then the design is classified as ductile and flexural resistance factor (ϕ_b) is taken as 0.9. The ϕ_b is 0.75 when the strain in the extreme fiber is below 0.002. A linear interpolation is used whenever the strain in the steel is in-between 0.002 and 0.005, as presented in Equation 2.6 (AASHTO, 2020).

$$\begin{aligned} \text{if } 0.005 > \varepsilon_t \geq 0.002 \text{ then } \phi_b &= 0.75 + \frac{0.15 (\varepsilon_t - 0.002)}{0.003} \\ \text{if } \varepsilon_t < 0.002 \text{ then } \phi_b &= 0.75 \end{aligned} \quad 2.6$$

The AASHTO NSM TiAB Guide provides hook diameters and overall tail lengths recommendations based on the size of TiAB as provided in Table 2-4, which were also used for the hooked-bonded and hooked-unbonded specimens in this project.

Table 2-4 Pin Diameters and Overall Tail Lengths (AASHTO, 2020)

Bar Designation	Pin Diameter, in.	Overall Tail Length, in.
#2	2	5
#3	2.75	5
#4	3	6
#5	3.75	6
#6	4.5	12

The AASHTO NSM TiAB Guide also provides groove dimensions and spacing requirements for NSM TiABs. Similar to the requirements in ACI 440.2 (2023), the groove width and depth are required to be 1.5 times the diameter of TiAB. The minimum clear spacing between the grooves must be twice the groove depth and the minimum edge distance must be four times the depth of the groove. The required groove dimensions and spacing according to bar specifications are provided in Table 2-5.

Table 2-5 Groove Dimension and Spacing Requirements (AASHTO, 2020)

Bar Designation	Square Groove Dimension, in.	Minimum Clear Spacing, in.	Minimum Edge Spacing, in.
#2	3/8	3/4	1 & 1/2
#3	9/16	1 & 1/8	2 & 1/4
#4	3/4	1 & 1/2	3
#5	15/16	1 & 7/8	3 & 3/4
#6	1 & 1/8	2 & 1/4	4 & 1/2

2.5.4 ACI 318-19: EFFECT OF STRESS DISCONTINUITY FOR INTERNAL BAR CUTOFF

In reinforced concrete beams, the reinforcement is placed near the tensile face of the beams to contribute to the tension resisting component of the internal resisting couple. To minimize bar lengths for economy and constructability, some of the bars can be terminated where their contribution is no longer necessary. It has been documented that the location of bar cutoff is influenced by four major factors (Wight and MacGregor, 2012):

- (i) bars are cutoff at points where they are no longer needed to withstand flexural tensile forces. The location of the bar cutoff is also a function of flexural tension forces resulting from bending moments and the effect of shear on the tensile forces;
- (ii) bars must be adequately extended on each side of every section to effectively develop the force in that bar at that section;
- (iii) stress concentration can occur if the tension bars are cutoff in a region with moderately high shear, potentially leading to the formation of an inclined crack at the bar cutoff point; and
- (iv) construction requirements outlined in the applicable code and guideline dictate certain practices that need to be followed for achieving good construction standards.

At the location where the bars are cut off, the stress in the cutoff bars reduces to zero, while the stress in the remaining bars increases. Consequently, a severe stress discontinuity occurs near the vicinity of the bar cutoff in the region of flexural tension, which ultimately leads to a reduction in shear capacity (Wight and MacGregor, 2012). As a result, an inclined crack initiates at or near the end of the bar cutoff. ACI 318 (2019) Section 9.7.3.5 prohibits bar cutoff unless one of the following is satisfied:

- (i) the factored shear force at the location of bar cutoff is not greater than the factored shear resistance, including the shear resistance provided by shear reinforcement;
- (ii) additional stirrups are provided along each terminated bar over a distance from the termination point not less than three-fourths the effective depth of the member;
- (iii) for No. 11 and smaller bars, the continuing reinforcement provides double the moment capacity compared to the moment demand at the location of bar cutoff, while ensuring that the factored shear force does not exceed three-fourths of the factored shear resistance.

Although ACI codes pertain to building designs, the same requirements used to be in the main specification of the AASHTO Standard Specifications for Highway Bridges (AASHTO, 2002) and have been moved to the commentary section of AASHTO LRFD Bridge Design Specifications (2020b). This is mentioned in Commentary Section C5.10.8.1.2a of the AASHTO LRFD Bridge Design Specifications (AASHTO, 2020b).

2.6 SUMMARY OF LITERATURE REVIEW AND KNOWLEDGE GAPS

This chapter summarized the past research and available design guidelines for implementing the NSM-FRP and NSM-TiAB strengthening techniques. Although extensive research has been conducted on NSM-FRP, due to the significant behavioral differences between FRP and TiAB, the applicability of the developed design guidance for NSM-FRP to TiAB is limited. The research conducted on NSM-TiAB is scarce when compared to FRP, with most studies performed by only

two institutions. Consequently, the design documents have been developed from limited studies and the bridge strengthening community could benefit from additional experimental research on this innovative technology.

In past TiAB development length studies, researchers have reported average bond strength values for use in design; however, none of the tests demonstrated the yielding of the tested TiAB. The load conditions for most of the conducted bond strength tests did not simulate the stress state that TiABs would be subjected to during a flexural strengthening application. Therefore, the literature review revealed a knowledge gap that requires more experimental work that involves development length tests that achieve TiAB yielding with an experimental setup simulating the conditions similar to tension reinforcement in a flexural member.

Past studies focused primarily on hooked-bonded NSM TiAB applications and limited results are available for straight-bonded NSM TiAB and hooked-unbonded TiAB applications. Due to the lack of experimental studies on anchorage types (hooked-bonded, straight-bonded, and hooked-unbonded) other than hooked-bonded TiAB, design guidance does not exist for implementing alternative anchorage options (straight-bonded and hooked-unbonded) in full-scale applications.

On the member-level studies of NSM-TiAB applications, the literature review revealed that very few large-scale tests were conducted, with the focus mainly on hooked-bonded TiAB applications. The full-scale tests using hooked-bonded TiAB replicated a critical load case for a bridge requiring strengthening, but the tested members were shear-deficient elements with TiAB bonded lengths maximized to the specimen support. Therefore, large-scale tests that utilize flexural strengthening with minimum bonded lengths to achieve desirable member performance are needed. The tests that utilized alternative anchoring methods (straight-bonded or hooked-unbonded) generally produced unsatisfactory results in small-scale tests that were not representative of full-scale bridge girders. Therefore, additional studies are needed to evaluate the performance and design methods of alternative anchorage methods to consider their potential use for bridge girder flexural strengthening.

Chapter 3

MATERIAL PROPERTIES

3.1 BACKGROUND

This chapter covers the materials used in both the material-level (Phase 1) and member-level (Phase 2) experimental work. The following sections describe the mechanical properties of these materials, which were measured either through testing according to the applicable ASTM standards or obtained from the manufacturer's documentation. The measured values were subsequently used in theoretical analyses and calculations.

3.2 CONCRETE

The concrete used in both the material-level and member-level beam tests was designed to simulate the concrete strength associated with bridges constructed in the 1960s. This choice was made because many bridges in Alabama, including the Cullman Bridge, were built during that period and are potential candidates for strengthening using this method. The Cullman Bridge was built in the early 1960s and had a reported long-term compressive strength of 4500 psi, as confirmed by concrete core strength testing as summarized in the Appendix A. Concrete proportions were prepared to achieve this strength as shown in Table 3-1.

Table 3-1 Concrete Mixture Proportions

Items	Value
Water Content	284 lbs/yd ³
Cement Content	535 lbs/yd ³
Fly Ash Content	0 lbs/yd ³
Coarse Aggregate (SSD)	1792 lbs/yd ³
Fine Aggregate (SSD)	1260 lbs/yd ³
Total Air Content	4%
Air-entraining Admixture	4.3 lbs/yd ³
Water-to-Cement ratio	0.53

For Phase 1, twelve 6"x12" cylinders were cast to evaluate the concrete strength as it matured. The cylinders were moist-cured for seven days, then demolded and air-cured to represent the conditions surrounding the beam specimens cured in laboratory conditions. Three cylinders were tested at 7, 28, 91, and 287 days in accordance with ASTM C39 (2021) to determine the concrete compressive strength. The 28-day compressive strength was 4380 psi, which was close to the target strength. Equation 3.1 from ACI 209R-92 (1992) was used to create a predictive curve for the concrete strength gain versus concrete age. This strength development plot and the points used to generate the curve are shown in Figure 3-1.

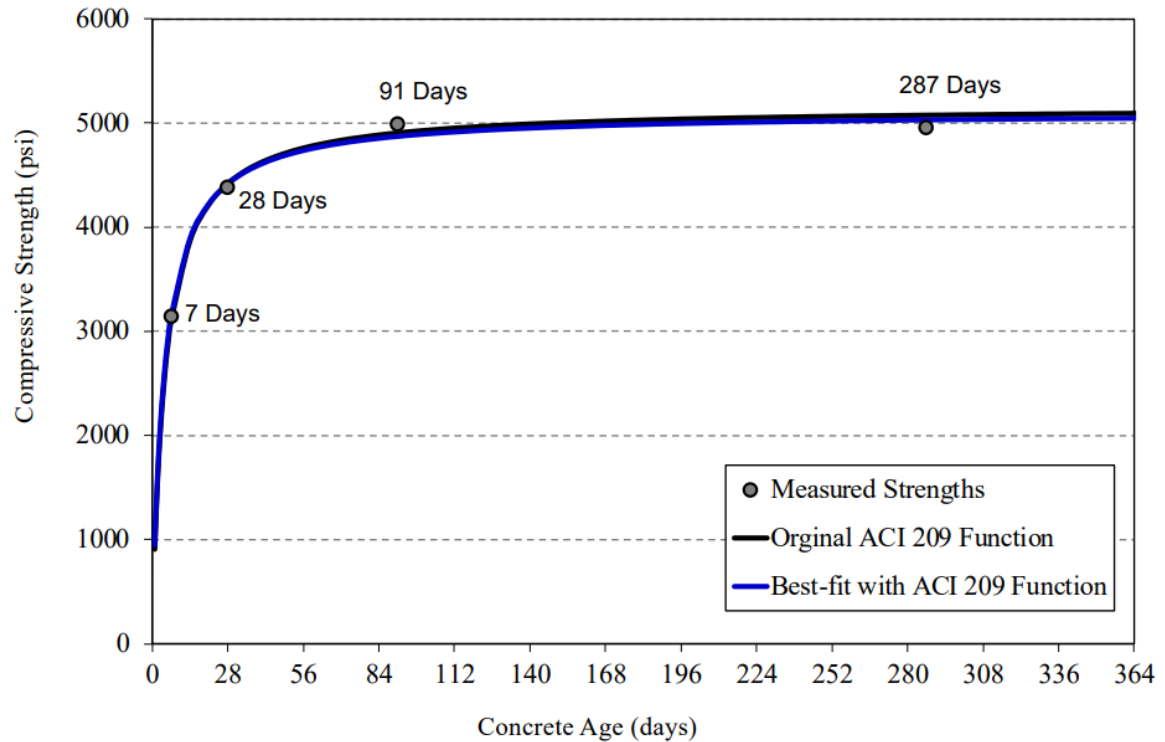


Figure 3-1 Compressive strength gain of concrete over time

$$(f'_c)_t = \frac{t}{\frac{\alpha}{\beta} + t} (f'_c)_u \quad 3.1$$

where, $(f'_c)_t$ is the concrete strength as a function of time, t is time in terms of days, α/β is the age of concrete in days at which one-half of the ultimate (in time) compressive strength of concrete is reached, and $(f'_c)_u$ is the ultimate concrete compressive strength.

In the member-level tests (Phase 2), the same concrete proportions were used as in Phase 1. The bridge girders were designed based on the concrete compressive strength obtained from cylinder cores taken from the Cullman Bridge. The concrete used to cast the specimens was

supplied by a local ready-mix company, and four batches were required to cast a total of sixteen large-scale beams. From each batch, three cylindrical concrete specimens (6 inches in diameter and 12 inches in height) were tested at 28 days to determine the compressive strength, following the guidelines of ASTM C39 (2021). At the time of testing, the average compressive strength of the concrete was slightly above 4320 psi, which is representative of the Cullman Bridge.

3.3 REINFORCING STEEL

ASTM A615 (2023) Grade 60 reinforcing rebars were used in both the material-level (Phase 1) and member-level (Phase 2) tests. Uniaxial tension tests were conducted to determine the yield strength, tensile strength, and elongation at fracture of the steel rebars. The tests conformed to ASTM E8 (2011) and were performed using a universal testing machine (UTM), as shown in Figure 3-2. Measurements were recorded using both strain gauges and clip-on extensometers. To investigate the sensitivity of the strength due to grinding the surface for strain gauge attachment, three regular bars and three ground bars (#4) were tested in the UTM, all from the same heat (mill certificates provided in the Appendix A). The test results indicated negligible differences in the behavior of ground bars, with necking and rupture even occurring outside the grinding locations.

The average values observed during the test and the certified mill test report (CMTR) values are presented in Table 3-2. Figure 3-3 shows a typical stress-strain curve obtained from the tension tests of the #4 bar used in Phase 1. The stress-strain response of #8 and #9 bars, used in Phase 2, is presented in Figure 3-4. The measured yield strength, tensile strength, and elongation at failure of the steel were 70 ksi, 101 ksi, and 16%, respectively.

Table 3-2 Reinforcing rebar tension test results of #4 bar

Bar Designation	Test No.	Yield Stress, ksi	Ultimate Stress, ksi	Elongation at fracture, %
Regular	1	67	105	9
	2	70	109	5
	3	69	107	6
	Average	69	107	7
Ground	1	65	104	16
	2	68	106	8
	3	70	108	10
	Average	68	106	11
		74 (from Mill certificate)	107 (from Mill certificate)	12 (from Mill certificate)



Figure 3-2 Tensile test of #4 reinforcing steel

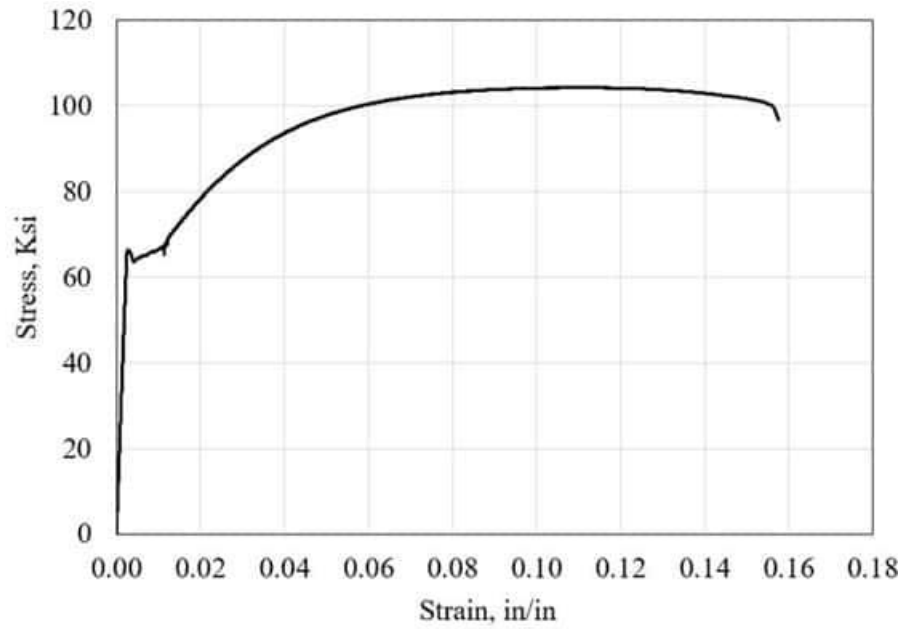


Figure 3-3 Stress-strain response of steel reinforcement tension test used in Phase 1 (#4 bar)

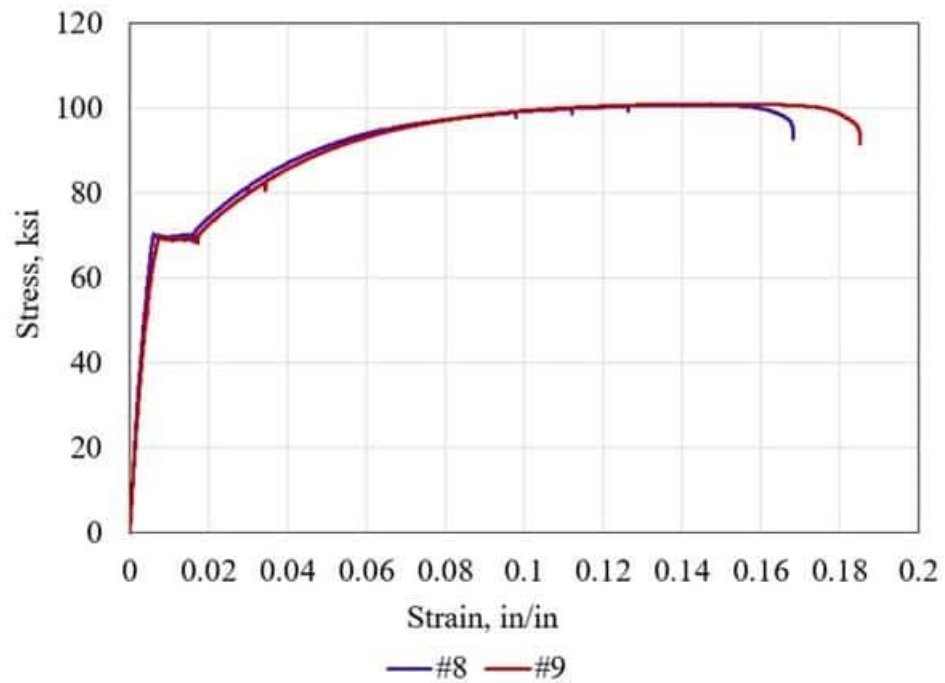


Figure 3-4 Stress-strain response of steel reinforcement tension test Phase 2 (#8 and #9 bar)

3.4 TITANIUM

The TiABs used in this study were Class 130 Ti-6Al-4V (Grade 5 according to ASTM B1009-20). The TiABs were supplied by the Perryman Company with an in-house classification of textured infrastructure bar (also marketed as Bridgealloy). Two types of TiABs with different surface deformations, referred to as Type 1 and Type 2, were used, as shown in Figure 3-5. The surface pattern on the Type 1 TiABs resembled threads on a threaded rod, with slightly rounded peaks and valleys to minimize stress concentrations (Amneus, 2014). Type 1 TiAB was used in material-level tests (Phase 1), while both Type 1 and Type 2 TiABs were used in member-level tests (Phase 2).

The mill certification obtained from the manufacturer conformed to the requirements of ASTM B1009-20 (2020). Tensile testing was also performed in the laboratory to verify the reported material properties and provide strength properties for calculations and analysis. The same type of titanium bars were rolled from the same heat (mill certification provided in Appendix A), and tension tests were completed on samples taken from several bars. The stress-strain responses obtained from testing both types of TiABs are presented in Figure 3-6. The TiABs exhibited a behavior without a well-defined yield point or yield plateau. Therefore, the 0.2% offset method was used to determine the yield stress. The elastic modulus was measured at 15,500 ksi, and elongation at fracture was measured at 10.6% over a 2-inch gauge extensometer. The AASHTO NSM TiAB guide requires a minimum elongation of 10% at fracture. The test results indicated a measured yield strength of 132 ksi, a tensile strength of 145 ksi, and an elongation at rupture of 9% for Type 1. For Type 2 TiAB, the measured yield strength and tensile strength were 142 ksi and 155 ksi, respectively, with an elongation at rupture of 10.6%. The tensile test measured values were slightly lower than the mill certificate (CMRT) values, so the measured values were used for all calculations and analysis. Type 1 TiABs were used for Phase 1 testing and both types of TiABs were used for Phase 2 testing.



Figure 3-5 The two TiAB types evaluated in this project

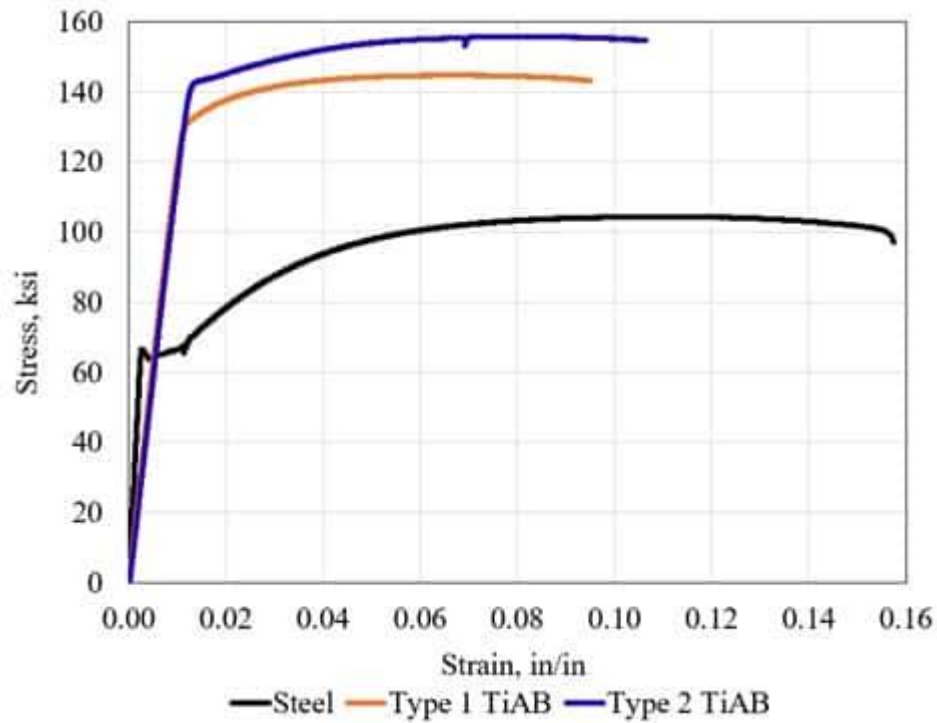


Figure 3-6 Comparison of stress-strain plot for both TiABs (Type 1 and Type 2 - #4 TiAB)

3.5 EPOXY

In both test phases (member-level and material-level), the epoxy used to bond the TiAB to the reinforced concrete member was Hilti's HIT-RE 500 V3 epoxy anchor (HILTI, 2021), which has been successfully used in previous studies by other researchers on both NSM FRP (Bertolotti, 2012) and NSM TiAB (Knudtsen, 2016). This epoxy is classified as a high-performance injectable epoxy mortar commonly used for rebar connections and heavy-duty anchoring. The mechanical properties provided by the manufacturer are shown in Table 3-3. The total curing time for the epoxy at room temperature (72°F) is 6.5 hours, as indicated on the product sheet provided in the Appendix A.

Table 3-3 Fully cured epoxy properties (HILTI, 2021)

HIT-RE 500V3 Full Cure Properties	
Bond Strength, psi	1690
Compressive Strength, psi	12000
Tensile Strength, psi	7150
Elongation at Break, %	1.1

Chapter 4

SPECIMEN AND TEST SETUP DETAILS FOR PHASE 1

4.1 INTRODUCTION

In this chapter, an overview of the test matrix, specimen design and construction, instrumentation, test setup, and testing protocol for Phase 1 is presented. This phase of experimental research was designed to characterize material-level behavior, focusing specifically on the effective bond strength required to achieve yielding (i.e., development length) of NSM TiABs. Previous studies have not clearly demonstrated this aspect of current design methodologies with different anchorage types. The anchorage cases included hooked-bonded anchorage, which was compared to the assumed 1.0 ksi average bond strength specified in current design guidelines. Additionally, the straight-bonded anchorage case was evaluated to recommend an average bond strength similar to the hooked-bonded case. Finally, the hooked-unbonded case was experimentally evaluated to investigate the feasibility of this anchorage method for large-scale applications. To achieve these objectives, small-scale beam tests were conducted to assess each strengthening option while realistically simulating the stress conditions that NSM TiABs would experience in flexural strengthening applications.

4.2 TEST MATRIX AND SPECIMEN DESIGN

Fifteen small-scale RC specimens were tested in this phase including a control specimen (conventional RC without strengthening). The specimens were 9 in. wide, 12 in. tall, and 10 ft long, with 6 in. overhangs beyond the centerline of the supports on both sides. The beam specimens were simply supported with a span of 9 ft and tested using a three-point loading arrangement. The specimens were constructed with an 8 in. long, reduced flexural-strength portion by discontinuing half of flexural tension reinforcement near the midspan. This was to concentrate any potential flexural failure in this region and clearly observe the effectiveness of the NSM TiAB strengthening method. This test configuration was based on a setup previously used by Hassan and Rizkalla (2003) and to investigate the bond strength between concrete and NSM CFRP strips, which is referred to in ACI 440.2 (2023) for bond strength.

The specimens were designed to minimize the possibility of diagonal shear cracks forming during the tests. The beam cross-section was determined such that only the concrete contribution to shear strength (V_c) was sufficient to resist the strengthened capacity and prevent shear failure, however additional shear reinforcement with stirrups (V_s) was still provided. The 9-foot span was chosen because it was the shortest span that could encompass all practical ranges of TiAB bonded

lengths needed to be tested. Three-point loading was used in these tests instead of four-point loading since it allowed for shorter specimens and align with the loading configuration used by Hassan and Rizkalla (2003).

The concrete used for this study was specifically proportioned to have strengths lower than what would be used in bridges built nowadays to represent an aged bridge strengthening application. Since the quality of the bond obtained between the epoxy and the concrete is a key aspect being evaluated, the use of lower-strength concrete is also conservative and appropriate to evaluate NSM TiAB to strengthen existing bridges. As shown in Figure 4-1, all the specimens were reinforced with six #4 ASTM A615 Gr. 60 longitudinal bars located in three layers (one top layer and two bottom layers). For stirrups, #3 ASTM A615 Gr. 60 bars were used that were spaced at 5 in. on center. The second layer from the bottom of longitudinal reinforcement terminates 4 in. before the midspan of the beam on both sides, which results in the 8 in. long center region with lower flexural capacity than the rest of the members.

The name configuration can be seen in Figure 4-2 where, R- rectangular beam, H- TiAB has hooked end anchorage, S- TiAB has straight end anchorage, B- TiAB is bonded, U- TiAB is unbonded along the length of the bar, l_d development length of TiAB. For example, HB40 represents a rectangular beam as shown in Figure 4-3 with hooked anchorages and bonded along the length (hooked-bonded) with 40 in. embedment length.

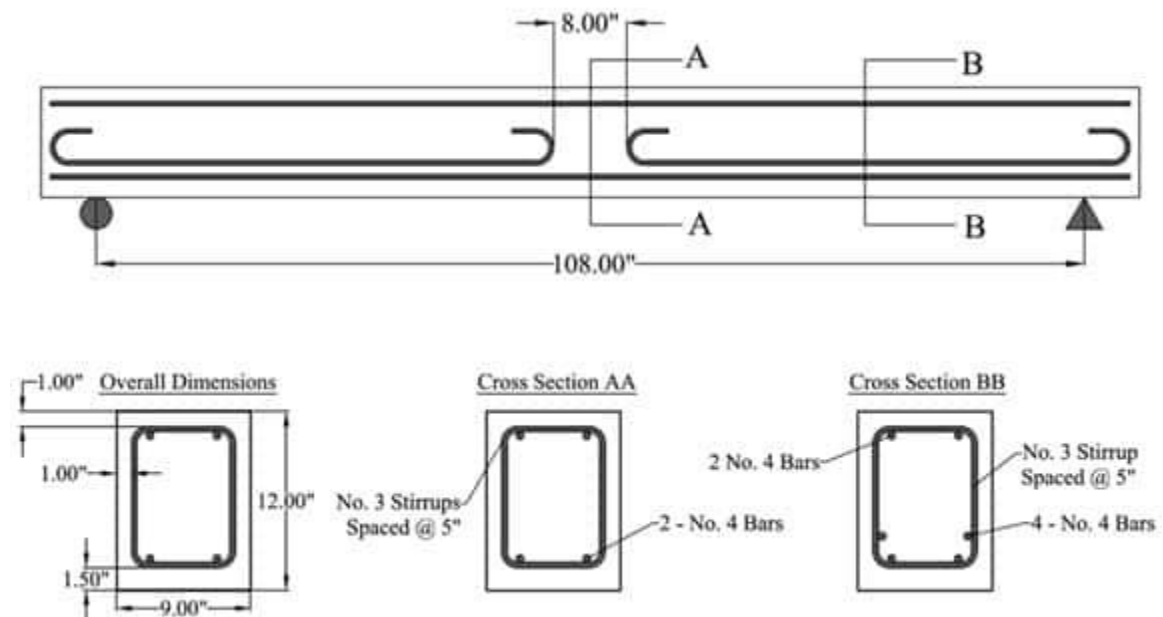


Figure 4-1 Beam sections and detailing of reinforcement

$$\frac{H/S}{B/U} \cdot \frac{1}{2 * l_d}$$

Figure 4-2 Specimen naming configuration

4.2.1 HOOKED-BONDED SPECIMENS

Five specimens with hooked-bonded TiAB were tested in this study. The specimens were named based on the bonded length, which was defined as the distance from the load point to the outer edges of the TiAB hooks. The TiAB was epoxied into a rectangular groove and drilled holes were cut in the soffit of the concrete beam. For instance, a specimen reinforced with a TiAB having a bonded length of 40 in. was referred to as HB40. Table 4-1 lists all the hooked-bonded specimens with their development and bonded lengths (l_{dTi} and l_{bond} , respectively). The expected average bond stress ($\overline{\mu_u}$) was calculated from Equation 2.5 using the measured f_{yTi}^* properties based on the assumption of TiAB achieving yielding, and the associated expected behavior was assigned based on the AASHTO NSM TiAB Guide recommendations of 1.0 ksi bond strength.

Table 4-1 Hooked-Bonded Test Matrix with TiAB embedment length

Specimen ID	l_{bond} (in.)	l_{dTi} (in.)	$\overline{\mu_u}$ (ksi)	Expected behavior
Control	0	0	N.A.	Tension-controlled
HB.15	15	7.5	2.18	Bond failure without yielding of TiAB
HB.20	20	10	1.64	Bond failure without yielding of TiAB
HB.30	30	15	1.09	Bond failure without yielding of TiAB
HB.40	40	20	0.82	Yielding of TiAB
HB.60	60	30	0.55	Yielding of TiAB

N.A.—not applicable

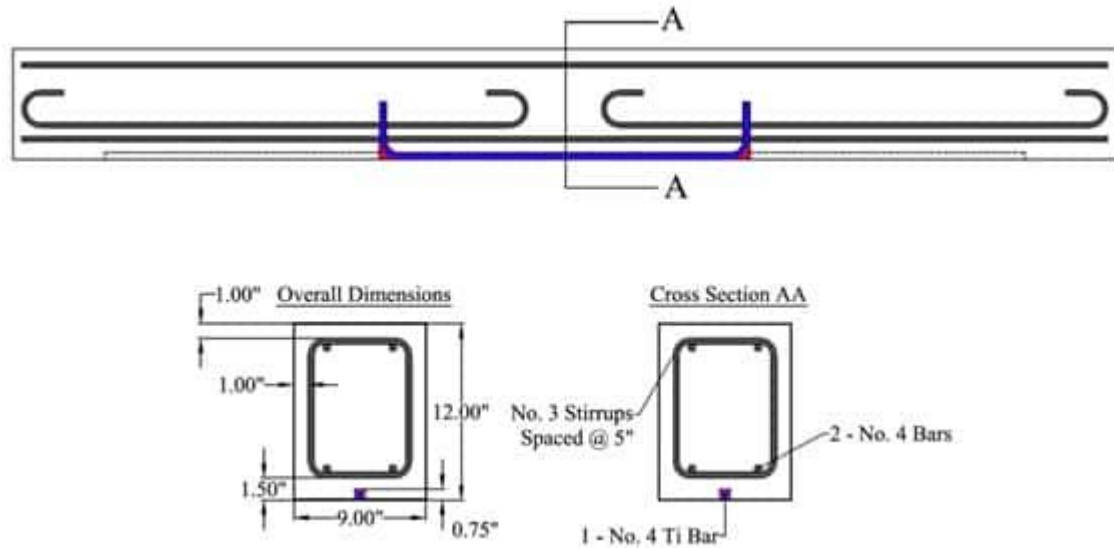


Figure 4-3 Hooked-bonded Specimen HB40

4.2.2 STRAIGHT-BONDED SPECIMENS

A similar effective bond stress approach was taken for the straight-bonded specimen with the 0.5 ksi being the transitioning effective bond stress to achieve the titanium bar yielding. This was decided based on the straight-bonded tests that (Vavra, E., 2016) conducted. Equation 2.5 was used to create a matrix of embedment lengths based on a series of bond stresses calculated according to potential TiAB yield. Table 4-2 displays the straight-bonded test matrix. The initial specimen design was based on the bond stresses calculated according to nominal TiAB yield strength of 120 ksi. The bond stresses were updated after obtaining TiAB measured yield strength of 131 ksi. Table 4-3 provides the bond stresses calculated according to nominal and measured properties based on the TiAB yield strengths (f_{yTi}). The remainder of the report refers to the bond stresses calculated based on the measured f_{yTi} .

Table 4-2 Straight-Bonded Test Matrix with TiAB embedment length

Specimen ID	l_d , in.	Embedment length, in.	Bond Stress (ksi)	Expected TiAB Performance
SB.30	15.0	30.0	1.00	bond failure
SB.40	20.0	40.0	0.75	bond failure
SB.60	30.0	60.0	0.50	yield
SB.80	40.0	80.0	0.38	yield
SB.96	48.0	96.0	0.31	yield

Table 4-3 Straight-Bonded Effective Bond Stresses using Nominal and Measured f_{yTi}

Specimen ID	Using Nominal f_{yTi} (ksi)	Using Measured f_{yTi} (ksi)
SB.30	1.00	1.09
SB.40	0.75	0.82
SB.60	0.50	0.55
SB.80	0.38	0.41
SB.96	0.31	0.34

4.2.3 HOOKED-UNBONDED SPECIMENS

The unbonded bars were different in the respect that Equation 2.5 was not used to design the TiAB lengths. Since the TiAB was not bonded, the strain in the bar remains unchanged along the length (Cairns and Rafeeqi 2002). This theory was used in the determination of the TiAB length. The test matrix is shown in Table 4-4.

Table 4-4 Hooked-Unbonded Test Matrix with TiAB length

Specimen ID	Half of the TiAB length, in.	Total TiAB length, in.
HU.10	5.0	10.0
HU.30	15.0	30.0
HU.40	20.00	40.0

4.3 SPECIMEN CONSTRUCTION

The formwork of the specimens was built using plywood and 2x4 in. wood pieces that were coated with polyurethane where in contact with concrete. The steel reinforcing bar cages were erected and tied by hand (Figure 4-4). The formwork ready for pouring is shown in Figure 4-5. The bars were then ground to accommodate strain gauges. Before placing the concrete, the steel reinforcing bars (both tension and compression) were instrumented with strain gauges at midspan. All specimens were cast from the same batch of concrete and a mechanical vibrator was used to ensure the proper consolidation of the concrete (Figure 4-7). The concrete's slump, air content, unit weight, and fresh temperature were all tested to ensure that the concrete was adequate. Those values can be seen in Table 4-5 below. Figure 4-6 shows the test cylinders being made for strength evaluation. Specimens were covered with water-soaked burlap and plastic sheets to moist cure the specimens for seven days. After curing, the specimens were removed from the forms and kept inside the laboratory (Figure 4-8).

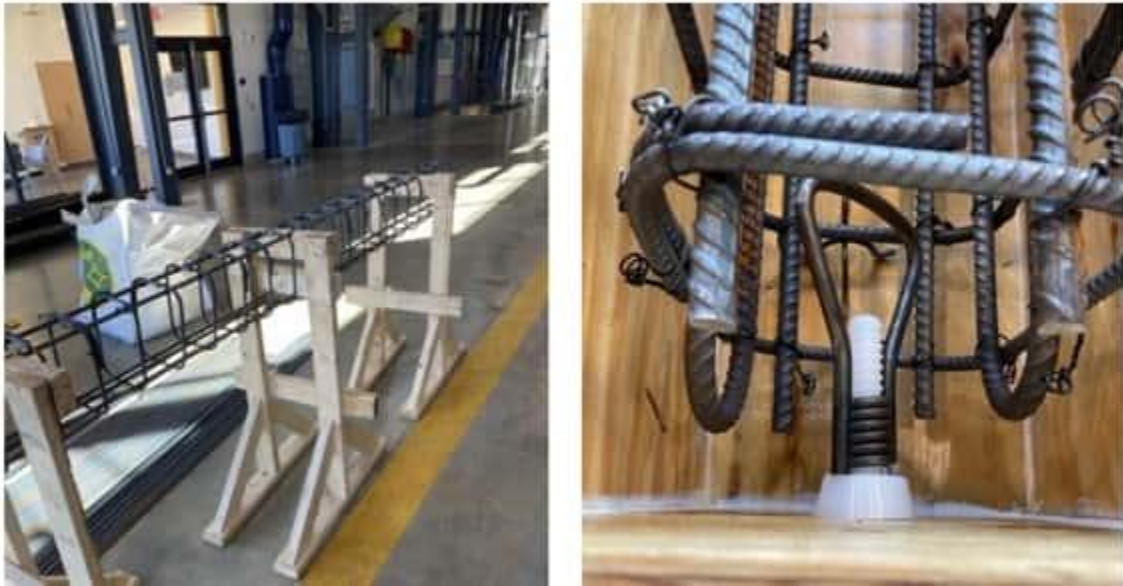


Figure 4-4 Rebar Cage (Left) and Lifting Hardware (Right)



Figure 4-5 Concrete forms and sliding funnel



Figure 4-6 Concrete casting, vibrating and finishing

Table 4-5 Concrete Properties

Date and properties of Concrete	
Placement Date	11/16/2021
Slump (in.)	4.0
Total air content (%)	4.0
Unit weight (pcf)	142.7
Fresh concrete temperature (°F)	71.0



Figure 4-7 Cylinder preparation for strength evaluation



Figure 4-8 Beam after placement (Left) and moist curing (Right)

4.4 INSTRUMENTATION

The test data were collected using several internal and external sensors for each specimen, as depicted in the instrumentation layouts shown in Figure 4-9 and Figure 4-10. The hydraulic actuator used for loading recorded the applied force through its internal load cell. The reinforcing steel was instrumented with strain gauges following the procedure described by the strain gauge manufacturer for embedding inside concrete. Polysulfide coating was used to protect the strain gauges from the fresh concrete during casting. Several strain gauges were also placed along the length of the TiAB: one at the center of the TiAB, two spaced at 4 in. on either 20 side of the center, and then spaced at 6 in. until the end of the TiAB. The proper installation of strain gauges to the TiAB was more challenging than the ones on steel reinforcing bars, which required a steady

application of glue for a longer time than recommended by the strain gauge manufacturer. The strain gauges installed on the TiAB were covered in epoxy directly without applying any coating because these were encapsulated with epoxy and not concrete. Four linear position transducers (LPTs) were mounted underneath the beams to measure the deflection. Two 10 in. stroke LPTs were attached at the midspan of the beam directly underneath the load point, and two 5-in. stroke LPTs in the shear spans 18 in. on either side of the load point. Two inclinometers were used to measure the rotation of the strengthened beams, which were mounted 8 in. apart and equal distance from the load point. Data was collected using internal and external sensors with GI.Bench software and Gantner hardware as the data acquisition system and recorded at a rate of 2 hertz.

The TiAB strain gauge spacing was modified for two specimens to prevent the edge strain gauges from being near the end of the bar. The 30-inch bonded TiABs (i.e., HB30 and SB30) had three strain gauges placed at 4 inches. For the hooked-unbonded bars, one gauge was placed at the center of the TiAB and one was placed at the quarter length on each side of the TiAB for a total of three strain gauges due to the expectation of constant stress along the bar.

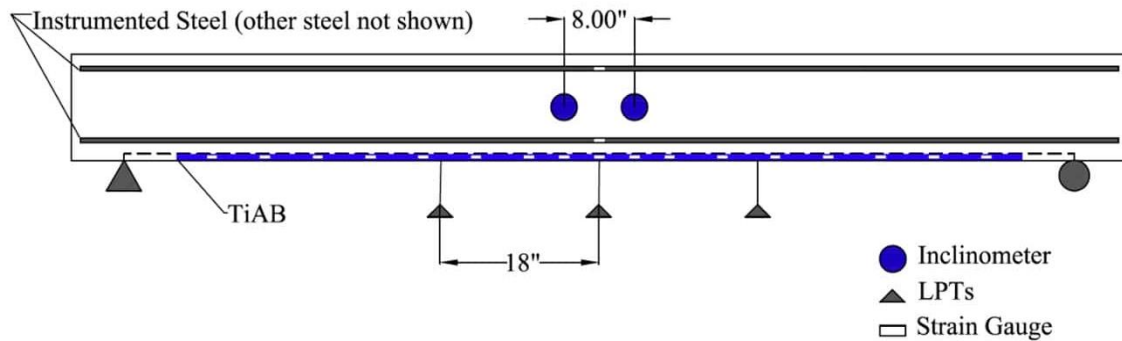


Figure 4-9 Instrumentation layout (Elevation View)

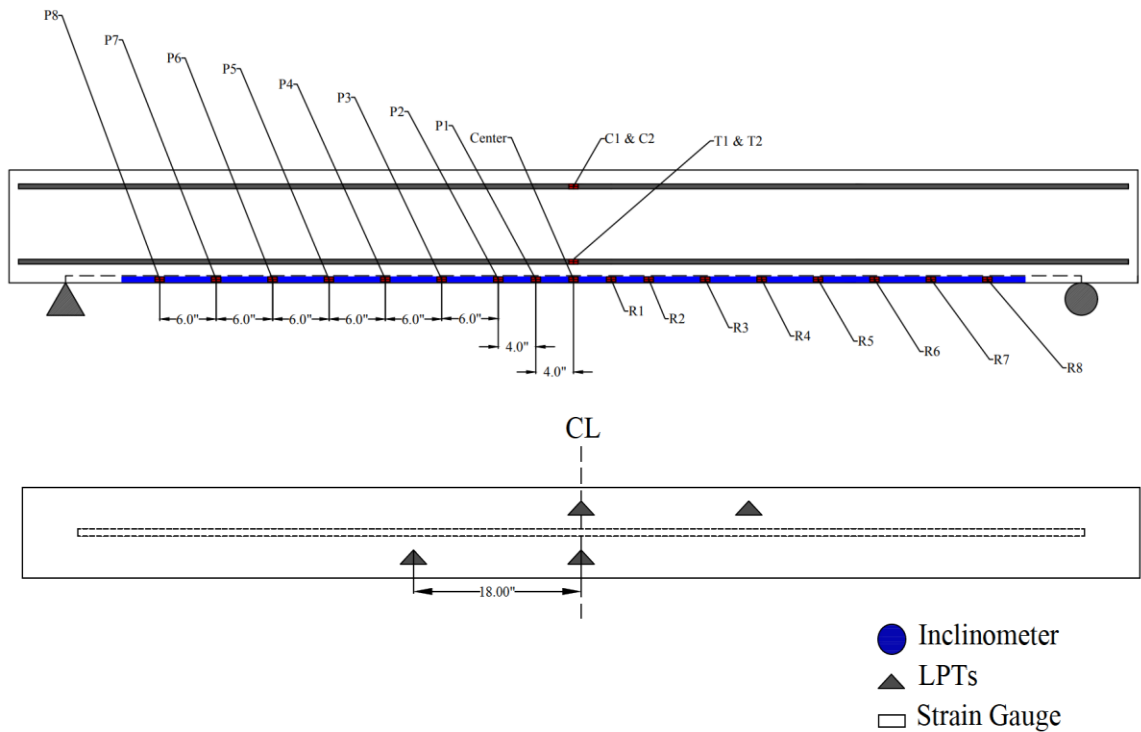


Figure 4-10 Instrumentation layout: strain gauges in TiAB (Top) and LPTs (Bottom)

4.5 NSM STRENGTHENING

In the following subsections, the process of pre-cracking, specimen preparation for TiAB installation, TiAB preparation before installation, and the comprehensive process of TiAB installation are described.

4.5.1 PRE-CRACKING

To accurately represent/simulate the in-service bridge condition, all the beam specimens were pre-cracked before strengthening. The beams were taken to 85% of steel yielding (this equated to about 2,000 $\mu\epsilon$ in the longitudinal steel). Eighty-five percent of yielding was chosen because the beams would be stressed beyond typical service load conditions but remain in the linear-elastic region. This was done using the same monotonic three-point loading configuration that was also used for the failure tests. The strains were monitored using the strain gauges that were attached to the tensile longitudinal reinforcement at the center of the beams. The cracks were marked with red permanent markers to distinguish them from the failure load cycle, and crack widths were measured at 1 kip intervals. Figure 4-11 shows the typical tensile strain and displacement variation plots during the cracking of the beams prior to installing the TiAB.

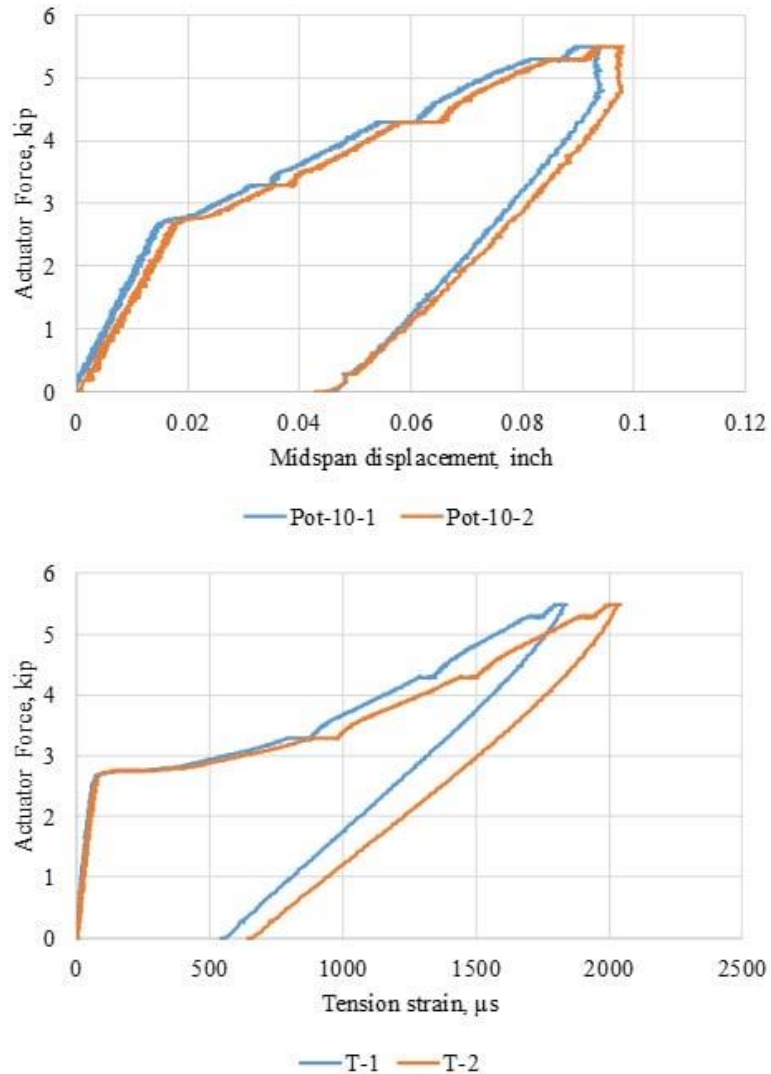


Figure 4-11 Example Load vs Displacement (Top) and Load vs Displacement (Bottom)

It has been consistently observed during the cracking process that the first crack would appear around 3 kips near the mid-span on either side of the center where stirrups were located. This crack was typically classified as a narrow (hairline) crack with a width of 0.003 inches. An example of crack initiation in a beam can be seen in Figure 4-12. As the load increased, the crack propagated toward the load point, and more cracks were initiated away from the center of the beam. When the steel reached 2000 $\mu\epsilon$, usually between 5 to 6 kips, the largest crack width for each beam varied from 0.008 inches to 0.012 inches. At the end of the pre-cracking stage, there were numerous cracks under the load point and in the shear span, as shown in Figure 4-12.

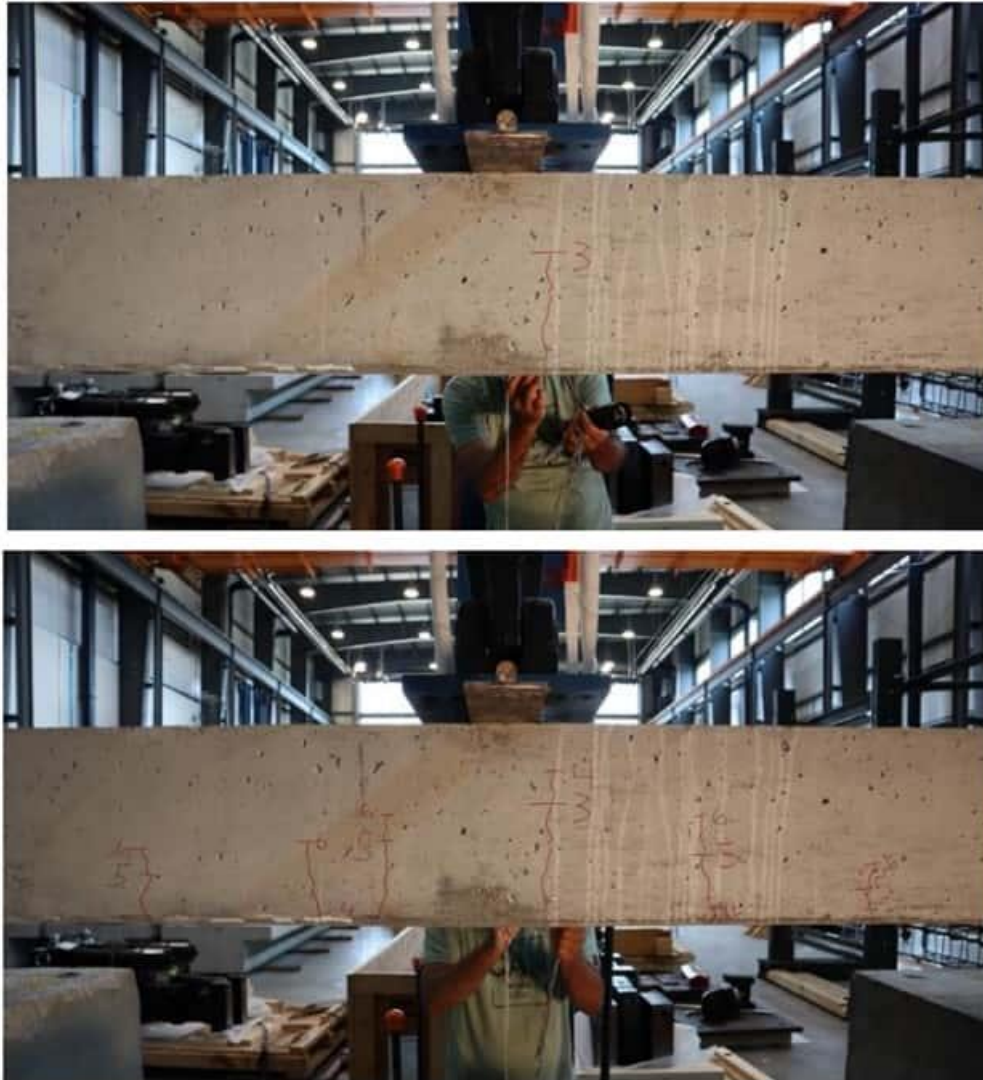


Figure 4-12 Crack initiation during pre-cracking (Top) and typical crack pattern at end of pre-cracking (Bottom)

Upon completion of cracking there was residual strain in the longitudinal reinforcement and permanent deformation of the beam. The residual strains ranged from 500-800 $\mu\epsilon$ and the residual displacement was in the range of 0.05 inches. The recorded residual strains and beam deformations obtained at the end of the cracking cycles were manually added to the plots of the final (failure) loading cycles.

4.5.2 PREPARING THE TiAB FOR INSTALLATION

The steps needed to be taken for NSM TiAB to be ready for mounting included; (i) cutting to length, (ii) heating and bending appropriately to form the anchorage hooks, (iii) grinding down the strain

gauge locations, (iv) attaching strain gauges along the bar length, (v) putting the wedges in place to keep the TiAB from falling out of the groove. The straight-bonded bars were cut to the representative length directly, while the hooked bars (both bonded and unbonded) had cut lengths that were calculated using the *Bar Bending Work Instructions* provided by the TiAB supplier (Perryman Company), to ensure that the TiAB were the proper length once bent (provided in Appendix B). The bars were cut and bent to desired lengths using the bending and cutting machine at the lab. For the hooked bars, the bar bending work instructions required that the bars be heated to approximately 1200°F and then placed in the bar bending machine at that temperature. TiAB naturally turns blue when heated to 1200°F making this process convenient and preventing cracking at the bend. An acetylenyl-oxygen torch with a rosebud tip was used to heat the TiAB. Figure 4-13 displays the TiAB being heated and bent.



Figure 4-13 TiAB heating (heating) and bending (right)

To keep the bars inside the cut grooves, a rubber hose with an inside diameter of 0.5 inches and an outside diameter of 0.75 inches was cut into quarter-inch segments to act as wedges. These wedges were slid onto the bar about every 18 inches to ensure the longest bar could be kept in place. For some cases, a small layer of electrical tape was added on the outside of the wedges for the TiAB to fit better with the walls of the groove. The last step to prepare the TiAB for installation was to add the strain gauges. Figure 4-14 depicts one of the wedges and two strain gauges attached on either side of the wedge.



Figure 4-14 TiAB with wedge and strain gauges

4.5.3 PREPARING THE SPECIMENS FOR NSM STRENGTHENING

The groove size and hook details of the TiAB conformed to the AASHTO NSM TiAB Guide recommendations. Figure 4-16 pictures the groove-cutting process into the flexural tensile surface of the concrete specimens. A single blade of 0.75 in. thickness (Figure 4-15) was used to cut the groove. The length of the groove was 104 in. for all the specimens, which accounted for the longest bonded TiAB length to be tested and provided flexibility in terms of revising the bonded lengths for the specimens, if deemed necessary. Standard 90-degree hooks were fabricated at the ends of TiABs with a hook length of 6 in. A conventional reinforcing steel-bending machine was used to form these hooks. Based on the TiAB manufacturer's recommendations, the TiABs were hot bent at the annealing temperature of 1200°F (after the heated TiAB region oxidized and turned blue) to prevent defects in the hook region, as pictured in Figure 4-13.

Oversized holes with 0.75 in. diameter were drilled to accommodate the hooked #4 TiAB with 0.5 in. nominal diameter. Figure 4-17 pictures the 6 in. deep hole drilling process using a hammer drill. The concrete substrate was chiseled to create a smooth curved transition between the groove and holes. A template was made from plywood to guide the hammer drill and shape the concrete substrate to the same radius as the TiAB hook. A chisel was then used to create the curved transition between the groove and the hole until the TiAB maintained a consistent distance from the curved concrete surface at both ends. The grooves and holes were cleaned by low-pressure water blasting (with masonry sand as the abrasive) according to the method prescribed in ACI 546R-14 (2014) to ensure a proper bond between the epoxy and concrete. Figure 4-18

contains pictures the grooves and holes being wet sandblasted at a pressure of 4000 psi to remove concrete dust, slurry, or other residues to prepare the concrete surface to achieve an improved bond.



Figure 4-15 Custom 0.75 in. wide blade and groove in the beam



Figure 4-16 Track saw mounted on beam



Figure 4-17 Hammer drill used for hole (left), beveling (middle), and chiseling to refine bevel



Figure 4-18 Low-pressure water blasting with abrasives

4.5.4 STRENGTHENING THE SPECIMENS

The TiAB were then epoxied into the grooves and holes from the underside of the specimen to simulate a realistic and worst-case strengthening application as shown in Figure 4-19. At high outdoor temperatures in summertime, the epoxy had low viscosity and the overhead groove prevented the epoxy from properly fill the grooves. To achieve appropriate epoxy viscosity, the epoxy was kept refrigerated at 41°F, and the TiAB installation was done early in the morning to ensure that the groove and holes were adequately filled. A trowel with a raised triangular prism tip was used to pack the first layer of epoxy into the corners of the groove, and the holes were prefilled with epoxy. The TiAB was then placed and held in place by wedges positioned along the length of the bar. A putty knife was used to place the rest of the epoxy over the bar until the groove was fully filled with epoxy. All the specimens were stored at indoor laboratory temperature conditions for seven days or longer before the load tests to allow for the epoxy to cure, which complied with the epoxy manufacturer recommendations.



Figure 4-19 First lift of epoxy application (left and middle), and Installed TiAB after final epoxy lift (right)

4.6 TEST SETUP AND LOAD PROTOCOL

The specimens were tested at the Advanced Structural Engineering Laboratory (ASEL) at Auburn University. An 82-kip force servo-hydraulic actuator that is capable of displacement- and force-control loading was used to monotonically load the specimens. After cutting the grooves, but prior to drilling the holes and mounting the TiAB, all the specimens were initially loaded to a service level

load of 85 percent of the steel reinforcing bar yielding strain under a force-controlled quasi-static loading protocol (1 kip/min.) to simulate the in-service bridge condition. The cracks were marked during these service-level loading cycles and the specimens were unloaded for TiAB mounting. The final load tests conducted after the TiAB mounting and epoxy curing began with force-controlled loading until the initiation of steel yielding, and then switched to displacement-controlled loading (0.02 in./min.) to better manage the loading rate in the yielding and post-peak regimes for each test. The test arrangement is shown in Figure 4-20.

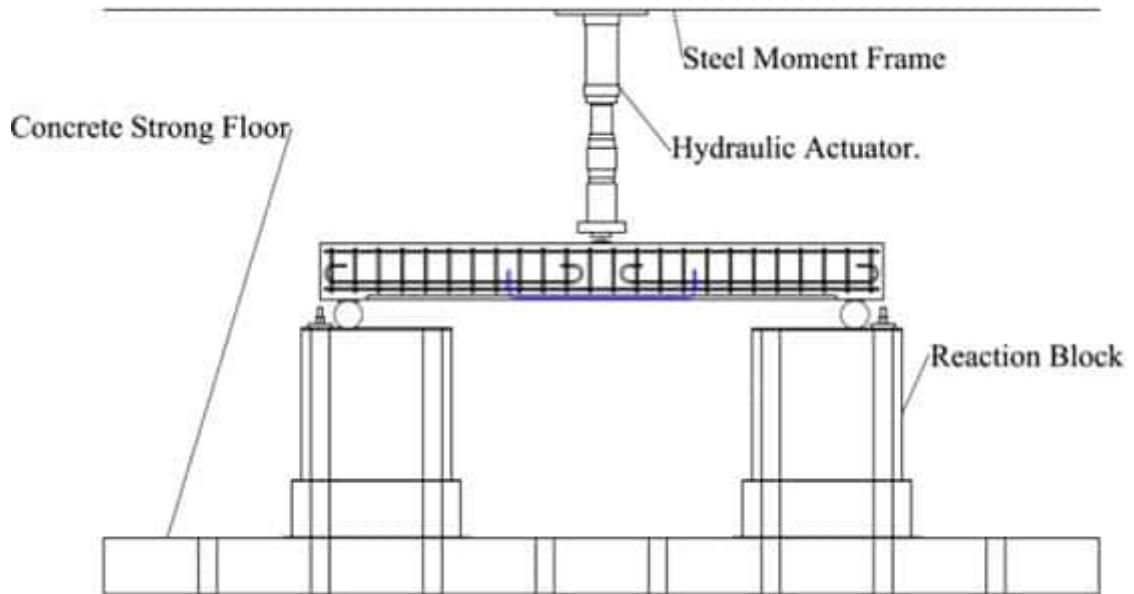


Figure 4-20 Test setup for NSM TiAB bond test (material-level test)

Chapter 5

TEST RESULTS, ANALYSIS, AND DISCUSSION FOR PHASE 1

5.1 INTRODUCTION

This chapter presents the experimental behavior, response, and post-test discussion from the failure load application of the material-level beam specimens strengthened with NSM TiABs. The beams failed in various modes, including TiAB rupture, epoxy rupture, concrete crushing, debonding, and anchorage slip. Upon data analysis, the failure of each specimen was defined as a peak load reduction of 5%. The peak and failure displacements were considered as the displacements that occurred at the peak and failure loads respectively. The calculated AASHTO NSM-TiAB capacity using experimental values of the concrete, steel, and TiAB was used to indicate when the TiAB yielded. The TiAB strain gauges that were not embedded in epoxy (i.e., the hooked-unbonded specimens) were capable of capturing TiAB strains in which case these strain values were used for determining TiAB yielding.

5.2 EXPERIMENTAL BEHAVIOR AND RESPONSE

The following sections discuss the experimental responses of the tested beam (hooked-bonded, straight-bonded, and hooked-unbonded). The load versus displacement graphs are marked with “X” markers that indicate major milestones that occurred during the test and associated pictures of the beams are provided for each test. Each section discusses the failure mode attributed to each beam’s strength loss as well as the displacement, rotation, and strain responses observed pre- and post-failure.

5.2.1 EXPERIMENTAL RESULTS OF HOOKED-BONDED SPECIMENS

The calculated load-carrying capacities (P_{pred}) for the control and strengthened specimens are reported in Table 5-1, which were calculated by following three methods: (i) using Equation 2.4 with the measured yield strength properties of the reinforcing steel and TiAB; (ii) a cross-sectional fiber analysis by considering the compression steel, using the measured stress-strain relationship including the post-yield strain hardening portions for the reinforcing steel and TiAB, and Hognestad’s parabolic stress model for the concrete; and (iii) using Equation 2.4 with the measured tensile strengths of the reinforcing steel and TiAB in place of the yield strengths, by assuming that strain hardening is reached at the ultimate loading stage. The calculated load capacities for the

specimens strengthened with NSM TiAB assumed strain compatibility for TiAB and no debonding failure occurs.

Table 5-1 Calculated strength for all Specimens based on different models and assumptions.

Specimen	Model	Input material properties	P_{pred} (kip)
Control	(i) Eq. 2.4	Measured f_y	9.6
	(ii) Sectional fiber analysis	Measured stress-strain response	10.7
	(iii) Eq. 2.4 w/ full strain hardening	f_s as measured f_u	14.8
Strengthened NSM TiAB	(i) Eq. 2.4	Measured f_y and measured f_{yTi}	19.8
	(ii) Sectional fiber analysis	Measured stress-strain responses	20.5
	(iii) Eq. 2.4 w/ full strain hardening	Measured f_{uTi} and f_s as measured f_u	25.5

Table 5-2 provides a summary of the loads and displacements reported at four stages of the specimen experimental response: i) steel tensile reinforcing bar yielding; ii) steel tensile reinforcing bar reaching 5000 $\mu\epsilon$ strain; iii) detection of concrete crushing; and iv) at the peak load. The first stage of reinforcement yielding corresponded to the bottom longitudinal steel reinforcing bars reaching the measured yield strain of 2345 $\mu\epsilon$ (i.e., f_y/E_s). The second stage of the bottom longitudinal steel reinforcing bar reaching 5000 $\mu\epsilon$ corresponded to the tension-controlled behavior requirements that exist in design codes to ensure ductile behavior. The third stage of the concrete compressive crushing was determined based on the top steel reinforcing bar strain that were extrapolated to the concrete surface. The sudden strain reversals observed in the top steel reinforcing bar from compressive to tensile strain were caused by a shift in the neutral axis depth due to concrete compressive crushing, which was consistent with visual observations. Finally, the peak load reporting stage corresponded to the maximum force recorded in the tests.

Table 5-2 Summary of experimental results (Hooked-bonded)

Specimen ID	$\varepsilon_s = \varepsilon_{sy}$		$\varepsilon_s = 0.005$		Concrete crushing		Peak load	
	Displ.	Load	Displ.	Load	Displ.	Load	Displ.	Load
	[in.]	[kip]	[in.]	[kip]	[in.]	[kip]	[in.]	[kip]
Control	0.129	8.2	0.193	9.3	1.826	14.4	2.717	14.8
HB15	0.257	11.6	0.312	13.1	1.289	15.6	1.238	15.7
HB20	0.269	12.1	0.548	14.8	1.496	16.9	1.419	16.9
HB30	0.237	11.3	0.292	13.0	1.576	22.1	1.719	22.2
HB40	0.227	11.3	0.295	13.6	0.726	19.2	1.931	23.5
HB60	0.237	12.9	0.265	13.3	0.840	20.5	2.443	24.5

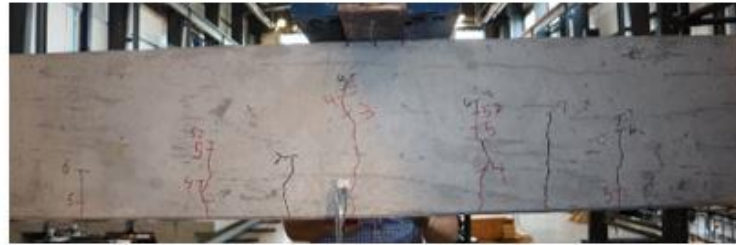
Pictures of the cracking conditions from the four reporting stages are shown in Figure 5-1 to Figure 5-3 where the vertical lines on the strengthened specimens represent the internal hook locations of the TiAB, while the horizontal lines mark the end of the TiAB hooks. Based on the experimental results in Table 5-2, accompanied by Figure 5-1 to Figure 5-3, the following observations were made:

- (i) The displacement and load at yielding of the tensile reinforcing bar for all strengthened specimens occurred at about 0.25 in. and 12 kip, respectively, which was about double the yield displacement of the control specimen. Pictures of the concrete cracking state from a side view during the yielding of the tensile reinforcing bar are shown in Figure 5-1.
- (ii) The displacement and load at the instant when the tension steel reached 5000 $\mu\epsilon$ for all the strengthened specimens except HB20 were approximately 0.30 in. and 13 kip, respectively, which are significantly higher than those for the control specimen. Specimen HB20 exhibited larger values of displacement and load compared to the other strengthened specimens at this stage. This outlier response was credited to the absence of a central crack where the strain gauges were located, as pictured in Figure 5-2c and Figure 5-3c. The limiting strain value for tension-controlled behavior of the

AASHTO NSM Guide was met for all the specimens shortly after reaching the yielding of the tension steel.

- (iii) For the control specimen, HB30, HB40, and HB60, the peak load occurred at displacements and loads higher than those when concrete crushing was observed. For HB15 and HB20, concrete crushing was detected at about the same load level as the peak load. Additionally, the peak loads measured for these two tests were marginally greater than the strength measured for the control specimen. Figure 5-2 and Figure 5-3 picture the specimen conditions during and after concrete crushing occurred, respectively.

Control



HB15



HB40



HB60



Figure 5-1 Condition of Specimens at yielding of the tension steel reinforcement.

Control



HB15



HB20



HB40

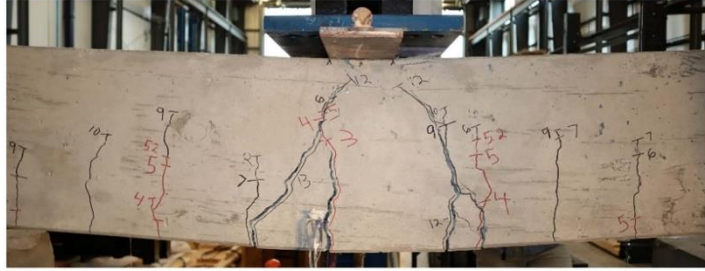


HB60



Figure 5-2 Condition of Specimens during detection of concrete crushing.

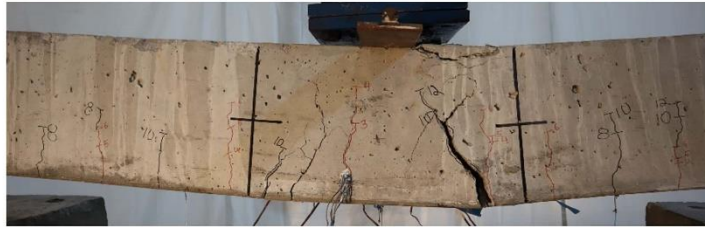
Control



HB15



HB20



HB30



HB40



HB60



Figure 5-3 Condition of Specimens after peak load.

5.2.1.1 Behavior and Responses of Hooked-bonded Specimens

Figure 5-4 includes the load-displacement response of all five TiAB Specimens, as well as the control specimen, and the calculated strength based on the AASHTO NSM Guide method

(Equation 2.4) using measured yield strength properties (f_y and f_{yT}). The response until concrete crushing was observed is represented with solid lines and switched to dashed lines beyond this stage. The entire load and displacement response of the beams are presented since the main objective of this research was to identify response limits and study the bond strength.

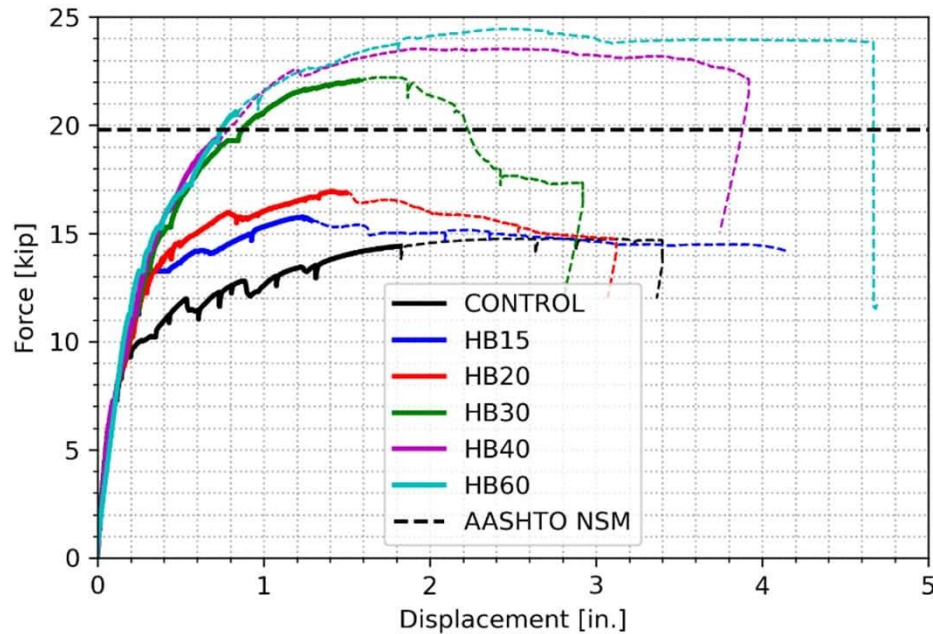


Figure 5-4 Load-displacement response for specimens and AASHTO NSM Guide strength prediction

The control specimen (without any strengthening) was tested to establish a baseline performance to compare against the specimens strengthened with NSM TiAB. As the applied force increased initially, the flexural cracks formed during the pre-crack load cycle widened and propagated, as well as new cracks formed and propagated toward the load point. The flexural cracks had almost constant spacing that approximately coincided with the stirrup locations. The specimen was loaded until the damage was considered excessive for safely continuing with the test, and the specimen was unloaded after it reached 3.4 in. of vertical displacement at midspan. The control specimen yielded and followed a hardening response until reaching concrete crushing near the peak load, thus exhibiting a tension-controlled failure mode. The peak load was considerably greater than the predictions (i) and (ii) reported in Table 5-1, but corresponded well with the prediction (iii), which indicates that significant strain hardening occurred in the tensile reinforcement, and the tensile strength of the steel reinforcing bars were reached.

Once the baseline behavior of the control specimen was obtained, specimens strengthened with NSM TiAB were tested. For the strengthened specimens, the pattern and development of cracks were similar to those observed in the control specimen.

Specimen HB15 exhibited yielding of the steel tensile reinforcing bars, followed by a critical shear crack forming near the TiAB hook anchorage zone which led to anchorage failure. Localized concrete crushing near the load point was also observed during the anchorage failure. As can be observed from Figure 5-3b, several inclined cracks formed near the TiAB anchorage zones with a wide crack near the hooked-end. The wide crack extended from the hooked-end and caused the TiAB to become ineffective before achieving yielding. Densely spaced cracking was also observed in the epoxy. After the peak load that corresponded to the anchorage failure, the strength gradually reduced to the force levels measured for the control specimen, as shown in Figure 5-4. The measured peak load was marginally greater than the control specimen (15.7 vs. 14.8 kips) and well below the calculated load-carrying capacity corresponding to TiAB yielding of 19.8 kips.

Specimen HB20 demonstrated similar overall behavior to HB15, with yielding of the steel tensile reinforcing bars, followed by a critical shear crack developing near the hook anchorage zone that led to anchorage failure. Localized concrete crushing near the load point was also observed during the failure. As can be observed from Figure 5-3c, a wide inclined crack propagated from an existing flexural crack within the strengthened region of the specimen, which widened and extended toward the load point. This wide inclined crack also propagated into the epoxy leading to TiAB ineffectiveness prior to achieving yielding. After the peak load that corresponded to the anchorage failure, the strength gradually reduced to the force levels measured for the control specimen, as shown in Figure 5-4. The peak load measured for the test was slightly greater than the control specimen (16.9 vs. 14.8 kips) but well below the calculated load-carrying capacity corresponding to TiAB yielding of 19.8 kips.

Specimen HB30 achieved yielding of the steel tensile reinforcing bars and TiAB, followed by concrete crushing near load point, and finally debonding failure of the TiAB. As can be observed from Figure 5-3d, several diagonal cracks propagated from existing flexural cracks within the TiAB strengthened region and wide cracks developed near the TiAB hook anchorage zone. The specimen achieved the calculated load-carrying capacity for the strengthened specimen at about 1 in. of vertical midspan displacement. Concrete crushing near the load point was observed beyond this level followed by a strain-hardening response. The load increased until two of the intermediate cracks became significantly wide and propagated through the epoxy causing debonding of the TiAB. After the peak load that corresponded to the TiAB yielding and tension steel strain-hardening, the strength dropped by about 22 percent. The peak load measured for the test was significantly

greater than the control specimen (22.2 vs. 14.8 kips) and exceeded the calculated load-carrying capacity corresponding to TiAB yielding of 19.8 kips.

Specimen HB40 achieved yielding of the steel tensile reinforcing bars and TiAB, followed by concrete crushing, and ultimately debonding of the TiAB due to the formation of a critical diagonal crack. The critical diagonal crack formed in the center region of the specimen, extended toward the load point and into the epoxy. As can be observed from Figure 5-3e, additional inclined cracks formed near the hooks and extended towards the center of the beam. The strength plateaued at around 23.5 kips that indicated that TiAB yielding and tension steel strain-hardening occurred. The peak load measured for the test was greater than the control specimen (23.5 vs. 14.8 kips) and exceeded the calculated load-carrying capacity corresponding to TiAB yielding.

Specimen HB60 demonstrated a similar behavior to HB40 while exhibiting a slightly higher peak load and deformation capacity. HB60 achieved yielding of the steel tensile reinforcing bars and TiAB, followed by concrete crushing, and ultimately rupturing the TiAB. Several flexural cracks extended diagonally towards the load point, and extensive cracking through the epoxy occurred, as can be observed from Figure 5-3f. After concrete crushing occurred, the peak load occurred at 24 kips that indicated that TiAB yielding and tension steel strain-hardening occurred. The beam was able to sustain the applied force until the TiAB ruptured at a midspan displacement of 4.65 in. The peak load measured for the test was greater than the control specimen (24.5 vs. 14.8 kips) and exceeded the calculated load-carrying capacity corresponding to TiAB yielding.

Figure 5-5 presents the moment-curvature plots for each strengthened specimen in which TiAB yielding was achieved. The average section curvature at midspan was calculated by taking derivatives of the rotations measured by the inclinometers on either side of the load point. Inclinometers were mounted on the side of the concrete beams and therefore the readings were susceptible to noisy response due to cracking occurring at the sensor attachment locations. Inclinometers also malfunctioned for the control specimen so it is not reported in the figure. The calculated moment-curvature response based on cross-sectional fiber analysis is also shown in Figure 5-5. The fiber model accounted for the compression steel, strain-hardening models for the steel tensile reinforcing bars and TiAB, and a parabolic stress model for the concrete while assuming a perfect bond (strain compatibility) between the TiAB and the concrete. It is observed that the initial flexural stiffness was captured reasonably well by the fiber analysis until the yielding of the bottom steel reinforcement at a moment of about 350 in.-kip. The fiber analysis diverged from the experimental response following the steel tensile reinforcing bar yielding, but the response converged with the experimental results at the ultimate curvature stage for the specimens achieved TiAB yielding.

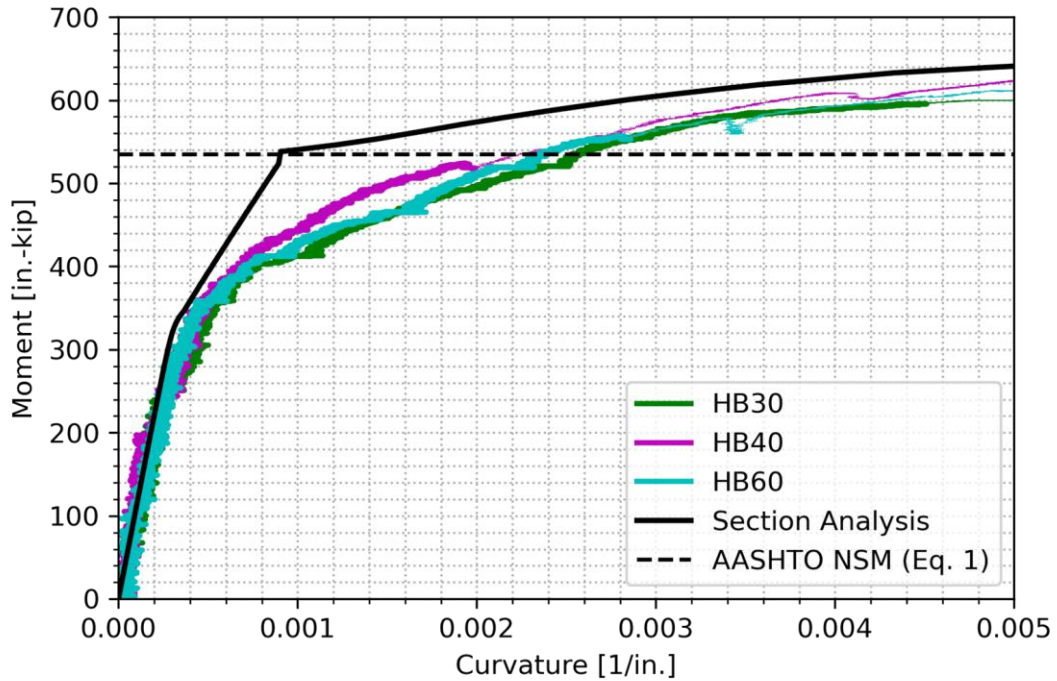


Figure 5-5 Moment-curvature response for strengthened specimens and section fiber analysis prediction

5.2.1.2 TiAB Bond Strength of Hooked-bonded Specimens

The TiABs were instrumented with strain gauges along its length, with the aim of calculating the stresses in the TiAB and measuring the bond stress with increasing load. Figure 5-6 shows the TiAB strain profiles obtained at different load levels for Specimen HB60 with strain gauge locations provided relative to the midspan. A nonlinear strain distribution is observed along the length of the TiAB. The strain measurements were recorded up to about 15 kips, due to strain gauges malfunctioning beyond this load level. The strain gauges on the TiABs were susceptible to cracking in the surrounding epoxy. It was consistently observed during the tests that the gauges would fail reporting values typically around $6000 \mu\epsilon$, which is prior to when TiAB yielding is expected to occur at around $8500 \mu\epsilon$. Therefore, direct measurement of bond stresses was not possible as the TiAB strains approached the yield strains.

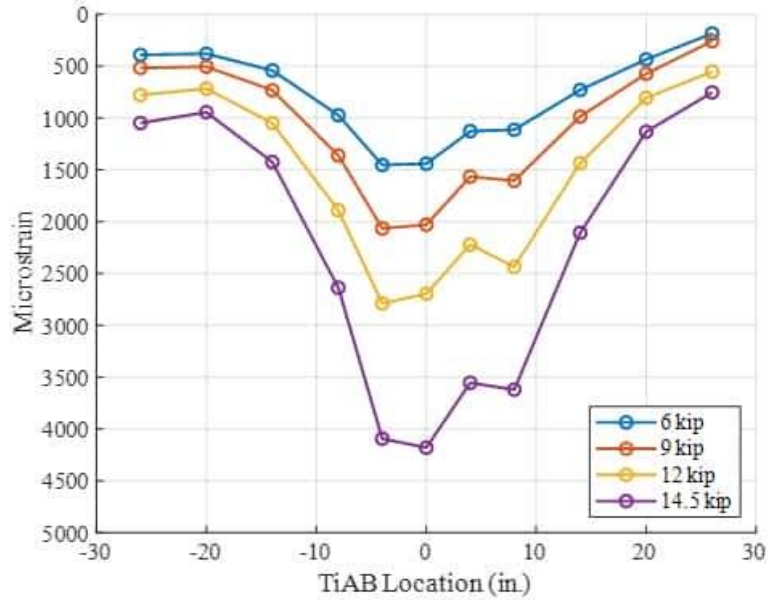


Figure 5-6 Strain profiles along the TiAB for HB60 at different force levels

In order to estimate the bond stress for specimens that achieved TiAB yielding, Equation 2.4 was employed to back-calculate the corresponding average bond strength (assuming, $A_{Ti}f_{yTi} = \bar{\mu}_u \pi D_{Ti}l_{Ti}$) to achieve the measured moment capacity. In the calculations, the stress in the steel at peak load was obtained from the fiber analysis which was approximately 90 ksi for HB30 and 100 ksi for HB40 and HB60, and the average bond strength ($\bar{\mu}_{Exp}$) was found by iterating to achieve the moment capacity. Table 5-3 presents the experimental average bond strengths obtained either from direct strain measurement or indirectly by back-calculating from the TiAB stress at the peak moment level.

Table 5-3 Bond stress at failure and observed behavior

Specimen ID	l_{bond} (in.)	l_{dTi} (in.)	$\bar{\mu}_{Exp}$ (ksi)	Observed behavior
HB15	15	7.5	0.86 ^m	Anchorage failure without yielding of TiAB
HB20	20	10	0.76 ^m	Anchorage failure without yielding of TiAB
HB30	30	15	1.08 ^{bc}	Yielding of TiAB with marked softening after peak load
HB40	40	20	0.82 ^{bc}	Yielding of TiAB with negligible softening after peak load
HB60	60	30	0.60 ^{bc}	Yielding of TiAB with negligible softening after peak load

*m—calculated from measured strain. bc—back-calculated from peak moment and Equation 2.4.

HB15 and HB20 exhibited a premature failure when the maximum strain in the TiAB were $3430\ \mu\epsilon$ and $3750\ \mu\epsilon$, which respectively corresponds to 51.4 ksi and 56.3 ksi of stress in the TiAB. Therefore, the average bond strength calculated at the peak moment based on the measured TiAB stresses was about 0.8 ksi. The back-calculated bond strength for HB30 at the peak moment was obtained as 1.08 ksi, which corresponded well with the initial prediction reported in Table 4-1. The estimated average bond stresses for specimens HB40 and HB60 that achieved yielding of the TiAB were calculated as 0.82 ksi and 0.55 ksi, respectively, indicating lower bond stress demands that prevented premature bond failure. Figure 13 pictures the post-test cracking condition of the NSM TiAB regions near the load point that either exhibited anchorage failure—i.e., HB15, HB20—or achieved yielding of the TiAB, and eventual debonding of the TiAB occurred later—i.e., HB30, HB40. It is observed that in all cases the major cracking was in the concrete or through the concrete-epoxy interface rather than the epoxy-TiAB interface.



Figure 5-7 Post-test specimen pictures of anchorage failure (HB 15 and HB20) or concrete-epoxy interface failure (HB30 and HB40)

5.2.1.3 Displacement Capacity of Hooked-bonded Specimens

All tested specimens met the AASHTO NSM Guide ductility requirement by exceeding the $5000\ \mu\epsilon$ strain limit in the tension reinforcing steel before exhibiting concrete crushing to ensure tension-controlled behavior. However, to emphasize the advantage of using a strengthening method based

on ductile materials like TiAB over non-ductile strengthening alternatives such as FRP, the study investigates the ability to impart significant inelastic displacements to the tested specimens by comparing the achieved deformation capacities without significant loss of load-carrying capacity.

Figure 5-8a presents the ratio of the displacement at peak load to the displacement at the initiation of yielding in the reinforcing steel. The calculated ductility ratios for strengthened specimens were lower than the control specimen but indicated an increasing trend with longer bonded length of the TiAB. Figure 5-8b presents the ratio of the displacement at peak load to the displacement at the initiation of yielding in the TiAB—only for specimens in which yielding of TiAB was achieved. Since the yielding of the TiAB was not measured directly, the displacement at TiAB yielding was assumed to be equal to the displacement when the load corresponding to the calculated capacity of the strengthened member was reached (i.e., 19.8 kips). Similar observations in terms of improved ductility are made as the peak-to-yielding displacement ratio based on TiAB yielding increases as the TiAB bonded length increases.

5.2.1.4 Discussion of Test Results of Hooked-bonded Specimens

The measured strength of the control specimen (14.8 kips) was consistent with calculations assuming the steel tensile reinforcing bars reached the tensile strength of the steel (f_u), which indicates that significant post-yield strain hardening of the reinforcing bars occurred in the tests. Similarly, the measured strengths for HB40 and HB60 were comparable to the flexural capacity calculated based on assuming that the tensile strength of the reinforcing steel bar (f_u) and TiAB (f_{uTi}) were both achieved. It was also observed that longer bonded TiAB resulted in increasing peak load and corresponding displacement. The tests with the shortest bonded TiAB lengths—i.e., HB15 and HB20—exhibited wide diagonal cracks forming near the anchorage zones, which prevented the TiAB from reaching the yield stress and limited its contribution to the member load-carrying capacity. It is observed in Table 5-2 and Figure 5-4 that HB15 and HB20 had a minor increase in strength relative to the unstrengthened control specimen, and the peak load was not sustained for large displacement levels. On the other hand, TiAB yielding was achieved for the strengthening cases where the provided development length was greater than the one calculated based on the AASHTO NSM TiAB Guide (based on an average bond strength of 1.0 ksi), i.e., HB40 and HB60. The load level corresponding to concrete crushing was calculated reasonably well by the strength calculated according to the AASHTO NSM TiAB Guide using Equation 2.4. The observed concrete crushing was not a strength-bounding limit state as the peak load for these specimens occurred beyond this load level. The reason for the excess capacity beyond the AASHTO NSM Guide calculated strength was credited to the strain hardening in the reinforcing steel and TiAB at large displacement levels.

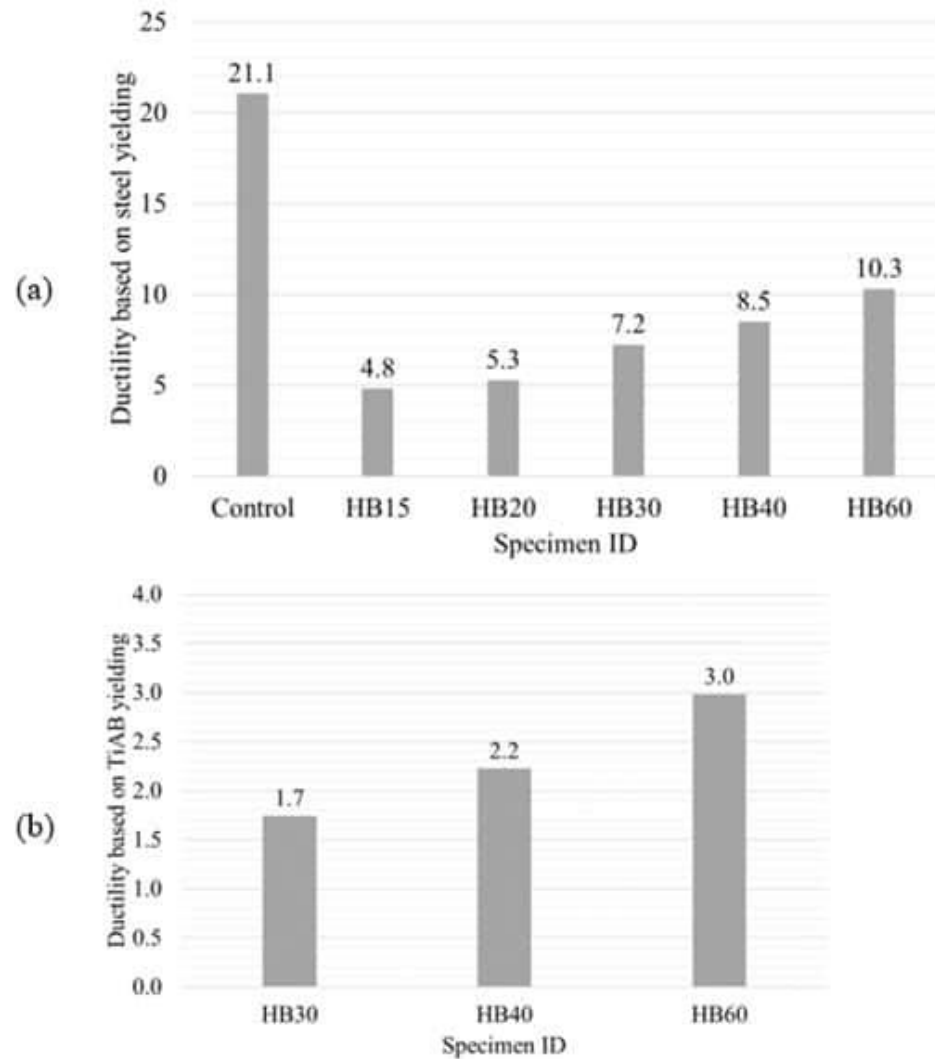


Figure 5-8 Displacement capacity ratio for each specimen: (a) measured from the yielding of the steel; (b) measured from the yielding of the TiAB

Figure 5-9 presents the load levels corresponding to observed concrete crushing and the peak load for the NSM TiAB strengthened specimen with different TiAB bonded lengths. The dashed vertical line indicates the TiAB bonded length calculated based on the AASHTO NSM TiAB Guide development length ($2 \cdot l_{dT}$) for TiAB using 1.0 ksi in Equation 2.5, while the dashed horizontal line is the strength calculated based on Equation 2.4 from the AASHTO NSM Guide using the measured material properties. It can be observed that Equation 2.4 provides an accurate estimate of the strength of the strengthened members HB30, HB40, and HB60. The measured peak loads of specimens HB40 and HB60 exceeded the prediction from Equation 2.4 by about 20 percent due to strain hardening of both the steel reinforcing bars and TiAB.

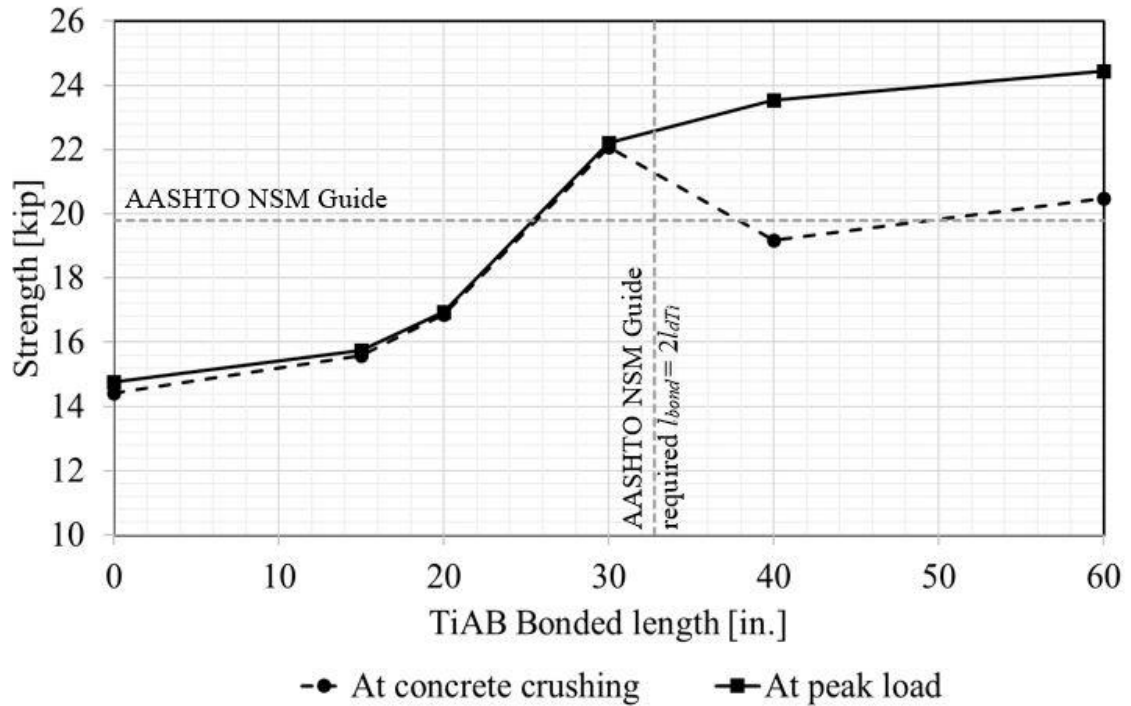


Figure 5-9 Measured load at concrete crushing and peak load for NSM TiAB strengthened specimens

The TiAB bonded length for HB30 was 2¾ in. shorter than the bond length required by the AASHTO NSM Guide based on measured properties. This shorter bonded length translated to a calculated average bond strength equal to 1.09 ksi using Equation 2.5 to achieve yielding in the TiAB (Table 4-1) and 1.08 ksi from the test result (Table 5-3), which was slightly greater than the specified design bond strength of 1.0 ksi. HB30 exceeded the flexural strength calculated according to the AASHTO NSM TiAB Guide, indicating both steel and TiAB yielding and exceeding the 5000 µε tension strain ductility threshold. Despite achieving the TiAB yielding, the specimen did not maintain strength with increasing displacement and exhibited over 20 percent strength loss soon after reaching the peak load. The overall response was found undesirable from a post-peak load behavior perspective which was improved with longer bonded lengths that comply with the development length required by the AASHTO NSM TiAB Guide.

5.2.2 EXPERIMENTAL RESULTS OF STRAIGHT-BONDED SPECIMENS

Table 5-1 calculated the load-carrying capacity of the control and strengthened specimens based on the three methods mentioned in section 5.2.1. The summary of the test results is reported in Table 5-4. The load-displacement values are presented at (i) steel tensile reinforcing bar yielding meaning the bottom longitudinal steel reinforcing bars reaching the measured yield strain of 2345

$\mu\epsilon$ (i.e., f_y/E_s); (ii) steel tensile reinforcing bar reaching 5000 $\mu\epsilon$ - the bottom longitudinal steel reaching 5000 $\mu\epsilon$ corresponded to the tension-controlled behavior requirements that exist in design codes (AASHTO LRFD) to ensure ductile behavior; and (iii) peak load – maximum recorded force in the tests.

Table 5-4 Summary of the experimental results (straight-bonded TiAB)

Specimen ID	$\epsilon_s = \epsilon_y$		$\epsilon_s = 0.005$		Peak Load	
	Displ. (in.)	Force (kip)	Displ. (in.)	Force (kip)	Displ. (in.)	Force (kip)
Control	0.079	6.29	0.19	9.3	3.16	14.74
SB30	0.15	9.58	0.28	13.25	0.39	15.08
SB40	0.14	9.89	0.42	16.83	0.58	18.56
SB60	0.13	9.32	0.22	12.53	1.26	23.15
SB80	0.094	7.92	0.23	12.83	2.41	24.33
SB96	0.14	8.77	0.25	12.85	1.94	23.85

The cracking condition of the specimens at steel yielding, at strain 0.005, and peak load are shown in Figure 5-10 to Figure 5-12 where the black vertical lines on the strengthened specimens represent the end of TiAB. Based on the experimental results in Table 5-4, accompanied by Figure 5-10 to Figure 5-12, the following observations were made:

Yielding of the tensile reinforcing steel: For SB30, SB40, and SB60, tension reinforcement yielded at around 0.15 in. of mid-span displacement and 9.50 kips load. For SB80 and SB96, the tension steel yield at 0.0944 in. of mid-span displacement, 9.50 kips load, and 0.14 in. of mid-span displacement, 9.50 kips load, respectively. The load was approximately 1.5 times higher, and mid-span displacement was about double compared to the control specimen. Pictures of the concrete cracking state from a side view during the yielding of the tensile reinforcing bar are shown in Figure 5-10.

The displacement and load at the instant when the tension steel reached 5000 $\mu\epsilon$ for all the strengthened specimens except SB40 were approximately 0.25 in. of mid-span displacement and 13 kip load, which are significantly higher than those for the control specimen. Specimen SB40 exhibited larger values of displacement and load compared to the other strengthened specimens at this stage. This outlier response was credited to the absence of a central crack where the strain gauges were located. The limiting strain value for the tension-controlled behavior of the AASHTO LRFD (2020) was met for all the specimens shortly after reaching the yielding of the tension steel.

For the SB30 and SB40, the peak load occurred at displacements and loads lower than 20 kips but higher than 14.74 kips (control specimen's peak load). For SB60, the measured peak load is 23.15 kips and a mid-span displacement is 1.26 in. For HS60 and HS80, the peak loads measured around 24 kips and mid-span displacement around 2.5 in. The specimen condition at peak load is shown in Figure 5-12.

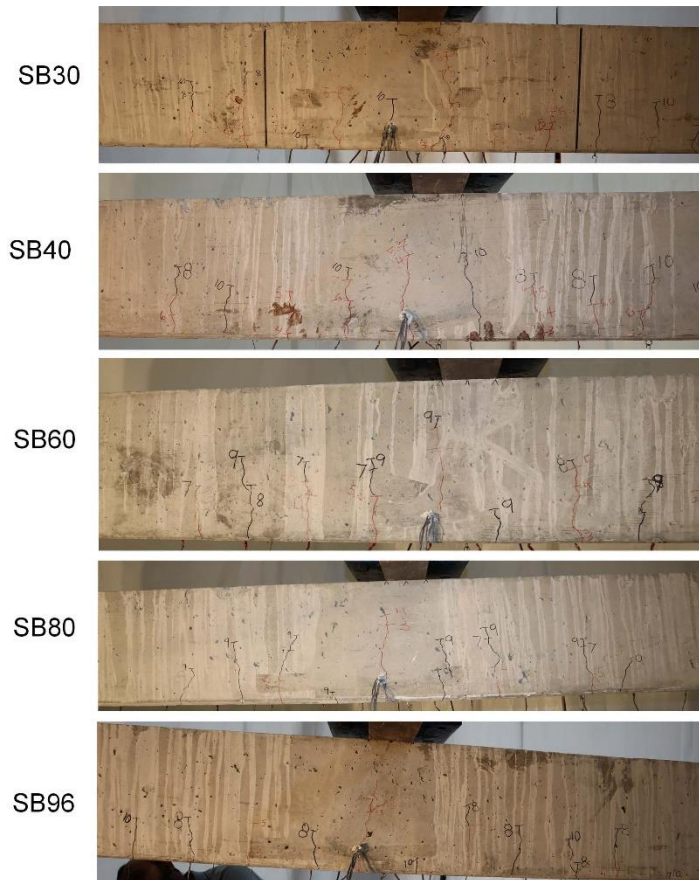
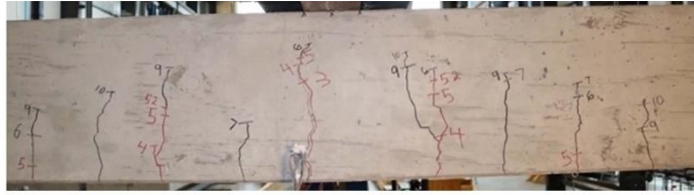


Figure 5-10 Cracking condition of specimens at yielding of the tension reinforcement steel

Control



SB30



SB60



SB80



SB96



Figure 5-11 Cracking condition of specimens at 0.005 steel strain

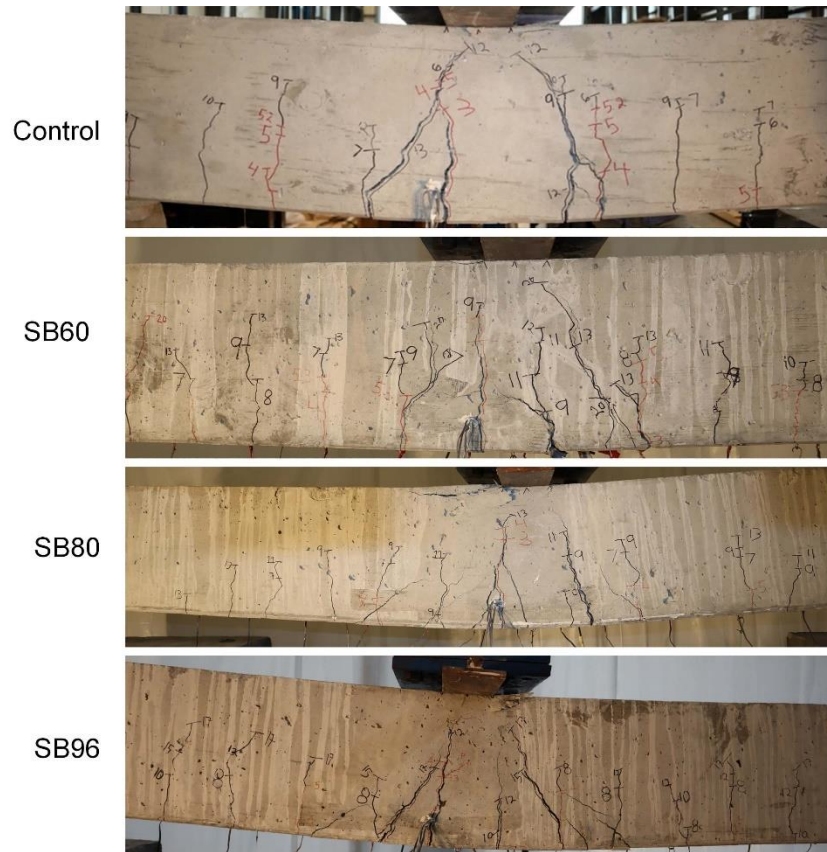


Figure 5-12 Cracking condition of specimens after peak load

5.2.2.1 Behavior and Responses of Straight-bonded Specimens

Figure 5-13 includes the load-displacement response of all five strengthened specimens, as well as the unstrengthened specimen, and the calculated strength based on the AASHTO NSM TiAB Guide (Equation 2.4) using measured yield strength properties (f_y and f_{yTi}). The entire load and displacement response of the beams are presented since the main objective of this research was to identify response limits and study the bond strength.

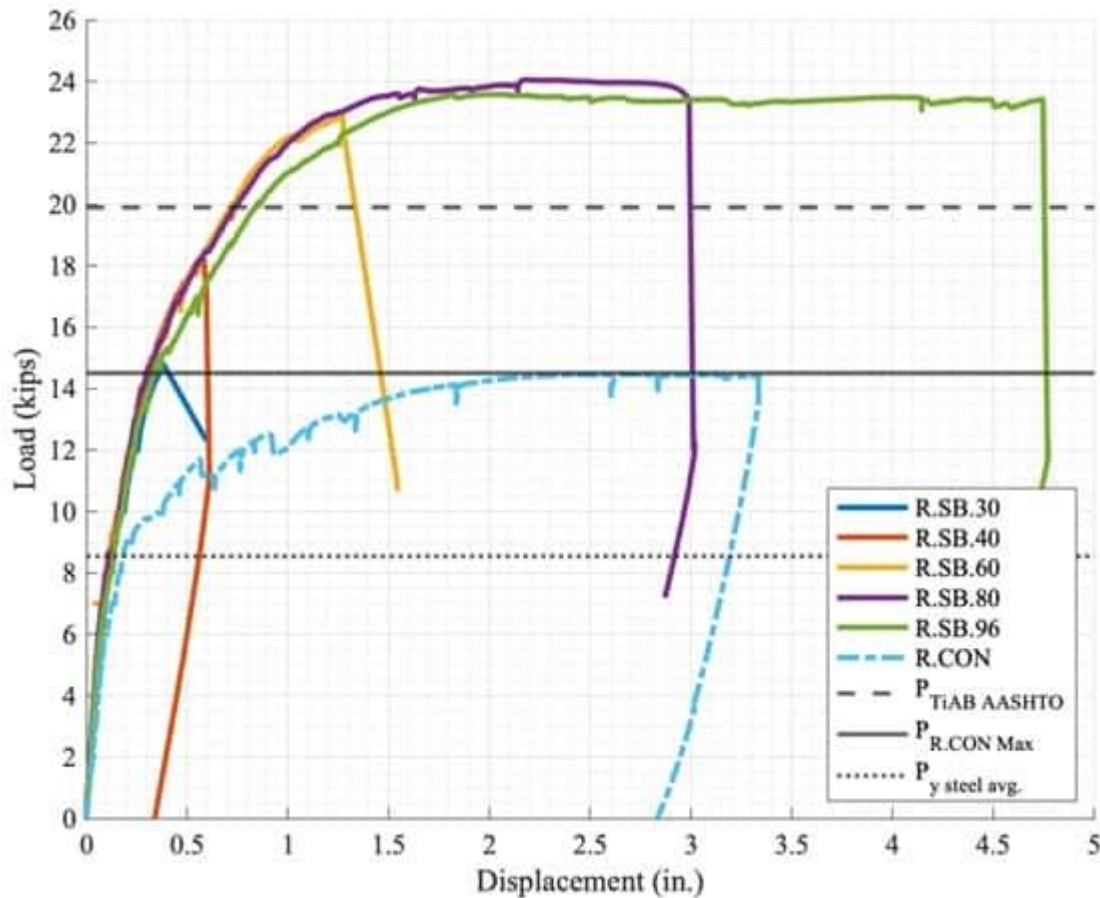


Figure 5-13 Load-displacement response for specimens and AASHTO NSM TiAB Guide strength prediction

The unstrengthened specimen was tested to establish a baseline performance to compare against the specimens strengthened with NSM TiAB. As the applied force initially increased, the flexural cracks formed during the pre-crack load cycle widened, and new cracks formed. The cracks propagated toward the load point and had almost constant spacing that coincided with the stirrup locations. The specimen was loaded until the damage was considered excessive for safely continuing with the test, and the specimen was unloaded after it reached 3.4 in. of mid-span displacement. The control specimen yielded and followed a hardening response, thus exhibiting a tension-controlled failure mode. The peak load was considerably greater than the predictions (i) and (ii) reported in Table 5-1, but corresponded well with the prediction (iii), which indicates that significant strain hardening occurred in the tensile reinforcement, and the tensile strength of the steel reinforcing bars were reached.

Specimen SB30 exhibited linear response until steel yielding (9.58 kips) and up to the applied force of about 13 kips. As the steel yielded, the actuator was in force-control and when the load exceeded the beam's resistance capacity, the actuator pushed the beam for its full stroke and

ruptured the bottom steel abruptly. The peak and failure load was 14.8 kips and 0.47 inches of mid-span displacement before the actuator induced the large deformation. The observed strength was negligibly higher than the control specimen (14.74 kips versus 15.08 kips) and considerably lower than the calculated strength that corresponding to the TiAB and steel rebar yielding (15.08 versus 19.8 kips). The observed failure mode was unclear due to not switching to a slower load rate (displacement-controlled loading) before the specimen failure. Maximum TiAB strain observed 4000 $\mu\epsilon$ before the beam failed ($\epsilon_{yTi} = 8450 \mu\epsilon$).

Specimen SB40 exhibited linear response until steel yielding (9.89 kips) and up to 13 kips. The generated flexural cracks were in a constant spacing until the load of 14 kips. The peak load occurred at 18.56 kips at a mid-span deflection of 0.58 inches. A diagonal crack formed in the left-central portion of the beam, which led to the concrete-epoxy interface delamination failure (Figure 5-14), and the TiAB ruptured. The load dropped suddenly to 11 kips where the beam was unloaded. The measured strength was larger than the control specimen but lower than the calculated strength based on the AASHTO NSM TiAB Guide (18.56 kips vs 19.8 kips). The recorded TiAB strain was 6000 $\mu\epsilon$ before the beam failed ($\epsilon_{yTi} = 8450 \mu\epsilon$).



Figure 5-14 a) Inclined crack formation and b) concrete-epoxy interface delamination of SB40

For specimen SB60, as the load increased, several diagonal cracks propagated from existing flexural cracks. The specimen exceeded the AASHTO NSM TiAB Guide calculated load-carrying capacity for the strengthened specimen by 17%. This strength increase could be credited to the yielding of tensile steel and TiAB. The peak load occurred at 23.15 kips at a mid-span deflection of 1.26 inches when the epoxy in the central portion of the beam fractured suddenly. The beam failed by epoxy rupture and debonding the TiAB after steel and TiAB yielding (Figure 5-15a). Although the strain in the TiAB was recorded at 4553 $\mu\epsilon$ which was less than the yield strain of TiAB 8450 $\mu\epsilon$, the measured capacity indicates that the tensile steel and TiAB yielded.

Specimen HS80 achieved yielding of the steel reinforcing bars and TiAB. Inclined diagonal cracks formed and extended toward the load point. The peak load of this specimen was 24.33 kips

with a mid-span displacement of 2.41 inches. This specimen also exceeded the AASHTO NSM TiAB Guide calculated capacity (19.8 kips) which was calculated (Equation 2.4) based on the yielding of tensile steel and TiAB. Therefore, the additional capacity beyond the calculated capacity could be credited to the strain hardening of tensile steel and yielding of TiAB. The load plateaued (Figure 5-13) was observed at around 24 kips with increasing midspan displacement until the debonding of TiAB and TiAB ruptured (Figure 5-15b) at 23.4 kips and 3.11 inches of displacement.

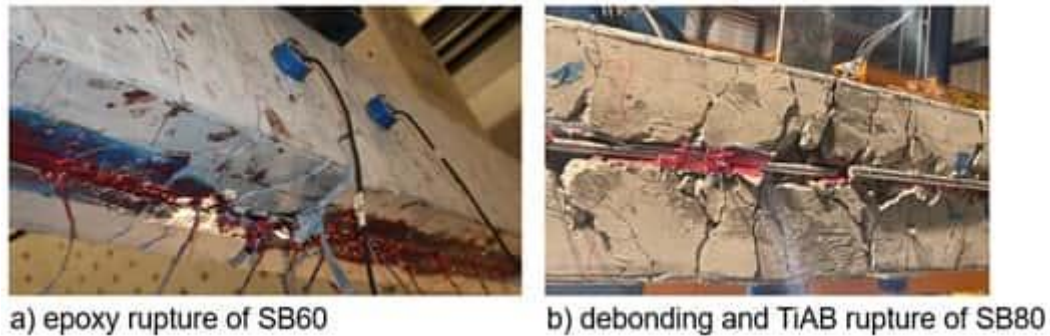


Figure 5-15 a) Epoxy rupture in SB60 and b) debonding and TiAB rupture in SB80

Specimen SB96 demonstrated similar behavior to SB80 while achieving yielding of the tensile steel reinforcing bars and TiAB. Several flexural cracks extended diagonally towards the load point and those diagonal cracks became prominent with increasing load. The peak load was 23.85 kips with a mid-span displacement of 1.94 inches. SB96 also exceeded the AASHTO NSM TiAB Guide calculated capacity by 20.5%, which was calculated (Equation 2.4) based on the yielding of tensile steel and TiAB. Therefore, the additional capacity beyond the calculated capacity could be credited to the strain hardening of tensile steel and yielding of TiAB. The load plateau (Figure 5-13) was observed in the force-displacement response. The central diagonal cracks severely widened and horizontal cracks formed in the shear span of the beam with the increase in load (Figure 5-16). The horizontal crack in the beam traveled along the length of the beam causing spalling of the concrete (23.5 kips and 4.75 inches of mid-span deflection) and leading to the failure of the beam with TiAB debonding.



Figure 5-16 Horizontal crack formation in the shear span of SB96

5.2.2.2 TiAB Bond Strength of Straight-bonded Specimens

To estimate the bond stress for specimens that achieved TiAB yielding, Equations 2.4(b) was employed to back-calculate the corresponding average bond strength to achieve the measured moment capacity. In the calculations, the stress in the steel at peak load was obtained using the yield stress of TiAB ($f_{yTi} = 132$ ksi and $f_{uTi} = 145$ ksi has 13 ksi difference, which was neglected in the calculation) in Equation 2.4, which was approximately 93 ksi, 101.6 ksi, 98 ksi for SB60, SB80, and SB96, respectively. The average bond strength ($\bar{\mu}_{Exp}$) was found using the above-mentioned steel yield stress to achieve the peak moment. Table 5-5 presents the experimental average bond strengths obtained indirectly by back-calculating from the TiAB stress at the peak moment level.

Table 5-5 Bond stress at failure and observed behavior

Specimen ID	l_{bond} (in.)	l_{dTi} (in.)	$\bar{\mu}_{Exp}$ (ksi)	$\bar{\mu}_{used}$ (ksi)	Observed behavior
SB30	30	15	0.66 ^m	1.09	Failure without yielding of TiAB
SB40	40	20	0.91 ^m	0.82	Failure without yielding of TiAB
SB60	60	30	0.56 ^{bc}	0.55	Yielding of TiAB with no softening after peak load
SB80	80	40	0.42 ^{bc}	0.41	Yielding of TiAB with negligible softening after peak load
SB96	96	48	0.35 ^{bc}	0.34	Yielding of TiAB with negligible softening after peak load

Note: m—calculated from measured strain. bc—back-calculated from peak moment and Equation 2.4.

SB30 and SB40 exhibited a premature failure when the maximum strain in the TiAB were 4000 $\mu\epsilon$ and 6000 $\mu\epsilon$, respectively. Therefore, for SB30 and SB40, the average bond strength calculated at the peak moment based on Equation 2.1 was about 0.66 ksi and 0.91 ksi, respectively. The measured strains for SB30 and SB40 proved to not reach yielding due to being well below the yielding strain of the TiAB. The back-calculated bond strength for SB60 at the peak moment was obtained as 0.56 ksi, which corresponded well with the initial prediction reported in Table 5-5. The estimated average bond stresses for specimens SB80 and SB96 that achieved yielding of the TiAB were calculated as 0.42 ksi and 0.35 ksi, respectively, indicating lower bond stress demands that prevented premature bond failure.

5.2.2.3 Displacement Capacity of Straight -bonded Specimens

All tested specimens met the AASHTO NSM TiAB Guide ductility requirement by exceeding the 5000 $\mu\epsilon$ strain limit in the tension-reinforcing steel before failure to ensure tension-controlled behavior. However, to evaluate the ductility characteristics of the NSM TiAB strengthening method, the inelastic displacements capability of the tested specimens were investigated by comparing the achieved deformation capacities without experiencing a significant loss of load-carrying capacity.

Figure 5-17a presents the ratio of the displacement at peak load to the displacement at the initiation of yielding in the tensile reinforcing. The calculated ductility ratios for strengthened specimens were lower than the control specimen but indicated an increasing trend with the longer bonded length of the TiAB (except SB96). Figure 5-17b presents the ratio of the displacement at peak load to the displacement at the initiation of TiAB yielding (only for specimens in which yielding of TiAB was achieved). Since the yielding of the TiAB was not measured directly, the displacement at TiAB yielding was assumed to be equal to the displacement when the load corresponding to the calculated capacity based on the AASHTO NSM TiAB Guide of the strengthened member was reached (i.e., 19.8 kips). Similar observations in terms of improved ductility are made as the peak-to-yielding displacement ratio based on TiAB yielding increases as the TiAB bonded length increases.

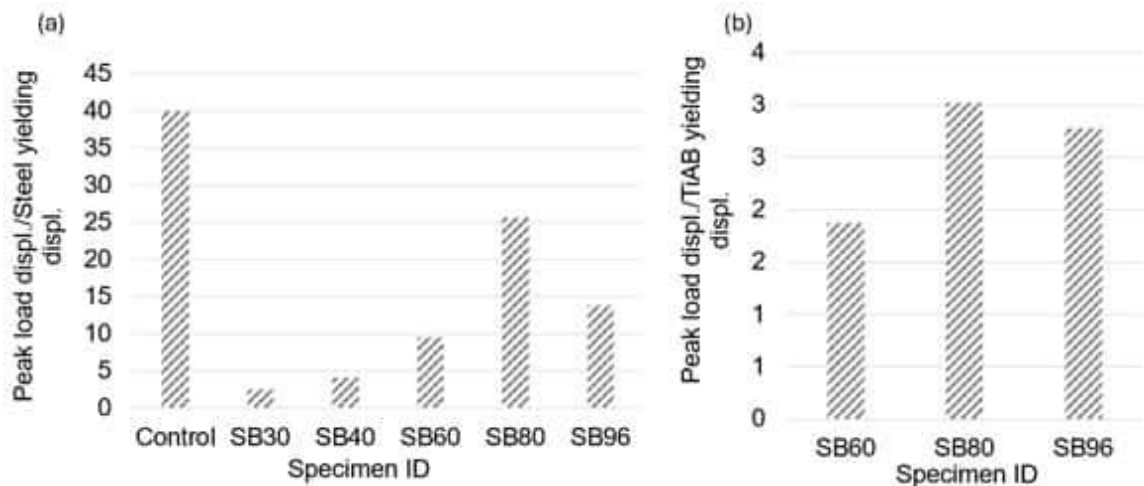


Figure 5-17 Displacement capacity ratio for each specimen: (a) measured from the yielding of the steel; (b) measured from the yielding of the TiAB

5.2.2.4 Discussion of Test Results of Straight -bonded Specimens

The measured strength of the control specimen (14.8 kips) was consistent with calculations based on the assumption that the tensile reinforcing bars reached their tensile strength (f_{us}), which indicates that significant post-yield strain hardening occurred during the tests. Similarly, the measured strengths for SB60, SB80, and SB96 were comparable to the flexural capacity calculated based on assuming that the tensile strength of the reinforcing steel bar (f_{us}) and TiAB (f_{uTi}) were achieved. Additionally, it was also observed that longer bonded TiAB led to an increase in peak load and corresponding displacement.

The specimen SB30, strengthened with the shortest bonded TiAB, failed by TiAB rupture. Similarly, SB40 failed exhibiting a wide diagonal crack, concrete-epoxy delamination, and TiAB rupture. These two specimens exhibited a minor increase in strength relative to the unstrengthened specimen (Table 5-4), and sudden failure occurred. On the other hand, TiAB yielding was achieved for specimens (SB60, SB80, and SB96) where longer bonded TiAB length was provided. The load exceeded the AASHTO NSM TiAB Guide calculated capacity which indicates the yielding of steel and TiAB.

Figure 5-18 presents the load levels corresponding to the peak load for the NSM TiAB strengthened specimen with different TiAB bonded lengths. The dashed horizontal line is the strength calculated based on Equation 2.4 from the AASHTO NSM TiAB Guide using the measured material properties. It can be observed that Equation 2.4 provides an accurate estimate of the strength of the strengthened members SB60, SB80, and SB96. The measured peak loads of these specimens exceeded the prediction from Equation 2.4 due to the strain hardening of both the steel and TiAB.

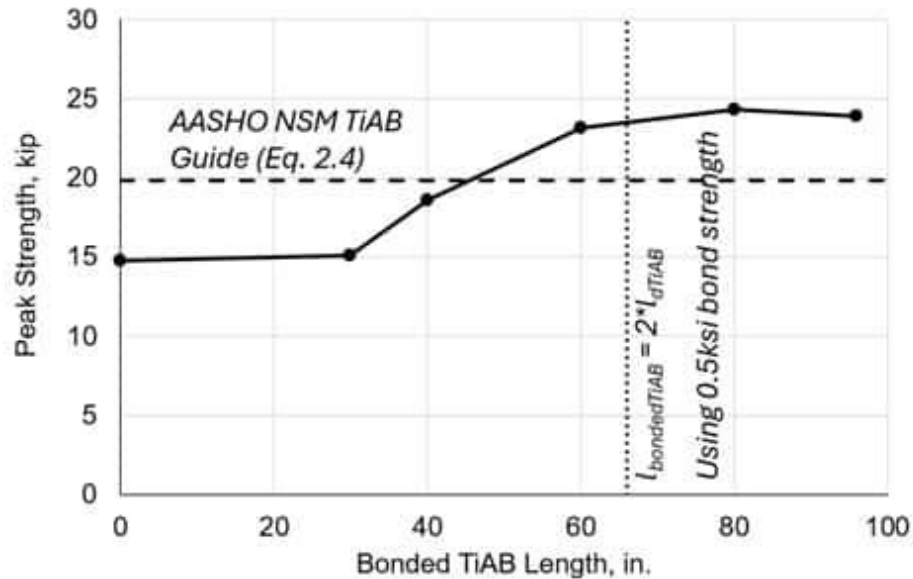


Figure 5-18 Measured load at peak load for NSM TiAB strengthened specimens

The TiAB bonded length for SB60 was 6 inches shorter than the bond length calculated using 0.5 ksi bond strength in the AASHTO NSM TiAB Guide provided equation (Equation 2.5). Specimen SB60 was strengthened providing a bonded TiAB length of 60 inches calculated using 0.55 ksi bond strength. This specimen exceeded the flexural strength calculated according to the AASHTO NSM TiAB Guide, indicating both steel and TiAB yielding and exceeding the 5000 $\mu\epsilon$ tensile steel strain ductility threshold. However, the specimen did not maintain strength with increasing displacement and failed suddenly with TiAB rupture after reaching the peak load.

5.2.3 EXPERIMENTAL RESULTS OF HOOKED-UNBONDED SPECIMENS

Table 5-1 calculated the load-carrying capacity of the control and strengthened specimens based on the three methods mentioned in section 5.2.1. The summary of the test results is reported in Table 5-6. The load-displacement values are presented at (i) steel tensile reinforcing bar yielding meaning the bottom longitudinal steel reinforcing bars reaching the measured yield strain of 2345 $\mu\epsilon$ (i.e., f_y/E_s); (ii) steel tensile reinforcing bar reaching 5000 $\mu\epsilon$ - the bottom longitudinal steel reaching 5000 $\mu\epsilon$ corresponded to the tension-controlled behavior requirements that exist in design codes (AASHTO LRFD) to ensure ductile behavior; and (iv) peak load – maximum recorded force in the tests.

Table 5-6 Summary of the experimental results (hooked-unbonded TiAB)

Specimen ID	$\epsilon_s = \epsilon_y$		$\epsilon_s = 0.005$		Peak Load	
	Displ.	Force	Displ.	Force	Displ.	Force
	in.	Kip	in.	Kip	in.	Kip
Control	0.079	6.29	0.19	9.3	3.16	14.74
HU10	0.18	9.23	0.91	12.31	2.46	14.09
HU30	0.11	7.56	0.37	13.52	0.76	18.25
HU40	0.094	6.91	0.20	10.94	1.37	23.19
HU60	0.140	7.23	0.27	11.01	1.67	23.36

The cracking condition of the specimens at steel yielding, at strain 0.005, and peak load are shown in Figure 5-19 to Figure 5-21 where the black vertical lines on the strengthened specimens represent the end of TiAB. Based on the experimental results in Table 5-6, accompanied by Figure 5-19-Figure 5-21, the following observations were made:

Yielding of the tensile reinforcing steel: For HU10, tensile reinforcement yielded at 6.29 kip of load and 0.18 inches of mid-span displacement; for HU30 it is 7.56 kips and 0.11 inch of mid-span displacement. For HU40 and HU60, tension reinforcement yielded at around 7.0 kips load. Pictures of the concrete cracking state from a side view during the yielding of the tensile reinforcing bar are shown in Figure 5-19.

The displacement and load at the instant when the tension steel reached $5000\mu\epsilon$ for HU40 and HU60, were approximately 11 kips, which are significantly higher than those for the control specimen. Specimens HU10 and HU30 exhibited larger values of displacement and load compared to the other strengthened specimens at this stage. This outlier response was credited to the absence of a central crack where the strain gauges were located. The limiting strain value for the tension-controlled behavior of the AASHTO LRFD (2020) was met for all the specimens shortly after reaching the yielding of the tension steel. The specimen condition at peak load is shown in Figure 5-20.

For Specimens HU40 and HU60, the peak load occurred at 23 kips which is higher than the calculated load (19.8 kips) for strengthened specimens. This indicates that adequate TiAB length was provided for the unbonded strengthening case. Specimens HU10 and HU30 did not exceed the calculated load for strengthened specimens. The specimen condition at peak load is shown in Figure 5-21.

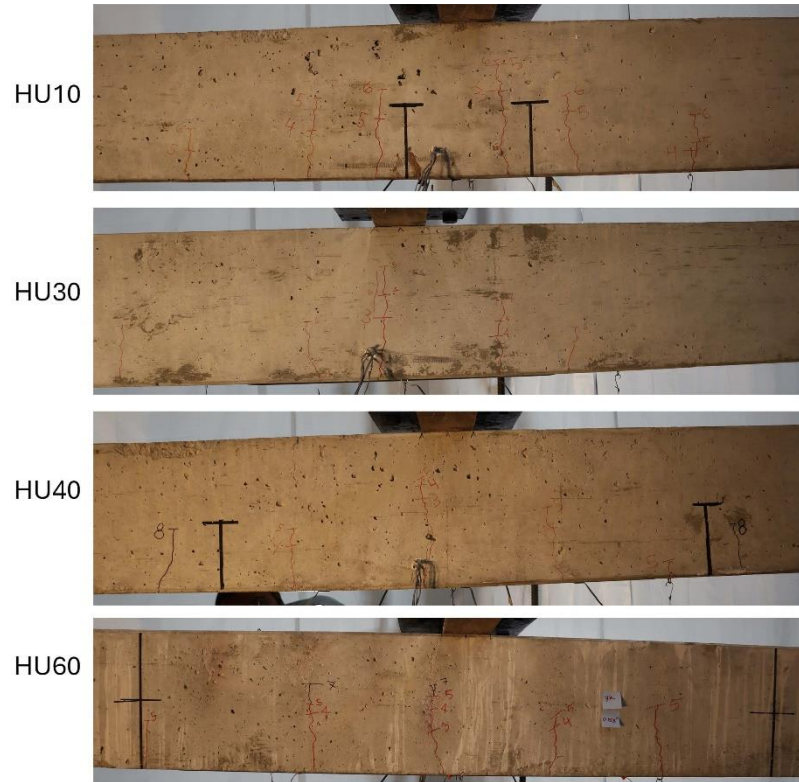


Figure 5-19 Cracking condition of specimens at yielding of the tension reinforcement steel

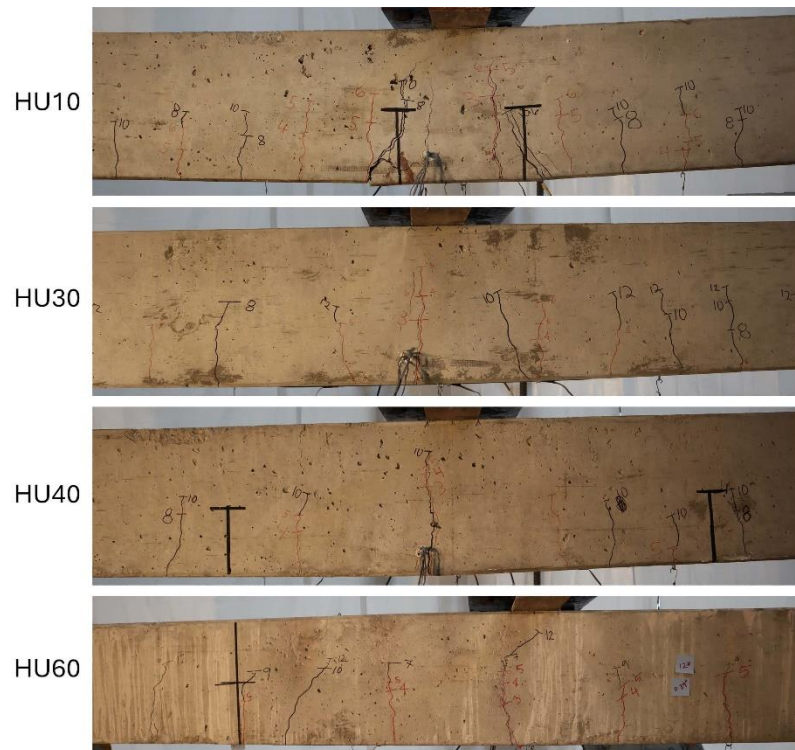


Figure 5-20 Cracking condition of specimens at 0.005 steel strain

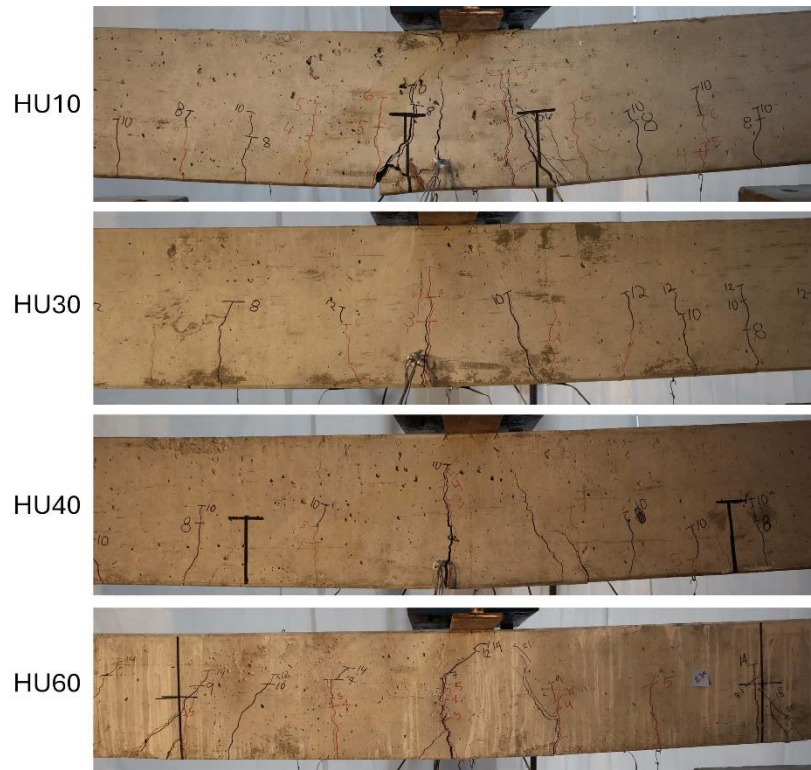


Figure 5-21 Cracking condition of specimens after peak load

5.2.3.1 Behavior and Responses of Hooked-unbonded Specimens

Figure 5-22 includes the load-displacement response of all strengthened specimens, as well as the unstrengthened specimen, and the calculated strength based on the AASHTO NSM TiAB Guide (Equation 2.4) using measured yield strength properties (f_y and f_{yTi}). The entire load and displacement response of the beams are presented since the main objective of this research was to identify response limits and study the influence of TiAB length on the strength.

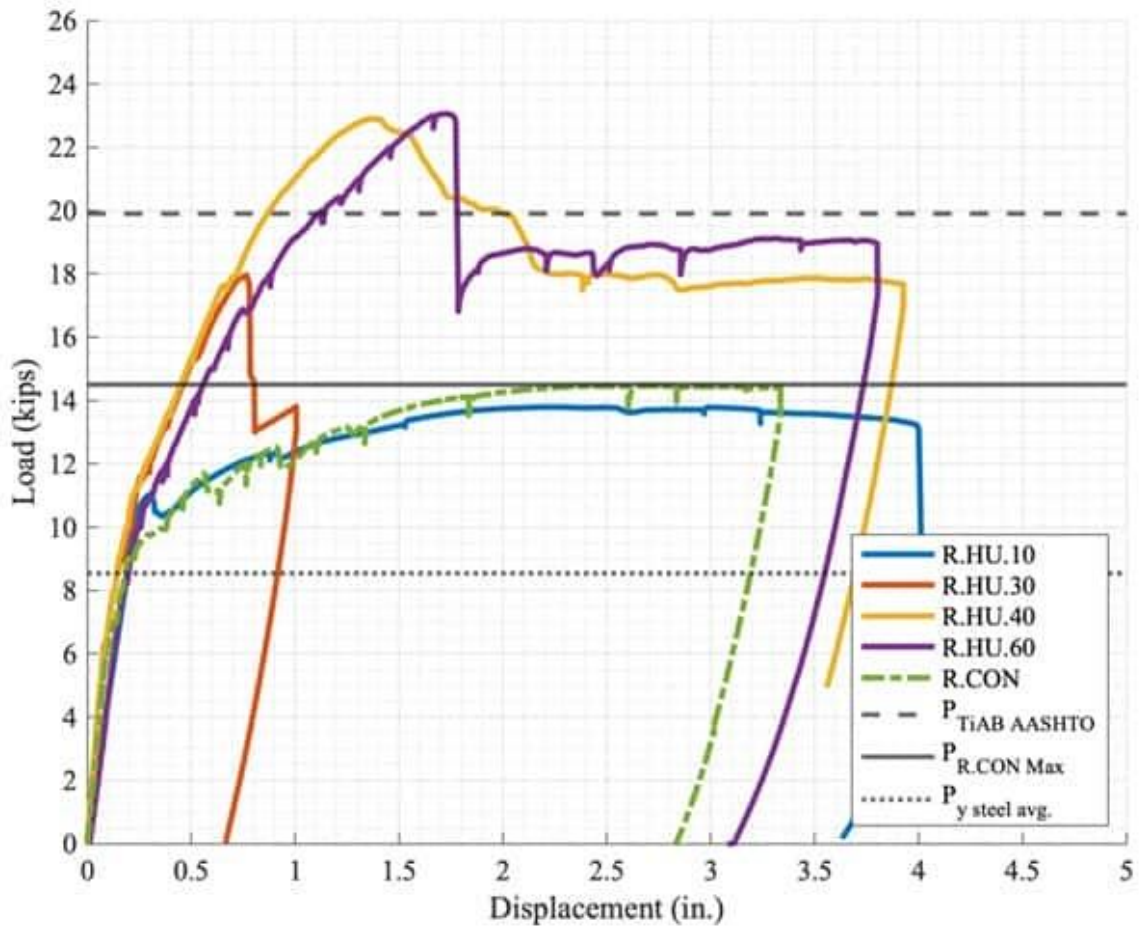
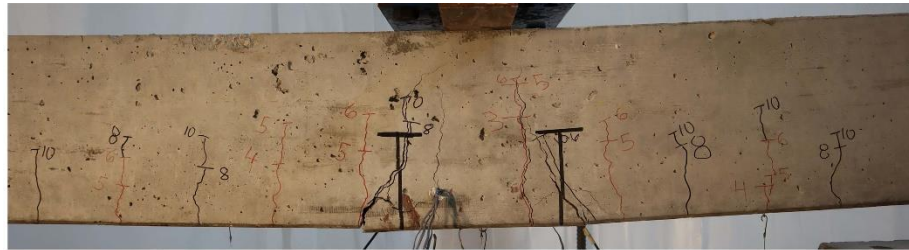


Figure 5-22 Load-displacement response for specimens and AASHTO NSM TiAB Guide strength prediction

The unstrengthened specimen was tested to establish a baseline performance to compare against the specimens strengthened with NSM TiAB. As the applied force initially increased, the flexural cracks formed during the pre-crack load cycle widened, and new cracks formed. The cracks propagated toward the load point and had almost constant spacing that coincided with the stirrup locations. The specimen was loaded until the damage was considered excessive for safely continuing with the test, and the specimen was unloaded after it reached 3.4 in. of mid-span displacement. The control specimen yielded and followed a hardening response, thus exhibiting a tension-controlled failure mode. The peak load was considerably greater than the predictions (i) and (ii) reported in Table 5-1, but corresponded well with the prediction (iii), which indicates that significant strain hardening occurred in the tensile reinforcement, and the tensile strength of the steel reinforcing bars were reached.

Specimen HU10 exhibited linear response even after steel yielding until 11 kips. As the load increased, inclined cracks were generated near crossing the hook ends at 10 kips, and the hooks became ineffective at 11 kips and the load dropped suddenly. These inclined cracks widened with the increase of load which is shown in Figure 5-23. Subsequently, the load-displacement response conversed to that of the control specimen which indicates the ineffectiveness of TiAB. The peak load was 14.09 kips and 2.46 inches of mid-span displacement. The specimen did not exceed the calculated strength of strengthened specimens (19.8 kips) which indicates the ineffectiveness of the provided TiAB length. Maximum TiAB strain observed 1370 $\mu\epsilon$ before the beam failed ($\epsilon_{yTi} = 8450 \mu\epsilon$).



a) Inclined crakes at hook ends (12.7 kips)



b) Widened inclined cracks at 13.8 kips

Figure 5-23 Inclined cracks formation near hook ends of HU10

Specimen HU30 exhibited an almost linear response until steel yielding (9.89 kips) and up to 12 kips. The generated flexural cracks were in a constant spacing aligning with stirrups. The inclined cracks started to form at around 10 kips. At peak load (18.25 kips), a diagonal crack was generated at the hook end on one side of the beam (Figure 5-24), which caused the hook to become ineffective, and the load dropped suddenly. The specimen did not take any more load and the specimen was subsequently unloaded. The recorded TiAB strain was 5930 $\mu\epsilon$ before the beam failed ($\epsilon_{yTi} = 8450 \mu\epsilon$).

Specimen HU40 exhibited an almost linear response until steel yielding (6.91 kips) and up to 11 kips, then the specimen showed a nonlinear response. Similar to the other specimens, the generated flexural cracks were in a constant spacing aligning with the internal stirrups. After the initiation of steel yielding, the cracks widened and propagated towards the load point. The central

crack was the widest. The peak load occurred at 23.19 kips at a mid-span deflection of 1.37 inches. Inclined cracks were also generated at the central region of the beam. At the peak load, the central crack was excessively wide and hairline cracks around the TiAB hook (on one side of the beam) indicated signs of distress (Figure 5-25). The load gradually dropped with increasing midspan displacement and eventually plateaued around 18 kips. The inclined cracks near the central region became wider. The beam was unloaded when the load dropped to 17.7 kips and 3.90 inches of displacement. The recorded TiAB strain was 10,060 $\mu\epsilon$ before the beam failed, and exceeded the yield strain of the TiAB ($\epsilon_{yTi} = 8450 \mu\epsilon$).



Figure 5-24 Inclined cracks formation near hook ends of HU30

Similar to other hooked-unbonded specimens, HU60 exhibited linear response until steel yielding (7.23 kips) and up to 11 kips. Flexural cracks were observed at almost constant spacing between the cracks until the yielding of the steel rebars. The inclined cracks started to generate at around 9 kips at the hook end. Diagonal cracks at the hook ends of the beam are shown in Figure 5-26. The hook became ineffective, and the load dropped suddenly to 17 kips without any noticeable change in the crack pattern on the sides of the beam. The test continued and the load plateaued to 18 kips, and then unloaded at 17.3 kips and a midspan deflection of 3.85 inches. The recorded TiAB strain was 8750 $\mu\epsilon$ before the beam failed ($\epsilon_{yTi} = 8450 \mu\epsilon$).



Figure 5-25 a) Widened and inclined cracks in the central region and b) widened cracks near hook ends of HU40

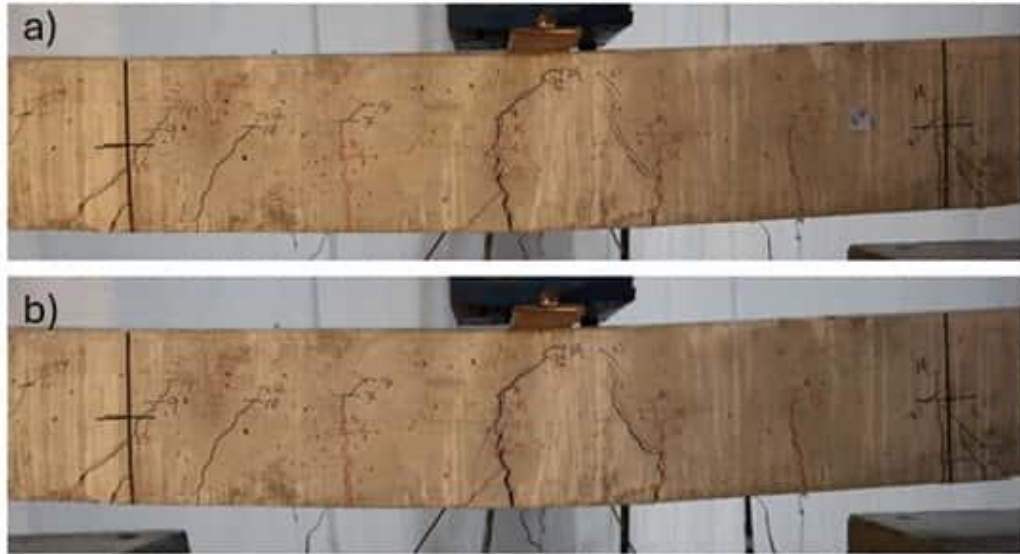


Figure 5-26 Cracking in the beam HU60 (a) at peak load (23.36 kips) (b) after failure

5.2.3.2 Displacement Capacity of Hooked-unbonded Specimens

All tested specimens except HU10 met the AASHTO NSM TiAB Guide ductility requirement by exceeding the 5000 $\mu\epsilon$ strain limit in the tension-reinforcing steel before failure to ensure tension-controlled behavior. HU10 failed before reaching 5000 $\mu\epsilon$. Figure 5-27a presents the ratio of the displacement at the peak load to the displacement at the initiation of yielding in the tensile steel. Figure 5-27b presents the ratio of the displacement at peak load to the displacement at the initiation of TiAB yielding (only for specimens in which yielding of TiAB was achieved). From the figure, the strengthened specimen showed ductility which indicates significant plastic deformation occurs before failure.

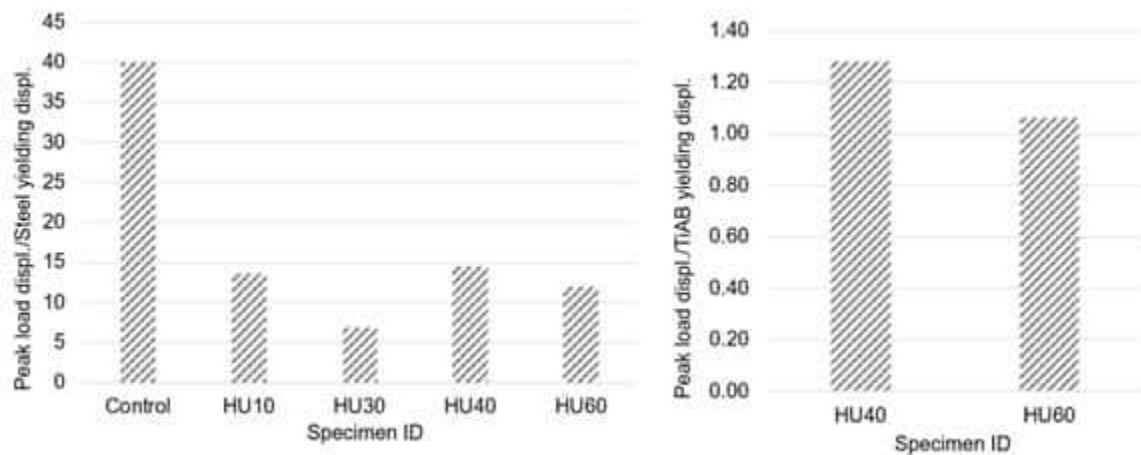


Figure 5-27 Displacement capacity ratio for each specimen: (a) measured from the yielding of the steel; (b) measured from the yielding of the TiAB

5.2.3.3 Discussion of Test Results of Hooked-unbonded Specimens

HU10 and HU30 failed before reaching AASHTO NSM TiAB Guide calculated capacity showing anchorage failure. Two other specimens, HU40 and HU60, exceeded the AASHTO NSM TiAB Guide calculated capacity. The measured TiAB strain in HU40 and HU60 are 10060 $\mu\epsilon$ and 8750 $\mu\epsilon$, respectively, which exceeded the TiAB yield strain ($\epsilon_{yTi} = 8450 \mu\epsilon$). The summary of the test results is shown in Table 5-7. It is also notable that HU60 achieved about the same capacity with the longer TiAB length and larger hook bend diameter of 4.5 inches compared to the standard 3-inch hooked bend diameter of HU40. Compared to the bonded specimens, the hooked unbonded specimens displayed larger cracks at lower displacements and exhibited lower stiffness. A comparison of the crack width with hooked-bonded and straight-bonded tested specimens at the same load is shown in Table 5-8.

Table 5-7 Summary of test results

Specimen ID	l_{bond} (in.)	Peak load (Kip)	Mid-span displacement at peak load (in.)	Observed behavior
HU10	10	14.09*	2.46*	Failed without yielding of TiAB
HU30	30	18.25	0.76	Failed without yielding of TiAB
HU40	40	23.19	1.37	Yielding of TiAB with negligible softening after peak load
HU60	60	23.36	1.67	Yielding of TiAB and sudden drop of load after peak load

*Peak load and mid-span displacement after anchorage failure

Table 5-8 Crack width comparison

Specimen ID	Load, kip	Crack width, in.
HB30		0.008
SB30	10	0.008
HU30		0.02
HB40		0.008
SB40	8	0.008
HU40		0.016
HB60		0.012
SB40	10	0.016
HU60		0.025

5.3 SUMMARY OF TESTED SPECIMENS

Figure 5-28 illustrates the load versus displacement of all the specimens. This figure indicates the consistent behavior before the initial softening for all beams.

The hooked-bonded specimens that had a TiAB development length of 15 in. (1.09 ksi of bond strength) and longer (bond strength < 1.09 ksi) exhibited desirable responses by achieving TiAB yielding, exceeding the nominal strength calculated based on NSM TiAB, and sustaining large

deformations at peak load levels after the yielding of both steel and TiAB. After undergoing significant deformation beyond the yielding of the bars, the specimens eventually either failed with titanium or epoxy rupture, which were sudden failure modes. Having the hooked ends significantly reduced the bonded length required to achieve the yielding of the TiAB.

Similarly, the straight-bonded specimens that had a TiAB development length of 30 in. (0.55 ksi of bond strength) and longer (bond strength < 0.55 ksi) exhibited desirable responses by achieving TiAB yielding, exceeding the nominal strength calculated based on NSM TiAB, and sustaining large deformations at peak load levels after the yielding of both steel and TiAB. Specimen SB80 failed due to TiAB rupture, indicating that the straight-bonded anchorage method can be utilized to achieve the full-strength from the TiAB, if sufficient embedment length is provided.

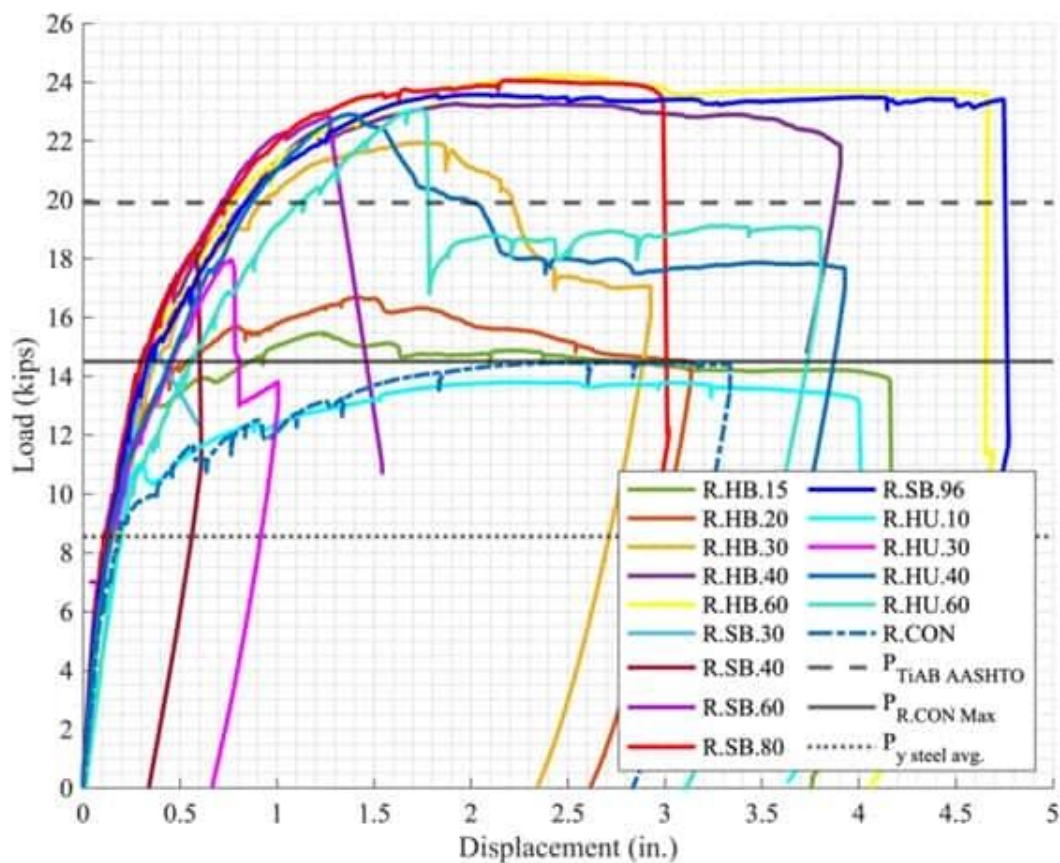


Figure 5-28 All Specimens Load versus Displacement Response

The hooked-unbonded specimens were capable of achieving plastic capacities similar to the bonded tests. Specimens HU40 and HU60 achieved the capacity calculated from Equation 2.4. Despite being able to achieve high resistance, the loads were not sustained through large displacements and indicated wide cracking that would be excessive for crack-controlling limits.

HB30, SB60, HU40, and HU60 all exhibited TiAB yielding, but without a post-peak plateau. HB40, HB60, SB80, and SB96 exhibited TiAB yielding with a post-peak plateau. Equation 2.4 in the AASHTO NSM TiAB guide assumes TiAB yielding when accounting for the titanium alloy contribution when calculating the nominal moment capacity. Therefore, the TiAB was considered to have yielded when the specimen achieved the strength calculated by the AASHTO NSM TiAB guide. Figure 5-29 illustrates each anchorage method's peak load versus TiAB length and Figure 5-30 depicts the displacement at failure for each beam that the TiAB yielded.

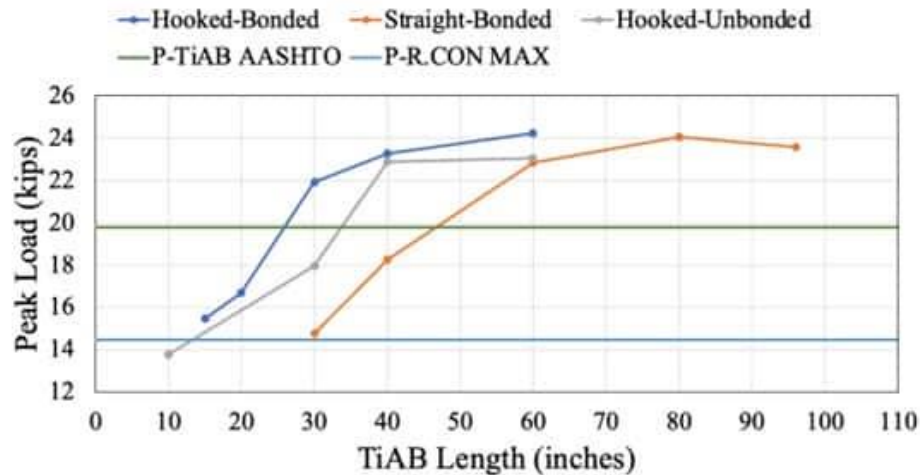


Figure 5-29 Peak Load versus TiAB Length for all Anchorage Methods

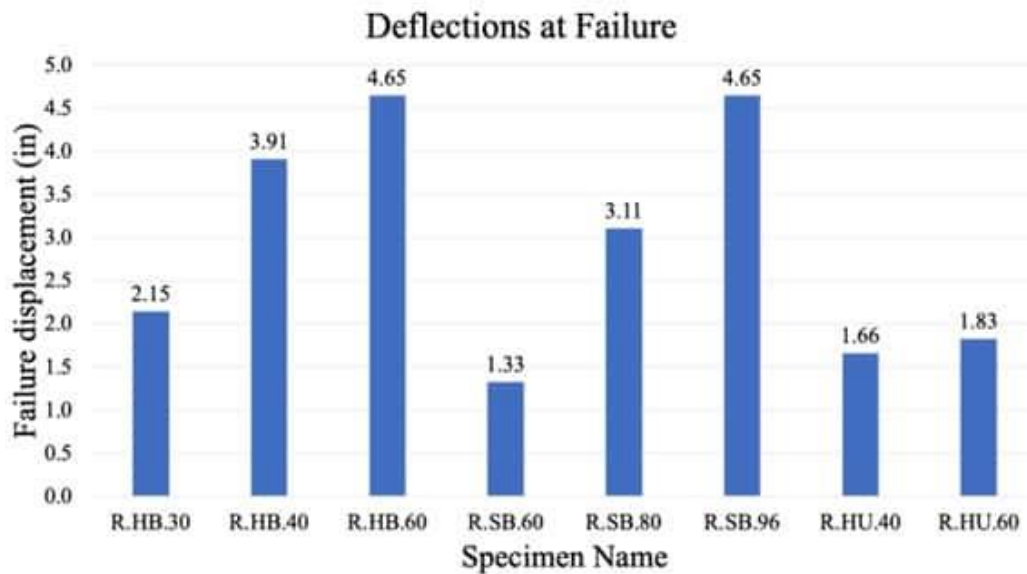


Figure 5-30 Deflections at Failure for Specimens that reached TiAB Yielding

These figures indicate that the bonded bars achieved larger inelastic deflections prior to failure with increasing embedment length. The loads achieved during these tests exceeded the calculated

nominal capacities while using measured material properties. Table 5-9 displays the calculated strengths; including the strengths of the control specimen, and the strengths of the beams that exceeded the AASHTO calculated capacity.

The measured strength of the control beam (Control) was 4.9 kips greater than the nominal flexural strength, calculated based only on the yielding of the steel reinforcing bars and assuming a rectangular stress block for concrete in compression. Similarly, HB60 was the specimen with the greatest flexural capacity after strengthening, and achieved 4.4 kips greater than the AASHTO calculation based on assuming yielding of both the steel reinforcing bar and TiAB, along with an assumed rectangular stress block for concrete in compression.

Table 5-9 Strength Comparison to Control

Specimens Name	Nominal Strength Based on Eq. 2.4 (kip)	Measured Strength (kip)	Strength Increase from Control
Control	9.6	14.5	N.A.
HB30	19.8	21.9	7.4
HB40	19.8	23.3	8.8
HB60	19.8	24.2	9.7
SB60	19.8	22.8	8.3
SB80	19.8	24.1	9.6
SB96	19.8	23.6	9.1
HU40	19.8	22.9	8.4
HU60	19.8	23.1	8.6

The reason for the increased measured strengths exceeding the calculated capacities is uncertain, but could be due to the variations in the support restraints (pin-pin type support versus pin-roller), contribution from strut and tie (arching) mechanism formation due to low aspect ratio, or the concentrated loads used in three-point loading test. Therefore, the measured strengths that exceeded the calculated capacities potentially discredit the AASHTO calculated capacity as an indicator of TiAB yield. The increase in member strengths due to TiAB yielding was calculated to contribute about 10.2 kips. As shown in Table 5-9, this calculated strength increase was consistent with the increase in strength observed for the strengthened specimens relative to the control specimen (Control).

5.4 RESULTS AND DISCUSSION OF HOOKED-BONDED SPECIMENS

The hooked-bonded specimens had increasing peak loads and failure displacements as the embedded/bonded length increased. This indicates better bond performance as the bonded length increased. HB30, HB40, and HB60 achieved the yielding of the TiAB and exceeded the AASHTO nominal moment capacity. The calculated capacities, peak and failure loads, peak and failure displacements, peak moments, and the maximum curvatures observed for each specimen are presented in Table 5-10. The load-displacement responses of the hooked-bonded specimens are plotted against the TiAB embedded length is plotted in Figure 5-29.

The AASHTO NSM TiAB guide uses 1.0 ksi of average bond strength to determine the minimum length to achieve TiAB yielding (development length) for bonded TiAB with hooked anchorages. HB30 was intended to represent approximately 1.0 ksi of average bond strength with a 15 in. development length. Using Equation 2.4 and the measured TiAB yield strength obtained from testing (131 ksi), HB30 was associated with 1.09 ksi of average bond strength. Even at this slightly higher average bond strength (shorted bonded length), the AASHTO calculated capacity of the beam was exceeded, which indicated yielding of the TiAB. This support the conclusion that the AASHTO recommended effective bond strength of 1.0 ksi to reach the member capacity with TiAB yielding is conservative. However, the ductile response that makes NSM TiAB advantageous over other strengthening methods (e.g., FRP strengthening) was better exhibited for the specimens with longer embedment lengths that corresponded to lower assumed average bond stresses ($l_d = 20$ [HB40], $\bar{\mu} = 0.82$ ksi and $l_d = 30$ [HB60], $\bar{\mu} = 0.55$ ksi).

Table 5-11 provides the failure mode, average bond strengths, development lengths, and the TiAB yielding based on the tests results of the hooked-bonded specimens. HB15 and HB20 did not reach the AASHTO NSM TiAB moment capacity, and therefore the associated bond strengths of 2.18 and 1.64 ksi, respectively, were not achieved. Figure 5-31 displays the load versus displacement response curves for the hooked-bonded TiAB test specimens.

Table 5-10 Hooked-Bonded Load and Displacements

Specimen	AASHTO Capacity, kip	Peak Load, kip	Deflection at Peak Load, in.	Load at Failure, kip	Deflection at Failure Load, in.	Peak Moment, k-in.	Maximum Curvature, in ⁻¹
Control	9.6	14.47	2.89	14.4	3.39	391	-
HB15	19.8	15.47	1.31	14.69	1.69	418	0.012
HB20	19.8	16.69	1.48	15.85	2.04	451	0.012
HB30	19.8	21.93	1.8	20.84	2.15	592	0.009
HB40	19.8	23.26	2.01	22.1	3.91	628	0.014
HB60	19.8	24.22	2.54	23.6	4.65	654	0.025

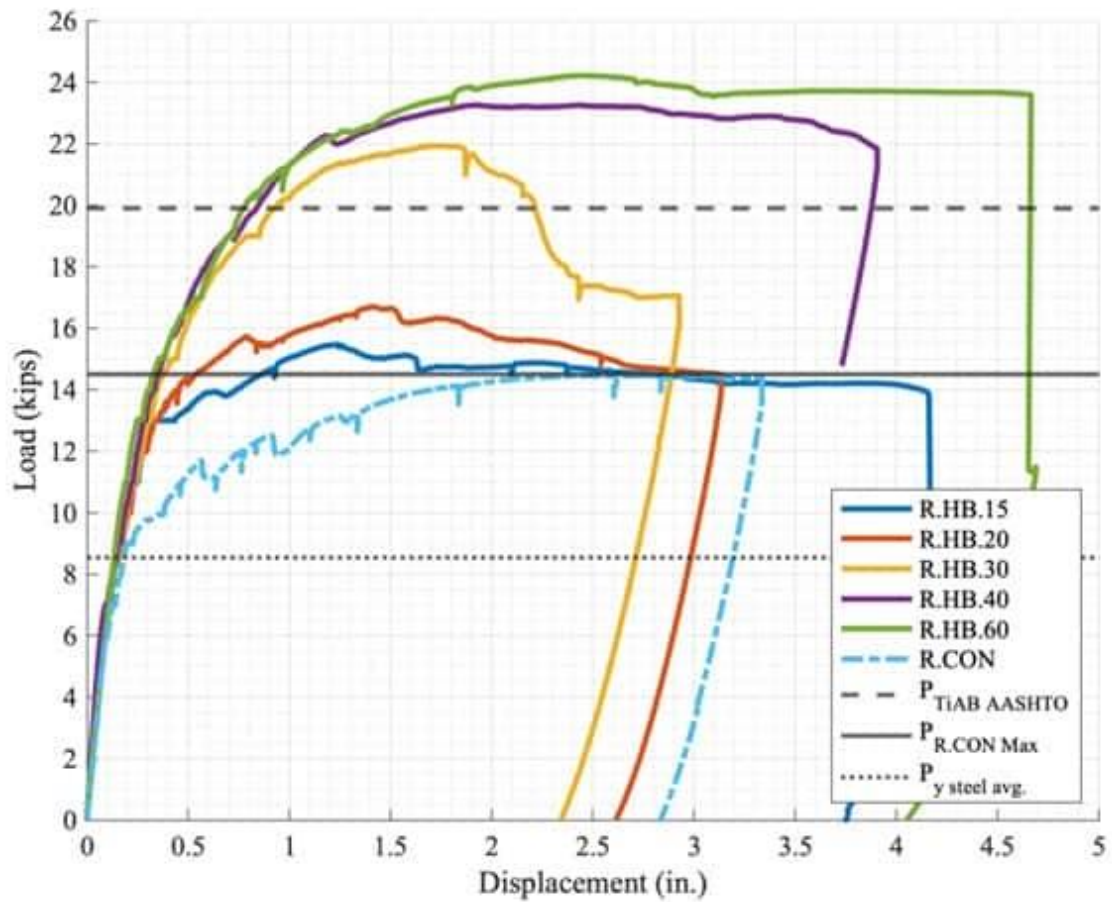


Figure 5-31 Hooked-Bonded TiAB Load versus Displacement

Table 5-11 Summary of Hooked-Bonded TiAB Results

Specimen	Failure Mode	Assumed Average Bond Strength (ksi)	l_d (in.)	TiAB Yield
HB15	Excessive Damage	2.18*	7.5	No
HB20	IC Debonding	1.64*	10	No
HB30	IC Debonding	1.09	15	Yes
HB40	CDC Debonding	0.82	20	Yes
HB60	TiAB Rupture	0.55	30	Yes

*These values were not achieved. IC – intermediate crack, CDC – critical diagonal crack.

5.5 RESULTS AND DISCUSSION OF STRAIGHT-BONDED SPECIMENS

The straight-bonded specimens had increasing failure load and displacements as the embedded length increased. SB60, SB80, and SB96 achieved yielding of the TiAB by exceeding the calculated AASHTO load capacity. The peak and failure loads and displacements are presented in Table 5-12. The peak load variation against the TiAB embedded length is plotted in Figure 5-29.

Table 5-13 provides the failure mode, average bond strengths, development lengths using Equation 2.5, and the TiAB yielding based on the tests results. 0.5 ksi was expected to be the required bond strength to achieve yielding of the TiAB. SB60 demonstrated that an average bond strength of 0.55 ksi for straight-bonded TiAB would reach the nominal AASHTO flexural capacity given in Equation 2.4. This proves that 0.5 ksi can be considered as a reasonable effective bond strength to reach the member capacity and yield the TiAB. However, the ductile response that makes NSM TiAB advantageous over other strengthening methods (e.g., FRP strengthening) was better exhibited in the longer embedment lengths/lower bond strengths ($l_d = 40$ [SB80], $\bar{\mu} = 0.41$ ksi and $l_d = 48$ [SB96], $\bar{\mu} = 0.34$ ksi). SB30 and SB40 did not achieve the expected capacity and therefore the associated calculated bond strengths of 1.09 ksi and 0.82 ksi, respectively, were not achieved. Figure 5-32 displays the load versus displacement response curves for all the straight-bonded specimens.

Table 5-12 Straight-Bonded Loads and Displacements

Specimen	AASHTO Capacity, kip	Peak Load, kip	Deflection at Peak Load, in.	Load at Failure, kip	Deflection at Failure Load, in.	Peak Moment, k-in.	Maximum Curvature, in ⁻¹
Control	9.6	14.47	2.89	14.4	3.39	391	-
SB30	19.8	14.77	0.47	14.77	0.47	399	0.001
SB40	19.8	18.26	0.67	17.44	0.68	493	0.001
SB60	19.8	22.84	1.33	22.73	1.33	617	0.003
SB80	19.8	24.06	2.31	23.40	3.11	650	0.012
SB96	19.8	23.60	1.86	23.40	4.65	637	0.016

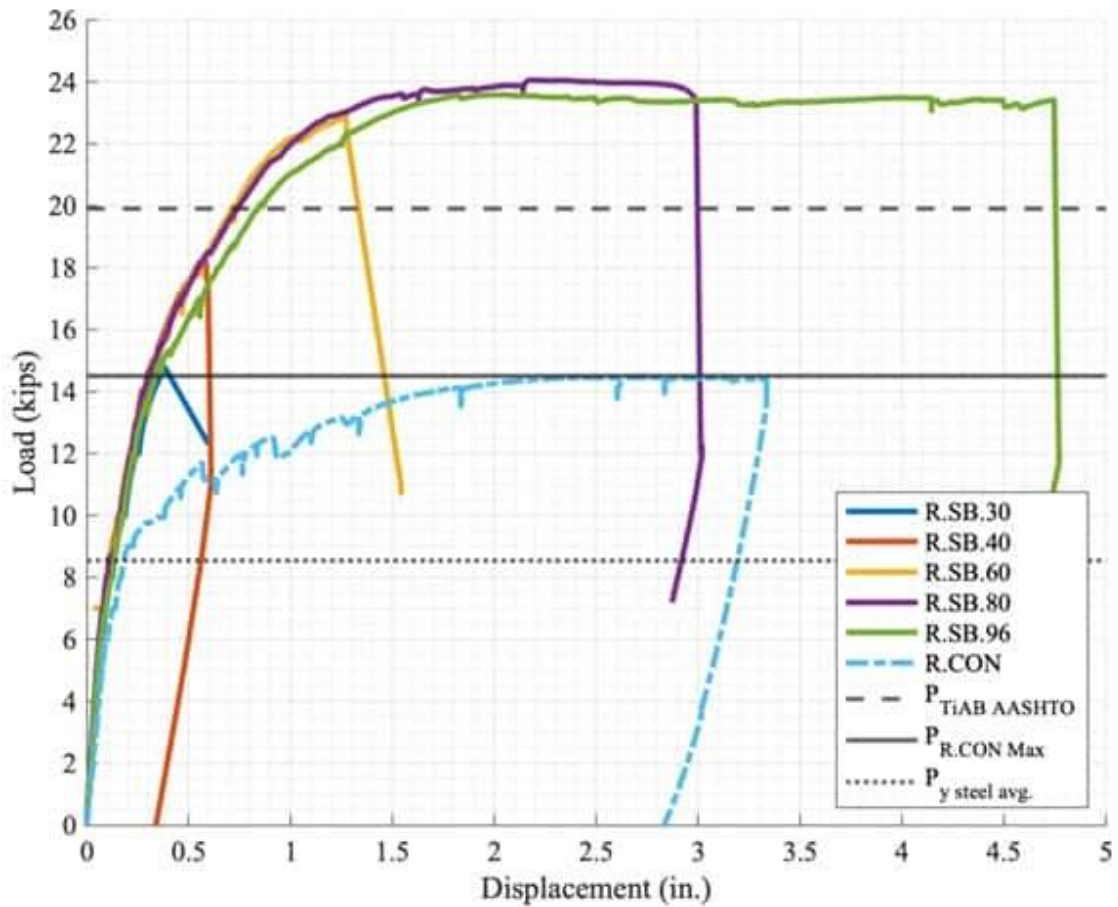


Figure 5-32 Straight-Bonded Load versus Displacement

Table 5-13 Straight-Bonded Yield Results

Specimen	Failure Mode	Assumed Average Bond Strength (ksi)	ld (in.)	TiAB Yield
SB30	Indeterminate	1.09*	15	No
SB40	CDC Debonding	0.80*	20	No
SB60	Epoxy Rupture	0.55	30	Yes
SB80	TiAB Rupture	0.41	40	Yes
SB96	Concrete Failure/Epoxy Shatter	0.34	48	Yes

*These values were not achieved, CDC – critical diagonal crack

5.6 RESULTS AND DISCUSSION OF HOOKED-UNBONDED SPECIMENS

HU40 and HU60 achieved TiAB yielding and exceeded the AASHTO NSM TiAB calculated capacity of the beam. The peak and failure loads and displacements, maximum curvature, and yielding of the TiAB are presented in Table 5-14. The peak load variation against the TiAB length is plotted in Figure 5-29. The trend indicates that the longer lengths achieved greater capacity.

It is also notable that HU60 achieved about the same capacity with the longer length and larger hook bend diameter of 4.5 inches compared to the standard 3-inch hooked bend diameter of HU40. The hooked unbonded specimens displayed larger cracks at lower displacements than the bonded specimens and exhibited lower stiffness. This is consistent with the research observed by Eric Vavra (2016) discussed in chapter 2. Figure 5-33 displays the load versus displacement response curves for all the hooked-unbonded specimens.

Table 5-14 Hooked-Unbonded Loads and Displacements

Specimen	AASHTO Capacity, kip	Peak Load, kip	Deflection at Peak Load, in.	Load at Failure, kip	Deflection at Failure Load, in.	Peak Moment, k-in.	Maximum Curvature, in ⁻¹	TiAB Yield
Control	9.6	14.47	2.89	14.4	3.39	391	-	N.A.
HU10	19.8	13.80	2.29	13.05	4.03	373	0.019	No
HU30	19.8	17.96	0.87	17.49	0.85	485	0.003	No
HU40	19.8	22.89	1.44	21.75	1.66	618	0.010	Yes
HU60	19.8	23.06	1.79	22.81	1.83	623	0.008	Yes

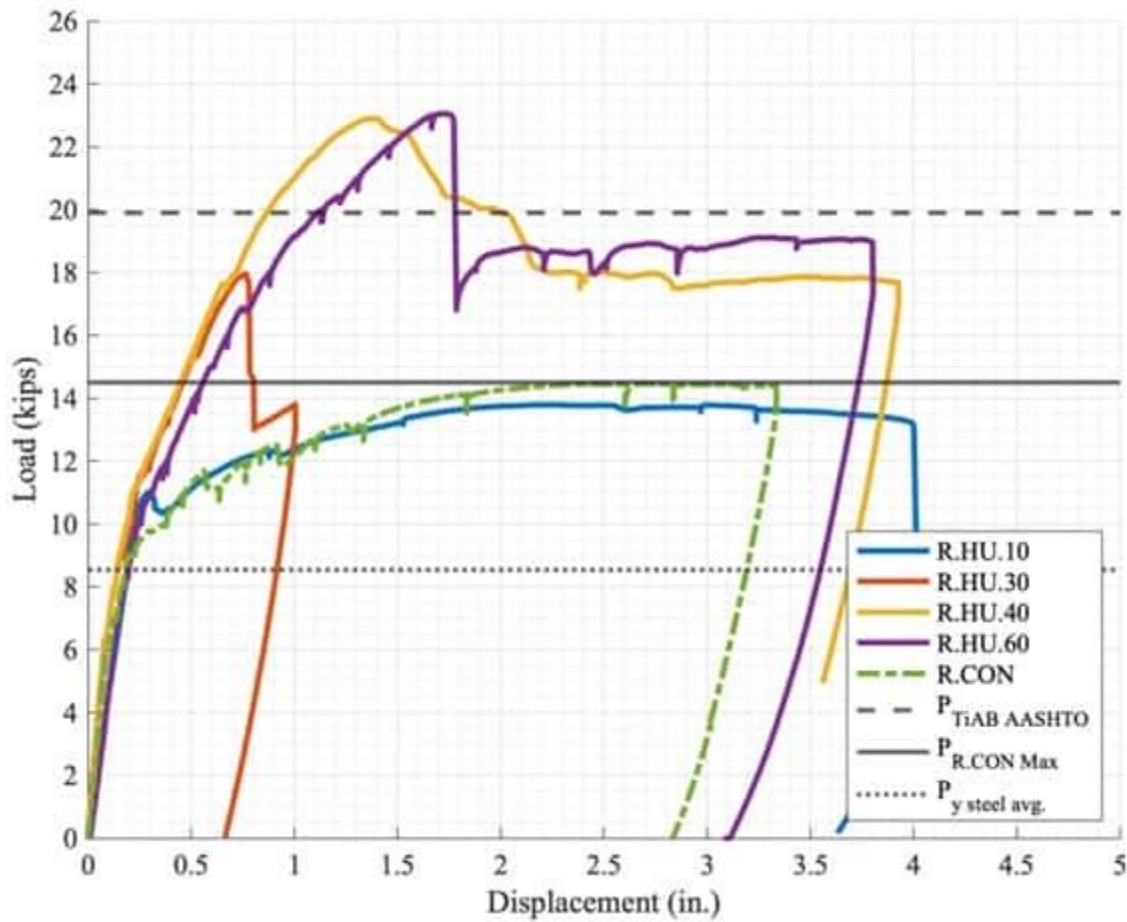


Figure 5-33 Hooked-Unbonded Load versus Displacement

5.7 SUMMARY AND CONCLUSIONS OF PHASE 1 TESTING

5.7.1 HOOKED-BONDED SPECIMENS

The hooked-bonded specimens exhibited increased peak loads and failure displacements as the bonded length increased, indicating improved bond performance with longer bonded lengths. Specimens HB30, HB40, and HB60 achieved TiAB yielding and exceeded the calculated capacity as per the AASHTO NSM TiAB Guide. The following conclusions can be drawn from the results of hooked-bonded specimens:

1. The AASHTO NSM TiAB Guide provides an accurate estimate of the flexural strength of strengthened members when sufficient TiAB bonded length is provided.
2. Specimens that achieved TiAB yielding exceeded the AASHTO NSM Guide predictions due to strain hardening of both the steel reinforcing bars and TiAB.

3. A TiAB bond strength of 1.0 ksi for appears to be reasonable for the hooked-bonded method because specimens with longer bonded lengths than the TiAB development length resulted in ductile load-displacement behavior, indicating that the AASHTO recommended bond strength is conservative.
4. Specimens with shorter bonded lengths did not achieve TiAB yielding, resulting in only marginal improvements in load-carrying capacity.
5. The specimen with a TiAB bonded length slightly less than the development length required by the AASHTO NSM Guide (i.e., HB30) achieved TiAB yielding before debonding occurred; however, the specimen did not sustain the high load levels at larger displacements and exhibited over a 20 percent strength loss soon after reaching the peak load.

5.7.2 STRAIGHT-BONDED SPECIMENS

The straight-bonded specimens also showed an increase in failure load and displacements with longer bonded lengths. Specimens SB60, SB80, and SB96 achieved TiAB yielding and exceeded the AASHTO NSM TiAB Guide's calculated capacity. The following conclusions can be drawn from the results of hooked-bonded specimens:

1. The AASHTO NSM TiAB Guide accurately predicts the strength of members with adequate bonded length.
2. Specimens with longer TiAB bonded lengths achieved TiAB yielding and exhibited desirable ductile behavior, while those with shorter TiAB bonded lengths did not.
3. A TiAB bond strength of 0.5 ksi appears to be reasonable for the straight-bonded method, though further experimental studies to check the fatigue performance of this method are recommended.

5.7.3 HOOKED-UNBONDED SPECIMENS

The hooked-unbonded specimens HU40 and HU60 achieved TiAB yielding and exceeded the calculated capacity of the beam, though HU60 performed similarly to HU40 despite having a longer length and larger hook bend diameter. The specimens displayed larger cracks at lower displacements and exhibited lower stiffness compared to the bonded TiAB specimens, indicating that the hooked-unbonded method may be better suited for temporary purposes. The following conclusions can be drawn from the results of hooked-unbonded specimens:

1. The AASHTO NSM Guide's strength predictions were achieved when adequate TiAB unbonded lengths are provided.

2. Longer TiAB lengths resulted in TiAB yielding and exceeded the calculated capacity, but the specimens could not maintain the load for extended periods.
3. The hooked-unbonded specimens displayed larger crack widths than the hooked-bonded and straight-bonded specimens and exhibited lower stiffness. Therefore, it is recommended to use the hooked-unbonded strengthening method only for temporary purposes.

Chapter 6

SPECIMEN AND TEST SETUP DETAILS FOR PHASE 2

6.1 INTRODUCTION

An overview of the specimen design and construction, instrumentation, test setup, strengthening of the specimens, and testing protocol for phase 2 are presented in this chapter.

6.2 TEST MATRIX

The experimental study of member-level tests (phase 2) focused on investigating the flexural behavior of full-scale bridge girders strengthened with near-surface mounted (NSM) TiABs. A total of 16 specimens were constructed for the purpose of positive- and negative-moment strengthening. Seven girders were prepared with hooked-bonded TiAB for testing including two control specimens. Five girders were prepared with straight-bonded TiAB and two were prepared with hooked-unbonded TiAB for testing. Two specimens were also prepared for fatigue test including one control specimen.

The test matrix, outlined in Table 6-1, provides the details of the parameters considered. The naming convention that pertained to the test matrix is as follows. The girder type is indicated by the first part of the designation such as TB for T-shaped girder. P and N represent the positive and negative moment-strengthening techniques, respectively. G, H, and S indicate the groove, hook, and straight, meaning TiAB were straight (S) bonded or hooked (H), and epoxied in a groove; and U and F represent unbonded and fatigue, respectively.

Table 6-1 Test Matrix for Member Level Test

Specimen ID	Strengthening Method	Ti application	End Anchorage	Number of tests
TB.P	Positive moment Control specimen	-	-	1
TB.N	Negative moment Control specimen	-	-	1
TB.G.H.P	Positive moment	Epoxied in Groove	Hooked	3
TB.G.S.P	Positive moment	Epoxied in Groove	Straight	3
TB.F.P	Positive moment Control specimen	-	-	1
TB.G.H.F.P	Positive moment	Epoxied in Groove	Hooked	1
TB.U.H.P	Positive moment	Unbonded	Hooked	2
TB.G.H.N	Negative moment	Epoxied in Groove	Hooked	2
TB.G.S.N	Negative moment	Epoxied in Groove	Straight	2

6.3 DESIGN OF SPECIMENS

This section presents the design of specimens for positive- and negative-moment tests.

6.3.1 POSITIVE-MOMENT TEST

As shown in Figure 6-1, the specimens had dimensions of 20 inches in total height, 6 inch flange height, 48 inch flange width, 24 inch web width, and a length of 16 feet with one foot overhand beyond the support on either side. The specimens' span, which refers to the distance between supports, was 14 feet with a 6 feet shear span. The girders were subjected to a four-point loading configuration with a 2-foot constant moment region at the center.

The girders were designed in such a way that they could produce equivalent internal forces in the positive moment region of a representative reinforced concrete bridge (e.g., Cullman Bridge). This design approach aimed to replicate the representative behavior of the selected ALDOT bridge. To achieve the nominal moment capacity of the representative bridge girder, two #9 reinforcement bars were placed at the bottom with two #8 and two #4 reinforcement bars at the top. The chosen reinforcement grade was A615 (ASTM A615, 2023) with a measured yield stress of 70 ksi. Longitudinal reinforcement was used at each corner bottom corner of the girder web to anchor the stirrups. To facilitate effective anchoring of #4 and #8 longitudinal bars in the flange, 45-inch long #4 transverse bars were placed at a 12-inch spacing. In terms of shear capacity, the specimens

were adequate with #4 stirrups every 12" on center even though the concrete contribution was sufficient to resist shear forces. The girders were designed with a shear span-to-depth ratio of 3.6 to ensure the flexure-dominated failure mode. This design approach ensured that the girders could effectively mimic the structural response and performance expected from a representative reinforced concrete bridge (e.g., similar to the Cullman Bridge).

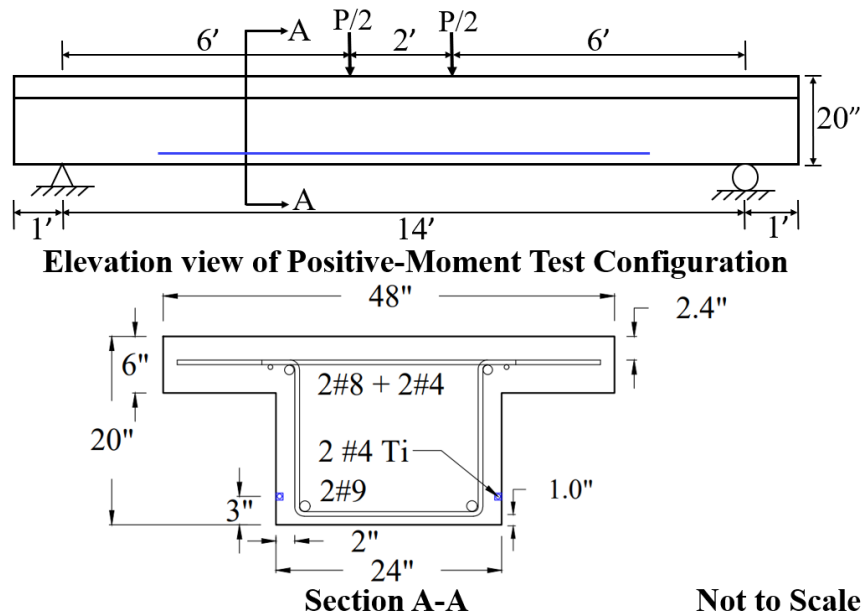
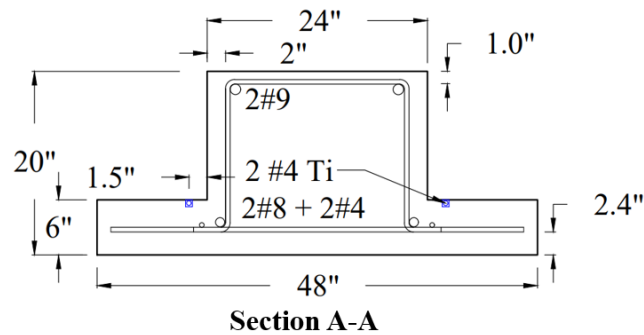
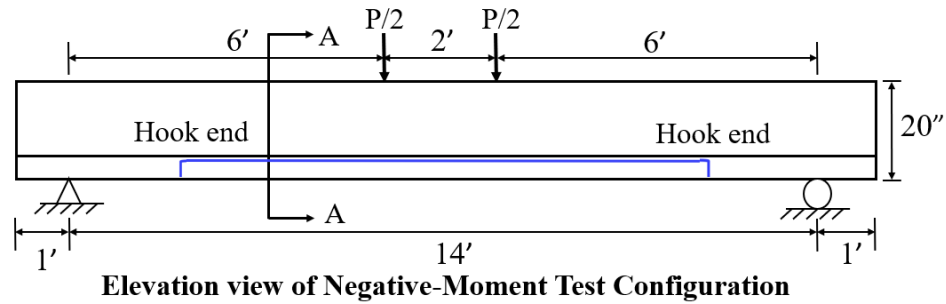


Figure 6-1 Specimen dimensions and reinforcement details for the positive-moment test configuration

6.3.2 NEGATIVE-MOMENT TEST

The same design approach was used for the negative-moment test specimens. These girders were designed in such a way that they could produce equivalent internal forces in the negative-moment region of a representative reinforced concrete bridge (e.g., Cullman Bridge). As shown in Figure 6-2, two #9 were used at the bottom with two #8 and two #2 at the top to obtain the same internal negative-moment resistance of the representative bridge. Therefore, the same specimens were flipped for the negative-moment test.



Not to Scale

Figure 6-2 Specimen dimensions and reinforcement details for the negative-moment test configuration

6.4 CONSTRUCTION OF SPECIMENS

All reinforcing bars were obtained from a local supplier. These bars were already cut and bent as required. The cages formed by these bars were set up and tied using a steel frame, as depicted in Figure 6-3. Lifting inserts were positioned near the top surfaces of the beams, as shown in Figure 6-3 (right).

To cast the specimens, the formwork was built using plywood and 2x4 lumber within the high-bay area of Auburn University's Advanced Structural Engineering Lab (ASEL). The specimens were cast in plywood formwork in the same orientation with the girder flange being on the top regardless of the testing configuration. With the help of the lifting hooks anchored at the top and bottom of the specimen and an overhead crane, the specimens were rotated to 45° first and then gradually rotated to 180° to flip the specimens for the negative-moment test. A polyurethane solution was applied to the formwork contact surfaces to ensure smooth concrete finishing and ease in stripping the specimens. Strain gauges were installed on the longitudinal #8 and #9 reinforcement bars at select locations before concrete placement. These gauges were used to measure and monitor the strain experienced by the specimens during testing. Before concrete placement, the strain gauges were strategically positioned and attached to the longitudinal

reinforcements. Polysulfide coating was used to protect the steel strain gauges from being damaged by fresh concrete.

Four specimens were cast per day, with two specimens from a single load of ready-mixed concrete. A mechanical vibrator was used to achieve proper consolidation. Slump tests (ASTM C143, 2020) and air content tests (ASTM C231, 2022) were performed to ensure that the concrete met ALDOT standards. After casting, the exposed surfaces were covered with water-soaked burlap and a plastic sheet to maintain wet-curing conditions for seven days. Following this curing period, the forms were removed, and the specimens were stored inside the laboratory until testing. Figure 6-4 shows the consolidation, air content test, and slump test during casting of some of the specimens. The constructed specimens and lifting of the specimen are shown in Figure 6-5.



Figure 6-3 Rebar cage formation (Left) and formwork ready for casting with lifting device (Right)

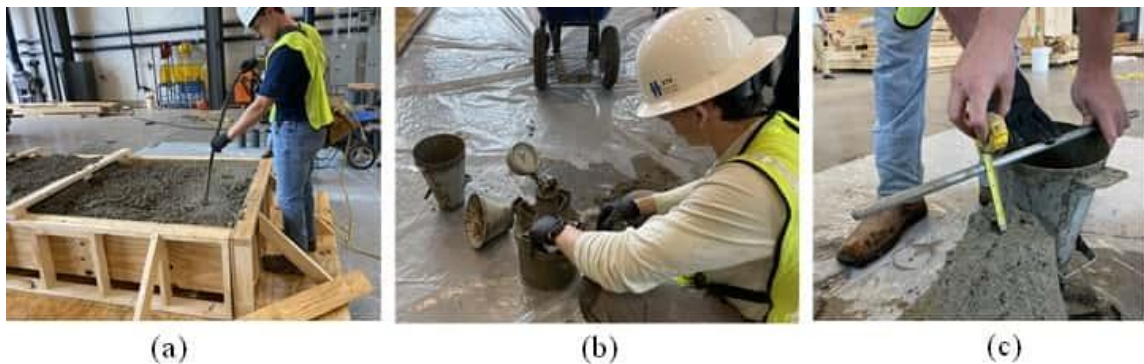


Figure 6-4 (a) Consolidation using vibrator, (b) air content test, and (c) slump test



Figure 6-5 Specimen after casting (Left) and Lifting of the specimen (Right)

Based on the compressive strengths of cores corresponding to a bridge in Alabama that was built in the 1960s that needs to be strengthened, the concrete for this study was intentionally proportioned to have strengths lower than what would be used in bridges built in the 2020s. The concrete mixture proportions and properties are shown in Chapter 3. The concrete specifically did not include fly ash because fly ash was not commonly used in the 1960s. A local ready-mixed concrete company supplied the concrete, and four batches were required to cast all specimens. The compressive strength was tested on 6×12 in. cylinders following ASTM C39 (2021). At the time of testing, the average compressive strength of the concrete was slightly above 4280-4940 psi, which is representative of older bridges.

6.5 INSTRUMENTATION

The reinforcing steel and TiABs were instrumented with strain gauges according to manufacturer's recommendations. The instrumentation layout is shown in Figure 6-6. For the steel reinforcing bars, two strain gauges in the constant-moment region were attached to each steel bar in the compression and tension regions to monitor the strain in the steel. To protect the strain gauges from being damaged during concrete placement, a polysulfide coating was used. In the case of TiABs, three strain gauges were attached in the constant-moment region to closely monitor the yielding of TiABs. At least three more strain gauges were also attached in the shear span on each TiAB to observe the development of strains along the TiAB length. For the fatigue test, there were three strain gauges in the shear span on one side, and on the other side of the shear span there were two strain gauges which is shown in Figure 6-7. Teflon tape was used to protect the strain gauges on the TiABs from adhering to the epoxy. For the hooked-unbonded test, only two strain gauges were used: one in the constant moment region and another at the end of TiAB. Since the strain distribution is expected to be uniform in the TiAB in the hooked-unbonded test, these two strain gauges were deemed enough for this part of the test.

Potentiometers were used to record girder vertical deflections. Four potentiometers with 20-inch stroke were placed in the constant moment region and two with 10-inch stroke positioned

in the shear spans. Additionally, two slip-sensors were mounted under each support to measure any potential vertical support displacement. Concrete strain was measured using two strain gauges attached to the top concrete surface within the constant moment region. Four inclinometers were used (two on each side of the beam) to measure the rotation of the section. The instrumentation layout is shown in Figure 6-6. The same instrumentation layout was used for both positive- and negative-moment bending tests. The strain gauge layout for the fatigue test specimens is shown in Figure 6-7.

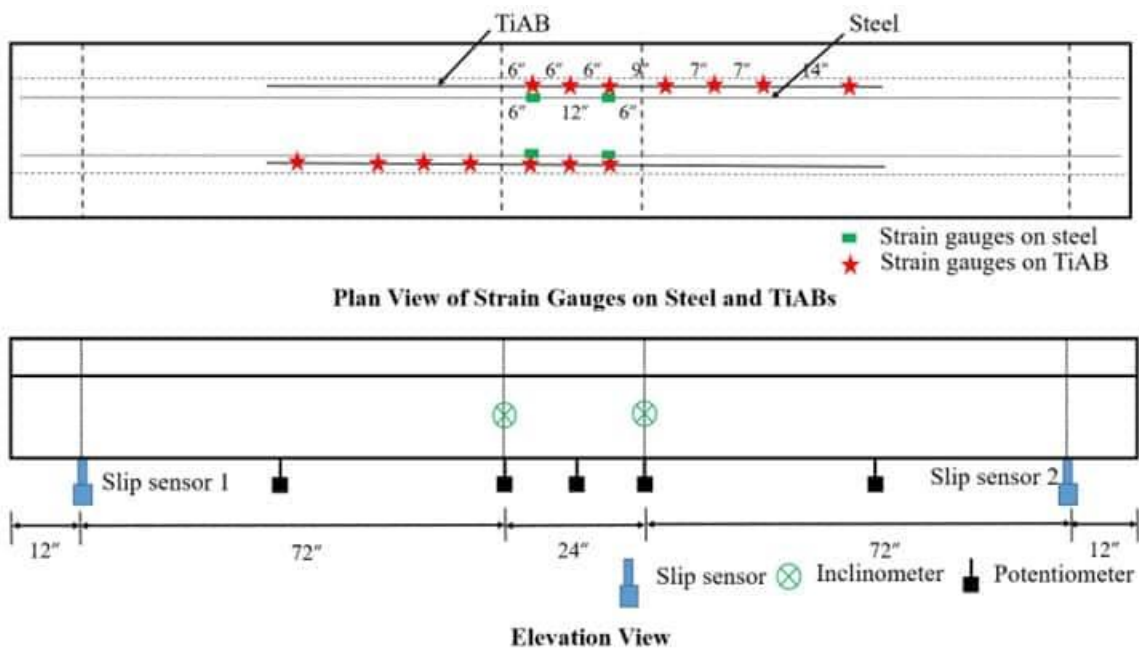
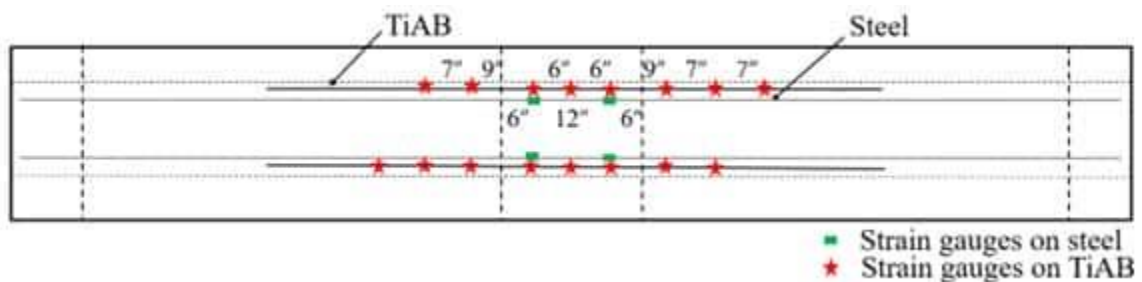


Figure 6-6 Instrumentation layout



6.6 TiAB NSM STRENGTHENING

In the following subsections, the process of pre-cracking, specimen preparation for TiAB installation, TiAB preparation before installation, and the process of TiAB installation are described.

6.6.1 PRE-CRACKING

To accurately simulate the in-service bridge condition of in-service bridge girders, all the specimens were pre-cracked prior to strengthening with TiAB. Although the beams in the first phase were pre-cracked up to 85% of steel yielding, the second phase specimens were pre-cracked up to $1000\ \mu\epsilon$ which is about half of the yield strain of the longitudinal steel (yields strain is $2,350\ \mu\epsilon$). Pre-cracking was done using the four-point loading configuration that was also used to fail the specimens. The strain levels were measured with strain gauges installed on the longitudinal reinforcement in the constant moment region of the girders. The cracks were marked at every 2 kips interval as well as the crack widths were measured at the same load intervals. Error! Reference source not found. shows typical tensile strain and displacement plots during the cracking of the beams prior to installing the TiAB.

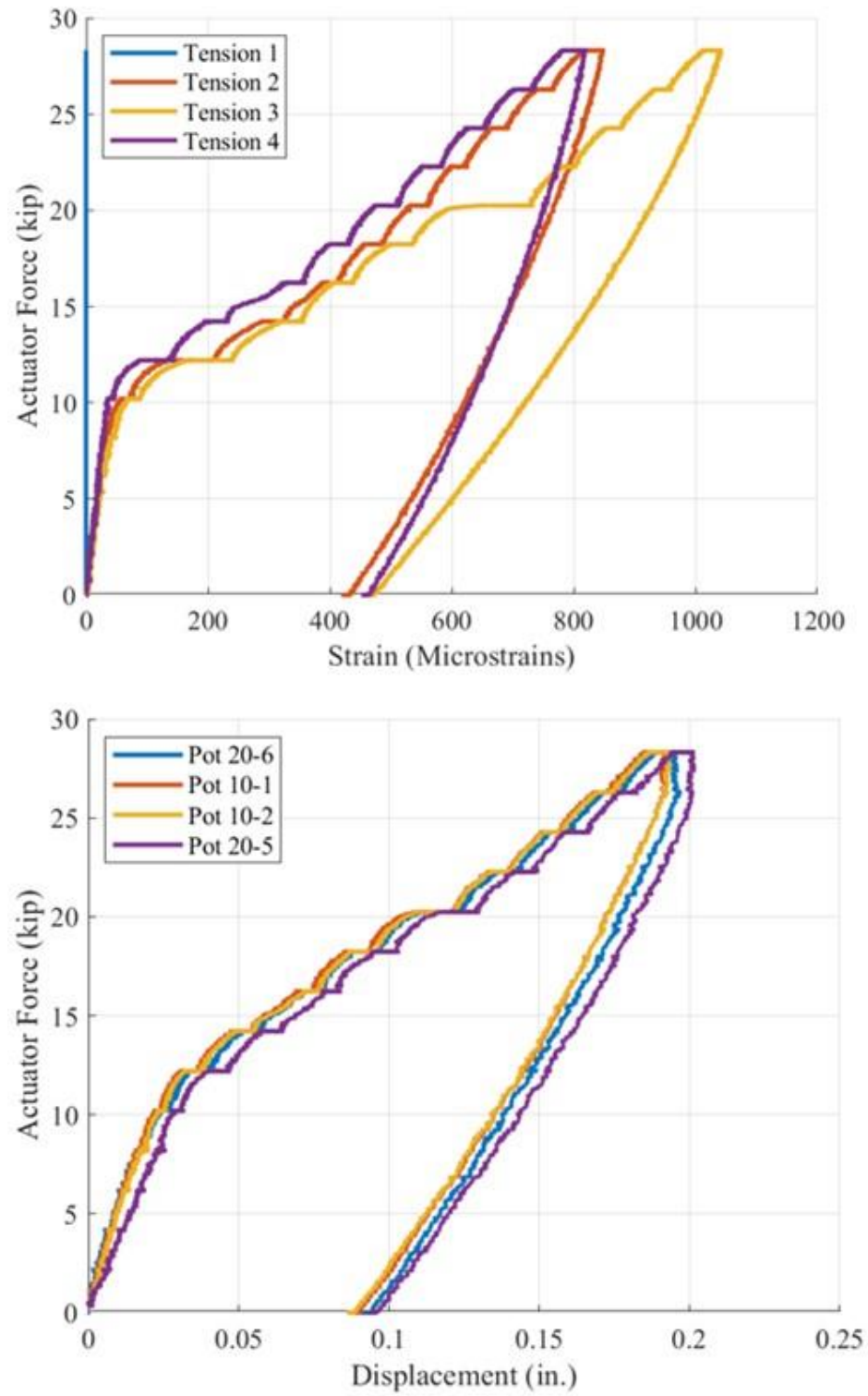


Figure 6-8 Load versus reinforcing rebar tensile strain in mid-span (Top), and load versus mid-span displacement (Bottom)

For the positive-moment test, the first crack appeared at around 3 kips at the constant moment region or under the loading point where stirrups were located. This crack was typically classified as a narrow (hairline) crack with a width of 0.003 inches. As the load increased, the crack generated in the shear span propagated toward the load point. When the steel reached 1000 $\mu\epsilon$, usually between 30 to 36 kips, the largest crack width for each beam varied from 0.012 inches to 0.016 inches. At the end of the pre-cracking stage, there were numerous cracks in the constant moment region as well as in the shear span, as shown in Figure 6-9. For the negative-moment test, one or two cracks appeared in the constant moment region under the load points or at the center of the girder. The crack propagated towards the top of the girder, and the crack width was 0.02 to 0.025 inch which was wider than the cracks in the positive-moment test. When the steel reached 1000 $\mu\epsilon$, the actuator force was usually between 23 to 26 kips. The cracks in the negative-moment test specimen are shown in Figure 6-10. The residual strains of about 500 $\mu\epsilon$ were in the tensile reinforcement after completion of the pre-cracking test. The recorded residual strains obtained at the end of the cracking cycles were manually added to the plots of the final (failure) loading cycles.

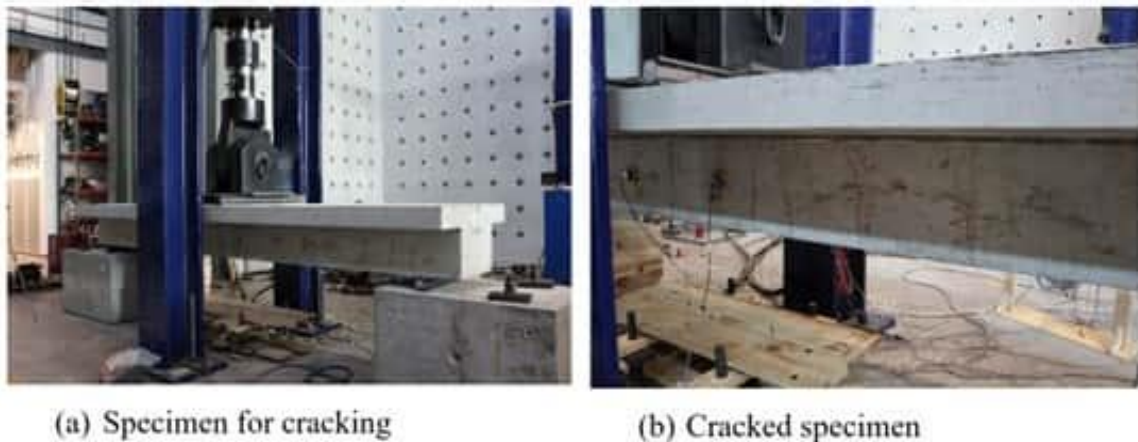


Figure 6-9 Cracks in the specimen (Positive-moment test)

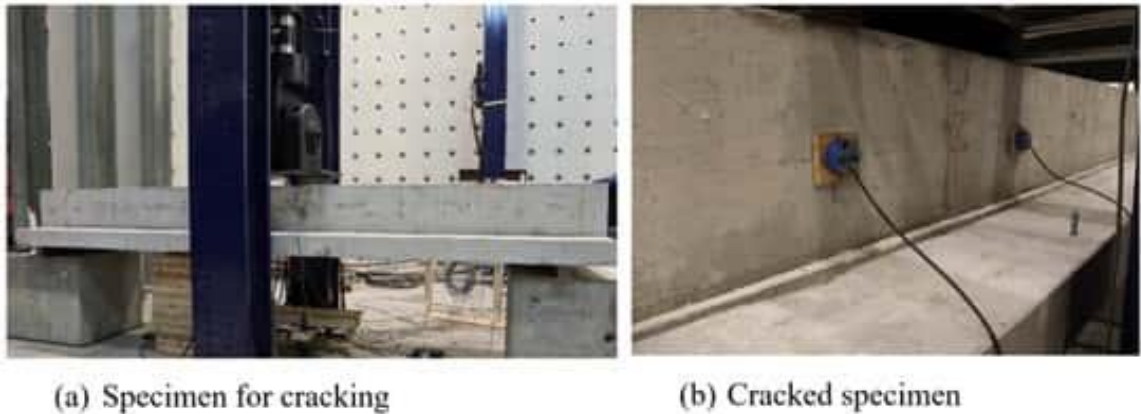


Figure 6-10 Cracks in the specimen (Negative-moment test)

6.6.2 PREPARING THE TiAB FOR INSTALLATION

The same steps were followed for the TiAB preparation in the second phase of the project as covered in Chapter 4 (Section 4.5.2) and in Appendix C. The main steps are: (i) cutting to length, (ii) heating and bending appropriately to form the anchorage hooks, (iii) grinding down the strain gauge locations, (iv) attaching strain gauges along the bar length, (v) putting the wedges in place to keep the TiAB from falling out of the groove. The straight-bonded bars were cut to the representative length directly, while the hooked bars (both bonded and unbonded) had cut lengths that were calculated using the Bar Bending Work Instructions (included in Appendix B) provided by the TiAB supplier (Perryman Company), to ensure that the TiAB were the proper length once bent.

The hook details of the #4 TiABs conformed to the requirements of the (AASHTO, 2020), with a tail length of 6 inches and a diameter of 3 inches. A conventional rebar cutting and bending machine was used to fabricate the TiABs hooks. To prevent cracking during the bending process, the TiABs were heated up to 1200°F until the bars turned blue, as recommended by the manufacturer (Perryman Company, 2021) and ASTM B1009 Specification (ASTM B1009-20, 2020). This temperature level for forming the hooks is below the annealing temperature of the specific titanium alloy used in this research, which ensured that no changes to the mechanical properties occur after cooling. A curved transition surface between the groove and hole in the concrete was carefully chiseled along a template with a small concrete jackhammer to accommodate the hook's radius as shown in Figure 6-11.

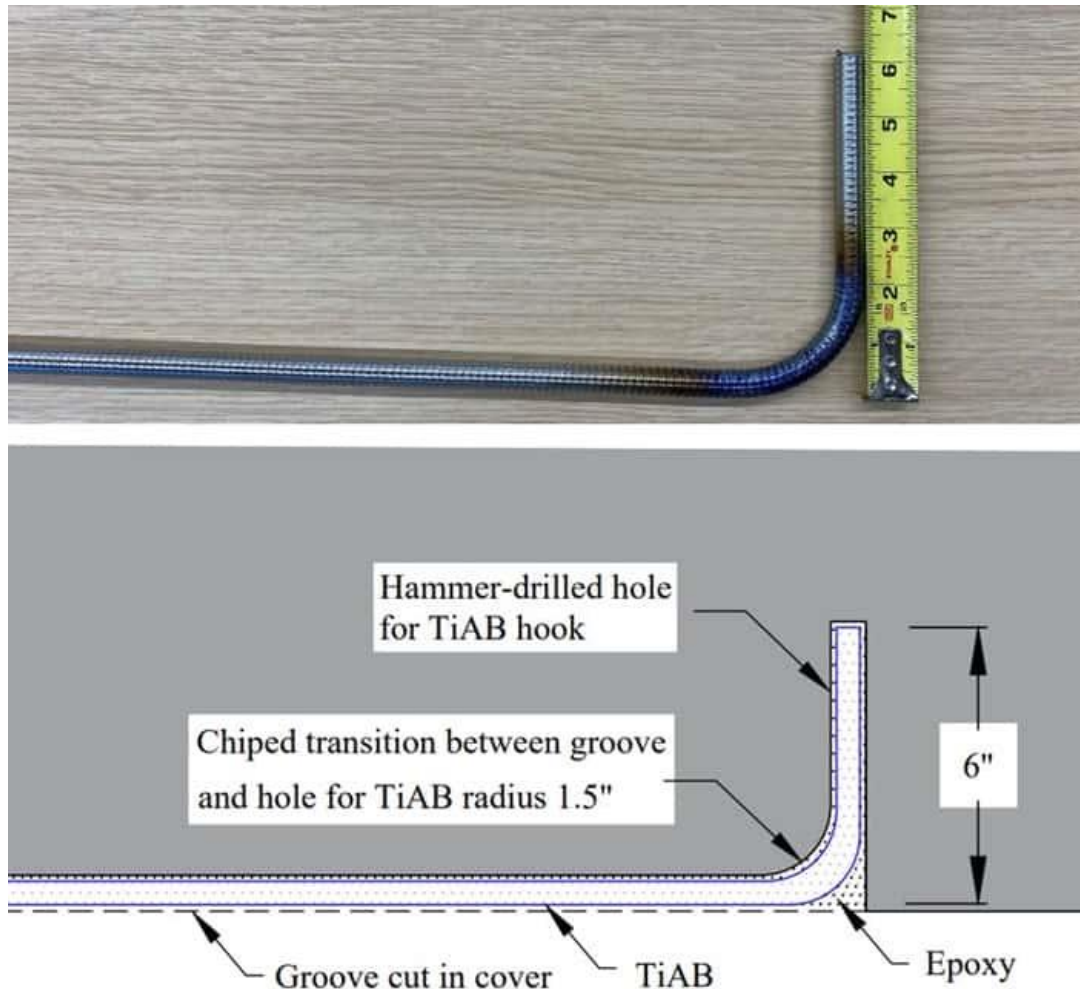


Figure 6-11 TiAB hook and section through hook end epoxied to concrete

6.6.3 PREPARING THE SPECIMENS FOR NSM STRENGTHENING

The location of the grooves for both positive and negative bending tests is shown in Error! Reference source not found. and Error! Reference source not found.. The concrete beams were prepared for NSM TiABs by cutting a 0.75 in. square groove in the web at 3 inches from the bottom of the beam for the positive bending test and at the soffit of the flange for the negative bending test. The grooves were cut using a track-mounted saw which is shown in Figure 6-12. The holes were made to accommodate the hook of TiAB. The drilling and chiseling of the concrete helped to accommodate the bend radius of the hooked TiABs. To ensure proper bonding between the concrete surface and adhesive, the grooves and holes were cleaned using low-pressure water blasting with masonry sand as an abrasive as described in ACI 546R-14 (2014). Sandblasting with

4000 psi pressure was used to eliminate any dust, slurry, or loose concrete particles (ACI 546R-14, 2014).

Drilling of the holes and chiseling to accommodate the bending diameter of the hook was required for hooked bonded and un-bonded specimens. On the other hand, the straight-bonded specimens only required groove cutting because there were no hooks to penetrate into the concrete. A single blade with 0.75-inch thickness was used to ensure the proper groove width. The girders were cut at full length because cutting all the girders to the maximum length provided flexibility in terms of revising the bonded length in the test matrix, if deemed necessary based on test results. The process is shown in Figure 6-13. The result is a clean and porous concrete groove suitable for good bonding between the concrete and epoxy. Therefore, the overall process to prepare the concrete girders was: (i) cutting a 0.75 in. square groove in the appropriate place of the girders, (ii) drilling holes and chiseling the concrete to accommodate the bend radius of the hooked TiABs, and (iii) low-pressure water blasting with abrasives for cleaning and achieving optimal bond performance.



Figure 6-12 Cutting groove for positive bending test (Top) and for negative bending test (Bottom)



Figure 6-13 Low-pressure water blasting to clean the groove (Left) and Cleaned groove (Right)

6.6.4 STRENGTHENING THE SPECIMENS

In this section, the each strengthening method of hooked-bonded, straight-bonded, and hooked-unbonded are described in detail. Four strategies were used to determine the TiAB bonded length for the specimens: (i) by providing a development length (l_{dT_i}) of 16.5 inches from the loading point, (ii) following the AASHTO Guide for NSM TiAB, (iii) ACI 318-19 by accounting for the effect of stress concentrations when terminating bars in the tension zone, and (iv) ACI 440.2 (2017)-23: by providing adequate length beyond the cracking moment. The first three methods were used for the hooked-bonded strengthening method and the fourth method was used for straight-bonded strengthening method.

6.6.4.1 Hooked-Bonded Specimens

For positive-moment strengthening, the following methods were applied: (i) by providing a development length (l_{dT_i}) of 16.5 inches from the loading point and (ii) ACI 318-19 by accounting for the effect of stress concentrations when terminating bars in the tension zone. The development length was calculated using Equation 2.5 assuming 1.0 ksi average bond strength along the embedded titanium bar (AASHTO, 2020) for hooked-bonded TiAB. The details of these strengthening methods are described in Chapter 2. In the case of the second condition, according to ACI 318-19, bar cutoff is prohibited unless one of the three conditions is satisfied which is outlined in Chapter 2, Section 2.5.4. In this case, the first ACI 318-19 condition was not satisfied, and the second condition was not applicable for this specific strengthening purpose. Therefore, the third ACI 318-19 condition was employed which required that the internal bars should offer double the required area to fulfill the flexural demand. The moment diagram of the hooked-bonded strengthened specimen is shown in Figure 6-14.

For the purpose of negative-moment strengthening, the methods used are: (i) following the AASHTO Guide for NSM TiAB (ii) ACI 318-19 by accounting for the effect of stress concentrations when terminating bars in the tension zone. Providing only the development length beyond the loading point did not work for the positive-moment strengthening and because of this, for negative-moment strengthening this method was not evaluated. The hooked-bonded TiAB specimens were thus strengthened by following the AASHTO NSM TiAB guide and ACI 319-19 requirements. The moment diagram of the hooked-bonded strengthened specimens is shown in Figure 6-15.

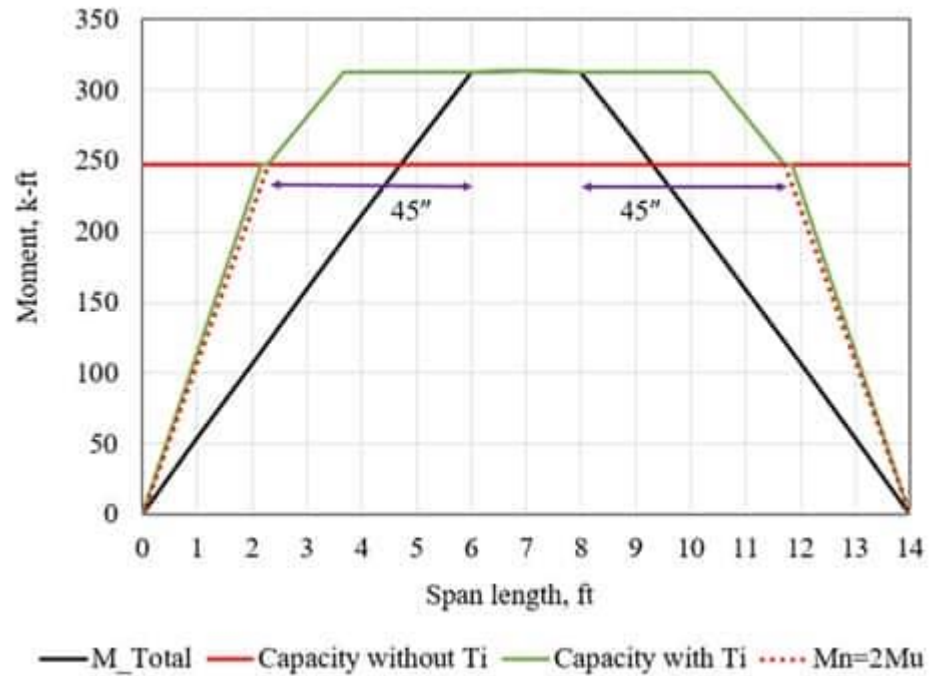


Figure 6-14 Moment diagram for hooked-bonded and un-bonded strengthened specimens (positive-moment test)

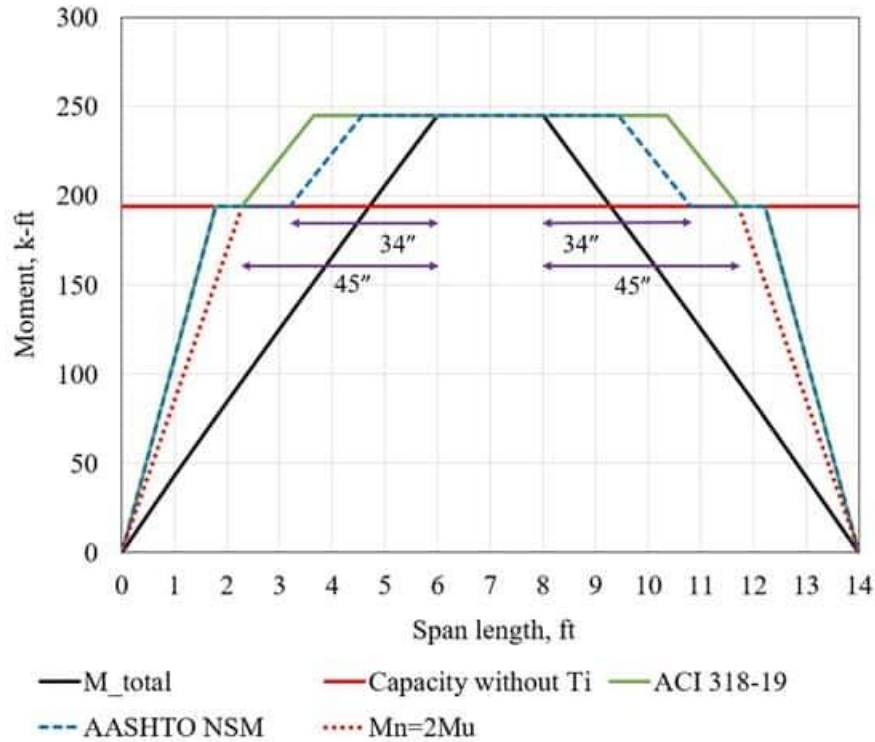


Figure 6-15 Moment diagram for hooked-bonded (negative-moment test)

6.6.4.2 Straight-Bonded Specimens

The details of the test parameters evaluated, and the naming convention assigned to each specimen are presented in Chapter 7. Due to the lack of guidance in using straight TiAB for strengthening RC members, the guidelines provided in relevant documents discussed in Chapter 2 were evaluated during the strengthening of some of these test specimens. The primary variable of the tests was the TiAB bonded length, which was determined based on three criteria; i) the presence of diagonal shear crack presented in the AASHTO NSM TiAB Guide, outlined in Figure 2-17, ii) preventing the concrete cover delamination failure mode as discussed in ACI 440.2 (2023), and iii) the calculated development length according to the AASHTO NSM TiAB Guide. The internal bar cutoff provisions of ACI 318 did not control over other criteria as it resulted in shorter TiAB bonded lengths, therefore these ACI 318 provisions did not impact the bonded length used for any of these the straight-bonded specimens.

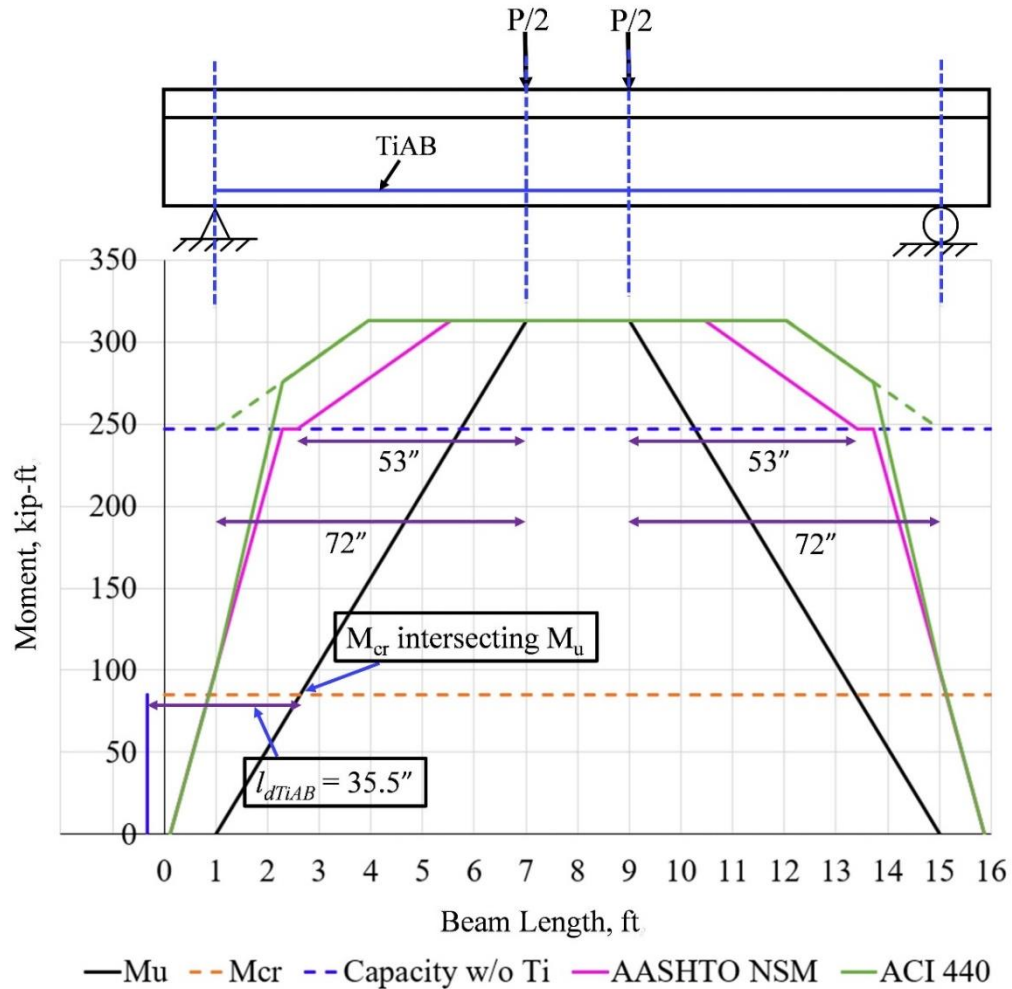


Figure 6-16 Moment diagram for straight-bonded strengthened specimens (positive-moment bending test)

6.6.4.3 Hooked-Unbonded Specimens

For the unbonded case, the strain in the TiAB is the same along the whole TiAB length (refer to total strain/uniform strain theory) (Cairns and Rafeeqi, 2002). Because the effect of stress discontinuity (ACI 318-19) worked well for both positive and negative-moment strengthening, total strain/uniform strain theory along with the effect of stress discontinuity (ACI 318-19) was used to calculate the TiAB length for one of the specimens and were calculated to be 45 in. For the other specimen, the TiAB length was calculated based on the following guidance provided in ACI 440.2 (2023) where the TiAB length was obtained from the distance from the loading point to the point where the moment equals the cracking moment (M_{cr}), with an additional 6 in. The calculated TiAB length is shown in Table 6-2.

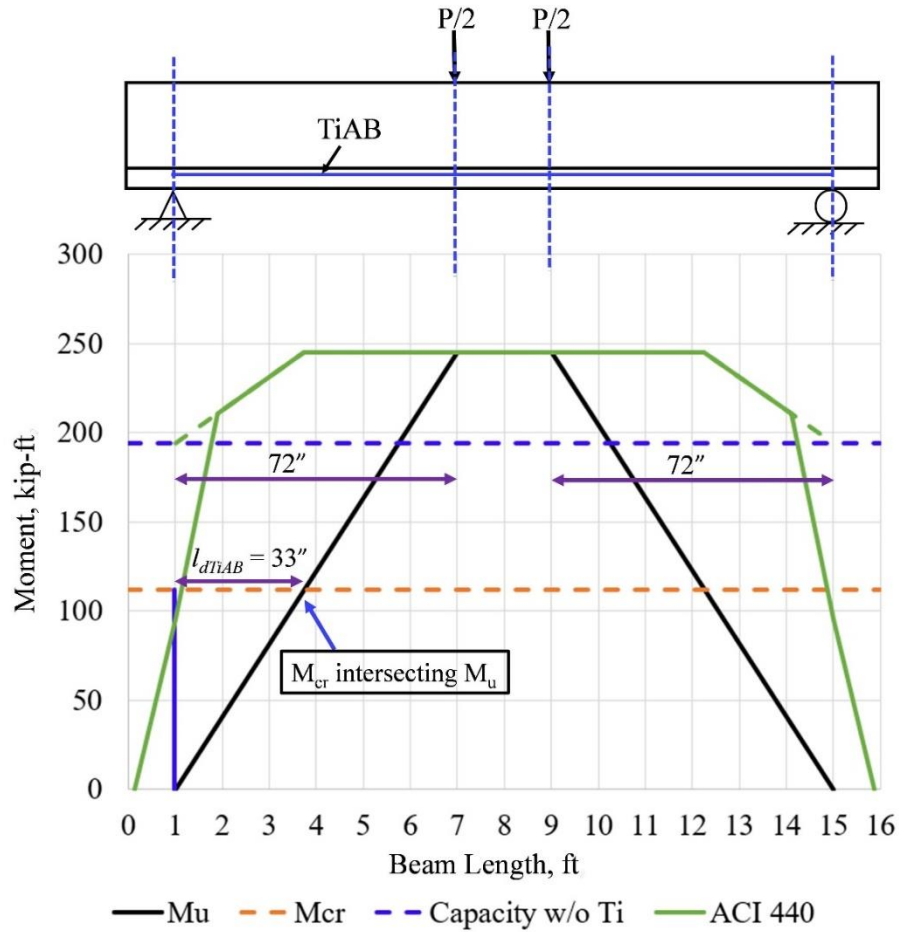


Figure 6-17 Moment diagram for straight-bonded strengthened specimens (negative moment bending test)

Table 6-2 TiAB length for hooked-unbonded specimen.

Assumption/Theory	Length from loading point, in.	Total length, in.
Effect of Stress discontinuity	45	114
M_{cr} section + 6"	59	142

The hook ends of TiABs were epoxied into the holes using Hilti HIT-RE 500 V3 epoxy (HILTI, 2021). The steps taken in the strengthening process are summarized as follows: i) drilling holes at TiAB mounting locations, ii) cutting the TiABs to length, iii) heating and bending of TiABs to form the end hooks, iv) attaching the strain gauges on TiABs, v) cleaning the holes, vi) filling the groove with epoxy, placing the TiABs, and applying the epoxy if needed. The specimens were kept in the laboratory for a duration of three days or more before testing to allow sufficient time to cure the

epoxy, as the minimum required curing time was 6.5 hours at 72°F (HILTI, 2021). In Appendix C, the major steps of strengthening are discussed in detail.

6.6.4.4 Fatigue Test Specimens

One control and one strengthened specimen using the hooked-bonded TiAB NSM anchorage method were tested to determine their performance during and after fatigue load testing. The specimen was strengthened according to ACI 318 (by accounting for the effect of stress concentrations when terminating the bars in the tension zone). The moment diagram for the strengthened specimen is shown in Figure 6-14.

6.7 TEST SETUP AND LOAD PROTOCOL

The girders were tested under flexure with a four-point loading scheme in the Advanced Structural Engineering Laboratory (ASEL) at Auburn University. The loading was applied at two points on top at 2-feet apart with 6-feet shear spans as shown in **Error! Reference source not found.** and **Error! Reference source not found.** A 446 kip-servo-hydraulic load- and displacement-control capable actuator was used for all tests. To replicate the service-level condition of a representative bridge, all specimens were cracked before installing TiABs. Each specimen was loaded until the steel strain reached 1000 $\mu\epsilon$, which is approximately 40% of its yield strain. Cracks were mapped at 2-kip intervals until the internal reinforcement reached the target strain. The specimens were unloaded after reaching the target strain and preparation started to strengthen the specimens with TiABs. There were about 400 - 500 $\mu\epsilon$ residual strain which was considered in the final analysis. The control specimen for each strengthening case (i.e., positive or negative) was first tested to failure. Thereafter, the remaining specimens were strengthened by installing and epoxying the TiABs into the grooves. After allowing sufficient time for the epoxy to cure, the strengthened girders were loaded until failure. The initial phase of each test was performed in a force-control mode at a rate of 1 kip/minute until reaching the initiation of yielding of the internal steel reinforcement ($\epsilon_y = 2413 \mu\epsilon$). Subsequently, the final phase of testing was conducted in the displacement-control mode with a loading rate of 0.05 inch/minute for better control over the loading in the post-yielding and failure regimes.

For fatigue loading, the specimens were first cracked by applying a service-level stress of 28 ksi to simulate the in-service condition of the girders. Following this, the load was applied as illustrated in Figure 6-18. Initially, load cycles A and B were applied, followed by 2 million cycles at a frequency of 1.2 Hz. The stress range in the outermost tension reinforcement rebar, used for fatigue, was 13.0 ksi, as determined from recent research (Chou et al., 2023; Higgins et al., 2007; Knudtsen,

2016). Subsequently, a cyclic loading test (CLT) was conducted by applying load cycles C to H, adopted from the studies by Casadei et al. (2005) and Ziehl et al. (2008).

Casadei et al. (2005), Ziehl et al. (2008), and Galati et al. (2008) investigated in-situ load testing procedures described in the ACI building code and proposed the CLT to assess the safety and serviceability of an existing structural system. They developed a novel in-situ load-testing method, the cyclic loading test (CLT), along with evaluation criteria to determine whether the existing structure requires strengthening. The loading protocol for this CLT test is shown in Figure 6-19.

Acceptance criteria proposed by Ziehl et al. (2008) should be checked during and after the load test to establish whether the tested member has passed the loading protocol. The three parameters used to analyze the behavior of a tested structure are: i) repeatability, ii) permanency, and iii) deviation from linearity. All three parameters are related to the structure's response in terms of displacement. This test was chosen to validate the performance of the girder strengthened with NSM TiAB and tested at ASEL.

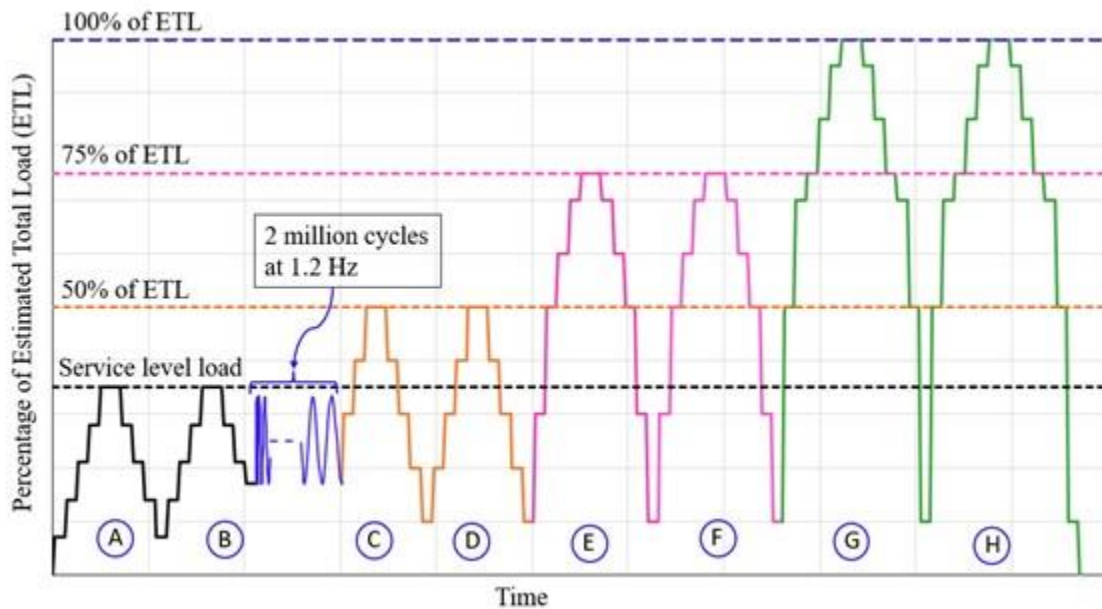


Figure 6-18 Fatigue test load protocol

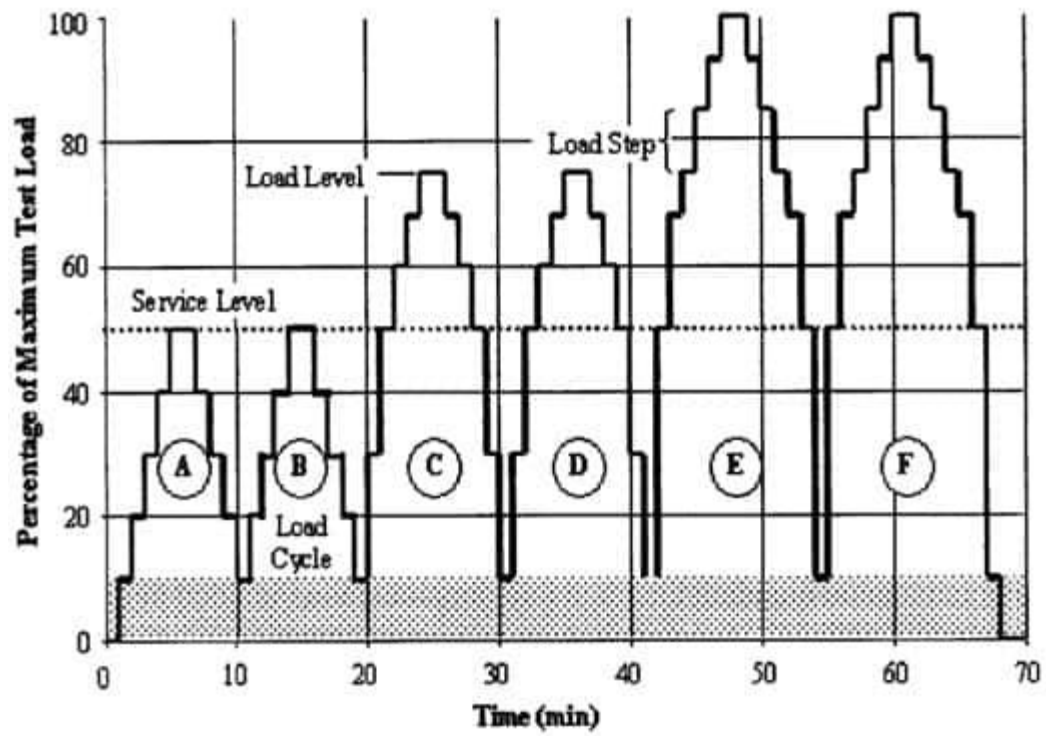


Figure 6-19 Load steps and cycles for a cyclic load test (Casadei et al., 2005)

Chapter 7

TEST RESULTS, ANALYSIS, AND DISCUSSION FOR PHASE 2

7.1 INTRODUCTION

This chapter presents the experimental behavior, response, and test result discussion of the member-level beam specimens simulating the Cullman bridge girders that were strengthened with NSM TiABs. Detailed discussions of each test are provided in the following sections that cover the test results and behavior of each specimen.

7.2 HOOKED-BONDED SPECIMENS

The method to determine the TiAB bonded length for the hooked-bonded specimens, the test results and a discussion of the test results are presented in this section. The test matrix in **Error! Reference source not found.** provides the overall parameters evaluated and the naming convention assigned to each specimen. More details of the naming convention were also covered in Chapter 6.

Table 7-1 Test Matrix and Specimen Designation for Hooked-bonded Specimens

Specimen Designation	Testing Configuration	TiAB Application	Anchorage	Bonded Length* (in.)	TiAB Type
TB.P.Control	Positive moment	N.A. (Control specimen)	N.A.	N.A.	N.A.
TB.G.H.P.01	Positive moment	Epoxied in groove	Hooked	16.5	1
TB.G.H.P.02	Positive moment	Epoxied in groove	Hooked	45	1
TB.G.H.P.03	Positive moment	Epoxied in groove	Hooked	45	2
TB.N.Control	Negative moment	N.A. (Control specimen)	N.A.	N.A.	N.A.
TB.G.H.N.01	Negative moment	Epoxied in groove	Hooked	34	1
TB.G.H.N.02	Negative moment	Epoxied in groove	Hooked	45	1

Notes: N.A. means not applicable and * denotes the length from the loading point to the nearest hook.

7.2.1 STRENGTHENING OF SPECIMENS

For positive-moment strengthening, a total of four specimens were tested, which included one control specimen as shown in **Error! Reference source not found.** Specimen TB.G.H.P.01 was strengthened by providing a bonded length of 16.5 in. from the loading point. The bonded length for this specimen was selected as the development length of a #4 TiAB, calculated using Equation 2.5 assuming 1 ksi average bond strength along the TiAB. Therefore, the total bonded length of the TiABs was 57 in. The second and third specimens (TB.G.H.P.02 and TB.G.H.P.03), were strengthened by accounting for the effect of stress discontinuity for internal bar cutoff described in ACI 318-19. As discussed in Chapter 6, a bar cutoff is not allowed unless one of the three conditions of ACI 318-19 Section 9.7.3.5 is satisfied. For these two specimens, the first condition was not satisfied, and the second condition was not applicable for this specific strengthening purpose. Therefore, the third condition was satisfied by ensuring that the continuing internal steel bars provided at least double the area required from the flexural demand at the TiABs termination location. The calculated TiAB length was 45 in. from the loading point, resulting in a total bonded length of 114 in. The moment diagram at the nominal strengthened capacity of specimens TB.G.H.P.02 and TB.G.H.P.03 ($M_n = 313$ k-ft, calculated according to Equation 2.4) is shown in Figure 6-14, along with the lines indicating twice the moment demand ($2M_u$). As presented in Table 7-1, Type 1 and Type 2 TiABs were used for TB.G.H.P.02 and TB.G.H.P.03, respectively. The two different types of TiABs are covered in more detail in Chapter 3.

Three specimens were tested for negative-moment strengthening, which included one control specimen. The first specimen (TB.G.H.N.01) was strengthened on the basis of AASHTO NSM TiAB Guide Section 9.8. This guideline requires strengthening the specimen to withstand the flexural tension demand in the presence of diagonal shear cracks as shown in Figure 2-17. Consequently, the calculated TiAB bonded length from the load point of 34 in. was necessary after adding $d_v \cot \theta$ (a term related to inclined shear cracking) to the development length ($l_d = 16.5$ in. for #4 TiAB), and this results in a total bonded TiABs length of 92 in. For the second specimen (TB.G.H.N.02), the TiABs length was determined using the approach outlined in ACI 318-19 Section 9.7.3.5, to account for the effect of stress concentrations at bar termination locations. The calculated TiAB length for this specimen was 45 in. from the load point that summed to a total bonded length of 114 in. The moment diagram with the strengthened capacities for TB.G.H.N.01 and TB.G.H.N.02 along with previously mentioned capacity ($2M_u$) are plotted in Figure 6-15.

7.2.2 TEST RESULTS

The load-deflection response of the positive-moment strengthened specimens is compared against the un-strengthened (control) specimen in Figure 7-1. In this figure, each **X** denotes when concrete

crushing occurred. The curves indicate very similar behavior for all specimens prior to yielding of the steel. The calculated strength of the control and strengthened specimens were 68 kips and 95 kips (97 kips for Type 2 TiAB), respectively, according to Equation 2.4 (omitting the TiAB terms for the control specimen calculations). It should be noted that TB.G.H.P.01 did not reach the AASHTO NSM TiAB Guide calculated capacity, indicating that bonded TiABs length was insufficient for this specimen. The measured strength of the other two strengthened specimens (TB.G.H.P.02 and TB.G.H.P.03) exceeded the AASHTO NSM TiAB Guide calculated capacity of 95 kips based on Equation 2.4 and exhibited a ductile failure mode similar to that observed for the control specimen.

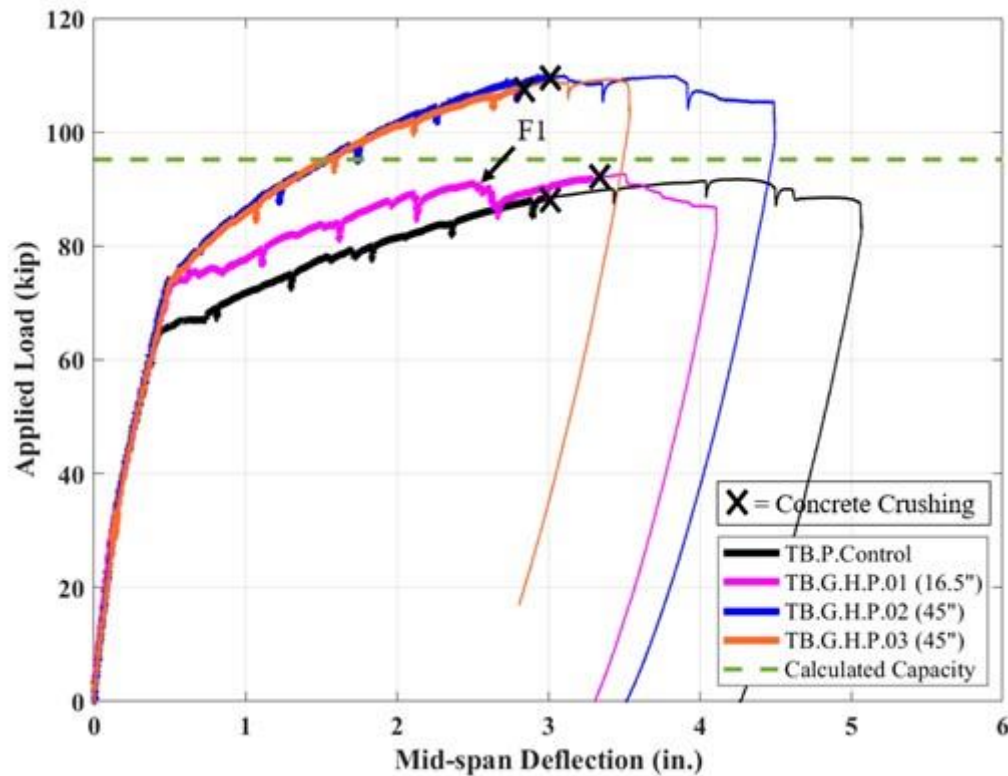


Figure 7-1 Load-deflection behavior of the positive-moment specimens (hooked-bonded specimens)

The load-deflection response of the specimens tested for the negative-moment strengthening is presented in Figure 7-2. The X denotes when concrete crushing occurred. The specimens exhibited similar load-deflection behavior prior to yielding of the steel. The calculated strength of the negative-moment control and strengthened specimens were 61 kips and 79 kips, respectively, according to Equation 2.4 (omitting the TiAB terms for the control specimen calculations). Notably, TB.G.H.N.01 did not reach the AASHTO NSM TiAB Guide calculated capacity indicating that the bonded TiABs length was insufficient for this case. Conversely,

TB.G.H.N.02 exceeded the AASHTO NSM TiAB Guide calculated capacity of 79 kips based on Equation 2.4 and exhibited a ductile failure mode similar to that observed for the control specimen.

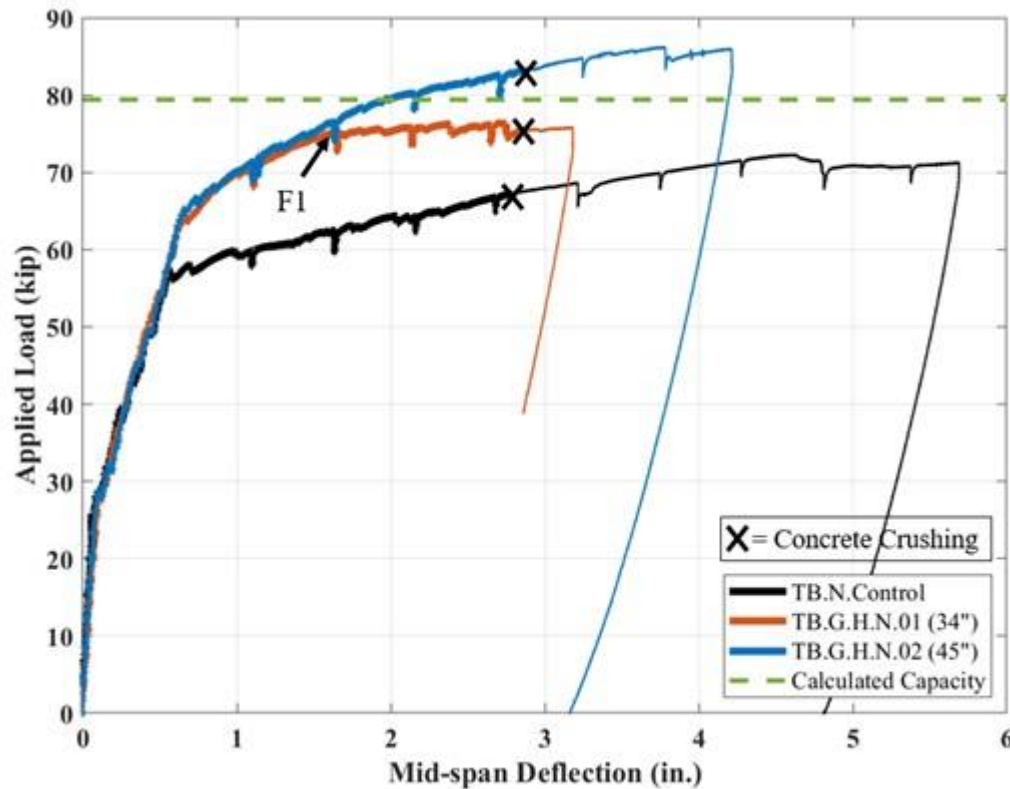


Figure 7-2 Load-deflection behavior of the negative-moment specimens (hooked-bonded specimens)

7.2.3 DISCUSSION OF TEST RESULTS

The hooked-bonded strengthened specimens including control (un-strengthened) specimens are discussed in this section.

7.2.3.1 Specimen TB.P.Control

The positive-moment control specimen exhibited a response characterized by steel yielding followed by a hardening region until concrete crushing failure, as shown in Figure 7-1. As the applied load increased, the flexural cracks formed in the pre-crack load cycle widened and further extended. New cracks also formed at relatively uniform intervals, aligning with stirrup locations. Beyond 60 kips, only a few new cracks formed. At 65 kips and at a mid-span deflection of 0.43 in., the longitudinal steel reached a strain of $2500 \mu\epsilon$ (including residual strain), indicating the onset of steel yielding. Concrete crushing was noticeable in the compression zone within the

constant moment region at 88 kips with a mid-span deflection of 3.00 in. The specimen was unloaded after reaching 5.00 in. of deflection. The measured flexural strength of 88 kips at concrete crushing exceeded the calculated capacity. This increase in moment capacity is attributed to the strain hardening of the tension steel and the unaccounted contribution from the compression reinforcement. The control specimen exhibited a ductile failure mode, which is evident based on the significant post-steel yielding displacement and the steel strains exceeding 20,000 $\mu\epsilon$ well above 5,000 $\mu\epsilon$ (0.005 in./in.).

7.2.3.2 Specimen TB.G.H.P.01

As load on Specimen TB.G.H.P.01 was increased, cracks from the pre-crack cycles widened and further extended, and new cracks also formed. Inclined shear cracks started to develop next to the TiABs hook locations at 50 kips that propagated inwards toward the flange with increasing load. Steel yielding occurred at 74 kips at a mid-span deflection of 0.51 inches. The post-steel yielding stiffness of this specimen was similar to the control specimen. The load-carrying capacity was slightly higher than the control specimen, but a sudden drop of load occurred at 91 kips and 2.50 inches of displacement due to anchorage failure at the hooked ends (point F1 on Figure 7-1). Beyond the failure stage, the hooks became ineffective because of the development of wide inclined shear cracks and losing part of concrete cover, as shown in Figure 7-3. Subsequently, the specimen response converged to that of the control specimen indicating the loss of the contribution of the TiABs. Specimen TB.G.H.P.01 did not exhibit significant strength increase because of the presence of wide inclined cracks and the TiABs not achieving yielding. The maximum strain measured on the TiABs was about 3900 $\mu\epsilon$ whereas the yield strain of Type 1 TiAB was 8516 $\mu\epsilon$. Although past the primary failure mode, with the application of more load, concrete crushing eventually occurred at 92 kips at a mid-span deflection of 3.30 inches. The measured capacity of the specimen did not reach the AASHTO NSM TiAB Guide calculated capacity for the strengthened specimen (95 kips) (Figure 7-1). Although this specimen was designed with a TiAB bonded length equal to the calculated development length (using Equation 2.5), the provided bonded length was insufficient to achieve the calculated load capacity. Additionally, the specimen did not exhibit a ductile failure mode as the other negative-moment specimens due to the sudden nature of the anchorage failure at Point F1.



Figure 7-3 Inclined shear cracks near hook ends and interface failure for Specimen TB.G.H.P.01

7.2.3.3 Specimen TB.G.H.P.02

As shown in Figure 7-1, steel yielding began at 73.8 kips and 0.48 inch of mid-span displacement, and a noticeable decrease in stiffness was observed after steel yielding. With increasing load, new cracks aligning with stirrup locations formed, and pre-existing cracks (cracks from cracking-load cycle) extended and widened. The TiABs yielded and contributed significantly to the increased strength of the specimen. At around 90 kips, localized inclined cracks developed at or near the concrete-epoxy interface. Concrete crushing was observed at 108 kips and a mid-span deflection of 2.98 inches. The primary failure mode of this specimen was thus concrete crushing in the flange near the top surface in the constant moment region, which occurred after both the steel and TiABs yielded. Visible delamination of the TiABs started at 109 kips and a mid-span displacement of 3.50 inch which led to a concrete-epoxy interface delamination failure, as shown in Figure 7-4. Although interface delamination occurred, the primary failure mode of the specimen was crushing of the concrete in the flexural compression zone. The specimen exceeded the capacity (95 kips) calculated by the AASHTO NSM TiAB Guide and carried 22.7% more load compared to the control specimen.



Figure 7-4 Concrete-epoxy interface failure for Specimen TB.G.H.P.02

7.2.3.4 Specimen TB.G.H.P.03

As previously discussed and shown in **Error! Reference source not found.**, the only difference between Specimens TB.G.H.P.02 and TB.G.H.P.03 was that the latter specimen used Type 2 TiABs that had different surface deformations and a slightly higher yield strength of 142 ksi. The test objective was to assess the effect of using a different TiAB type on the specimen strength and behavior. When comparing the responses of TB.G.H.P.02 and TB.G.H.P.03 in Figure 7-1, their responses were similar, indicating that the different TiAB types had no discernible effect on the flexural behavior. For TB.G.H.P.03, steel yielding occurred at 74 kips and 0.50 inches of mid-span displacement. Concrete crushing occurred at 108 kips and 2.90 inches of mid-span displacement. The primary failure mode was thus concrete crushing on the top (compression) surface in the constant moment region, which occurred after the steel and TiABs yielded. Some localized inclined cracks developed at or near the concrete-epoxy interface at 108 kips and 2.80 inch of mid-span displacement. At 110 kips and 3.30 inches of displacement, the concrete-epoxy interface delamination became highly prominent (Figure 7-5) and subsequently caused the detachment of a portion of concrete below the TiAB at a displacement of 3.52 inches. Despite the delamination, the primary failure mode of this specimen was concrete crushing in the flexural compression zone. The specimen exceeded the AASHTO NSM TiAB Guide capacity (97 kips) and carried 22.7% more load when compared to the control specimen.

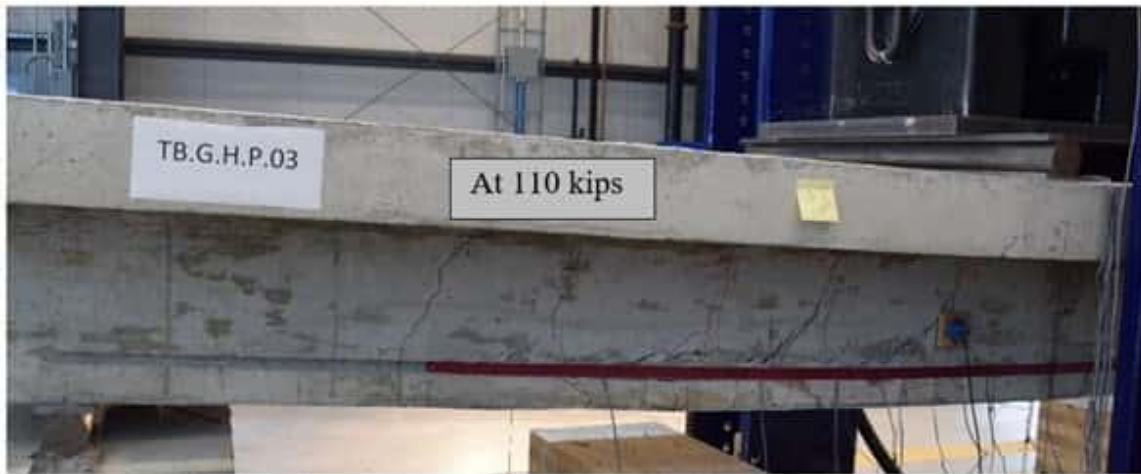


Figure 7-5 Concrete-epoxy interface failure for Specimen TB.G.H.P.03

7.2.3.5 Specimen TB.N.Control

This control specimen exhibited behavior characterized by steel yielding followed by concrete crushing failure at the top of the specimen in the constant moment region. In the negative-moment test configuration, the control specimen exhibited a different crack pattern compared to the control specimen of the positive-moment test configuration. It exhibited much fewer cracks in the constant-moment region, but these cracks were wider and extended further. At 45 kips, inclined cracks initiated and propagated toward the loading points and these cracks widened as the load increased. Flexural tension steel yielding occurred at 57 kips and 2500 $\mu\epsilon$, including the residual strain from pre-cracking loading cycles. After steel yielding, a visible reduction in stiffness was observed. Concrete crushing occurred at 67 kips and 2.78 inches of mid-span deflection, as shown in Figure 7-2. The load was then further increased; reaching a maximum load of approximately 73 kips at a displacement of 4.50 inches. The specimen was unloaded once it was no longer able to take any more load. The capacity of this specimen exceeded the calculated AASHTO NSM TiAB Guide capacity of 61 kips.

7.2.3.6 Specimen TB.G.H.N.01

The crack pattern of this specimen resembled that of the control specimen (TB.N.Control). As the load increased, new cracks formed, and all the cracks (new and pre-existing cracks) widened and propagated toward the loading points. Steel yielding occurred at 63.8 kips and a mid-span displacement of 0.63 inch. At 75 kips and 1.63 inches of displacement (Point F1 on Figure 7-2), the specimen experienced a stiffness change due to wide cracks that developed near the hooked end. These cracks initially formed at the hook end locations at 55 kips and gradually

became wider; eventually causing the hook anchorage to become ineffective. From Figure 7-2, it can be seen that the specimen capacity reached a plateau after Point F1. With further displacement, cracks at the hook ends led to the delamination of one end of the concrete-epoxy interface, as shown in Figure 7-6. Concrete crushing was observed at 75 kips and 2.85 inches of mid-span displacement. The maximum TiAB strain was about $8000 \mu\epsilon$, which is less than the yield strain ($8516 \mu\epsilon$). The measured peak load was 77 kips, which is below the AASHTO NSM TiAB Guide calculated capacity of 79 kips. The primary failure mode of the specimen was due to the loss of hook anchorage caused by wide cracks at the location of hook ends, leading to the delamination at the concrete-epoxy interface. The test demonstrated that the addition of $d_v \cot \theta$ to the development length in accordance with the AASHTO NSM TiAB Guide was insufficient to achieve the desired flexural strength for this specimen. Additionally, the specimen did not exhibit a failure mode as ductile as obtained for the other negative-moment specimens.



Figure 7-6 Crack formation at the hook and delamination for Specimen TB.G.H.N.01

7.2.3.7 Specimen TB.G.H.N.02

The crack pattern observed for this specimen closely resembled those of the previously discussed negative-moment load configuration specimens. Inclined cracks initiated at 55 kips and propagated toward the loading points. With increasing load, both new and existing cracks widened and extended. Steel yielding began at 65 kips and a mid-span displacement of 0.65 inches. The TiABs also yielded at 78 kips at 1.86 inches of deflection and contributed to the overall strength of the specimen. Concrete crushing occurred at 83 kips and 2.86 inches of mid-span displacement. Cracking was observed in the epoxy but there was no significant distress related to delamination

or hook anchorage ineffectiveness. A small crack appeared near the hook end at 55 kips, but it did not significantly widen or lead to any failure. The specimen reached its maximum load at 86 kips at a displacement of 3.77 inches, which exceeded the calculated AASHTO NSM TiAB Guide capacity of 79 kips. The load was further increased until the specimen could no longer take any additional load, and was subsequently unloaded at 4.21 inches of displacement. The crack pattern of the specimen prior to unloading is shown in Figure 7-7. The primary failure mode of this specimen was concrete crushing in the flexural compression zone and the specimen exceeded the calculated capacity of the AASHTO NSM TiAB Guide and resisting about 24% more load when compared to the control specimen.



Figure 7-7 Cracking in Specimen TB.G.H.N.02 at 86 kips

7.3 STRAIGHT-BONDED SPECIMENS

The bonded length used for the TiAB in the straight-bonded specimens, the test results and a discussion of the test results are presented in this section. The test matrix in **Error! Reference source not found.** provides details of the parameters evaluated and the specimen designation. More details of the naming convention were covered in Chapter 6.

Table 7-2 Test Matrix and Specimen Designation for Straight-bonded Specimens

Specimen Designation	Testing Configuration	TiAB Application	Anchorage	Bonded Length* (in.)	TiAB Type
TB.P.Control	Positive moment	N.A. (Control specimen)	N.A.	N.A.	N.A.
TB.G.S.P.01	Positive moment	Epoxied in groove	Straight	53	2
TB.G.S.P.02	Positive moment	Epoxied in groove	Straight	72	1
TB.G.S.P.03	Positive moment	Epoxied in groove	Straight	72	2
TB.N.Control	Negative moment	N.A. (Control specimen)	N.A.	N.A.	N.A.
TB.G.S.N.01	Negative moment	Epoxied in groove	Straight	33	1
TB.G.S.N.02	Negative moment	Epoxied in groove	Straight	72	1

Notes: N.A. means not applicable and * denotes the length from the loading point to the nearest hook.

7.3.1 STRENGTHENING SPECIMENS

For positive-moment strengthening, four specimens were tested, including one control specimen. TB.G.S.P.01 was strengthened based on AASHTO NSM TiAB Guide Section 9.8. This guideline requires strengthening of the specimen to withstand the flexural tension demand in the presence of diagonal shear cracks as shown in Figure 2-17. Consequently, the calculated TiAB bonded length from the load point was 53 inches after adding $d_v \cot \theta$ (the term accounting for the inclined shear crack horizontal distance) to the development length ($l_{dTiAB} = 35.5$ in. for #4 Type 2 TiAB based on measured yield strength) while assuming an average bond strength of 0.5 ksi for straight TiAB based the findings of Phase 1 testing as covered in Section 5.7.2. This resulted in a total bonded TiAB length of 130 inches.

Specimen TB.G.S.P.02 and TB.G.S.P.03 were strengthened by providing a TiAB bonded length of 72 inches from the loading point. The TiAB bonded length for these specimens was selected by accounting for the effect of concrete cover delamination as discussed in ACI 440.2 (2023) Section 14.1.2 (Criterion ii). The addition of development length (l_{dTiAB}) beyond the cracking moment (M_{cr} = modulus of rupture of the cross-section) resulted in a TiAB bonded length of 88 inches from the loading points. This calculated TiAB bonded length exceeded the specimen length; therefore, a bonded length of 72 inches was provided from the load points to the support points. The total bonded length of the TiAB was 168 inches for these specimens, which is equal to the span length (i.e., the distance between the two supports). The flexural demand and capacity

diagrams of the positive moment strengthened specimens are shown in Figure 6-16, along with the lines indicating $I_{dT_{iAB}}$ beyond the cracking moment (M_{cr}).

Three specimens were tested to evaluate negative-moment strengthening, which included one control specimen. TB.G.S.N.01 was strengthened by providing a TiAB bonded length equal to the development length of a #4 TiAB Type 1 from the loading points. The TiAB development length ($l_{dT_{iAB}} = 33$ inches) was calculated using Equation 2, while using measured yield strength for TiAB Type 1 and assuming average bond strength of 0.5 ksi. The total TiAB bonded length for this specimen was 90 inches.

For TB.G.S.N.02, the TiAB length was determined using the approach provided in ACI 440.2 (2023), to accommodate the effect of concrete cover delamination at bar termination locations. The calculated TiAB bonded length for this specimen was 72 inches from the load point; summed to a total TiAB bonded length of 168 inches. The flexural demand and capacity diagrams of the negative-moment strengthened specimens are shown in Figure 6-17.

7.3.2 TEST RESULTS

The load-deflection responses of the positive-moment strengthened specimens are plotted against the control specimen (TB.P.Control) in Figure 7-8. In this figure, each X denotes when concrete crushing occurred. The curves indicated very similar responses for all specimens until the steel reinforcement yielded. The calculated nominal strength was 68 kips for the control (unstrengthened) specimen, 95 kips for the specimen strengthened using TiAB Type 1, and 97 kips for the specimen strengthened using TiAB Type 2 according to Equation 2.4. TB.G.S.P.01 exceeded the AASHTO NSM TiAB Guide calculated capacity, but concrete-epoxy interface failure occurred before concrete crushing, indicating that the provided TiAB bonded length was insufficient for this specimen. The measured strength of TB.G.S.P.02 and TB.G.S.P.03 exceeded the AASHTO NSM TiAB Guide calculated capacities, achieved concrete crushing, and exhibited a ductile failure mode similar to the one observed for the control specimen.

The load-deflection responses of the specimens tested for the negative-moment strengthening are presented in Figure 7-9. The X marks correspond to when concrete crushing occurred. The specimens exhibited similar load-deflection responses until the steel yielded. The calculated nominal strength for the control specimen was 61 kips, whereas the specimens strengthened with TiAB Type 1 was 79 kips, according to Equation 2.4. Notably, TB.G.S.N.01 did not reach the AASHTO NSM TiAB Guide calculated capacity indicating that the provided TiAB bonded length was insufficient for this specimen. Conversely, TB.G.S.N.02 exceeded the AASHTO NSM TiAB Guide calculated capacity, achieved concrete crushing, and exhibited a ductile failure mode similar to the one observed for the control specimen.

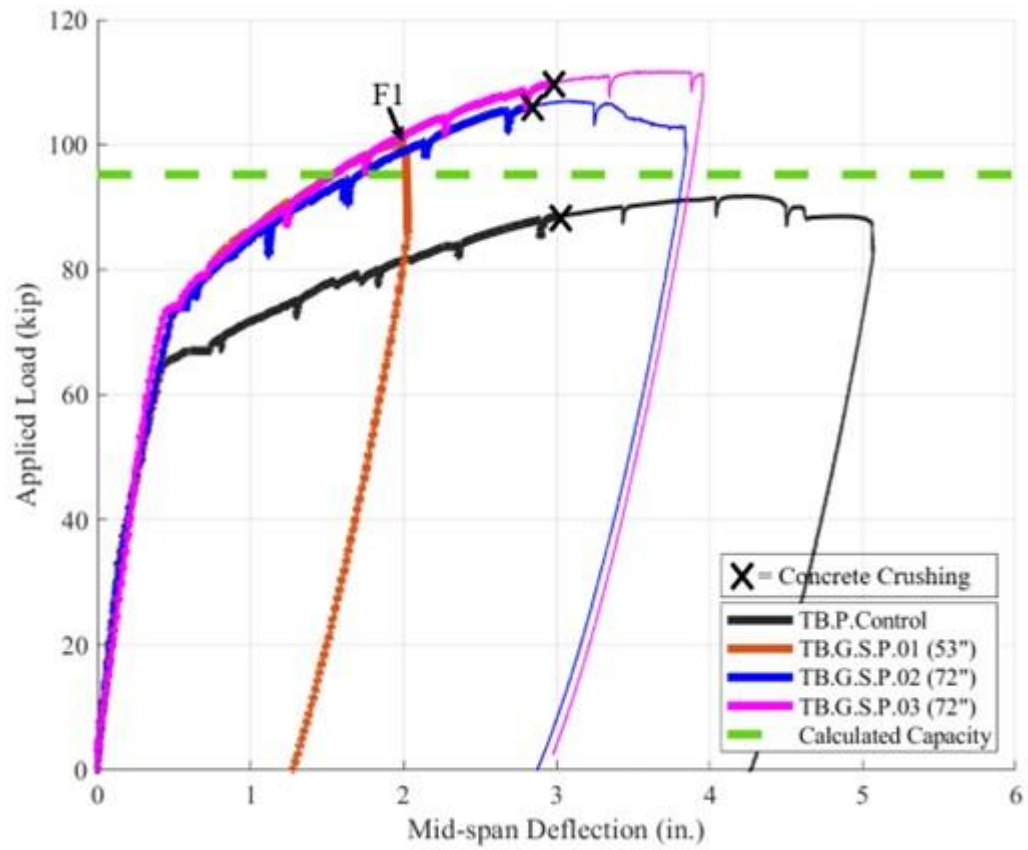


Figure 7-8 Load-deflection behavior of the positive-moment specimens (straight-bonded specimens)

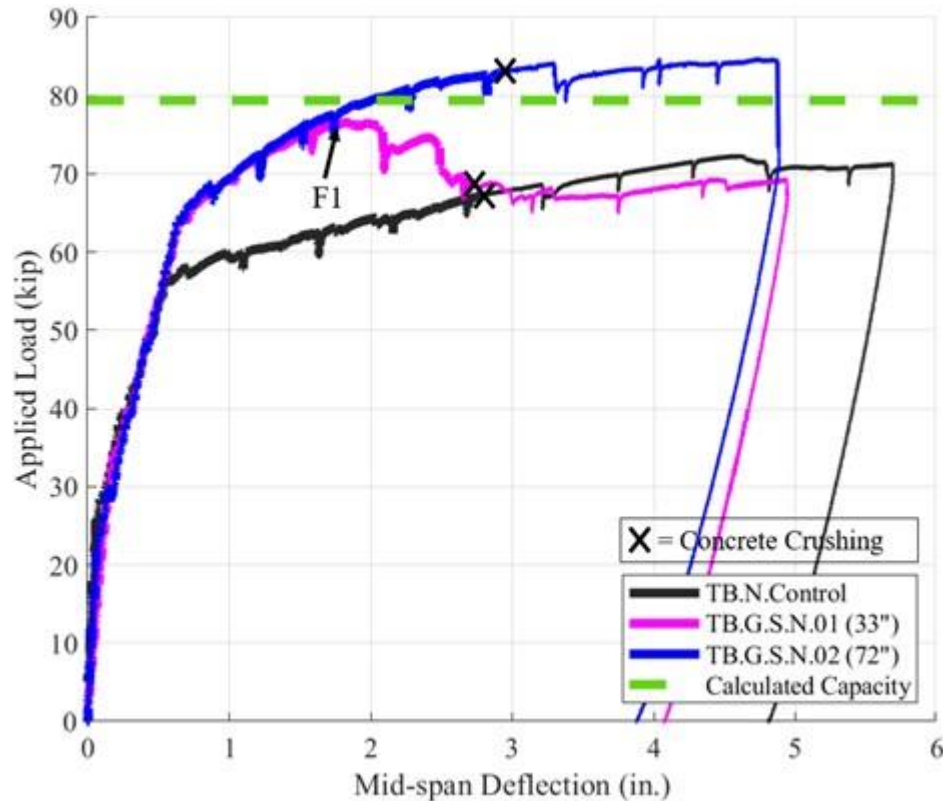


Figure 7-9 Load-deflection behavior of the negative-moment specimens (straight-bonded specimens)

7.3.3 DISCUSSION OF TEST RESULTS

The results of the control specimens were discussed with the results of the hooked-bonded specimen; therefore, only the results of the straight-bonded strengthened specimens will be covered in this section.

7.3.3.1 Specimen TB.G.S.P.01

This specimen was strengthened with TiAB Type 2 and the provided bonded length was determined according to the guidance in the AASHTO NSM TiAB Guide. As the load on Specimen TB.G.S.P.01 increased, cracks from the pre-crack cycle widened and further extended, and new cracks also formed. Inclined cracks started to develop at 55 kips that propagated inwards toward the flange with increasing load. Steel yielding occurred at 74 kips at a mid-span deflection of 0.53 inch. A visible stiffness change occurred after steel yielding. The load-carrying capacity was higher than the control specimen, but a sudden drop of load occurred at 2.0 inches of mid-span displacement due to concrete-epoxy interface failure near the TiAB termination region on one side of the specimen, as shown in Figure 7-10. Following the concrete-epoxy interface failure (point F1

on Figure 7-8), this specimen's load-displacement response suddenly dropped. Failure of this specimen was deemed to occur at 100 kips due to the large drop in its load resistance and it was unloaded after this occurred.

The measured capacity of the specimen exceeded the AASHTO NSM TiAB Guide calculated capacity for the strengthened specimen (95 kips) but concrete-epoxy interface failure occurred in a brittle fashion before concrete crushing occurred. Although this specimen was designed with a TiAB bonded length based on the AASHTO NSM TiAB Guide ($l_{dTiAB} + d_v \cot \theta$), the provided TiAB bonded length was insufficient to achieve the desired ductile failure mode. Despite exceeding the calculated nominal flexural strength, the specimen did not exhibit a ductile failure given the sudden nature of the concrete-epoxy interface failure.



Figure 7-10 Concrete-epoxy interface failure for Specimen TB.G.S.P.01 at 100 kips

7.3.3.2 Specimen TB.G.S.P.02

This specimen was strengthened with TiAB Type 1 ($f_y = 132$ ksi) and the provided bonded length was determined according to the guidance available in ACI 440.2 (2023). Similar behavior in the initial parts of the load response was observed for Specimen TB.G.S.P.02 as the previous specimen. New cracks formed that aligned with the stirrup spacing, and pre-existing cracks (cracks formed in the pre-strengthening load cycle) extended and widened. A few inclined cracks started to form after a load of 50 kips. Steel began to yield at a load of 73 kips with 0.50 inch of mid-span deflection as shown in Figure 7-8. The post-steel yielding stiffness of this specimen was similar to the other strengthened specimens. TiAB strains indicated initiation of TiAB yielding at a load of 90 kips and 1.30 inches of displacement. Concrete crushing was observed at 107 kips with a mid-span deflection of 2.81 inches.

The primary failure mode of this specimen was concrete crushing at the top surface in the constant-moment region, which occurred after both steel and TiAB yielding. At 95 kips, localized inclined cracks developed near the concrete-epoxy interface. Prior to unloading, the specimen exhibited visible concrete-epoxy delamination at 108 kips and a mid-span deflection of 3.31 inches, as pictured in Figure 7-11. The specimen exceeded the AASHTO NSM TiAB Guide calculated capacity of 95 kips and carried 22.7% more load when compared to the control specimen.



Figure 7-11 Concrete-epoxy interface failure for Specimen TB.G.S.P.02 at 108 kips load

7.3.3.3 Specimen TB.G.S.P.03

As previously discussed and shown in Table 7-2, Specimens TB.G.S.P.02 and TB.G.S.P.03 had identical TiAB bonded lengths but the latter specimen used TiAB Type 2 that had different surface deformations and yield strength ($f_y = 142$ ksi). The test objective was to assess the effect of using a different TiAB type on the specimen strength and behavior. When comparing the responses of TB.G.S.P.02 and TB.G.S.P.03 in Figure 7-8, their responses were similar except TB.G.S.P.03 carried slightly more load than TB.G.S.P.02. The load capacity difference is potentially due to the yield strength difference between the two TiAB types; however, the different TiAB types caused no real significant difference in flexural behavior. For TB.G.S.P.03, steel yielding occurred at 73 kips and 0.44 inches of mid-span deflection. TiAB strains indicated initiation of TiAB yielding at 94 kips load and 1.45 inches of displacement. Concrete crushing occurred at 110 kips and 2.97 inches of mid-span displacement.

The primary failure mode was thus concrete crushing on the top (compression) surface in the constant-moment region, which occurred after the steel and TiAB yielded. Some localized

inclined cracks developed at or near the concrete-epoxy interface at 100 kips and 1.97 inches of mid-span deflection. At 112 kips and 3.47 inches of displacement, the concrete-epoxy interface delamination became highly prominent, and the specimen was subsequently unloaded (Figure 7-12). The specimen exceeded the AASHTO NSM TiAB Guide capacity of 97 kips and carried 25% more load when compared to the control specimen.



Figure 7-12 Concrete-epoxy interface failure for Specimen TB.G.S.P.03 at 112 kips load

7.3.3.4 Specimen TB.G.S.N.01

This specimen was strengthened with TiAB Type 1 and the provided bonded length was equal to the TiAB development length (l_{dTiAB}) calculated according to an assumed average bond strength of 0.5 ksi according to Equation 2.5. The crack pattern of this specimen resembled the negative-moment control specimen. As the load increased, new cracks formed, and all the cracks (new and pre-existing cracks) widened and propagated toward the load points. Inclined cracks formed at 40 kips and propagated toward the load points. Steel yielding occurred at 64 kips and a mid-span displacement of 0.66 inches. At 76 kips and 1.76 inches of displacement (Point F1 in Figure 7-9), the inclined cracks formed near the TiAB termination regions became wider and the specimen exhibited a stiffness change. The specimen capacity decreased soon after Point F1 with increasing displacement. Widening of the cracks at the TiAB ends developed with increasing displacement which was followed by the delamination of the concrete-epoxy interface, as shown in Figure 7-13. Concrete crushing was observed after a significant load drop at 69 kips and 2.72 inches of mid-span displacement. The maximum TiAB strain was recorded as 4740 $\mu\epsilon$, which was less than the TiAB yield strain (8516 $\mu\epsilon$).

The measured peak load was 76 kips, which is below the AASHTO NSM TiAB Guide calculated capacity of 79 kips. The primary failure mode of the specimen was due to concrete-

epoxy interface delamination caused by wide cracks at the ends of the TiAB. The test demonstrated that providing only development length as the bonded length was insufficient to achieve the targeted flexural strength.



Figure 7-13 Wide crack formation at the end of TiAB and concrete-epoxy interface delamination for Specimen TB.G.S.N.01

7.3.3.5 Specimen TB.G.S.N.02

This specimen was strengthened with TiAB Type 1 and the provided bonded length was determined according to the requirements of ACI 440.2. The initial crack pattern observed for this specimen closely resembled those of the previously discussed negative-moment specimens. Inclined crack formation initiated at 50 kips and propagated toward the load points. With increasing load, both new and existing cracks widened and extended. Steel yielding began at 64 kips and a mid-span displacement of 0.64 inches. The TiAB also yielded at 77 kips and 1.66 inches of deflection. Concrete crushing on the top surface occurred at 83 kips and 2.94 inches of mid-span displacement. Some cracking in the epoxy was also observed at this load level. A small crack appeared near the concrete-epoxy interface at 78 kips, but it did not significantly widen or lead to any failure.

The specimen reached its maximum load at 84 kips at a displacement of 3.30 inches, which exceeded the AASHTO NSM TiAB Guide calculated capacity of 79 kips. At this load, a visible

concrete-epoxy delamination failure was observed, and a sudden, but small drop in force occurred. The load was further increased until the specimen could no longer take any additional load and was subsequently unloaded at 4.87 inches of displacement. The crack pattern of the specimen prior to unloading is shown in Figure 7-14. The primary failure mode of this specimen was concrete crushing in the flexural compression zone. The specimen exceeded the calculated capacity of the AASHTO NSM TiAB Guide and resisted about 22% more load when compared to the control specimen.



Figure 7-14 Concrete cracking pattern for Specimen TB.G.S.N.02 at 4.44 inches of mid-span displacement

7.4 HOOKED-UNBONDED SPECIMENS

The TiAB length of the hooked-unbonded specimens, the test results, and a discussion of the test results are presented in this section. The test matrix in Table 7-3 **Error! Reference source not found.** provides details of the parameters evaluated and the specimen designation. More details of the naming convention are also discussed in Chapter 6.

Table 7-3 Test Matrix and Specimen Designation for Hooked-unbonded Specimens

Specimen Designation	Testing Configuration	TiAB Application	Anchorage	TiAB Length* (in.)	TiAB Type
TB.P.Control	Positive moment	N.A. (Control specimen)	N.A.	N.A.	N.A.
TB.U.H.P.01	Positive moment	Unbonded	Hooked	45	2
TB.U.H.P.02	Positive moment	Unbonded	Hooked	59	2

Notes: N.A. means not applicable and * denotes the length from the loading point to the nearest hook.

7.4.1 STRENGTHENING OF SPECIMENS

Two hooked-unbonded strengthened specimens were tested as shown in **Error! Reference source not found.** and compared against the control specimen. The specimens were tested only with the positive-moment test configuration. Specimen TB.U.H.P.01 was strengthened by considering the effect of stress discontinuity for the internal bar cutoff, as described in ACI 318-19. The details of the effect of stress discontinuity for internal bar cutoff are described in Chapter 6. This same condition was used for hooked-bonded strengthening method that performed as desired. The calculated TiAB length was 45 in. from the loading point, resulting in a total TiAB length of 114 in. Specimen TB.U.H.P.02 was strengthened providing a TiAB length that extends 6 inches beyond the distance from the loading point to the section where the moment demand exceeds the calculated cracking moment (M_{cr}). The TiAB length for the second specimen was 59 in. from the loading point, resulting in a total TiAB length of 142 in. Type 2 TiAB was used to strengthen both TB.U.H.P.01 and TB.U.H.P.02.

7.4.2 TEST RESULTS

The load-deflection responses of the positive-moment strengthened (hooked-unbonded) specimens are compared against the control specimen in Figure 7-15. In this figure, X denotes when concrete crushing occurred in the control specimen. The curves indicate very similar responses for all specimens prior to yielding of the steel. The calculated strength of the control and strengthened specimens were 68 kips and 97 kips, respectively, according to Equation 2.4 (omitting the TiAB terms for the control specimen calculations). It should be noted that TB.U.H.P.01 and TB.U.H.P.02 did not reach the AASHTO NSM TiAB Guide calculated capacity, indicating the ineffectiveness of the *unbonded* TiAB strengthening method for these specimens.

7.4.3 DISCUSSION OF TEST RESULTS

7.4.3.1 Specimen TB.U.H.P.01

As the load on Specimen TB.U.H.P.01 was increased, cracks from the pre-crack cycles widened and further extended, and new cracks also formed. Inclined shear cracks started to develop at 55 kips. Flexural cracks began to form next to the TiABs hook locations that propagated inwards toward the flange with increasing load. Steel yielding occurred at 67 kips at a mid-span deflection of 0.45 inches. The post-steel yielding stiffness of this specimen was noticeable. The load-carrying capacity was higher than the control specimen, but a sudden drop of load occurred at 95 kips and 2.03 inches of displacement due to anchorage failure at the hooked end (point F1 on Figure 7-15) on one side of the specimen due to losing a part of the concrete cover, as shown in Figure 7-16. Before this anchorage failure, numerous cracks were generated near the hook end. The specimen continued to be loaded, and concrete failure occurred on the other side of the girder at the hook end location. A sudden drop of force occurred at 97 kips at a mid-span deflection of 2.67 inches (point F2 on Figure 7-15). Subsequently, the specimen was unloaded. The maximum strain measured on the TiABs was about $7828 \mu\epsilon$ which was less than the yield strain of Type 2 TiAB of $9161 \mu\epsilon$. The measured capacity of the specimen did not reach the AASHTO NSM TiAB Guide calculated capacity for the strengthened specimen of 97 kips (Figure 7-15). Additionally, specimen TB.U.H.P.01 did not exhibit a significant strength increase because of the anchorage failure prior to the TiABs achieving yielding.

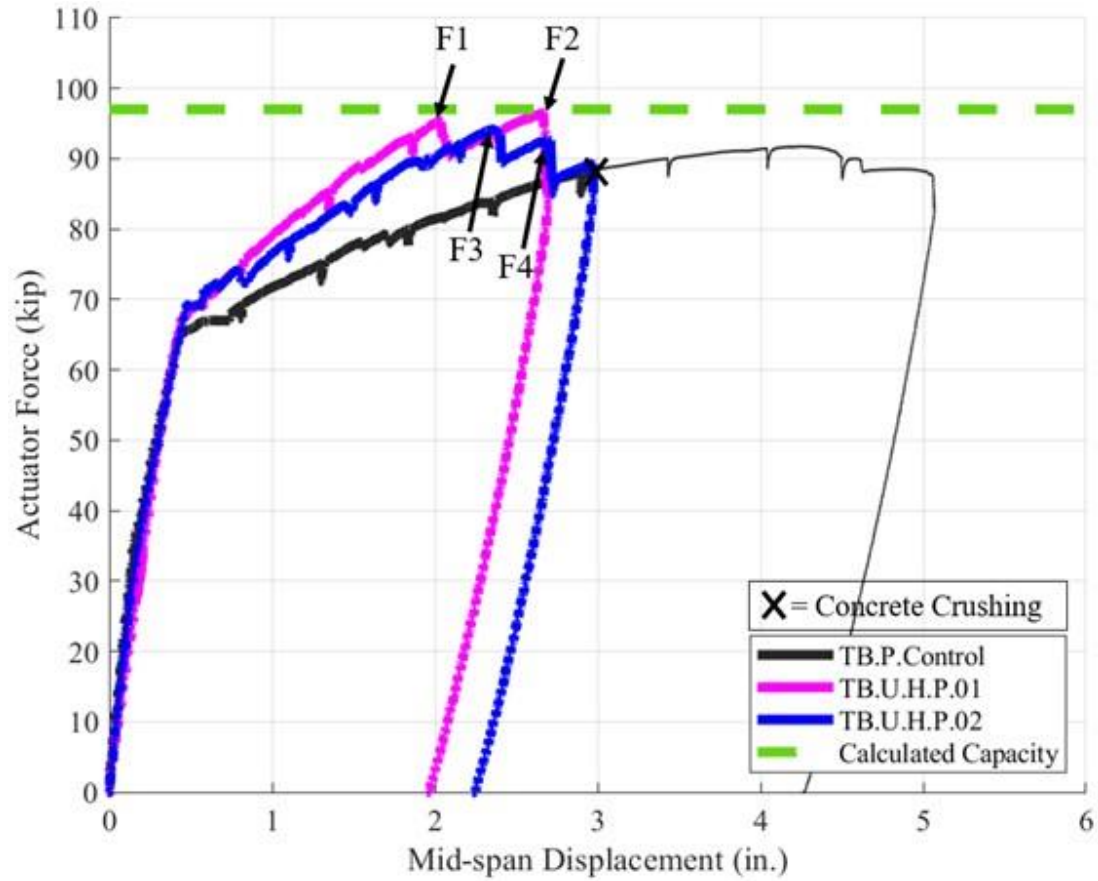


Figure 7-15 Load-deflection behavior of the positive-moment specimens (hooked-unbonded specimens)



Figure 7-16 Anchorage failure of Specimen TB.U.H.P.01

7.4.3.2 Specimen TB.U.H.P.02

As the load on Specimen TB.U.H.P.02 was increased, cracks from the pre-crack cycles widened and further extended, and new cracks also formed. Inclined shear cracks started to develop at 50 kips that propagated inwards toward the flange with increasing load. Steel yielding occurred at 69 kips at a mid-span deflection of 0.47 in. The post-steel yielding stiffness of this specimen was less than the first strengthened specimen with the hooked-unbonded method (Figure 7-15). The load-carrying capacity was higher than the control specimen, but a sudden drop of load occurred at 94 kips and 2.36 in. of mid-span displacement due to the loss of concrete cover on one side end of the TiAB (point F3 on Figure 7-15). The load was further increased but another sudden drop of load occurred at 93 kips at a mid-span deflection of 2.73 inches (point F4 on Figure 7-15). Because of the decrease in load resistance, the specimen was considered failed and unloaded. The maximum strain in the TiAB was about $6935 \mu\epsilon$ which was less than the yield strain of Type 2 TiAB was $9161 \mu\epsilon$. The measured capacity of the specimen did not exceed the AASHTO NSM TiAB Guide calculated capacity for the strengthened specimen of 97 kips (Figure 7-15). Specimen TB.U.H.P.02 did not exhibit a significant strength increase because of the anchorage failure near the hook ends as shown in Figure 7-17.



Figure 7-17 Anchorage failure of Specimen TB.U.H.P.02

7.5 FATIGUE LOAD TEST

The fatigue testing of a TiAB NSM strengthened specimen using the hooked-bonded method is presented in this section. The test matrix in **Error! Reference source not found.** provides details of the parameters evaluated and the specimen designation. More details of the naming convention are also discussed in Chapter 6.

Table 7-4 Test Matrix and Specimen Designation for Fatigue Load Test

Specimen Designation	Testing Configuration	TiAB Application	Anchorage	Bonded Length* (in.)	TiAB Type
TB.F.P.Control	Positive moment	N.A. (Control specimen)	N.A.	N.A.	N.A.
TB.F.H.P	Positive moment	Bonded	Hooked	45	2

Notes: N.A. means not applicable and * denotes the length from the loading point to the nearest hook.

7.5.1 STRENGTHENING OF SPECIMENS

Two specimens were tested using the fatigue load test protocol which included one control specimen as shown in **Error! Reference source not found..** Specimen TB.F.H.P was strengthened by accounting for the effect of stress discontinuity for the internal bar cutoff described in ACI 318-19 as described in Chapter 6. Specimen TB.F.H.P. was strengthened by providing a bonded length of 45 in. from the loading point, resulting in a total bonded length of 114 in. The moment and resistance diagrams at the nominal strengthened capacity of specimens TB.F.H.P. ($M_n = 313$ k-ft, calculated according to Equation 2.4) is shown in Figure 6-14, along with the lines indicating twice the moment demand ($2M_u$). Type 2 TiAB was used to strengthen Specimen TB.F.H.P. The details of the types of TiABs are covered in Chapter 3.

7.5.2 DISCUSSION OF TEST RESULTS

The control (unstrengthened) specimen was tested for comparison with the strengthened specimen. Both specimens were pre-cracked to simulate the in-service condition of the bridge girder by applying load until the tensile steel reached $1000 \mu\epsilon$. The control specimen was then subjected to fatigue load, while the other specimen was strengthened with two #4 NSM TiAB bars with hook ends according to the ACI318-19 guideline to account for the stress concentration at the bar termination locations. Two #4 TiABs (Type 2) were placed on the side of the web at 3 in. from the bottom of the specimen. The strengthened specimen was then tested under fatigue load test protocol. The fatigue loading, using a sinusoidal load at 1.2 Hz with a target stress range of 13 ksi, was applied for 2.0 million cycles. A four-point loading configuration was used for cracking, fatigue testing, and post-fatigue (step-load application) testing. After the fatigue load cycles, step loads (as discussed in Section 6.7) were applied to evaluate the remaining capacity of the bridge girder. The fatigue test results and measured behavior are covered in the following sections.

7.5.2.1 Fatigue test results

The strain variation in the tensile steel with the number of cycles is shown in Figure 7-18. The target stress range was 13 ksi with a maximum strain of 965 $\mu\epsilon$ and minimum strain of 517 $\mu\epsilon$ (corresponding to cycling between 5 ksi and 18 ksi), as indicated by the blue lines in the figure. After starting the test, the strain (both maximum and minimum) in the tensile steel increases above the target strain for both the control and strengthened specimen which is considered conservative for the purposes of this study.

The initial stress levels in the reinforcing steel that were targeted as the upper and lower bounds for fatigue loading gradually increased throughout the tests. For the control specimen, the initial stress range was 14.4 ksi which increased to 14.9 ksi by the end of the 2.0 million cycles. The applied load range was 21.0 kips with a maximum load of 24.3 kips and a minimum load of 3.3 kips.

For the strengthened specimen, the initial stress range was 14.6 ksi but it increased to 16.5 ksi at 0.65 million load cycles. The stress range was then adjusted, which is visible in Figure 7-18. Following the adjustment, the stress range remained at 13.5 ksi for the remainder of the test. The applied load range was 20.5 kip (with a maximum load of 25 kips, and a minimum load of 4.5 kips) to achieve the desired stress range. The strain in the TiAB varied in the range of 40 $\mu\epsilon$ to 800 $\mu\epsilon$, which is less than one-tenth of the TiAB yield strain ($\epsilon_{yTi} = 9161\mu\epsilon$). The mid-span TiAB strain gauge measurements cycled between 100-530 $\mu\epsilon$, while in some other locations, it was ranged between 250-800 $\mu\epsilon$, 203-626 $\mu\epsilon$, and 270-600 $\mu\epsilon$.

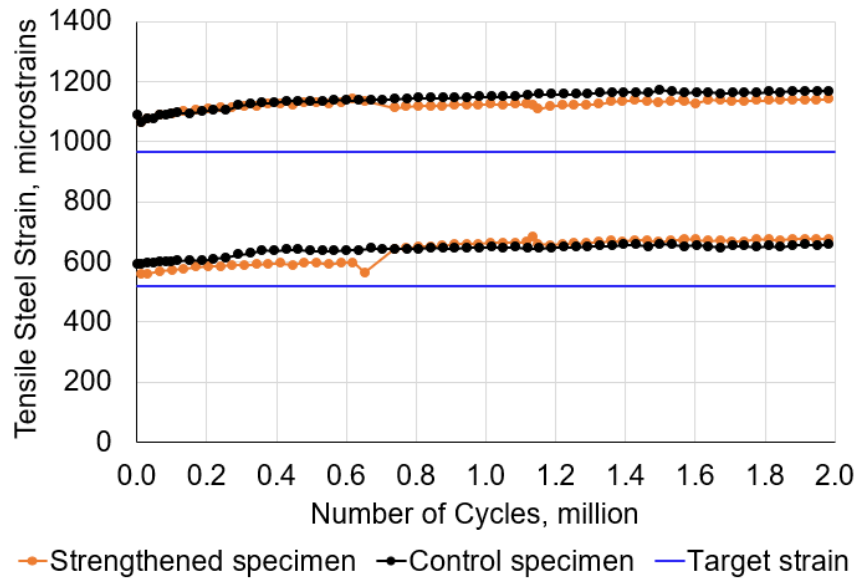


Figure 7-18 Strain variation in tensile steel under fatigue load cycles

Figure 7-19 shows the variation of mid-span displacement of the specimen versus the number of load cycles. For the control specimen, the mid-span displacement gradually increased with the increase of the number of fatigue cycles. The maximum displacement reached at the end of the fatigue cycles was 0.163 inches. For the strengthened specimen, the mid-span displacement increased until 0.62 million cycles and thereafter remained nearly constant. As expected, the mid-span displacement in the strengthened specimen was less than that of the control specimen.

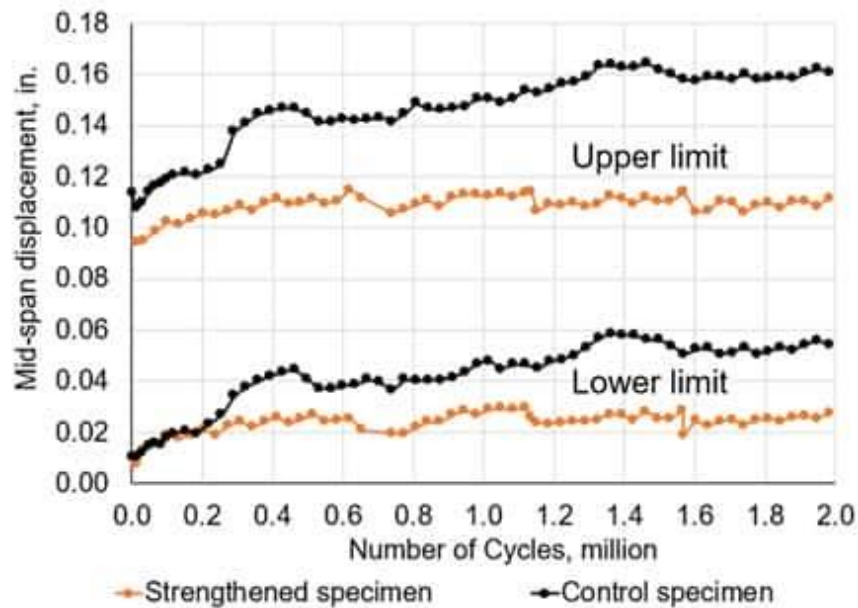


Figure 7-19 Variation of mid-span displacement under fatigue load

7.5.2.2 Post-fatigue test results

After the fatigue cycles, the step loads from C to H shown in Figure 7-20 were applied. The estimated total load (ETL) was calculated to be 76 kips and 102 kips for the control and strengthened specimen, respectively. The applied load and mid-span displacement response of the specimens during these step loads is shown in Figure 7-22. For the control specimen, the maximum strain in the tensile steel was $2805 \mu\epsilon$ during the step-load cycles (load cycles G and H) following the fatigue loading. Once the step loads were successfully completed for the control specimen, monotonic loading with a load rate of 0.02 in./minute was applied until failure. The applied load and mid-span displacement response is shown in Figure 7-21. The response was linear until steel yielding and visible stiffness changes occurred after steel yielding. Strain hardening contributed to the strength, which is visible from the post-steel yielding response and the measured ultimate strength of this specimen exceeded the calculated capacity of 76 kips.

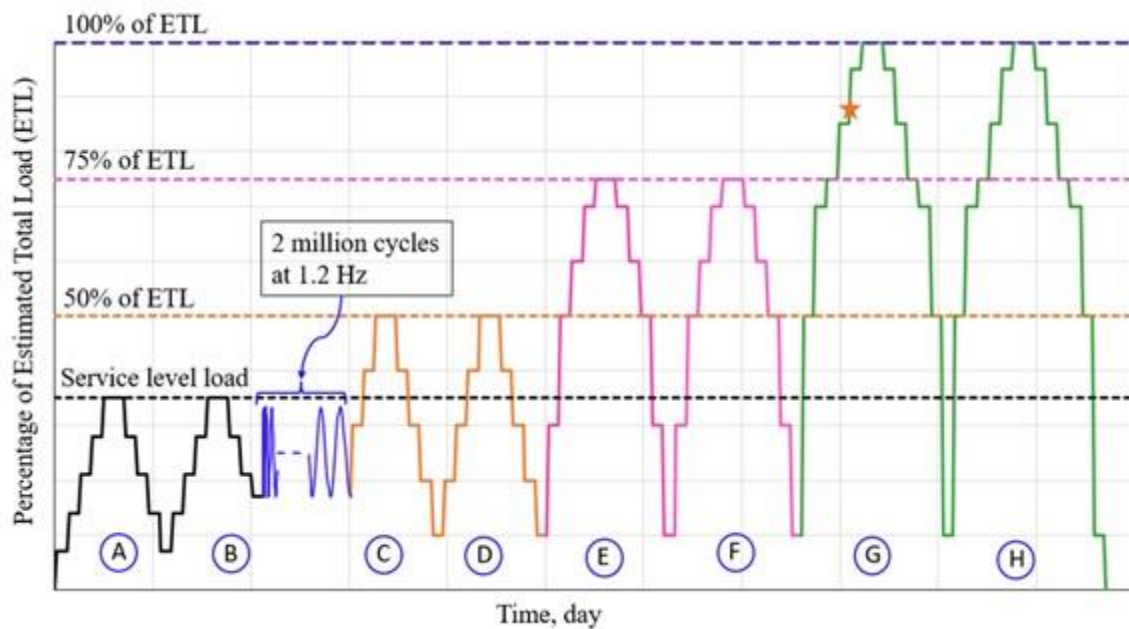


Figure 7-20 Loading protocol for fatigue test

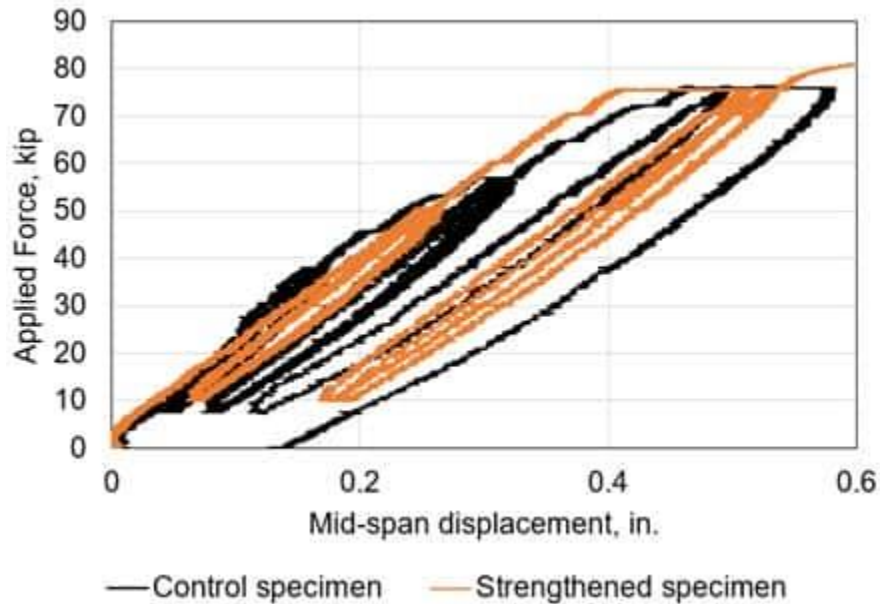


Figure 7-21 Mid-span displacement versus applied force response during step loads

The initial load cycles and fatigue cycles were successfully completed for the strengthened specimen (TB.F.H.P). During the application of step load G for the strengthened specimen, the hydraulic actuator abruptly started to vibrate. This instant is shown as an orange star mark on load step G in Figure 7-20 and corresponded to near the yielding of the steel reinforcement. Due to the significant change in the member stiffness due to steel yielding and the use of load-control protocol to control the actuator, the specimen experienced large displacement during the abrupt vibration stage. Figure 7-23 illustrates the applied load and mid-span displacement response of the strengthened specimen during step load and the actuator started to vibrate at point A. The actuator force rapidly fluctuated from 47 kips to 133 kips during this vibration stage which exceeded the calculated capacity of the specimen (102 kips) and resulted in failure by concrete crushing and TiAB rupture. The calculated capacity was based on Equation 2.4 using measured yield strengths of the steel reinforcement and TiAB. The maximum strain in the steel reinforcement was $3029 \mu\epsilon$ before the actuator entered the abrupt vibration stage.

As discussed above, due to the excessive hydraulic actuator vibration that occurred during the failure load cycles the strengthened fatigue load specimen failed unexpectedly. The fatigue performance of the strengthened specimen could thus not be properly evaluated, making the test results inconclusive. Discussions with hydraulic actuator manufacturer representatives revealed the reason for the unexpected vibration behavior to lack of valve tuning of the actuator when performing under force-controlled loading mode. To eliminate such unexpected actuator vibration response, the final load stage of future fatigue tests will be conducted in displacement-controlled loading mode.

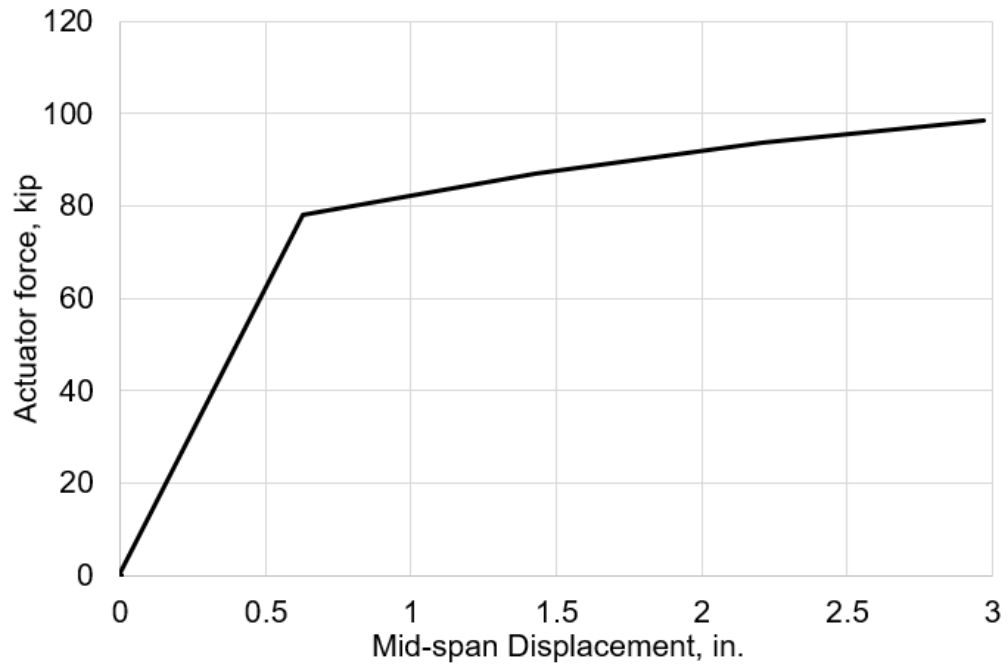


Figure 7-22 Applied load versus mid-span displacement response of control specimen post-fatigue testing

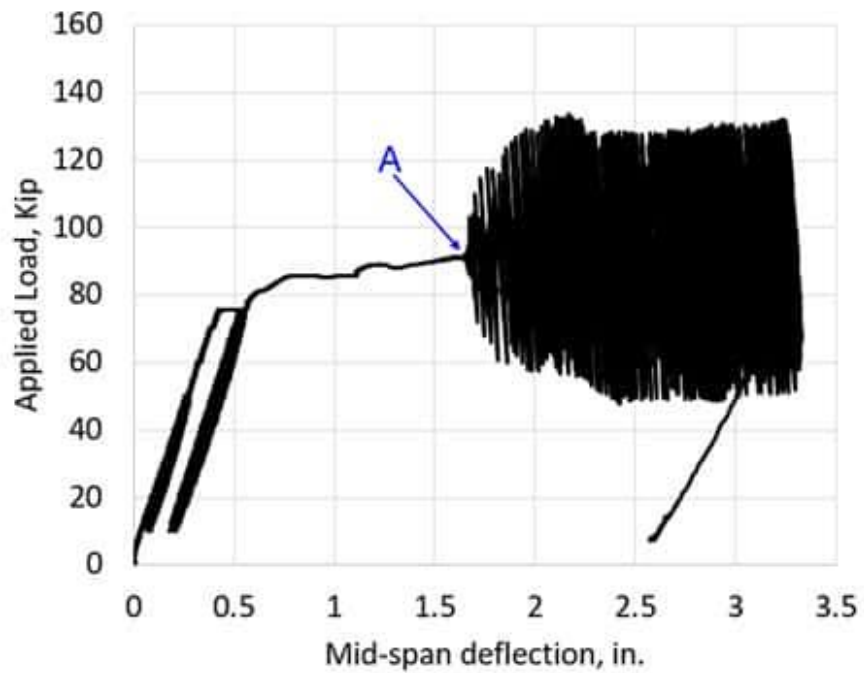


Figure 7-23 Applied load versus mid-span displacement during step loads for the strengthened specimen

7.5.2.3 Fatigue behavior of TiAB

To determine whether the TiAB had an impact on failure, two TiABs were tested in tension in accordance with ASTM E8. The TiABs were subjected to fatigue load cycles (sinusoidal shaped) at 2 Hz frequency for 2 million cycles using a strain range of 200-800 $\mu\epsilon$. The strain range was selected from the strain reading of TiAB from the tested beam discussed above. Since each TiAB strain gauge had cycled in a slightly different range during the fatigue loading of the beam tests, a range of 200-800 $\mu\epsilon$ was chosen as a worse-case strain range to capture the bounds of the TiAB strain gauge readings from the beam tests, as discussed in the previous section. After 2 million cycles tension test was performed to measure the stress-strain response after fatigue loading. A direct tension test was performed on a TiAB using displacement-control (DC) loading protocol mentioned in ASTM E8, and for another TiAB, a direct tension test was performed using force-control (FC) loading protocol with a rate of 1kip/min. until yielding and then 0.5 kip/min. until failure. The tension test results of the TiABs with fatigue and without fatigue load cycles are shown in Figure 7-24. The unfatigued TiAB has a yield strength of 142 ksi with a yield strain of 0.0095 and the ultimate stress was 155 ksi with an ultimate strain of 0.107.

From the results in Figure 7-24, the TiAB tested using DC loading protocol has around 5% less strength than the unfatigued TiAB. The yield strength of this specimen is 136 ksi with a yield strain of 0.0096 and the ultimate stress was 150 ksi with an ultimate strain of 0.16. Therefore, the results of this specimen are similar to those measured to the unfatigued TiAB specimen and exhibited similar good ductility.

The TiAB tested using FC loading protocol has around 8% less strength than the unfatigued TiAB. The yield strength of this specimen is 130 ksi with a yield strain of 0.0099 in./in. and the ultimate stress was 146 ksi with an ultimate strain of 0.0312 in./in. This specimen failed at a strain of 0.0312 in./in.

Therefore, from the above-mentioned test results, it can be concluded that the force control (FC) loading protocol has an impact on the performance of the TiAB. However, in all cases when the TiAB was tested in direct tension, the TiAB was able to exceed yield strains which did not occur during fatigue testing of the large-scale girder. From the direct tension results, it can be concluded that the vibration of the actuator led to the failure of the large-scale girder during fatigue testing. The post-fatigue testing behavior of a large-scale girder will thus be re-tested using displacement-control loading protocol.

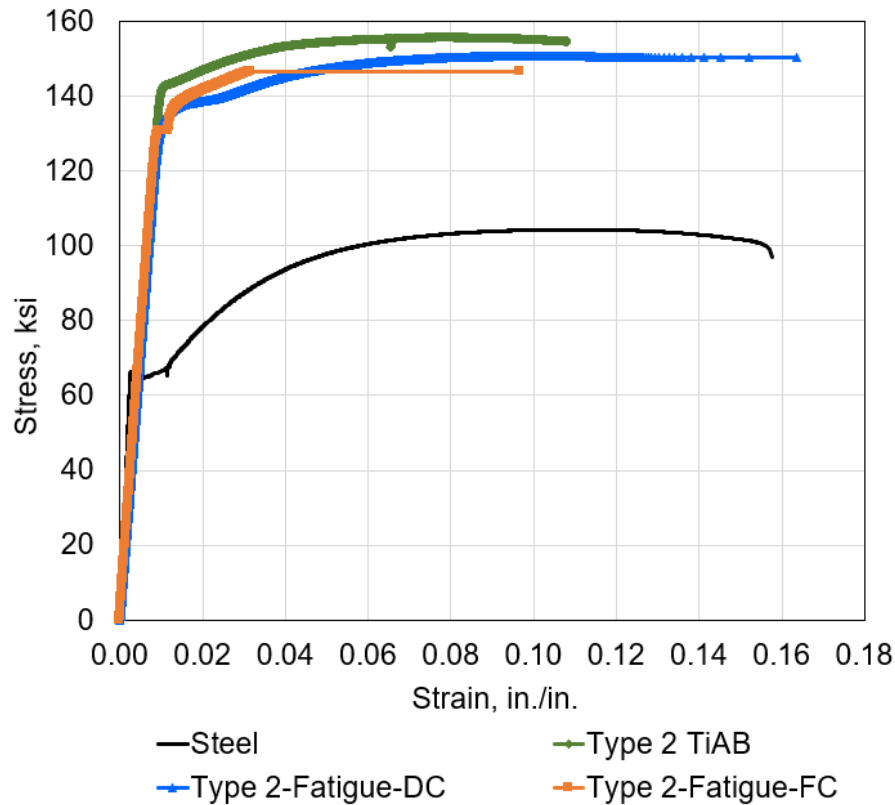


Figure 7-24 Tension test results of steel and TiAB (with and without fatigue load cycles)

7.6 SUMMARY AND CONCLUSIONS OF PHASE 2 TESTING

7.6.1 HOOKED-BONDED SPECIMENS

The results about the failure load and mode of all the tested specimens are provided in **Error! Reference source not found..** The primary failure mode of the control specimen for the positive moment case (TB.P.Control) was concrete crushing at the concrete compression zone at a load of 88 kips and displacement of 3.00 in. Specimen TB.G.H.P.01 for which the bonded TiABs length was equal to the development length calculated according to the AASHTO NSM TiAB Guide, failed at a load of 91 kips due to anchorage failure around the TiAB hooked ends. Specimen TB.G.H.P.01 carried only 3.4% more load than the positive-moment control specimen at primary failure. Specimens TB.G.H.P.02 and TB.G.H.P.03 for which the bonded TiABs length was selected by considering the effect of stress concentrations of terminating bars according to ACI 318-19, both exhibited concrete crushing at the concrete compression zone as their primary failure modes at a load of 108 kips and displacements of 2.98 and 2.90 in., respectively. Specimens TB.G.H.P.02 and TB.G.H.P.03 carried 22.7% more load at primary failure mode than the positive-moment control

specimen and exceeded the AASHTO NSM TiAB Guide calculated capacity by 13% and 11%, respectively.

Table 7-5 Summary Results of Hooked-bonded Tested Specimens

Specimen Designation	Testing Configuration	Bonded Length*, in.	Load at Primary Failure, kips	Strength calculated based on Equation 1, kips	Displ. at Primary Failure, in.	Primary Failure Mode
TB.P.Control	Positive moment	N.A.	88	68	3.00	Concrete crushing
TB.G.H.P.01	Positive moment	16.5	91	95	2.50	Anchorage failure
TB.G.H.P.02	Positive moment	45	108	95	2.98	Concrete crushing
TB.G.H.P.03	Positive moment	45	108	97	2.90	Concrete crushing
TB.N.Control	Negative moment	N.A.	67	61	2.78	Concrete crushing
TB.G.H.N.01	Negative moment	34	75	79	1.63	Anchorage and delamination failure
TB.G.H.N.02	Negative moment	45	83	79	2.86	Concrete crushing

Notes: N.A. means not applicable and * denotes the length from the loading point to the nearest hook.

For the negative-moment strengthening tests, the primary failure mode of the control specimen (TB.N.Control) was concrete crushing at the concrete compression zone at a load of 67 kips and displacement of 2.78 in. Specimen TB.G.H.N.01 for a bonded TiAB length of 48 in. was provided according to the AASHTO NSM TiAB Guide, failed at a load of 75 kips due to anchorage failure at the TiAB hooked ends followed by delamination failure at the concrete-epoxy interface. Specimen TB.G.H.N.01 carried about 12% more load than the negative-moment control specimen at their primary failure modes. Specimen TB.G.H.N.02 for which the bonded TiAB length was selected by considering the effect of stress concentrations when terminating bars in the tension zone according to ACI 318-19, carried a load of 83 kips at a mid-span displacement of 2.86 in. and failed due to concrete crushing at the concrete compression zone. Specimen TB.G.H.N.02 carried 24% more load than the negative-moment control specimen at their primary failure modes and exceeded the AASHTO NSM TiAB Guide calculated capacity by 4.5%.

In order to compare the serviceability performance of the strengthened specimens, crack width measurements taken during the tests are compared against permissible crack widths provided in

the AASHTO LRFD Specification in Table 7-6. Crack widths are compared at a load level that corresponds to a maximum service-level stress ($0.6f_y \leq 36$ ksi) in the reinforcement bar according to the AASHTO LRFD Specification. The load levels corresponding to $0.6f_y$ and measured crack widths at these load levels are compared against the permissible crack width for Class 1 exposure in the AASHTO LRFD Specification. This crack width class is characterized by a reduced concern for appearance, corrosion, or both. The comparisons indicated that for both positive- and negative-moment tests, the measured crack widths were all within the AASHTO permissible limit.

Table 7-6 Service-Level Crack Width Comparisons (hooked-bonded specimens)

Specimen Designation	Max. Service level stress, ksi	Calculated force using elastic crack section analysis, kip	Measured crack width, in.	Permissible crack width, in.
TB.P.Control	36	33.8	0.016	0.017
TB.G.H.P.01			0.012	
TB.G.H.P.02			0.012	
TB.G.H.P.03			0.016	
TB.N.Control	36	30.2	0.008	0.017
TB.G.H.N.01			0.016	
TB.G.H.N.02			0.016	

Based on the results obtained from testing girders strengthened with hooked-bonded TiAB NSM, the following conclusions can be drawn:

- Providing only the development length of TiABs as the bonded length was not sufficient to achieve the full-strength contribution of TiABs through yielding. Even the addition of $d_v \cot \theta$ to the development length in accordance with the AASHTO NSM TiAB Guide was not sufficient to achieve the desired strength.
- Formation of inclined shear cracks due to stress concentrations near hook end locations causes hook anchorage failure, which can result in the ineffectiveness of NSM TiAB strengthening. Therefore, the effect of inclined shear cracks must be taken into consideration when designing for flexural strengthening using NSM TiAB with hook ends.
- Flexural strengthening using NSM TiABs with hooked ends is effective when the TiAB bonded length is determined to prevent excessive inclined shear cracks cracking at the TiAB termination locations in the tension region. ACI 318-19 requirements for internal reinforcement cut-off were found applicable and adequate to account for the impact of stress concentrations at TiABs hook ends. It is recommended to include the design considerations from ACI 318-19 to account for the effect of stress concentration at the end of the cutoff bar in the flexural tension zone in the AASHTO NSM TiAB Guide.
- Two different TiAB types were evaluated, and they provided similar flexural response and behavior, so either type can be used to strengthen reinforced concrete bridge girders.

7.6.2 STRAIGHT -BONDED SPECIMENS

The results of all the tested specimens and failure modes are summarized in Table 7-7. The primary failure mode of the TB.P.Control specimen was concrete crushing in the concrete compression zone. The TiAB bonded length for TB.G.S.P.01 was determined according to the AASHTO NSM TiAB Guide. TB.G.S.P.01 exceeded the strengthened nominal capacity but suddenly failed due to concrete-epoxy delamination before reaching concrete crushing, indicating that the provided TiAB bonded length was insufficient. Specimens TB.G.S.P.02 and TB.G.S.P.03 for which the bonded TiAB length was calculated according to ACI 440.2, both achieved concrete crushing as their primary failure modes, exhibited ductile failure modes, and exceeded the AASHTO NSM TiAB Guide calculated capacity by 12.6% and 13.4%, respectively. For the negative-moment tests, the primary failure mode of the TB.N.Control specimen was concrete crushing in the concrete compression zone. The TiAB bonded length for TB.G.S.N.01 was equal to the TiAB development length calculated using an average bond strength of 0.5 ksi. The specimen failed due to concrete-epoxy interface delamination near the TiAB termination regions. Specimen TB.G.S.N.02 for which the TiAB bonded length was 72 inches from the load points and determined based on ACI 440.2, failed due to concrete crushing in the concrete compression zone. Specimen TB.G.S.N.02 exceeded the AASHTO NSM TiAB Guide calculated capacity by 5.1%.

Table 7-7 Summary Results of Straight-bonded Tested Specimens

Specimen Designation	Testing Configuration	Bonded Length*, in.	Load at Primary Failure, kips	Strength calculated based on Equation 1, kips	Displ. at Primary Failure, in.	Primary Failure Mode
TB.P.Control	Positive moment	N.A.	88	68	3.00	Concrete crushing
TB.G.S.P.01	Positive moment	53	100	97	2.00	Delamination failure
TB.G.S.P.02	Positive moment	72	107	95	2.81	Concrete crushing
TB.G.S.P.03	Positive moment	72	110	97	2.97	Concrete crushing
TB.N.Control	Negative moment	N.A.	67	61	2.78	Concrete crushing
TB.G.S.N.01	Negative moment	33	76	79	1.76	Delamination failure
TB.G.S.N.02	Negative moment	72	83	79	2.94	Concrete crushing

Notes: N.A. means not applicable and * denotes the length from the loading point to the nearest hook.

To compare the serviceability performance of the strengthened specimens, crack width measurements taken during the tests are compared against permissible crack widths provided in the AASHTO LRFD Specification (2024) in Table 7-8. Crack widths are compared at a load level that corresponds to a maximum service-level stress ($0.6f_y \leq 36$ ksi) in the reinforcement bar according to AASHTO LRFD Specification. The load levels corresponding to $0.6f_y$ and measured crack widths at these load levels are compared against the permissible crack width for Class 1 exposure in the AASHTO LRFD Specification. This crack width class is characterized by a reduced concern for appearance, corrosion, or both. A comparison of the crack widths in **Error! Reference source not found.** indicate that the measured crack widths for both positive- and negative-moment tests that achieved yielding of the TiAB were all within the AASHTO permissible limit, except for the TB.G.S.N.01 specimen that failed before the TiAB yielded.

Table 7-8 Service-Level Crack Width Comparisons (straight-bonded specimens)

Specimen Designation	Max. Service level stress, ksi	Calculated force using elastic crack section analysis, kip	Measured crack width, in.	Permissible crack width, in.
TB.P.Control	36	33.8	0.016	0.017
TB.G.S.P.01			0.012	
TB.G.S.P.02			0.012	
TB.G.S.P.03			0.012	
TB.N.Control	36	30.2	0.008	0.017
TB.G.S.N.01			0.020*	
TB.G.S.N.02			0.012	

Table note: *this specimen did not achieve yielding of the TiAB prior to failure.

The following conclusions can be drawn based on testing girders strengthened with straight-bonded TiAB NSM:

- Providing only the TiAB development length as the TiAB bonded length was insufficient to achieve the full-strength contribution of TiAB through yielding. Even the addition of $dvCot\theta$ to the development length in accordance with the AASHTO NSM TiAB Guide did not result in satisfactory overall performance.
- When insufficient TiAB bonded length is provided, cracks in the concrete-epoxy interface close to the TiAB termination regions cause delamination failure, which can result in the ineffectiveness of the NSM TiAB strengthening. Therefore, the effect of delamination failure must be taken into consideration when designing for flexural strengthening using NSM TiAB with straight bars.
- ACI 440.2 requirements to determine the bonded length of TiAB were found applicable and adequate to eliminate the impact of concrete cover delamination or concrete-epoxy

interface delamination. Therefore, it is recommended to use Section 14.1.2 of ACI 440.2 when designing with straight TiAB for NSM applications to address the concrete-epoxy interface delamination.

- Both TiAB types used in the study provided similar flexural responses, so either type can be used to strengthen RC bridge girders with NSM using straight TiAB.

7.6.3 HOOKED-UNBONDED SPECIMENS

The failure load and mode results of all hooked-unbonded tested specimens are provided in Table 7-9. Specimen TB.U.H.P.01 for which the provided TiABs length was based on considering the effect of stress concentrations when terminating bars in the tension zone according to ACI 318-19, failed at a load of 95 kips with a displacement of 2.03 inches due to anchorage failure around the TiAB hooked end. Specimen TB.U.H.P.01 carried only 8% more load than the positive-moment control specimen at primary failure. Specimens TB.U.H.P.02 had a TiAB length equal to the distance from the loading point to the point where the cracking moment (M_{cr}) intersected the moment demand, plus an additional 6 inches. The specimen TB.U.H.P.02 failed at 94 kips load and 2.36 inches of midspan deflection exhibiting anchorage failure as the primary mode of failure. It carried only 6.8% more load at its primary failure mode compared to the positive-moment control specimen. Due to anchorage failure, none of the specimens achieved TiAB yielding nor reached the AASHTO NSM TiAB Guide calculated capacity.

Table 7-9 Summary Results of Hooked-unbonded Tested Specimens

Specimen Designation	Testing Configuration	TiAB Length*, in.	Load at Primary Failure, kips	Strength calculated based on Equation 1, kips	Displ. at Primary Failure, in.	Primary Failure Mode
TB.P.Control	Positive moment	N.A.	88	68	3.00	Concrete crushing
TB.U.H.P.01	Positive moment	45	95	97	2.03	Anchorage failure
TB.U.H.P.02	Positive moment	59	94	97	2.36	Anchorage failure

Notes: N.A. means not applicable and * denotes the length from the loading point to the nearest hook.

Based on the results obtained from testing girders strengthened with hooked-unbonded TiAB NSM, the following conclusions can be drawn:

- Formation of inclined cracks due to stress concentrations near hook end locations causes hook anchorage failure, which can result in the ineffectiveness of hooked-unbonded TiAB strengthening.

- Because of hook end/anchorage failure, the strength contribution was marginal, therefore it is recommended to use the hooked-unbonded strengthening method only for temporary (i.e., emergency) purposes.

7.6.4 FATIGUE TEST SPECIMENS

The final two tests of the large-scale testing program aimed to evaluate the fatigue performance of the TiAB NSM strengthened specimen. The load protocol included performing two million load cycles before loading the specimens to failure. However, due to an unexpected response in the hydraulic actuator during the failure load cycles, the fatigue performance of the strengthened specimen could not properly be evaluated, rendering the test results inconclusive. Direct-tension tests were performed with fatigue cycles on TiAB. The TiAB was able to exceed yield strains which did not occur during fatigue testing of the large-scale girder. From the direct tension results, it can be concluded that the TiAB is not susceptible to high-cycle fatigue, and the high-load cycles during the vibration of the actuator led to the failure of the large-scale girder during fatigue testing. Since fatigue loading is common for bridges due to vehicle crossings, experimental demonstrations of fatigue performance are necessary to provide final recommendations to ALDOT on using this novel strengthening method. Funding through an Auburn University Highway Research Center (HRC) study will be used to conduct additional fatigue testing. These tests will investigate the fatigue performance of specimens by replicating the beams tested in the ALDOT research project, which simulated the strength-deficient Cullman bridge girders.

The tests will essentially repeat the testing of the two specimens planned for the original test program; however, displacement-control loading will be used because it was concluded that load-control loading can lead to erratic actuator response. These tests will include one control (unstrengthened) and one strengthened specimen. Including a new control specimen will facilitate direct comparison of results because both specimens will be made from the same reinforcing steel and concrete.

The final report will include a summary of test results and comparisons with prior tests and calculations. The outcomes of this HRC project may be incorporated into this ALDOT final report to complete the missing fatigue performance, ensuring the ALDOT project final report serves as a comprehensive document providing recommendations and guidance for using the NSM TiAB strengthening method for ALDOT bridges.

Chapter 8

PROPOSED STRENGTHENING METHOD FOR THE CULLMAN BRIDGE

8.1 INTRODUCTION

This chapter provides an overview of the proposed strengthening details to address the identified flexural deficiencies of the bridge in Cullman, Alabama. A draft special provision to implement the proposed strengthening method for the Cullman Bridge is presented in Appendix C.

8.2 OVERALL BRIDGE DESIGN

The Cullman Bridge is a three-span, continuous reinforced-concrete bridge built in the early 1960's in Cullman (NBI ID: 7755). The bridge is on US Route 278 (State Route 74) that is part of main Street (3rd St.) of downtown Cullman. As shown in Figure 1-1, this bridge is an overpass over the S&N Alabama subdivision railroad line of CSX Transportation. The bridge has been weight-restricted due to positive- and negative-moment strength deficiencies for several truck types, as shown in Figure 1-1. The bridge is 102 ft long and has two lanes. The exterior spans are 30 ft and the interior span is 42 ft in length. The bridge consists of five continuous, reinforced concrete girders per direction with parabolic haunches at interior supports. The bridge deck is 6 inches thick with a roadway width of 26 ft. Girders are spaced at 6 ft 6.5 in. center to center laterally, and the curb is located 3.0 ft from the centerline of the exterior girder on each side of the bridge. A simplified plan and cross-sectional view of the bridges are shown in Figure 8-1 and Figure 8-2, respectively. The sectional view of the bridge girder with reinforcement detailing and overall dimension is shown in Figure 8-3. The bridge girder has a 1.0 in. clear cover at the bottom of the slab, 1.5 in. clear cover at the top of the slab, and 1.94 in. clear cover at the side and bottom of the web as shown in the Figure 8-3.

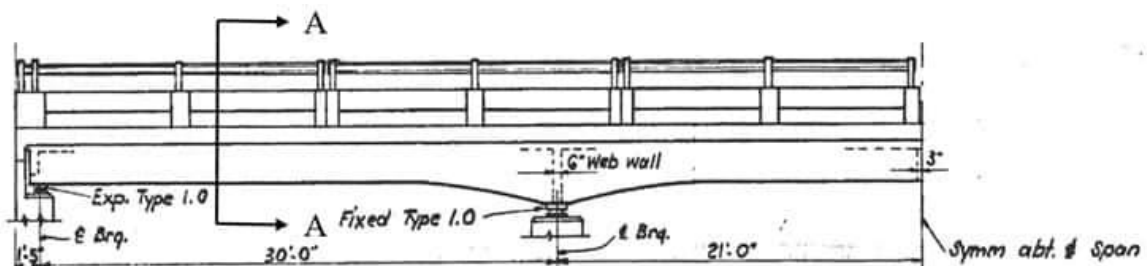


Figure 8-1 Plan View Showing Half of the Cullman Bridge (courtesy of ALDOT)

8.3 BRIDGE DEFICIENCIES

The structural analysis of the Cullman Bridge was evaluated by the ALDOT Bridge Rating and Load Testing engineers using AASHTOWare Bridge Rating (BrR) software. Table 8-1 summarizes the locations with insufficient flexural strength for the Emergency Vehicle (EV3) loading case obtained from the BrR software for Span 1. Load rating factors (LRF) calculated at these critical locations indicate flexural strength deficiencies in the range of 20% (See Table 8-1: Span 1, section at 19 ft, LRF = 0.791 [positive moment in yellow], and section at 21.29 ft, LRF = 0.821 [negative moment in orange]). These critical locations coincide with reinforcement cutoff locations at the ends of the haunch regions where the section depth parabolically decreases from 3'-0" to 1'-8", as shown in Figure 8-4. The BrR results also indicate insufficient flexural capacity (LRF<1.0) for the Tri-Axle and Concrete truck load cases at the same locations in Span 1 as highlighted in Table 8-1.

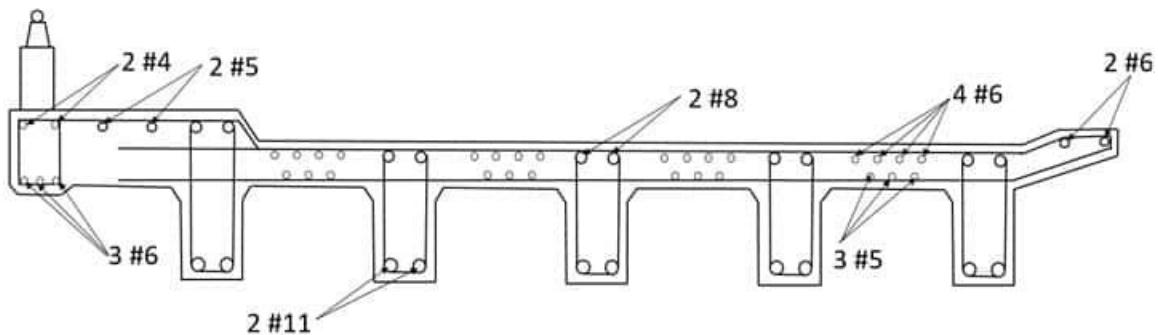


Figure 8-2 Cross Section at Mid of the Span (Section A-A in Figure 8.1) of the Cullman Bridge (figure not to scale)

Table 8-1 and Figure 8-4 indicates that both positive- and negative-moment strengthening is required at the reinforcement cutoff locations in the two end spans (e.g. Section A-A in Figure 3.4). Since the bridge passes over the railroad line, there is also limited clearance and access to perform any work under the bridge (positive-moment strengthening). Therefore, the bridge has been selected to be an ideal candidate to demonstrate the use of titanium-alloy reinforcement as the strengthening method to address both negative- and positive-moment deficiencies. The final design of the strengthening method has been determined through laboratory testing and analytical work considering the limited access to strengthen the Cullman Bridge.

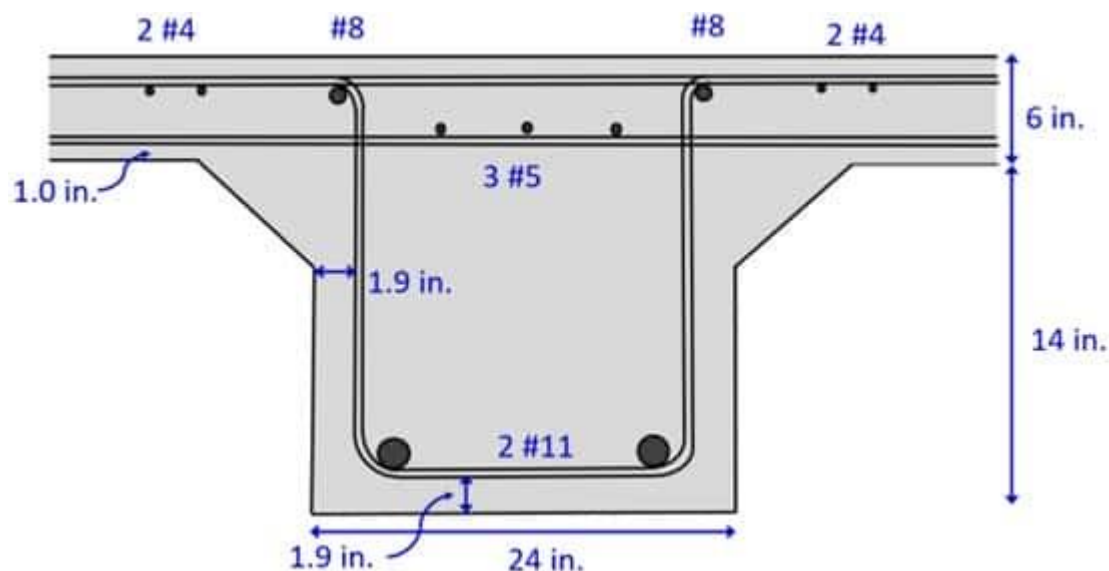


Figure 8-3 Sectional view of the bridge girder with reinforcement detailing

Table 8-1 Locations with Flexural Strength Deficiencies Based on EV3 Load Case (Positive Mom. in Yellow, Negative Mom. in Orange, Most Critical Locations Circled)

Span 1							Operating	Operating
Location							Rating	Load
(ft)	Percent	Limit State	Units	Capacity	DL + Adj -LL*	LL	Factor	Rating
15.42	51.4	Flexure	kip-ft	328.46	23.66	211.99	1.080	46.45
18.00	60.0	Flexure	kip-ft	-163.77	8.68	-143.05	0.941	40.48
19.00	63.3	Flexure	kip-ft	185.31	1.21	178.72	0.791	34.01
21.00	70.0	Flexure	kip-ft	-205.50	-16.26	-166.89	0.850	36.54
21.29	71.0	Flexure	kip-ft	-205.50	-19.11	-169.21	0.821	35.32
21.49	71.6	Flexure	kip-ft	-211.19	-21.04	-170.79	0.828	35.60
21.50	71.7	Flexure	kip-ft	-211.44	-21.15	-170.87	0.828	35.61
Span 2								
10.83	25.8	Flexure	kip-ft	185.31	7.08	154.41	0.877	37.73
11.00	26.2	Flexure	kip-ft	192.85	8.67	157.82	0.885	38.05
31.00	73.8	Flexure	kip-ft	192.85	6.93	153.20	0.923	39.69

8.3.1 PRELIMINARY ANALYTICAL WORK

The primary advantage of titanium-alloy bars is the high yield strength that allows the use of less reinforcement area to develop the same force as compared to other conventional alternatives. This strength advantage can translate into using reduced quantity or smaller diameter reinforcement to

achieve a certain level of strength increase. For example, a #6 Grade 60 conventional bar develops approximately the same strength as a #4 Grade 140 titanium-alloy bar, or the total tension force developed with 7x#4 conventional steel bars can be achieved using 3x#4 titanium-alloy bars. The reduction in the rebar quantity or size makes it easier to physically install and leads to significant cost savings during the field strengthening application, which offsets the higher material cost of titanium alloy bars.

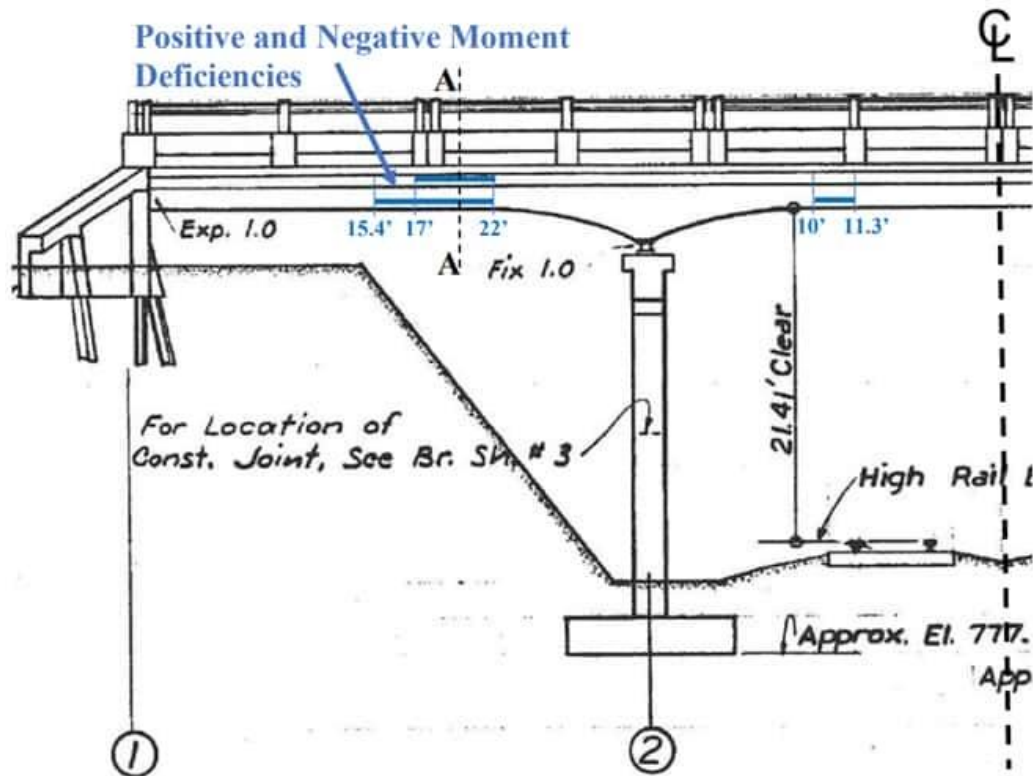


**Figure 8-4 Illustration of Portions with Insufficient Flexural Strength of the Cullman Bridge
(Delineated with blue lines)**

To demonstrate the potential flexural strength benefits of using titanium-alloy reinforcement for the girders of the Cullman Bridge, preliminary analytical studies were conducted, and their results are presented in Figure 8-5. The results shown were obtained by performing sectional moment-curvature calculations for both the positive- and negative-moment cases at the locations with flexural strengths deficiencies (Section A-A in Figure 8-4). The graphs include the moment-curvature response plots for the existing and strengthened cases. For the strengthened case, two #4 ($A_s = 2 \times 0.2 \text{ in}^2 = 0.4 \text{ in}^2$) titanium-alloy bars were added to each girder at the identified cross-section to gain additional flexural capacity. In both cases, the analytical strength increase was sufficient to exceed the required moment capacity as indicated by the demand line shown in Figure 8-5.

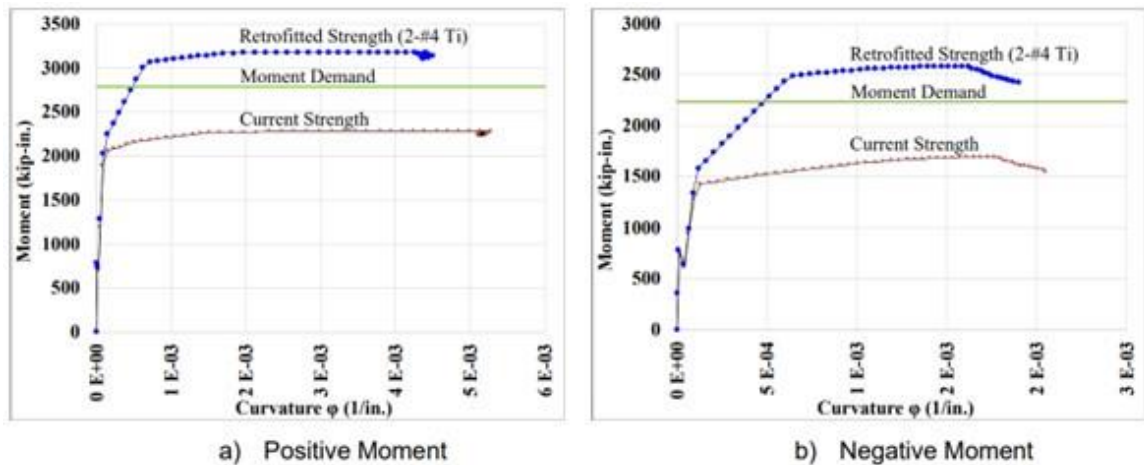


Figure 8-5 Moment-curvature Comparison Plots using Titanium-Allow Reinforcement to Strengthen the Cullman Bridge

8.3.2 DETAILED STRUCTURAL ANALYSIS AND PROPOSED STRENGTHENING METHOD

ALDOT analyzed the Cullman Bridge using BrR software for different types of vehicles. The results for the Emergency Vehicle (EV3) loading were used to check the moment deficiencies because this loading type created the most critical moment (both positive and negative) as shown in Figure 8-6 and Figure 8-7 for span 1 and span 2, respectively. The exterior girders did not have any moment deficiencies, but the interior girders did. Span 1 exhibited both positive- and negative-moment deficiencies (green circle in Figure 8-6), while span 2 had only positive-moment deficiency (green circle in Figure 8-7). The black line is the unstrengthened girder capacity based on the ALDOT analysis (using BrR software). The girder capacity was calculated assuming a rating factor of 1.0 (orange line in Figure 8-6 and Figure 8-7), and was calculated based on AASHTO Specifications (AASHTO, 2020b) including dead load, live load, and impact load, with operating level factors applied.

To address these deficiencies, hooked-bonded TiAB NSM was selected to strengthening the Cullman Bridge because this method is currently the only permitted anchorage method by the AASHTO NSM TiAB Guide. The experimental studies conducted using this anchorage method also demonstrated satisfactory performance for strengthening the specimens when provision of ACI 318-19 for considering the effect of stress discontinuity at internal bar cutoff locations were followed for determining the TiAB bonded length. ACI 318-19 Section 9.7.3.5 specifies that bars should not be terminated in a tension zone unless one of three conditions is met: (i) the factored shear force is not greater than the design shear resistance, including that provided by shear reinforcement; (ii) additional stirrups are provided along each terminated bar over a distance of no less than three-

fourths the effective depth of the member; or (iii) for No. 11 and smaller bars, the continuing reinforcement provides double the flexural capacity compared to the moment demand, while ensuring that the factored shear force does not exceed three-fourths of the design shear resistance. In this study, the third condition of ACI 318-19 was satisfied and was used to design the NSM TiAB strengthening for the Cullman Bridge girders. The details of the strengthened and moment-deficient regions are shown in Figure 8-8, where blue lines indicate the moment-deficient portion and orange lines represent the strengthened portion.

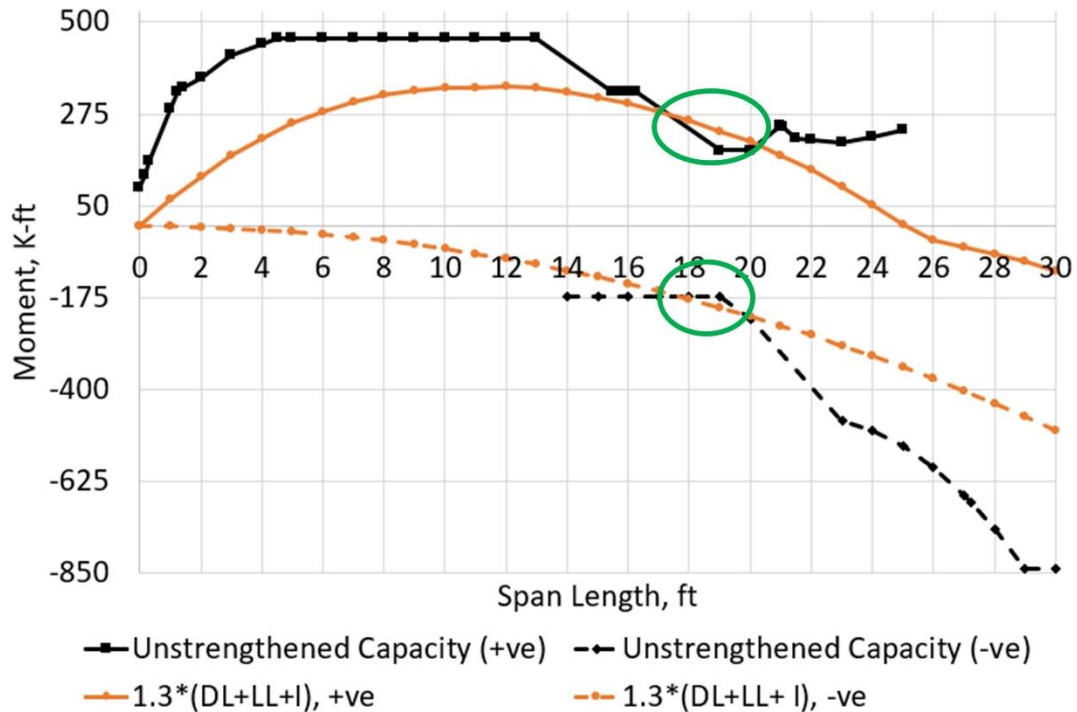


Figure 8-6 Positive- and Negative-moment Deficiencies for Span 1 (green circle)

For positive moment strengthening, the TiAB was designed to be placed 5 inches from the bottom of the web along the sides of the girders on both sides, due to the railroad passing under the bridge. For negative-moment strengthening, the TiAB will be installed at the bottom of the slab on both sides to minimize any disruption to the vehicle traffic over the bridge. Two #5 TiAB bars were found to be sufficient to achieve the desired moment capacity for the positive-moment deficiencies, while four #3 TiAB bars were determined to be used for the negative-moment deficiencies. The bar sizes for positive- and negative-moment strengthening were selected based on providing adequate strength and safety margin while accounting for the available concrete cover in the region that grooves need to be cut.

According to the AASHTO NSM TiAB Guide, the groove depth and width for a #5 bar is 15/16 inches (0.94 inches), which is close to the 1.0-inch cover available at the bottom of the slab. On

the other hand, #4 and #3 TiAB bars have groove dimensions of 0.75 inches and 9/16 inches (0.56 inches), respectively. Therefore, after discussions with ALDOT, #3 TiAB was selected for negative-moment strengthening. For positive-moment strengthening, #5 TiAB was chosen for positive-moment strengthening to provide a greater safety margin and the bar size (and corresponding groove size) is manageable from a constructability perspective, as the web has a 1.94-inch clear cover on the side of the girders. The groove size and moment capacity details of the strengthened bridge girders, with a safety margin, are illustrated in Figures 8.9 to 8.12. For positive-moment strengthening, the TiAB will be placed at 5" from the bottom of the web along the side of the girders on both sides to avoid reducing the overheight clearance of the rail track under the bridge. For negative-moment strengthening, the TiAB will be placed at the bottom of the slab on both sides of the slab to avoid closing the bridge to traffic during the repair. Before cutting any grooves, it is recommended to use ground-penetrating radar to measure the as-built cover to verify that there is sufficient cover to accommodate the groove depths required to mount the #3 and #5 TiAB.

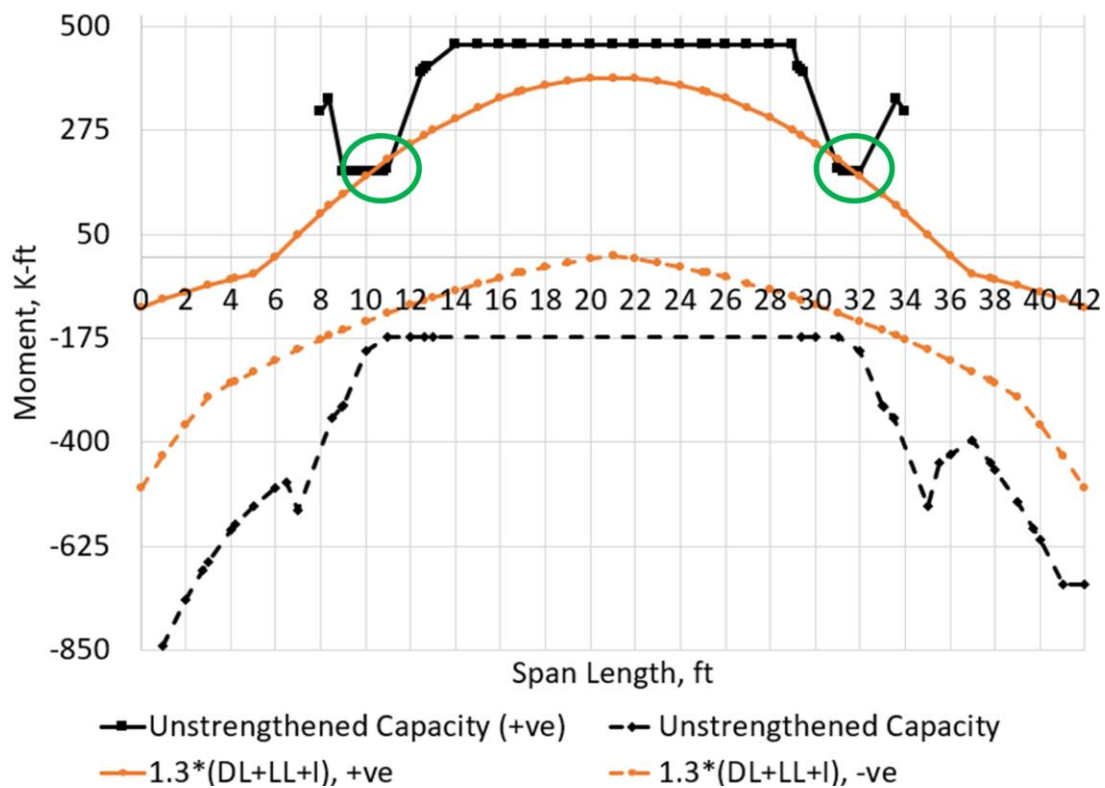


Figure 8-7 Positive-moment deficiencies for Span 2 (green circle)

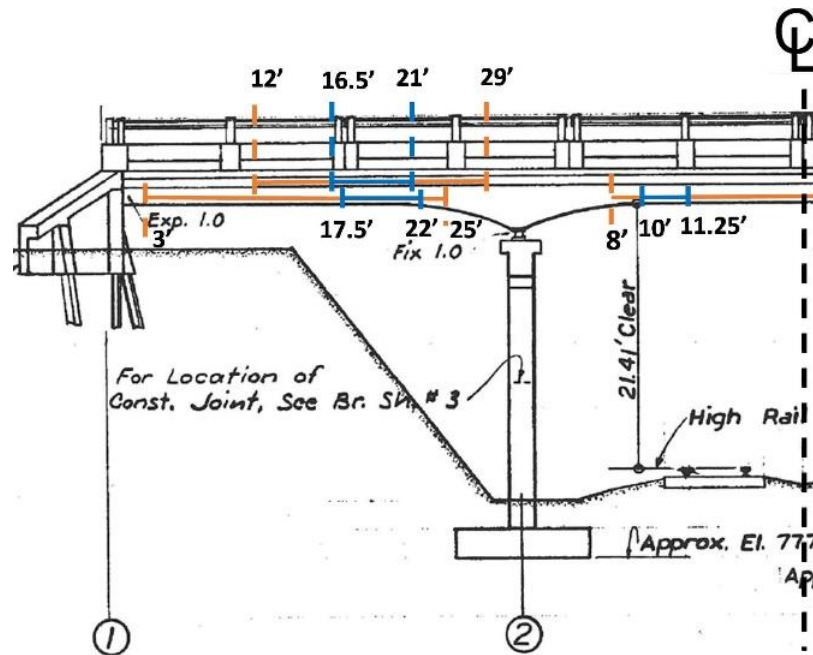


Figure 8-8 Strengthened and moment-deficient lengths in the Cullman Bridge

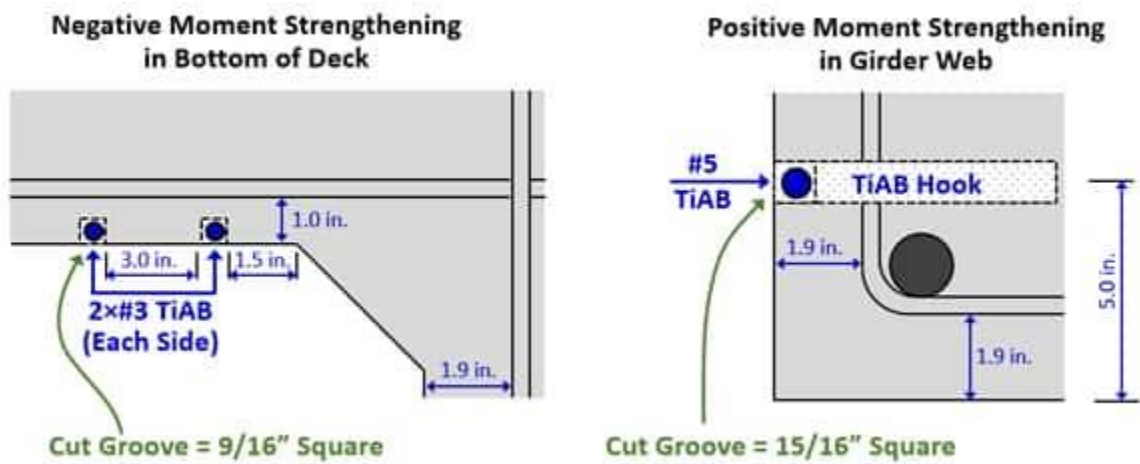


Figure 8-9 Groove size and location for #5 and #3 TiAB

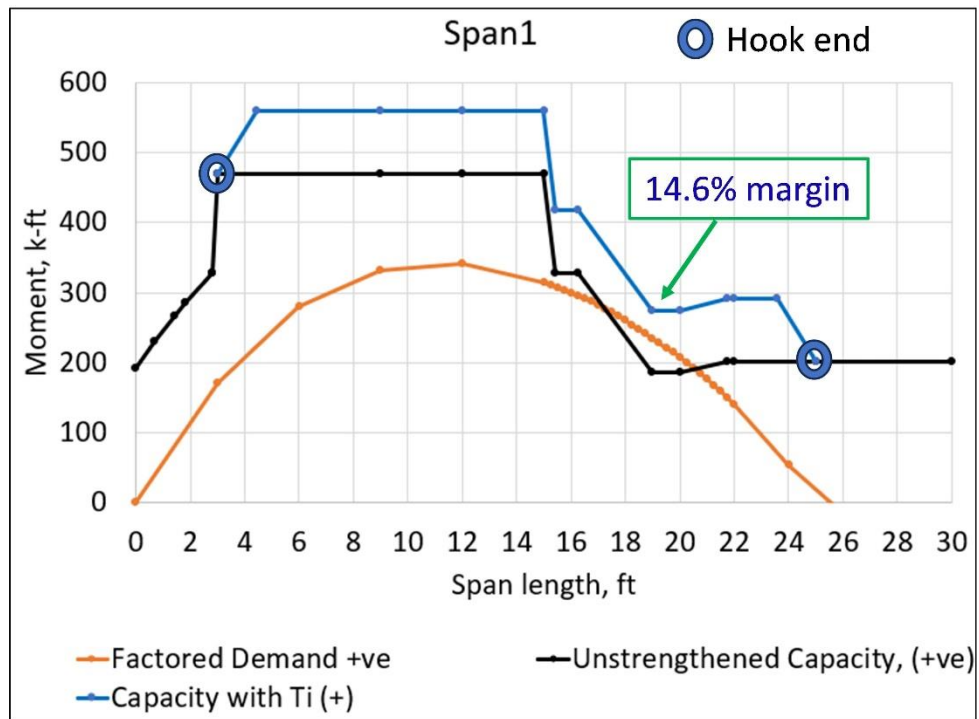


Figure 8-10 Positive-moment strengthened capacity for span 1

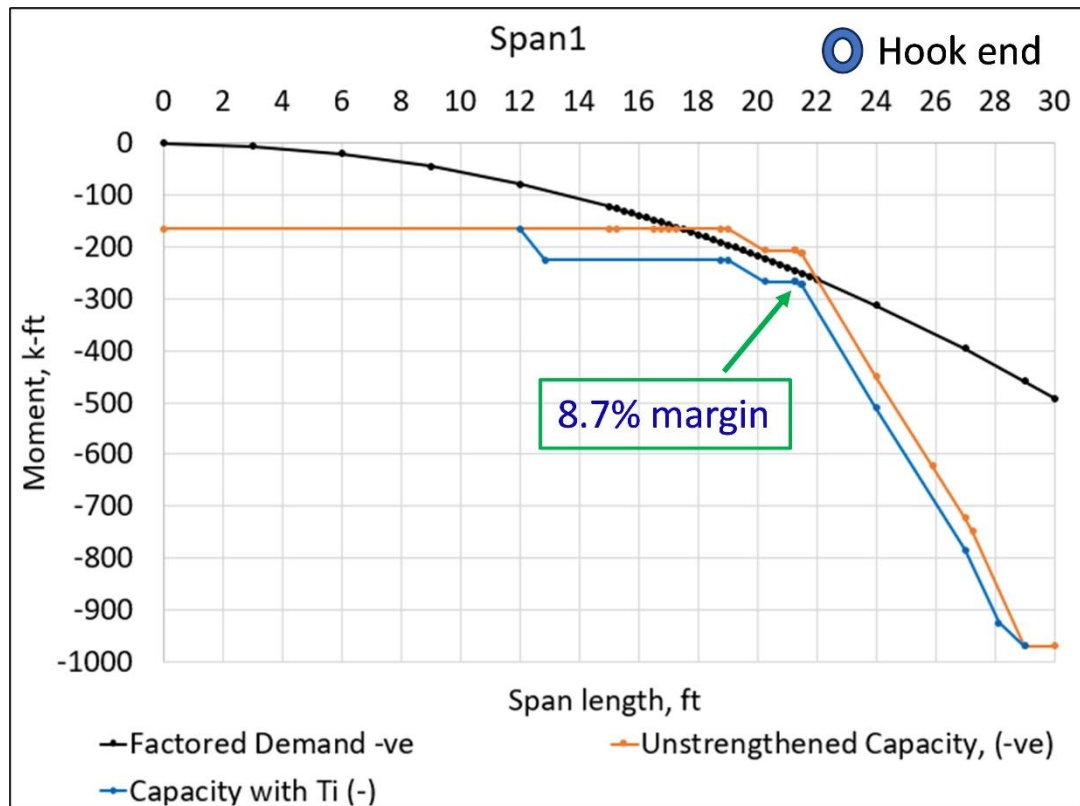


Figure 8-11 Negative-moment strengthened capacity for span 1

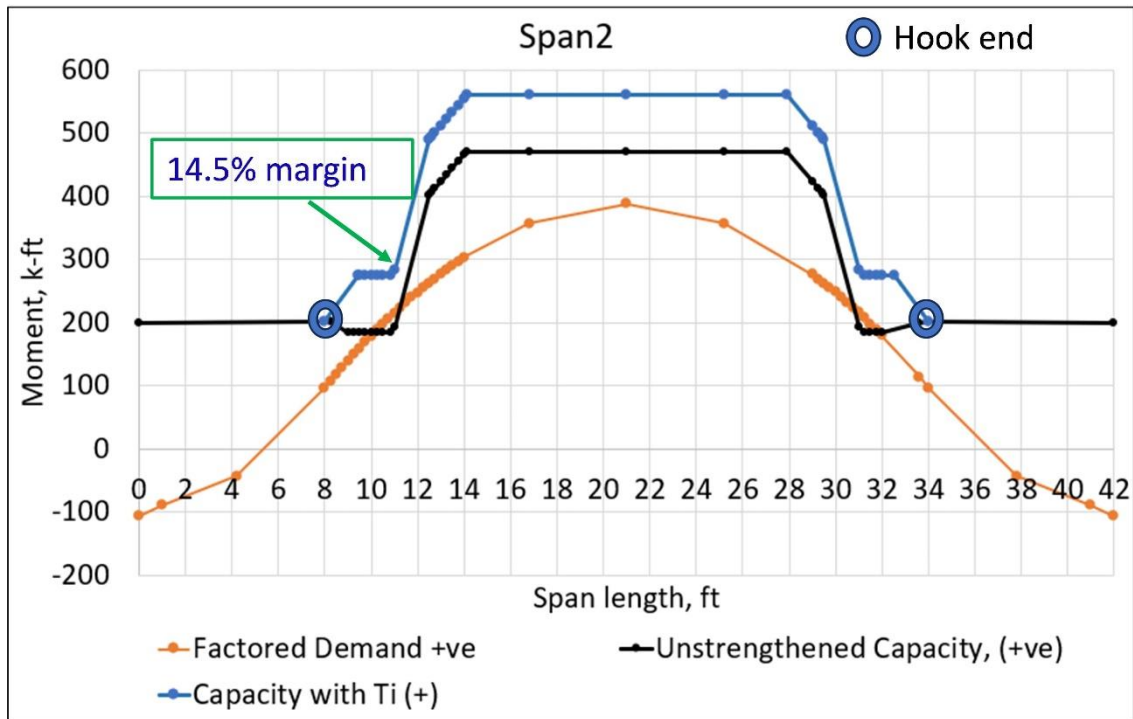


Figure 8-12 Positive-moment strengthened capacity for span 2

Chapter 9

SUMMARY, CONCLUSIONS, AND RECOMMENDATIONS

Strengthening reinforced concrete (RC) members using near-surface mounted titanium-alloy bars (NSM TiAB) has emerged as a promising alternative to traditional methods, such as NSM with carbon fiber-reinforced polymers (CFRP). To assess the feasibility of NSM TiAB for strengthening RC members, experimental work was conducted involving both material- and member-level studies on beam specimens. The study also included unstrengthened control specimens for comparison purposes. The test results were used to evaluate the flexural behavior with varying TiAB bonded lengths and to evaluate the applicability and accuracy of the design provisions in the AASHTO NSM TiAB Guide, particularly concerning flexural strength and TiAB development length. This chapter presents conclusions and recommendations drawn from the test results of both Phase 1 and Phase 2 performed for this project.

9.1 PHASE 1 WORK

In this phase, small-scale experimental studies were performed to assess the accuracy of AASHTO NSM TiAB Guide for hooked-bonded strengthened specimens and provide the appropriate guidance for straight-bonded and hooked-unbonded specimens. The strength predictions according to AASHTO NSM TiAB Guide were achieved when adequate TiAB bonded lengths were provided. For the bonded TiAB mounting methods, specimens with longer TiAB bonded lengths reached TiAB yielding and demonstrated ductile behavior compared to those with shorter bonded lengths. For the hooked-unbonded specimens, specimens with longer TiAB lengths resulted in TiAB yielding and exceeded the AASHTO NSM TiAB Guide predicted capacity, but the specimens could not maintain the load for extended periods due to the development of large cracks near the TiAB hook ends.

9.1.1 CONCLUSION OF PHASE 1 WORK

The following conclusions can be drawn from the results of Phase 1 work:

1. Hooked-bonded specimens with adequate bonded length achieved TiAB yielding and exceeded the strength calculated with the AASHTO NSM TiAB Guide. These specimens also demonstrated that an average TiAB bond strength of 1.0 ksi, as provided in the AASHTO NSM TiAB Guide, appears to be reasonable for the hooked-bonded TiAB anchorage method.

2. Straight-bonded specimens with adequate bonded length achieved TiAB yielding and exceeded the strength calculated with the AASHTO NSM TiAB Guide. These specimens also demonstrated that a TiAB bond strength of 0.5 ksi appears to be reasonable for the straight-bonded method, though further experimental studies to check the fatigue performance of this method are recommended.

3. Hooked-unbonded specimens exhibited greater crack widths and lower stiffness compared to both hooked-bonded and straight-bonded specimens. Therefore, it is recommended that hooked-unbonded specimens be used only for temporary (i.e., emergency) purposes.

9.2 PHASE 2 WORK

In this phase, a total of 16 specimens were tested simulating the Cullman Bridge, Alabama, which has flexural strength deficiencies. The specimens were strengthened using NSM TiAB using hooked-bonded, straight-bonded, and hooked-unbonded anchorage methods, and tested to evaluate the positive- and negative-moment capacities and behavior. Two specimens were tested to assess the fatigue performance, including one control specimen. These two specimens were tested for positive- moment strengthening purposes only and one specimen was strengthened using hooked-bonded TiAB NSM with the bonded length meeting the requirements of ACI318-19 Section 9.7.3.5. Due to malfunctioning of the hydraulic actuator, the results from the fatigue tests were inconclusive and two more specimens will be tested with the funding provided by Auburn University Highway Research Center.

9.2.1 CONCLUSION OF PHASE 2 WORK

Based on the results obtained from Phase 2 work, the following conclusions can be drawn:

- The use of hooked-bonded and straight-bonded near-surface mounted (NSM) TiABs is an effective method to strengthen reinforced concrete bridge girders provided that anchorage and concrete-epoxy delamination failure do not occur.
- Providing only the development length of TiABs as the bonded length was not sufficient to achieve the full-strength contribution of TiABs through yielding. Even the addition of $d_v \cot \theta$ to the development length in accordance with the AASHTO NSM TiAB Guide was not sufficient to achieve the desired strength and ductile behavior.
- Flexural strengthening using NSM TiAB with hooked ends is effective when the TiAB bonded length is determined to prevent excessive inclined shear cracking at the TiAB termination locations in the tension region. ACI 318-19 Section 9.7.3.5 requirements for internal reinforcement cut-off were found applicable and adequate to account for the impact of stress concentrations at TiABs hook ends.

- For the straight-bonded NSM TiAB, the provisions in ACI 440.2 to determine the bonded length of TiAB were found applicable and adequate to eliminate the impact of concrete cover delamination or concrete-epoxy interface delamination. Therefore, it is recommended to use Section 14.1.2 of ACI 440.2 when designing with straight TiAB for NSM applications to address the concrete-epoxy interface delamination.
- Hooked-unbonded strengthening method was not effective due to the formation of inclined cracks near hook end locations because of stress concentrations, therefore it is recommended to use only for temporary (i.e., emergency) purposes.
- Two different TiAB types were evaluated, and they provided similar flexural response and behavior, so either type can be used to strengthen reinforced concrete bridge girders.

9.3 RECOMMENDATIONS

The following recommendations are offered based on the results obtained in this study:

- For hooked-bonded TiAB NSM design, it is recommended to use a bond strength of 1.0 ksi.
- For straight-bonded TiAB NSM design, it is recommended to use a bond strength of 0.5 ksi.
- For hooked-bonded TiAB NSM applications, the provisions in Section 9.7.3.5 of ACI 318-19 should be included in the AASHTO NSM TiAB Guide to account for the effect of stress concentrations at bar termination locations in the flexural tension zone.
- For straight-bonded TiAB NSM applications, the provisions in Section 14.1.2 of ACI 440.2 should be used to avoid cover or concrete-epoxy interface delamination.
- It is recommended to strengthen the Cullman Bridge by using TiAB NSM as presented in Chapter 8 with the Special Provisions covered in Appendix C. Since this will be the first bridge in Alabama strengthened with TiAB NSM, it is recommended to instrument and test the bridge to determine the effectiveness of this strengthening method. Before cutting any grooves in the Cullman Bridge, it is recommended to use ground-penetrating radar to measure the as-built cover to verify that there is sufficient concrete cover to accommodate the groove depths required for TiAB NSM installation.

References

- AASHTO. 2002. "Standard Specifications for Highway Bridges." Washington, D.C.: American Association of State Highway and Transportation Officials.
- . 2020a. "Guide for Design and Construction of Near-Surface Mounted Titanium Alloy Bars for Strengthening Concrete Structures." 1 st. Washington, DC: American Association of State Highway and Transportation Officials.
- . 2020b. "LRFD Bridge Design Specifications." American Association of State Highway and Transportation Officials.
- ACI 318. 2019. "Building Code Requirements for Structural Concrete." Farmington, MI, 2019: American Concrete Institute.
- ACI 440-23. 2023. "Design and Construction of Externally Bonded Fiber-Reinforced Polymer (FRP) Systems for Strengthening Concrete Structures-Guide." Farmington Hill, Mich., USA: American Concrete Institute.
- ACI 546R-14. 2014. "Guide to Concrete Repair." American Concrete Institute.
- Adkins, J., & George, W. 2017. "Titanium Finds a Home in Civil Engineering."
- Amneus, D.,. 2014. "Methods for Strengthening Flexural Steel Details in Reinforced Concrete Bridge Girders Using a Near-Surface Mounted Retrofitting Technique." Oregon State University.
- ARTBA. 2023. "State Bridge Profile- Alabama." American Road and Transportation Builders Association.
- ASTM A615. 2023. "Standard Specification for Deformed and Plain Carbon-Steel Bars for Concrete Reinforcement." West Conshohocken, PA, 2022: ASTM International.
- ASTM B1009-20. 2020. "Standard Specification for Titanium Alloy Bars for Near Surface Mounts in Civil Structures." ASTM International, West Conshohocken, PA., American Society for Testing and Materials International.
- ASTM C39. 2021. "Test Method for Compressive Strength of Cylindrical Concrete Specimens." ASTM International. https://doi.org/10.1520/C0039_C0039M-14.
- ASTM C143. 2020. "Standard Test Method for Slump of Hydraulic-Cement Concrete." ASTM International. https://doi.org/10.1520/C0143_C0143M-20.
- Barker, L. 2014. "Flexural Anchorage Performance and Strengthening on Negative Moment Regions Using Near-Surface Mounted Retrofitting in Reinforced Concrete Bridge Girders." Oregon State University.
- Barris, C., P. Sala, J. Gómez, and L. Torres. 2020. "Flexural Behaviour of FRP Reinforced Concrete Beams Strengthened with NSM CFRP Strips." *Composite Structures* 241 (June):112059. <https://doi.org/10.1016/j.compstruct.2020.112059>.
- Barris, C., L. Torres, J. Comas, and C. Miàs. 2013. "Cracking and Deflections in GFRP RC Beams: An Experimental Study." *Composites Part B: Engineering* 55 (December):580–90. <https://doi.org/10.1016/j.compositesb.2013.07.019>.
- Bomberger, H. B., P. J. Cambourelis, and G. E. Hutchinson. 1954. "Corrosion Properties of Titanium in Marine Environments." *Journal of The Electrochemical Society* 101 (9): 442. <https://doi.org/10.1149/1.2781297>.

- Cairns, J., and S. F. A. Rafeeqi. 2002. "Analysis of Reinforced Concrete Beams Strengthened by External Unbonded Bars." *Magazine of Concrete Research* 54 (2): 141–53. <https://doi.org/10.1680/mac.2002.54.2.141>.
- Chajes, M., Rollins, T., Dai, H., & Murphy, T. 2019. "Report on Techniques for Bridge Strengthening: Main Report." Technical FHWA-HIF-18-041. U.S. Department of Transportation, Federal Highway Administration.
- Chou, J., Y. Liu, H. Guo, J. Zhang, and H. Peng. 2023. "Fatigue Behavior of Reinforced Concrete Beams Strengthened with Prestressed Near-Surface-Mounted Carbon-Fiber-Reinforced Polymer Strips." *Composite Structures* 308 (March):116689. <https://doi.org/10.1016/j.compstruct.2023.116689>.
- Daly, A., Shave, J., & Denton, S. 2006. "Strengthening of Concrete Structures Using Near-Side Surface Mounted FRP Reinforcement." PPR053. United Kingdom: TRL.
- Flowers, J. C.,. 2024. "Determination of the Effective Bond Strength for Near-Surface Mounted Titanium-Alloy Bars in Reinforced Concrete." Auburn University.
- Hassan, T., and S. Rizkalla. 2003. "Investigation of Bond in Concrete Structures Strengthened with Near Surface Mounted Carbon Fiber Reinforced Polymer Strips." *Journal of Composites for Construction* 7 (3): 248–57. [https://doi.org/10.1061/\(ASCE\)1090-0268\(2003\)7:3\(248\)](https://doi.org/10.1061/(ASCE)1090-0268(2003)7:3(248)).
- Higgins, C., Amneus, D., & Barker, L. 2015. "Titanium Alloy Bars for Strengthening a Reinforced Concrete Bridge." In *Sustainable Bridge Structures*. New York City, USA: CRC Press.
- Higgins, Christopher, Jonathan Knudtsen, Deanna Amneus, and Laura Barker. 2017. "Shear and Flexural Strengthening of Reinforced Concrete Beams with Titanium Alloy Bars." In . <https://doi.org/10.11159/icsenm17.141>.
- HILTI. 2021. "HIT-RE 500 V3 Epoxy Adhesive Anchoring System 3.2.4." Technical Datasheet. HILTI.
- Klaiber, F.W., Dunker, K.F., Wipe, T.J., and Sanders, W.W., eds. 1987. *Methods of Strengthening Existing Highway Bridges*. National Cooperative Highway Research Program Report 293. Washington, D.C: Transportation Research Board, National Research Council.
- Lorenzis, L. De, and A. Nanni. 2001. "Characterization of FRP Rods as Near-Surface Mounted Reinforcement." *Journal of Composites for Construction* 5 (2): 114–21. [https://doi.org/10.1061/\(ASCE\)1090-0268\(2001\)5:2\(114\)](https://doi.org/10.1061/(ASCE)1090-0268(2001)5:2(114)).
- Perryman Company. 2021. "Bridge Bar Bending Work Instructions." B 9.5 WI.
- Platt, S., and K. A. Harries. 2018a. "Geometry, Material Properties and Bond Performance of Prototype Titanium Reinforcing Bars." *Construction and Building Materials* 187 (October):1253–66. <https://doi.org/10.1016/j.conbuildmat.2018.08.074>.
- . 2018b. "Study of Galvanic Corrosion Potential of NSM Titanium Reinforcing Bars." *Case Studies in Construction Materials* 9 (December):e00175. <https://doi.org/10.1016/j.cscm.2018.e00175>.
- Platt, S. L. 2018. "Galvanic Corrosion Potential and Material and Bond Properties of Titanium Reinforcing Bars," 196.
- Platt, S. L., K. A. Harries, and M. J. McCabe. 2020. "Reinforced Concrete Bridge Deck Repair with Titanium NSM." In *ICSBE 2018*, edited by R. Dissanayake and P. Mendis, 44:447–57. Lecture Notes in Civil Engineering. Singapore: Springer Singapore. https://doi.org/10.1007/978-981-13-9749-3_39.
- Razaqpur, A. G., M. Shedid, and D. Petrino. 2011. "Behavior of Beams Strengthened with Novel Self-Anchored Near-Surface-Mounted CFRP Bars." *Journal of Composites for Construction* 15 (4): 625–34. [https://doi.org/10.1061/\(ASCE\)CC.1943-5614.0000183](https://doi.org/10.1061/(ASCE)CC.1943-5614.0000183).

- Sharaky, I.A., L. Torres, and H.E.M. Sallam. 2015. "Experimental and Analytical Investigation into the Flexural Performance of RC Beams with Partially and Fully Bonded NSM FRP Bars/Strips." *Composite Structures* 122 (April):113–26. <https://doi.org/10.1016/j.compstruct.2014.11.057>.
- Smith, S.T, and J.G Teng. 2002. "FRP-Strengthened RC Beams. II: Assessment of Debonding Strength Models." *Engineering Structures* 24 (4): 397–417. [https://doi.org/10.1016/S0141-0296\(01\)00106-7](https://doi.org/10.1016/S0141-0296(01)00106-7).
- Subagia, I.D.G. A., and Y. Kim. 2014. "Tensile Behavior of Hybrid Epoxy Composite Laminate Containing Carbon and Basalt Fibers." *Science and Engineering of Composite Materials* 21 (2): 211–17. <https://doi.org/10.1515/secm-2013-0003>.
- Teng, J. G., L. De Lorenzis, B. Wang, R. Li, T. N. Wong, and L. Lam. 2006. "Debonding Failures of RC Beams Strengthened with Near Surface Mounted CFRP Strips." *Journal of Composites for Construction* 10 (2): 92–105. [https://doi.org/10.1061/\(ASCE\)1090-0268\(2006\)10:2\(92\)](https://doi.org/10.1061/(ASCE)1090-0268(2006)10:2(92)).
- Vavra, E.,. 2016. "Application of Titanium Alloy Bars for Strengthening Reinforced Concrete Bridge Girders in Flexure." Thesis, Oregon State University.
- Wight, J. K. and MacGregor, J. G. 2012. *Reinforced Concrete: Mechanics and Design*. 6th Edition. Pearson Education, Inc.
- Yost, J. R., Shawn P. G., David W. D., and Jason J. M.,. 2007. "Flexural Behavior of Concrete Beams Strengthened with Near-Surface-Mounted CFRP Strips." *ACI Structural Journal* 104 (4).
- Zhang, S.S., Y. Ke, E. Chen, H. Biscaia, and W.G. Li. 2022. "Effect of Load Distribution on the Behaviour of RC Beams Strengthened in Flexure with Near-Surface Mounted (NSM) FRP." *Composite Structures* 279 (January):114782. <https://doi.org/10.1016/j.compstruct.2021.114782>.

Appendix A: Material Properties Used in this Project

Concrete Core Test of Cullman Bridge

ALABAMA DEPARTMENT OF TRANSPORTATION

LAB NO:	FGR- 512-19	PROJECT NO(S): 99-500-680-000-401
COPIES TO:	File Physical Laboratory Division Project Engineer	COUNTY: Statewide DIVISION: DATE: October 2, 2019

BMT-16, Rev. 10/87

REPORT OF)INSPECTION
)ANALYSIS ON SAMPLE OF ... DRILLED CONCRETE CORE

DATE RECEIVED: 09/27/2019
DATE TESTED: 10/02/2019
PRODUCER:
IDENTIFICATION MARKS:
SOURCE OF MATERIAL:
QUANTITY (REPRESENTED):
SAMPLED BY/DATE:
SUBMITTED BY/DATE:
REMARKS:
TESTED BY: Weiss/Barker

TEST RESULTS

CORE NUMBER	1	2	3	4	5	6
DIAMETER, (IN)	2.988	2.986	2.989	2.896	2.987	2.987
AREA, SQUARE INCHES	7.012	7.003	7.017	6.587	7.007	7.007
LOAD @ RUPTURE (LB)	34300	28600	28700	42000	33100	31700
COMPRESSIVE PSI	4890	4080	4090	6370	4720	4530
CORRECTED COMPRESSIVE PSI (H/D RATIO)	4690	3960	(2.00)	6050	4520	4390
LENGTH OF CORE: SAWED (IN)						
LENGTH OF CORE: CAPPED (IN)	4.471	4.868	5.981	3.976	4.347	4.308

jm

Steven Ingram
Testing Engineer

Mill certificate of #4 bar for material-level test

phase -1
NUCOR

Mill Certification 01/13/2021

MTR#: 590440-2
Lot #: 380001667620
3630 Fourth Street
Flowood, MS 39232 US
601 939-1623
Fax: 601 936-6202

Sold To: SABEL STEEL SERVICE INC
PO BOX 4747
MONTGOMERY, AL 36103 US

Ship To: SABEL STEEL SERVICES INC
704 LAFAYETTE ST
MONTGOMERY, AL 36104 US

Customer PO	06-2020-087	Sales Order #	37014179 - 9.1
Product Group	Rebar	Product #	1053861
Grade	A615 Gr 60/AASHTO M31	Lot #	380001667620
Size	#3	Heat #	3800016676
BOL #	BOL-667443	Load #	590440
Description	Rebar #3/10mm A615 Gr 60/AASHTO M31 40' 0" [480"] 2001-6000 lbs	Customer Part #	
Production Date	12/18/2020	Qty Shipped LBS	25265
Product Country Of Origin	United States	Qty Shipped EA	1680
Original Item Description		Original Item Number	

I hereby certify that the material described herein has been manufactured in accordance with the specifications and standards listed above and that it satisfies those requirements.

Melt Country of Origin : United States

Melting Date: 12/11/2020

C (%)	Mn (%)	P (%)	S (%)	Si (%)	Ni (%)	Cr (%)	Mo (%)	Cu (%)	V (%)	Nb (%)
0.39	0.82	0.011	0.026	0.210	0.10	0.10	0.03	0.25	0.029	0.001

Other Test Results

Yield (PSI) : 73400

Tensile (PSI) : 100000

Average Deformation Height (IN) : 0.031

Elongation in 8" (%) : 18.8

Bend Test : Pass

Weight Percent Variance (%) : -3.09

Comments:

Nucor Steel Jackson, Inc. is ISO 9001:2015, 14001:2015, and ABS certified. All manufacturing processes of the steel materials in this product, including melting, have occurred within the United States. Mercury, in any form has not been used in the production or testing of this material. Manufactured in the US and complies with the Buy American Act. No weld repair was performed.

Mill certificate of #8 bar for member-level test

NUCOR

Mill Certification

06/02/2021

MTR#:703103-2
Lot #:370002085920
2301 F.L. Shuttlesworth Drive
Birmingham, AL 35234 US
205 250-7400
Fax: 205 250-7465

Sold To: SABEL STEEL SERVICE INC
PO BOX 4747
MONTGOMERY, AL 36103 US

Ship To: SABEL STEEL SERVICES INC
704 LAFAYETTE ST
MONTGOMERY, AL 36104 US

Customer PO	06-2021-133	Sales Order #	37016305 - 17.1
Product Group	Rebar	Product #	3020138
Grade	A615 Gr 60/AASHTO M31	Lot #	370002085920
Size	#8	Heat #	3700020859
BOL #	BOL-792167	Load #	703103
Description	Rebar #8/25mm A615 Gr 60/AASHTO M31 60' 0" [720"] 6001-10000 lbs	Customer Part #	
Production Date	06/02/2021	Qty Shipped LBS	30760
Product Country Of Origin	United States	Qty Shipped EA	192
Original Item Description		Original Item Number	

I hereby certify that the material described herein has been manufactured in accordance with the specifications and standards listed above and that it satisfies those requirements.

Melt Country of Origin : United States

Melting Date: 06/01/2021

C (%)	Mn (%)	P (%)	S (%)	Si (%)	Ni (%)	Cr (%)	Mo (%)	Cu (%)	V (%)	Nb (%)
0.36	0.78	0.016	0.030	0.200	0.11	0.18	0.03	0.50	0.024	0.002

Tensile testing

	Yield (PSI)	Tensile (PSI)	Elongation in 8" (%)
(1)	74400	103900	13.0

Mechanical

	Average Deformation Height (IN)	Bend Test
(1)	0.061	Pass

Other Test Results

Weight Percent Variance (%) : -4.27

Comments:

Nucor-Birmingham is ISO 9001-2015 and ISO 14001 certified. All manufacturing processes of the steel materials in this product, including melting, have occurred within the United States. Mercury, in any form has not been used in the production or testing of this material. Meets (FTA) Buy America Requirements (49 C.F.R. part 661). Radium, or Alpha source materials in any form have not been used in the production of this material. All Products are manufactured in the United States and comply with Title 23 CFR 635.410 of the "Buy America Requirements". No weld repair was performed. Parts meet the requirements of the purchase order and have been produced under the Nucor Steel Birmingham quality manual rev 8 dated 9/14/2017.

Mill certificate of #9 bar for member-level test

NUCOR

Mill Certification

03/02/2021

MTR#:631099-1
Lot #:370001740820
2301 F.L. Shuttlesworth Drive
Birmingham, AL 35234 US
205 250-7400
Fax: 205 250-7465

Sold To: SABEL STEEL SERVICE INC
PO BOX 4747
MONTGOMERY, AL 36103 US

Ship To: SABEL STEEL SERVICES INC
704 LAFAYETTE ST
MONTGOMERY, AL 36104 US

Customer PO	06-2021-105	Sales Order #	37015142 - 7.1
Product Group	Rebar	Product #	2110350
Grade	A615 Gr 60/AASHTO M31	Lot #	370001740820
Size	#9	Heat #	3700017408
BOL #	BOL-707218	Load #	631099
Description	Rebar #9/29mm A615 Gr 60/AASHTO M31 50' 0" [600"] 6001-10000 lbs	Customer Part #	
Production Date	01/25/2021	Qty Shipped LBS	46750
Product Country Of Origin	United States	Qty Shipped EA	275
Original Item Description		Original Item Number	

I hereby certify that the material described herein has been manufactured in accordance with the specifications and standards listed above and that it satisfies those requirements.

Melt Country of Origin : United States

Melting Date: 01/22/2021

C (%)	Mn (%)	P (%)	S (%)	Si (%)	Ni (%)	Cr (%)	Mo (%)	Cu (%)	V (%)	Nb (%)
0.38	0.84	0.010	0.032	0.263	0.12	0.15	0.03	0.40	0.027	0.001

Mechanical

	Average Deformation Height (IN)	Bend Test
(1)	0.067	Pass

Tensile testing

	Yield (PSI)	Tensile (PSI)	Elongation in 8" (%)
(1)	70900	105800	14.0

Other Test Results

Weight Percent Variance (%) : -5.00

Comments:

Nucor-Birmingham is ISO 9001-2015 and ISO 14001 certified. All manufacturing processes of the steel materials in this product, including melting, have occurred within the United States. Mercury, in any form has not been used in the production or testing of this material. Meets (FTA) Buy America Requirements (49 C.F.R. part 661). Radium, or Alpha source materials in any form have not been used in the production of this material. All Products are manufactured in the United States and comply with Title 23 CFR 635.410 of the "Buy America Requirements". No weld repair was performed. Parts meet the requirements of the purchase order and have been produced under the Nucor Steel Birmingham quality manual rev 8 dated 9/14/2017.

Mill certificate of #4 Type 1 TiAB



Perryman company

213 Vandale Drive Houston, PA 15342 USA

phone: 724-746-9390 fax: 724-746-9392

Customer: Auburn University
311 Ingram Hall
Auburn, AL 36849

Heat No: PVD7162
Melting Source: Perryman Company, USA
Work Order No: 159425

Certified Test Report

Date: 8/9/2021
Quantity: 369 FT

Customer Order No: Donation

Specification: ASTM B1009 Class 130 (2020)

Product: Ti 6Al-4V 0.500" +/-0.001" Dia. Bridgealloy X 15'-20' lengths
Straight lengths - no hooks

Condition: Annealed 1400 F - 2 hours

Chemistry	Wt %	ASTM E 1447:	Post processing Hydrogen Determination		H: .0007
Metallographic Examination:		ASTM E407:	Microstructure -	Equiax alpha-beta	ASTM E 407: Surface Contamination -
Etchant: PER1 & PER2					No alpha case 500x
Mechanical Properties		Tensile	2% Yield	Elongation	
ASTM E8/EN 2002-001:2005E		Strength	Strength	4D	
Condition		ksi	ksi	%	
As Shipped		152.4	137.1	11	
		150.4	135.9	13	

Bend Tests acceptable.

Calculated cross sectional area = 0.1899 in²

Tensile Modulus = 15.2 Msi

This is to certify that all test results conform to the specifications listed above and that all tests required were performed by Perryman Company.

The material did not come in contact with Mercury or radioactive contamination at Perryman.

Attached is a copy of the Ingot Chemistry. All testing performed at room temperature unless otherwise noted.

The test results relate only to the lots tested and are contained in the records of Perryman Company. The Certified Test Report cannot be reproduced except in full, without written approval. Made in USA.

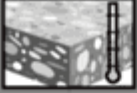


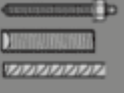



Page 1 of 1

Zachary S. Degan
Laboratory Manager


8/9/2021

Nadcap
ACCREDITED
Materials Testing Laboratory

Curing Time of HIT-RE 500 V3 epoxy

					
	[°F]	[°C]	 t_{work}	 $t_{cure, ini}$	 $t_{cure, full}$
	23	-5	2 h	48 h	168 h
	32	0	2 h	24 h	36 h
	40	4	2 h	16 h	24 h
	50	10	1.5 h	12 h	16 h
	60	16	1 h	8 h	16 h
	72	22	25 min	4 h	6.5 h
	85	29	15 min	2.5 h	5 h
	95	35	12 min	2 h	4.5 h
	105	41	10 min	2 h	4 h

APPENDIX B: TiAB bending Work Instructions

 Perryman company	Corporate Address: 213 Vandale Drive Houston, PA 15342	Document Title: Bridge Bar Bending Work Instructions
	P: 724.746.9390 F: 724.746.9392	Document Number: B 9.5 WI
		Revision Number: 1
		Effective:
		Page: 1 of 7

1.0 Scope

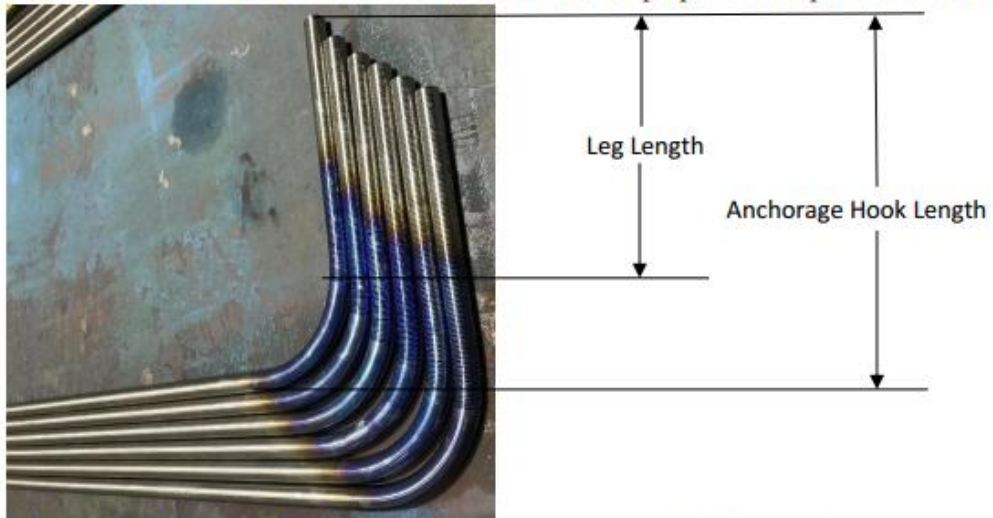
- 1.1 This work instruction provides a guideline to bend the 90° anchorage hook on the textured or untextured Bridgealloy™ bars.
- 1.2 This can also be used as a guideline for general bending of titanium bars.
- 1.3 It can be applicable for other angles.

2.0 References


- 2.1 PC-1200 Bridgealloy™ Materials Specification
- 2.2 CRSI Manual of Standard Practice

3.0 Definitions

- 3.1 **Leg distance** – Straight portion of anchorage hook.
- 3.2 **Anchorage hook length** – Leg length + mandrel radius + bar diameter or measurement from end of hook to outside diameter of perpendicular portion of bar.



- 3.3 **Hydraulic rebar bender** – Portable machine used to quickly fabricate rebar on the job or at the shop. The machine used at Perryman Company is **FASTCUT** FR-800 ReBar Bender.
- 3.4 **Mandrel** – A cylindrical rod around which metal or other material is shaped. The mandrels used at Perryman Company were manufactured in house from 304 stainless steel. Mandrel diameter will be dependent on job requirement.
- 3.5 **CRSI** – Concrete Reinforcing Steel Institute
- 3.6 **Bar size numbers** – Rebar size numbering system measured in 1/8" increments. For example, bar size 5 is equivalent to 5/8" diameter.

 <p>Corporate Address: 213 Vandale Drive Houston, PA 15342</p> <p>P: 724.746.9390 F: 724.746.9392</p> <p>Perryman company</p>	Document Title: Bridge Bar Bending Work Instructions
	Document Number: B 9.5 WI
	Revision Number: 1
	Effective:
	Page: 2 of 7

4.0 Safety

- 4.1 Safety glasses.
- 4.2 Face shield.
- 4.3 Heat resistant gloves.
- 4.4 Ear protection.
- 4.5 Personal protective equipment on job site as required.

5.0 Responsibilities

- 5.1 Bar Mill operators will follow these work instructions.
- 5.2 Bar Mill supervisors will make sure operators follow these work instructions.
- 5.3 Site contractor and employees will follow these work instructions when bending on site.

6.0 Procedure

- 6.1 Calculate cut length of straight bars using the following equation if both ends are being bent: +

$$L = (W - D - 2R) + (H - R - D/2)2 + \pi R$$

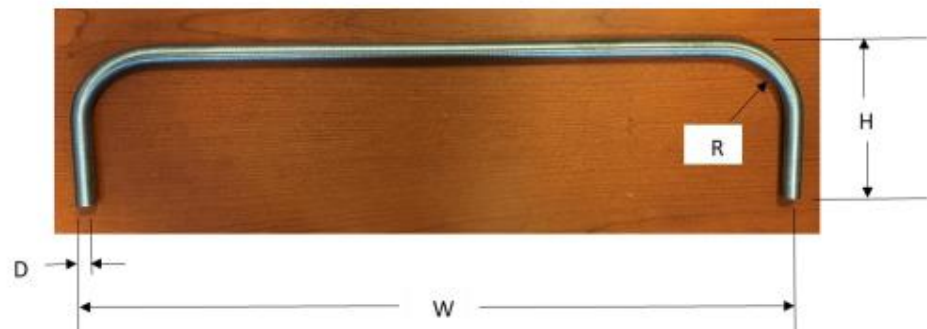
L = bar length prior to bending

W = Straight length


D = Bar diameter

H = Anchorage length

R = Mandrel radius



- 6.1.1 Cut bars to length.
- 6.2 Acquire a scrap bar equivalent in size to prime bars to set up prior to bending prime bars.
 - 6.2.1 Check bar for irregularities, such as cracks, prior to bending.
- 6.3 Set mandrel on hydraulic rebar bender to job required diameter.
- 6.4 Set bender for 90° with overbend (2°) to account for spring back.

 <p>Corporate Address: 213 Vandale Drive Houston, PA 15342</p> <p>P: 724.746.9390 F: 724.746.9392</p> <p>Perryman company</p>	Document Title: Bridge Bar Bending Work Instructions
	Document Number: B 9.5 WI
	Revision Number: 1
	Effective:
	Page: 3 of 7

6.4.1 Measure angle after bending and adjust as necessary.

6.5 Measure leg distance from center of mandrel to bar stop. For set up of the bar stop, subtract the radius of the bar from the leg length.

6.5.1 Example:

Diameter of bar = 0.625"

Leg length = 3.5"

Stop position = $3.5 - 0.625/2 = 3.1875$ " from center of mandrel

See diagram below:



6.6 Turn on hydraulic rebar bending machine.

6.7 Define heating area on the bar starting 3" before the bend area and ending 3" past the bend area.


6.8 Heat bar.

6.8.1 Use a propane/oxygen torch with rosebud torch tip. Use the hottest point of the torch about 1"-1.5" from tip.

6.8.2 Proximity of torch heating needs to be close enough to the hydraulic rebar bender for quick transfer.

6.8.3 The bar needs to be positioned on top of something fire resistant (such as a metal vice) for ease of rotating and stabilizing.

6.8.4 Heat the bend area while rotating bar until the bar turns blue. For example, a 0.625" diameter bar it should take approximately 1 minute 45 seconds.

 <p>Corporate Address: 213 Vandale Drive Houston, PA 15342</p> <p>P: 724.746.9390 F: 724.746.9392</p> <p>Perryman company</p>	Document Title: Bridge Bar Bending Work Instructions
	Document Number: B 9.5 WI
	Revision Number: 1
	Effective:
	Page: 4 of 7



6.8.4.1 Straw or yellow color equates to approximately 900°F. Too cold for bending. Continue to heat until blue.




6.8.4.2 Blue color equates to approximately 1200°F. This is the desired color and temperature.

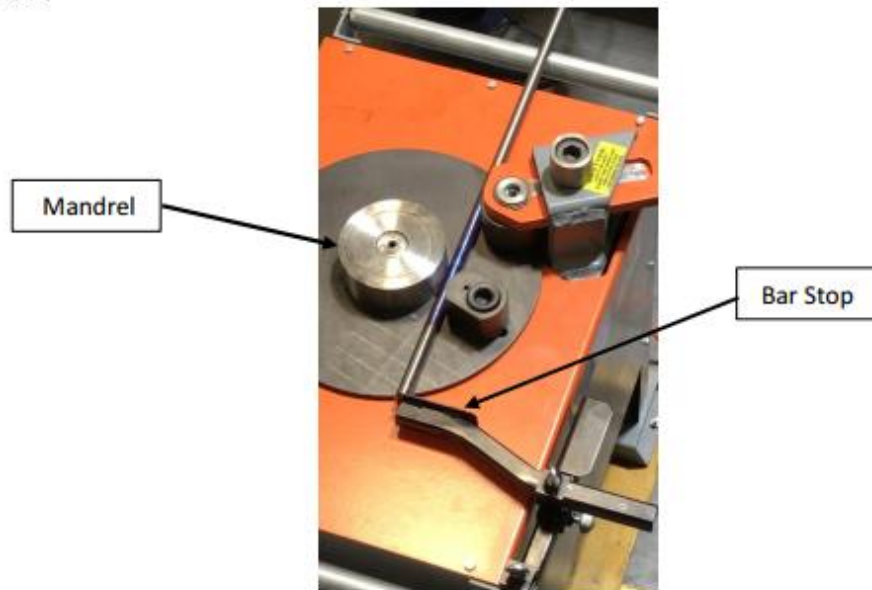


6.8.4.3 If the bar turns red hot, it indicates it is overheated. Contact supervisor for disposition of bar if overheated.

6.8.4.4 If necessary, temperature sticks can be used to confirm temperature.

 <p>Corporate Address: 213 Vandale Drive Houston, PA 15342</p> <p>P: 724.746.9390 F: 724.746.9392</p> <p>Perryman company</p>	Document Title: Bridge Bar Bending Work Instructions
	Document Number: B 9.5 W1
	Revision Number: 1
	Effective:
	Page: 5 of 7


6.9 Immediately move bar to rebar bender and insert the bar to the stop or a designated mark.



6.9.1 Bend bar immediately while hot.



6.9.2 If one end already has a hook, direction of bar and flatness will be critical. Ensure that hook lays on flat surface while bending the other hooked end.


 <p>Corporate Address: 213 Vandale Drive Houston, PA 15342</p> <p>P: 724.746.9390 F: 724.746.9392</p> <p>Perryman company</p>	Document Title: Bridge Bar Bending Work Instructions
	Document Number: B 9.5 W1
	Revision Number: 1
	Effective:
	Page: 6 of 7

6.9.2.1 Flat surface can be any type of table that is on the same plane as the rebar bender.

- 6.10 Bar can be water quenched for handling purposes.
- 6.10.1 This can be accomplished with a hose or bucket of water and will cool in seconds once in contact with water.
- 6.11 Check the bend angle for perpendicularity and anchorage length.
- 6.11.1 Bend angle can be checked with machinist square.
- 6.11.2 Per CRSI Manual of Standard Practice, Angular Deviation – maximum $\pm 2 \frac{1}{2}^\circ$ or $\pm \frac{1}{2}$ in./ft. but not less than $\frac{1}{2}$ in. on all 90° hooks and bends.
- 6.11.3 Anchorage hook length can be checked with tape measure.
- 6.11.4 Per CRSI Manual of Standard Practice, for bar sizes #3 through #11 (see definitions), the dimensional tolerance for leg length = $\pm 1"$. Perryman aims at $\pm \frac{1}{4}"$. +



- 6.12 Make necessary adjustments and repeat with scrap bar. When all criteria are met, begin bending prime bars.
- 6.13 If bars are textured on the bend, use a die grinder assembled with a 40 grit flat wheel to remove the texture on inside diameter of the bend. +
- 6.13.1 Grind in longitudinal direction perpendicular to the transverse texture.
- 6.13.2 Removal amount is approximately 0.010". +

 <p>Corporate Address: 213 Vandale Drive Houston, PA 15342</p> <p>P: 724.746.9390 F: 724.746.9392</p>	Document Title: Bridge Bar Bending Work Instructions
	Document Number: B 9.5 WI
	Revision Number: 1
	Effective:
	Page: 7 of 7



7.0 Revision History

REVISION	DESCRIPTION OF CHANGE
0	Original
1	6.1 Added equation to calculate the straight lengths prior to bending. 6.11 Added photo. 6.13 Changed tool for grinding bend ID and added photos.

APPENDIX C: DRAFT ALDOT SPECIFICATION
ALABAMA DEPARTMENT OF TRANSPORTATION

Date: September 15, 2024

Special Provision No. xx-xxxx

Subject: Use of titanium alloy reinforcement to strengthened bridge girders in Alabama

Alabama Standard Specifications, 2022 Edition, shall be amended by the addition of a new Section xxx as follows:

SECTION XXX

NEAR-SURFACE-MOUNTED TITANIUM-ALLOY REINFORCEMENT

xxx.01 Description.

This section covers strengthening of reinforced concrete bridge girders with near-surface-mounted (NSM) titanium alloy bars (TiABs). The NSM TiABs shall be installed in grooves cut into the concrete surface to increase the flexural strength of a structure.

xxx.02 Materials.

(a) Titanium Alloy Bar (TiABs)

The NSM TiAB (Ti 6Al-4V) shall conform to the requirements of ASTM B1009-20. The mechanical properties of the TiAB shall conform to the mechanical property requirements given in ASTM B1009-20 (Table 1). Yield strength (based on 0.2% offset) of Class 120 and Class 130 bars shall not be less than 120 ksi and 130 ksi, respectively, as tested per ASTM E8/E8M, Test Methods for Tension Testing of Metallic Materials and the elongation should be at least 10%. Material test certificates for each production lot of the TiAB used shall be furnished to the Engineer no later than 15 calendar days prior to installation in the structure. All manufacturer instructions for the TiAB shall be followed. The two classes of TiAB—Class 120 and Class 130—can be obtained from the Perryman Company, 213 Vandale Drive Houston, PA 15342, USA.

Furnished uniform deformations shall be equally spaced along the TiABs with a minimum deformation height of 0.01 inch and a maximum spacing of 0.06 inch. The deformations shall not have sharp stress risers. The final cross-sectional area of the bars including the deformations shall not be less than 96 percent of the nominal area of undeformed bars.

(b) Injectable adhesive

The injectable adhesive to bond the TiABs to the concrete shall be HIT-RE 500 V3 supplied by Hilti, Inc., PO Box 21448, Tulsa, OK 74121-1148, (800)879-8000. The system to dispense the

injectable adhesive shall be selected by the Contractor. All manufacturer instructions for the injectable adhesive shall be followed.

Material safety data sheets (MSDS) for the adhesive shall be obtained from the manufacturer and shall be accessible at the job site at all times. All adhesive handling instructions defined by the manufacturer shall be followed.

xxx.03 Construction Requirement.

(a) Cooperation of the Contractor

The Engineer will obtain the assistance of a representative of the Auburn University Highway Research Center in inspecting and documenting the work. The Contractor shall provide assistance to this representative as directed by the Engineer.

Auburn University Highway Research Center Contact:

Dr. Kadir C. Sener

Phone: (334) 844-6268, Email: sener@auburn.edu

238 Harbert Engineering Center, Auburn University, AL 36849-5337

(b) Preparation and protection of construction site

The Contractor shall provide the necessary pathway, scaffolding, and other essential methods of reaching the project site and the designated installation area for personnel, equipment, and materials. The Contractor shall remove and reinstall all obstructions as directed by the Engineer without additional compensation.

The Contractor shall provide the necessary equipment (e.g. GPR or other approved devices) for detecting existing reinforcement within a depth 0.1 inch and to determine the thickness of the concrete cover. Before constructing anchor holes and grooves, the Contractor shall provide the Engineer with a summary of cover thickness and clear distance measurements between existing reinforcement and the planned titanium alloy reinforcement bars and end hooks.

The Contractor shall provide the Engineer with documentation, which can include photographs or drawings, for all materials the Engineer designates to be reinstalled after the installation of the NSM TiAB. The materials shall not be removed until the Engineer informs the Contractor that the documentation is acceptable.

The Contractor shall be provided with necessary support to coordinate with any other organization/agency which might be in charge of other portions (e.g. rail track) associated with the bridge(s). The work delay due to this arrangement shall be taken into consideration.

Bridge testing instrumentation (sensors, wires, etc.) shall not be removed from the bridge without the prior written approval of the Engineer.

(c) Contractor's installation plan

The Contractor shall submit **four copies** of a proposed NSM TiAB installation plan. The plan shall include the following:

- Manufacturer documentation that covers physical and chemical properties
- Equipment and procedures for locating, cutting, and preparing grooves and end hooks for installation
- Equipment and procedures to collect, contain, and dispose of debris generated by groove cutting, hole drilling, and concrete surface preparation.
- TiAB and adhesive installation procedure including sequence and timing of operation
- Materials and procedures for the protection of the NSM TiAB during installation and curing
- Weather restrictions (temperature, humidity, etc.)
- Installation tolerances
- Quality control plan
- Procedures for documentation of the installation

The submittal will not be approved by the Engineer but will be reviewed for completeness. The installation of the TiAB shall not begin until the Engineer informs the Contractor in writing that the submittal is complete.

Incomplete submittals will be returned to the Contractor for completion and the resubmittal of four copies.

(d) Storage and handling of TiAB

1. Storage requirements

All components of the NSM TiAB system shall be delivered and stored in the original factory sealed, unopened packaging or appropriately labeled containers, which should include details like the manufacturer, brand name, system identification number, manufacturer date, shelf life, and expiration date. Components shall be stored following the manufacturer's instructions. All components shall be protected from dust, moisture, chemicals, direct sunlight, physical damage, fire, and temperatures beyond the range specified in the manufacturer data sheets. Any component

found to have been stored in conditions differing from the prescribed storage conditions shall be discarded.

2. Shelf life

Any component of the NSM TiAB system that has been stored longer than the shelf life shown on the manufacturer data sheet shall be discarded.

3. Handling

All components of the NSM TiAB system shall be handled with care according to the manufacturer's recommendations. Careful handling shall be done to protect the components from damage.

4. Cleaning construction site

The Contractor is responsible for the clean-up of the equipment and the project site using appropriate solvents, as shown in the NSM TiAB installation plan.

5. Disposal of materials

Any component of the NSM TiAB system that has exceeded its shelf life or pot life, has not been properly stored, or has been contaminated, and any unused or excess material considered as waste, shall be disposed of following the manufacturer's instructions and in compliance with state and federal environmental control regulations.

6. Material sampling

The Contractor shall provide sufficient material for the Engineer to select four samples from each lot of titanium alloy reinforcement delivered to the site, for testing by the Agency. Samples will be a minimum of 4 feet in length.

(e) Concrete preparation

1. Groove cutting

Groove locations shall be reviewed and confirmed by the Engineer prior to cutting. If a groove location is designated as moveable on the plans, the entire groove may be shifted laterally or longitudinally by up to 3 inches to avoid an obstruction with prior approval of the Engineer. Grooves shall be cut using a diamond-blade concrete wet saw. The width and depth of the groove shall be at least 1.5 times the diameter of the TiAB used for strengthening. The minimum edge distance must be at least 6 times the diameter of the TiAB and the clear spacing between the grooves must be at least 3 times the diameter of the TiAB. The tolerance for these dimensions and clearance requirements must fall within $\pm 1/8$ inch. Misaligned ends of discontinuous cuts that form a single groove shall be ground smooth to create a smooth transition. A smooth transition with the

radius of the bending radius of TiAB shall be installed to fit the hook in the groove and hole as shown in Figure 1. This can be achieved with a hammer and chisel. The Contractor shall periodically check to ensure that the transition has the correct radius and that too much concrete is not being taken off because the bearing area between the concrete and the TiAB is critical for proper anchorage of the TiAB reinforcement. The generated slurry from the wet-cutting shall be collected by using an industrial wet-dry vacuum and disposed following state rules and regulations. Do not cut into existing rebar while cutting grooves, shaping smooth transitions, or drilling holes for end hooks. The Contractor shall notify the Engineer when any existing reinforcement is damaged or cut while preparing the existing concrete for TiAB installation.

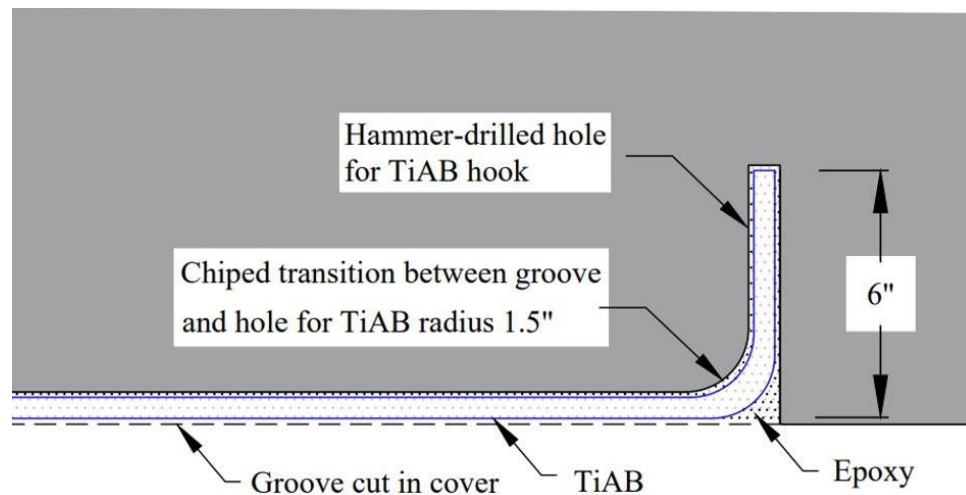


Figure 1: Smooth transition between concrete and bent TiAB

2. Groove cleaning

The inside faces of the groove and holes (for the hook) shall be cleaned with low-pressure water blasting with abrasive to allow the adhesive to securely bond to the concrete. This can be done using a 1500-5000 psi pressure washer with a nozzle attachment that feeds sand (abrasive) into the high-pressure stream in accordance with ACI 546R (2014). After using abrasive cleaning, a high-pressure water and no abrasive shall be used to clean the groove and holes of any residual abrasive. At the time of NSM TiAB installation, each groove and anchor hole shall be free of dust, sand, oil, moisture, laitance, grease, curing compounds, and other compounds that may interfere with the bond. The surfaces of the groove and anchor holes shall be dry when the adhesive is applied. Compressed air can be used for drying but the concrete surface shall be free of water, oil, or any other material detrimental to the bond between the concrete and adhesive. Do not directly apply a flame to the groove surface.

3. Masking

Temporary masking of the concrete surface adjacent to each groove is allowed to facilitate the removal of excess adhesive after installation. Masking material must be fully removed before completion of the project.

(f) Installation of NSM TiABs

1. TiAB preparation

The appropriate length of TiAB shall be cut while accounting for the additional hook lengths as needed. The following formula can be followed in calculating the TiAB length for the hooked bar. An acetylene-oxygen torch with a rosebud torch shall be used to heat the bend area to make the hooks. At 900°F the TiAB will turn a straw color and at 1200°F it will turn blue in color. Do not heat the TiAB more than 1300 °F (red hot) and discard any bars that turned red hot (overheated). While the TiAB is still at 1200°F (blue in color) place it in the bar bending machine equipped with the mandrel radius matching the desired radius of the TiAB.

The formula to calculate the TiAB length:

$$L = (W - D - 2R) + 2 \left(H - R - \frac{D}{2} \right) + \pi R$$

Where, L is the bar length prior to bending, W is the straight length, D is the bar diameter, H refers to anchorage length, and R refers to mandrel radius.

2. Temporary protection

Temporary protection may be required during TiAB installation and until the adhesive has cured. Both the TiAB and uncured adhesive shall be protected from direct contact by rain, dust, dirt, and vandalism. Keep the epoxy refrigerated at its lowest allowed temperature (41° F for HIT-RE-500 V3) if placing the epoxy in the groove on a hot day. For normal day operation, the epoxy shall be stored at 70° F or as specified by the manufacturer. Concrete temperature shall not exceed 120°F during adhesive installation and curing. Do not place the titanium alloy bars and epoxy when the concrete temperature is below 50°F, unless otherwise advised by the epoxy manufacturer's recommendation and approved by the Engineer. Strengthened structural components shall not be subjected to direct traffic loading during the initial curing time specified by the adhesive manufacturer.

3. Initial adhesive injection and consolidation

The adhesive shall be mixed and injected into the grooves in accordance with the manufacturer's recommended procedures. All adhesive and reinforcement placement operations for a single TiAB shall be completed within the adhesive manufacturer's recommended working time for the ambient conditions encountered during installation. If a sample shows any visual

evidence of improper proportioning or mixing, work shall be suspended until the equipment or procedures are corrected. Prior to the insertion of TiAB, complete filling the holes for the hooks and at least half of the groove depth with adhesive, and the adhesive shall be consolidated to remove entrapped air voids. Manual consolidation may be performed using a putty knife.

4. TiAB placement

Each element of TiAB shall consist of a continuous bar or hooked bar. Splicing of TiAB is not permitted. Sections of rubber hose/tube with a length of less than 0.25 in. with the same inside diameter as the TiAB bar diameter and the same outside diameter as the groove can keep the bar from falling out and center the bar inside the groove. It is recommended to place the rubber hose/tube at 18-inch intervals which is typically sufficient to hold the bar. The TiAB shall be inserted into the groove after applying the first layer of epoxy filling at least half of the groove depth. The TiAB shall then be approximately centered in the groove, and then seated to the specified depth applying even pressure along the whole length of the bar. A concrete grooving trowel may be used to seat the TiAB. The seated TiAB shall be at least 1/8 inch below the concrete surface, and adhesive shall be present between the TiAB and three (bottom and two sides) groove surfaces.

5. Final adhesive injection

After the TiAB is properly seated and while the initially injected adhesive remains workable, the final layer of epoxy shall be placed to cover the TiAB and to fill any remaining space in the groove. A putty knife can be used to smooth the surface of the epoxy and remove the excess epoxy from outside of the groove. Sufficient time for full curing shall be provided following the manufacturer's recommendations.

6. Final surface cleaning

The masking or tape used around the groove shall be removed after finishing the epoxy injection. It is recommended to wait a sufficient amount of time so that the epoxy is not removed up around the edge of the groove while removing the tape/mask. Water blasting shall be permitted for surface cleaning any adhesive.

(g) Repair of defects

The Contractor shall be responsible for proposing and constructing a repair procedure for all defects or damage caused by the installation of the NSM TiAB system as designated by the Engineer.

xxx.04 Method of Measurement.

The near-surface-mounted (NSM) Titanium Alloy Bar (TiAB) will be measured in units of linear feet of length of NSM TiAB installed, regardless of the required width or depth of the TiAB installation.

xxx.05 Basis of Payment.

(a) Unit price coverage

The near-surface-mounted (NSM) Titanium Alloy Bar (TiAB) will be paid for at the contract unit price which shall be full compensation for furnishing all materials, equipment, tools, labor, submittals, and incidentals necessary to complete this item of work.

(b) Payment will be made under Item No.:

xxx-A Near-surface-mounted Titanium Alloy Bar (TiAB) – per liner foot